Effects of ion beam irradiation on transition metals embedded polymer matrix

A thesis Submitted to the
The Maharaja Sayajirao University of Baroda, Vadodara

For the Degree of

Doctor of Philosophy

In

Physics

By

Chaitali Gavade

Under the Supervision of

Prof. N. L. Singh

Department of Physics, Faculty of Science
The M.S.University of Baroda, Vadodara-390002, India

June 2014

DEDICATED TO

....MY BELOVED PARENTS

DECLARATION BY THE CANDIDATE

I hereby declare that the thesis entitled ***“Effects of ion beam irradiation on transition metals embedded polymer matrix”*** is the results of the investigations carried out by me under the guidance of Prof. N. L. Singh at Department of Physics, The Maharaja Sayajirao University of Baroda, Vadodara. The work is approved by Council of Post-Graduate Studies and Research. Further, I have put in research work for requisite number of terms as required by the University.

I further declare that to the best of my knowledge, this thesis has not been submitted for the award of any degree, diploma, associateship, fellowship etc. of any university or institute.

Chaitali Gavade

CERTIFICATE

This is to certify that the thesis entitled ***"Effects of ion beam irradiation on transition metals embedded polymer matrix***" is a piece of research work done by **Ms. Chaitali Gavade**, under my supervision and guidance for the degree of **Doctor of Philosophy in Physics at The Maharaja Sayajirao University of Baroda.** To the best of my knowledge and belief the thesis

1. embodies the work of the candidate herself
2. has duly been completed
3. fulfils the requirements of the ordinance relating to the PhD degree of the University
4. is up to the standard both in respect of content and language for being referred to examiner.

Forwarded through

(Prof. N. L. Singh)
Thesis supervisor

Department of Physics
Faculty of Science
The Maharaja Sayajirao University of Baroda
Vadodara-390 002,Gujarat,India

ACKNOWLEDGEMENTS

All praises to Almighty God, the Omnipotent, the Omnipresent, the most Merciful, the most Compassionate, the most Perfect and exalted among and of ever born on the surface of Earth, who is always torch of guidance and knowledge of humanity as a whole.

*The work presented in this thesis was accomplished under the inspiring guidance, generous assistance and enlightened supervision of **Prof. N. L. Singh**, Department of Physics, The Maharaja Sayajirao University of Baroda, Vadodara. I express my deep sense of gratitude and respectful regards to him for putting me at ease and affectionately inspiring me during my research studies.*

*My sincere gratitude and thanks to **Prof. Nikhil Desai**, former Dean, Faculty of Science, The Maharaja Sayajirao University of Baroda for all the valuable support. I am thankful to **Prof. A.C. Sharma**, Dean, Department of Physics, Faculty of Science, The Maharaja Sayajirao University of Baroda for all the help during my stay in the department. I express my heartiest thank to P**rof. P. K. Mehta** for his cooperation and encouragement during this work. Thanks are also due to **Prof. C. F. Desai, Prof. D. K. Kanchan, Prof. J. P. Singh, Prof. S. Mukharjee, Dr. M. B. Sureshkumar, Dr. D. G. Rathod, Dr. K. R. Jotania, Dr. Keyur Vyas, Dr. Mitesh Sarkar, Dr. P. H. Soni and Shri N. V. Patel,** for their co-operation.*

I am also grateful to The Maharaja Sayajirao University of Baroda, Vadodara for providing me infrastructure and research facility. I am thankful to the fellowship provided by UGC and CSIR, New Delhi.

I would like to thank each and every non-teaching staff of my Physics department for their timely help. I am also thankful to faculty office staff for all the help.

*Valuable suggestions and constant support are greatly acknowledged and appreciated which I had during the discussions with **Dr. P. K. Khanna**, Dept. of Applied Chemistry, Defence Institute of Advanced Technology (DIAT), Govt. of India, Girinagar, Pune.*

*I thank Fr.Director- Inter University Accelerator Centre (IUAC), **Dr Amit Roy** for encouragement and financial support during my work and stay at the centre. I would like to express special gratitude and thanks to **Dr. D. Kanjilal (Director-IUAC), Dr. D. K. Awasthi, Dr. S. Chopra, Dr. F. Singh, Dr. A. Tripathi** and scientists for constant support and fruitful discussions extended to me during experimental work carried out at IUAC, New Delhi.*

I would like to thank ***Dr. Ajay Gupta****, Fr. Center Director,* IUC-UGC-CSR, *Indore and* ***Dr. V. Ganesan (****Center Director,* IUC-UGC-CSIR, *Indore****), Dr. D. Alok Benerjee, Dr. Ram Janay Choudhary****, for providing laboratory facility. I would like to thank* **Dr. V Shrinet** *(ERDA, Vadoadara) and* ***Dr. Sunil Shah, Dr. Sanjeev kapoor*** *(DDU, Nadiad) for providing laboratory facility.*

No work is accomplished without appreciation and healthy environment we receive from friends and well-wishers. I wish to record my deep gratitude to my colleague ***Dr. Sejal Shah, Dr. Bhagwati Bishnoi, Dr. Poonam Sharma, Dr. Anjum Qureshi, Dr. Dolly Singh, Dr. Devang Shah, Dr. Satish Pelagde, Dr. Prashant Kumar Rath, Ms. Anamika Panihari, Dr. Paresh Prajapati, Mr. Aditya Patel, Mr. Gaurang Patel, Mrs. Purvi Patel, Dr. Sagar Ambavale, Ms. Sangeeta Kishore, Dr. Kanti Bhambhariya, Mr. Gyansagar Patel , Dr. Nirali, Prajkata, Gargi, Dr. Nikit Deshmukh, Manishbhai*** *and many others.*

*I am very much grateful for the moral support of my parents throughout the period of my research work. I am very indebted to them without whose help I could not have finished my work. Without their several sacrifices, it would not have been possible for me to accomplish whatever I have achieved in my life so far. I am short of words to express my deep gratitude to my Father (***Mr. Dilip Gavde***) and my dearest and most loving Mother (***Mrs. Nayna Gavde***), brother (***Mr. Kunal Gavde***) along with my dear and loving bhabhi (***Mrs. Pratibha Gavde***) and little* ***Nachiket*** *for their constant support throughout my thesis work and encouraged me to complete my work. I like to thank my relatives who support and motivate me throughout my work.*

I also express deep gratitude to my in-laws and sister-in-law who also stood beside me in all hardships. I therefore would like to thank them from the bottom of my heart. I am very much thankful to my loving and caring Husband ***(Mr. Sandeep Kulkarni)*** *whose constant support and encouragement has led me to complete my thesis. Finally I again thank to the almighty for giving such a supportive and loving family being with us in all the ups and downs of life.*

Date: **CHAITALI GAVADE**

PLACE: VADODARA

PREFACE

The rapid pace of advances in polymers, with only few decades separating their first commercial development from their present pervasive use, has been remarkable. Although progress to date in polymer science can be considered revolutionary, opportunities are abundant to create new polymeric materials and modifying existing polymers as per different applications. Inclusions of nanoparticles in polymers offer to novel materials/ nanocomposites which are proposed important technological advances in the field of battery, gas sensors, photo electronic devices, catalysis, electrochemistry, photoluminescence and separation membranes. However, for most of these highly specialized applications, there is a practical need to disperse the nanoparticles in polymeric materials. As useful feature of polymer host matrices is that they provide the possibility of mediating magnetic interactions between particles in these nanocomposites including dipolar, exchange (isotropic and anisotropic), super exchange and magnetoelastic interactions. Polymers have traditionally been considered as an excellent host matrix for composite materials. Several advanced polymer composites have been synthesized with a wide variety of inclusions like metals, semiconductors, carbon nanotubes and magnetic nanoparticles. Many attractive properties of polymers like non-corrosiveness, light weight, mechanical strength, dielectric tenability and able to provide required immobilisation of the nanoparticles avoiding their coalescence or segregation, thus protecting the novel size-dependent properties of nanomaterials can be utilized along with magnetic and optical properties of nanoparticles to make multifunctional material.

Research in the use of noble nano materials has surged over the last few decades and considerably numerous works have been carried out to understand the nanomaterials and their assemblies. By confinement of materials in nanometre spatial dimensions, small size effect, surface effect, quantum size effect and macroscopic quantum tunnel effect can alter the optical, magnetic, electrical and structural properties of nanomaterials. Whereas, composites are materials in which two or more distinct, structurally complementary substances combine to produce some structural or functional properties not present in any individual component and to combine some of the advantages of the component materials forming some novel ones.

Unlike applications of nanotechnology in the photonics and electronics areas, the use of the polymer nanocomposites in the field of dielectrics and electrical insulation has not attracted a lot of interest until very recently. The current growing need for high-power density and high voltage capacitors, gate dielectrics, memories, sensors, shielding and power-storage devices has stimulated a new wave of research interest in polymer nanocomposites. By incorporating high permittivity inorganic nanoparticles like metal nanoparticles into a polymer matrix with low dielectric loss and high dielectric strength, one may be able to develop new composite materials that have improved dielectric properties (resistivity, dielectric strength, permittivity and dielectric losses) and retain the unique attributes of polymers such as ease of production and often ductilility, etc.. By varying the size and percentage of filler nanoparticles, the polymer nanocomposites may be fabricated with tailored dielectric properties for specific applications.

The high energy ion beam irradiation effects in polymers have fascinated considerable attention for purposes of polymers in radiation environment and also in the improvement of new electronic devices. The deposited energy may be converted into atomic motion and finally leads to the structural and chemical modifications within a cylindrical zone of several nanometers in diameter and new structural arrangements may appear. Swift heavy ion irradiation tends to damage polymers significantly by two ways mainly, electronic excitation and ionization. The nature of defects and the relative radiative sensitivity of different polymers depend on the properties such as their composition and molecular weight, on the charge, mass and energy of the ion and also on the environmental conditions during irradiation. Irradiation effects in inorganic materials are manifested as changes in physical properties such as refractive index, magnetization and hardness. Some of the work reported on the modification of ion beam irradiation on organometallic / metal polymer composites. It is observed that dielectric properties enhances on increasing the organometallic/metal particles content in polymer matrix and also upon ion beam irradiation.

In the present work, three different types of conductive nanoparticles were used as filler viz. silver (Ag), copper (Cu), nickel (Ni). Poly methyl methacrylate (PMMA) and polystyrene (PS) were used as polymer matrices for making polymer nanocomposites. The films were prepared by casting technique. The irradiation effect on these nanocomposite films was studied with respect to ion specie, energy and fluence. For this purpose 120 MeV Si Ni^{10+}, 85 MeV C^{6+}beams were used. AC electrical/dielectric, structural, chemical, thermal, optical, magnetic properties and surface morphology of pristine and irradiated nanocomposites were investigated by means of various techniques.

The present work is categorized into the following chapters:

Chapter 1 will be the general introduction of state of art of the applications of polymer based nanocomposites in packing and shielding application. The importance of ion beam irradiation in the field of nano science and technologies is explained on the basis of energy loss of ion beam in the polymeric samples. This also deals with literature survey with reference to ion beam irradiation of polymeric materials and motivation for present work.

Chapter 2 presents a brief review of the concept of polymer composites and general descriptions of the experimental methods and tools used are given in this chapter. The working principles and operation of Pelletron Accelerators has been conversed. Three different types of conductive nanoparticles were used as filler viz. silver (Ag), copper (Cu), nickel (Ni). Poly methyl methacrylate (PMMA) and polystyrene (PS) were used as polymer matrices for making polymer nanocomposites. Different characterization techniques have been used to do off-line analysis of the pristine and irradiated samples. These techniques with their proper specifications and operating principle have been described.

Chapter 3 This chapter describes the comparative study of characterization of conductive filler, silver (Ag) dispersed PMMA and PS polymers nanocomposites. These composites were irradiated with 85 MeV C^{+6} ions and 120 MeV Si^{+10} ions at fluences of $1x10^{11}$ and $1\ x10^{12}$ ions/cm^2. The various results of experimentations before and after ion beam irradiation are explained. Scientific explanations of various properties e.g., structural, optical, thermal, electrical properties and surface morphology of conductive composites are given. The results obtained from various characterization techniques show the dependence of different properties of composites upon matrix, ion beam irradiation and filler concentrations. Structural properties were studied by means of X-ray diffraction. The band gap of materials decreases with filler concentrations and also upon irradiation. Thermal property of the composite was studied by DSC analysis and it reveals about the glass transitions temperature (Tg). The glass transition temperature increases on increasing the filler concentration and decreases upon ion beam irradiation with fluences in PMMA and increases in PS nanocomposites. The average surface roughness of the composites also changed as revealed from SEM studied. The results of all characterization techniques have been correlated to give a better and clear view of dielectric, structural, mechanical, chemical, thermal properties and surface morphology. It was observed that dielectric properties and microstructure of polymer composites enhanced after irradiation.

Chapter 4 illustrates the study of characterization of conductive filler, Copper (Cu), dispersed PMMA and PS polymers nanocomposites. These composites were irradiated with 85 MeV C^{+6} ions and 120 MeV Si^{+10} ions at fluences of $1x10^{11}$ and 1 $x10^{12}$ ions/cm^2. The various results of experimentations before and after ion beam irradiation are explained. Scientific explanations of various properties e.g., structural, optical, thermal, surface morphology and electrical properties of conductive composites are given. The results obtained from various characterization techniques show the dependence of different properties of composites upon ion beam irradiations and filler concentrations. The structural, thermal, dielectric analysis was carried out by X-ray diffraction, DSC and Impedance phase gain analyzer respectively. The surface morphology of the composites is studied by SEM. It was observed that dielectric properties of polymer composites enhanced after irradiation. The results give the chain scissioning in Cu/PMMA composites and cross linking in the Cu/PS composites.

Chapter 5 describes the study of characterization of conductive filler, nickel (Ni), dispersed PMMA and PS polymers nanocomposites. These composites were irradiated with 85 MeV C^{+6} ions and 120 MeV Si^{+10} ions at fluencies of $1x10^{11}$ and 1 $x10^{12}$ ions/cm^2. The various results of experimentations before and after ion beam irradiation are explained. We have studied changes in the optical, structural, dielectric, magnetic and thermal properties of composites due to swift heavy ion irradiation by means of UV–visible spectroscopy, X-ray diffraction, differential scanning calorimetry, impedance gain phase analyzer and SQUID. The ion beam irradiation of polymer nanocomposites leads to chain scission and cross linking, which leads to increase the free radicals, unsaturation etc. As a result of that there are changes in magnetic and dielectric properties. The magnetic properties enhanced after irradiation which may be attributed to the exchange dipolar interaction of particles in the matrix and generation of free radicals. AC electrical and dielectric properties of PMMA/Ni and PS/Ni nanocomposites were studied over a wide range of frequency as a function of filler concentrations. Both the dielectric constant and the electrical conductivity of the composites increased with the increase of Ni content. These phenomena could be interpreted from interfacial polarization of heterogeneous system.

Chapter 6 This chapter summarizes the results obtained by $Si^{10+}$and C^{6+} beam irradiations. It also gives conclusions derived from the present work. Future perspectives, as well as possible extension of the present work have been explained.

*The references are numbered in square bracket in the text and are listed at the end of the respective chapters.

List of Publications

List of publications:

1. “Optical and Dielectric Properties of Ion Beam Irradiated Ag/Polymethyl Methacrylate Nanocomposites” Chaitali Gavade, N.L. Singh, P.K. Khanna. *Journal of nanoscience and nanotechnology* 14 (2014)1-6.

2. “Effect of swift heavy ion irradiation on copper/polymethyl methacrylate Nanocomposites”Chaitali Gavade, Sangeeta Kishore, N.L. Singh, P.K. Khanna. *Radiation Effects & Defects in Solids* 168(7–8) (2013) 504–511.

3.”Swift Heavy Ion Induced Modification in Physical Properties of Poly methylmethacrylate (PMMA)/Nickel (Ni) nanocomposites“ N. L. Singh, Chaitali Gavade, and P. K. Khanna . *Defect and Diffusion Forum* 341 (2013) 51-68.

4. “The effect of SHI irradiation on structural, thermal and dielectric properties of silver Nanoparticle-embedded polystyrene matrix” Chaitali Gavade, N.L. Singh, Anita Sharma, P.K. Khanna and Fouran Singh. *Radiation Effects & Defects in Solids* 166 (8-9) (2011) 585-591.

5. “Ion Beam Induced Modification of Metal Oxide Nanoparticles Dispersed Polyaniline Films” Sangeeta Kishore , Chaitali Gavade, Dolly Singh and N. L. Singh. *Radiation Effects & Defects in Solids* 166 (8-9) (2011) 606-614.

6. “Effect of SHI on dielectric and magnetic properties of metal oxide/PMMA nanocomposites” Chaitali Gavade, N.L.Singh, D.K.Avasthi, Alok Banerjee. *Nuclear Instruments and Methods in Physics Research B* 268 (2010) 3127–3131.

7. “Study of dielectrical properties of swift heavy ion induced modifications in metal oxide/PMMA nanocomposites” Chaitali Gavade, N. L. Singh, Dolly Singh, Sejal Shah, A. Tripathy, D. K. Avasthi. *Integrated Ferroelectrics*, 117 (2010) 76–84.

8. “ Ion beam induced modification of metal nanoparticles dispersed polymeric films” Sejal Shah, N L Singh, Chaitali Gavade, V Shivakumar, Indra Sulania, A. Tripathi, F Singh, D K Avasthi, R.V.Upadhyay. *Integrated Ferroelectrics* 117(2010) 97–103.

9. “ Electrical and thermal studies on the polyvinylchloride/carbon black composites induced by high energy ion beam” Dolly Singh, N.L. Singh, Anjum Qureshi, Chaitali Gavade, D.K. Avasthi, Arif N. *Integrated Ferroelectrics* 117(2010) 85-96.

Papers in Proceedings:

1. Synthesis of Silver Polymer Nanocomposites and Their Antibacterial Activity, Chaitali Gavade, Sunil Shah, N.L.Singh.55th DAE Solid State physics, AIP Conf. Proc. 1349 (2011) 168-169.

2. Effect on Optical Properties of Silver/PVA Nanocomposites Influenced by SHI Irradiation, Chaitali Gavade, Sunil Shah, N.L.Singh. Proceeding of International Symposium of Materials Chemistry, 6-11 Dec, 2010, BARC, Mumbai, India

3. Effect of SHI irradiation on dielectric and thermal properties of metal oxide/PMMA nanocomposites, Chaitali Gavade, Dolly Singh, N.L.Singh, D.K.Avasthi, V.Ganesan. Proceedings of the DAE Solid State Physics Symposium, Vol.54(2009)221.

4. Optical and electrical properties of polypropylene/glass fiber composites by 140MeV Ag^{11+} ion irradiation, Dolly Singh, Anjum Qureshi, Chaitali Gavde,

N.L.Singh, Ambuj Tripathi, D.K. Avasthi. Proceedings of the DAE Solid State Physics Symposium, Vol.54 (2009) 223.

5. Temperature Dependent Impedance Spectroscopic Studies of Solid Polymer Electrolyte:a: x) PEO: x Ni-DMG,Sangeeta, Dolly Singh, Chaitali Gavade and N. L. Singh. Proceedings of the DAE Solid State Physics Symposium, Vol.54(2009) 829.

6. Study of AC Electrical Properties of Proton Irradiated Polymer Composite, Sejal Shah, Dolly Singh, Anjum Qureshi, Chaitali Gavde, N.L. Singh, K.P.Singh. Proceedings of the DAE Solid State Physics Symposium Volume 52 (2007) 179.

7. Effect of SHI irradiation on NIO doped PMMA composites, Chaitali Gavde, Sejal Shah, Dolly Singh, N. L. Singh, A.Tripathi and D.K.Avasthi. Proceedings of the DAE Solid State Physics Symposium, Volume 53 (2008) 593.

List of abbreviations

AC	Alternating current
CMC	Ceramic matrix composites
DSC	Differential scanning calorimetry
Eg	Energy band gap
EMI	Electromagnetic interference
F	Frequency
keV	Kilo electron volt
LET	Linear energy transfer
MeV	Mega electron volt
MMC	Metal matrix composites
PMC	Polymer matrix composites
PMMA	Polymethyl methacrylate
PS	Polystyrene
S_e	Electronic energy loss
SE	Shielding effectiveness
SEM	Scanning electron microscopy
SHI	Swift heavy ion
S_n	Nuclear energy loss

SQUID	Superconducting Quantum interference device
SRIM	Stopping range of ions in material
Tg	Glass transition temperature
THF	Tetrahydro furan
XRD	X-ray diffraction
ZFC/FC	Zero-field- cooled/Field –cooled

List of Figures

Chapter – I

Chapter – II

Chapter – III

Chapter – IV

Chapter – V

Chapter – VI

List of Tables

Chapter – II

Chapter – III

Chapter – IV

Chapter – V

Chapter – VI

Contents

Chapter I Introduction

Chapter II Materials and Experimental Techniques

Chapter – III Effect of swift heavy ions on physical properties of PMMA/Ag and PS/Ag nanocomposites

Chapter – IV Effect of swift heavy ions on physical properties of PMMA/Cu and PS/Cu nanocomposites

Chapter –V Effect of swift heavy ions on physical properties of PMMA/Ni and PS/Ni nanocomposites

Chapter – I

Introduction

Abstract

This chapter concerns with the fundamentals of polymers composites and nano composites. The importance of ion beam irradiation in the field of nano science and technologies is explained on the basis of energy loss of ion beam in the polymeric samples. The effects of ion beam irradiation on physical properties of nano composites are explained. The purpose of this chapter is to describe the context of the work, the overall objectives of the study and the structure of the thesis.

1.0Introduction to rapid pace of polymers and polymer composites:

Polymers are a large class of materials consisting of many small molecules (called monomers) that can be linked together to form long chains, thus they are known as macromolecules. On the basis of different chemical structures, physical properties, mechanical behaviour, thermal characteristics, stereochemistry, polymers can be classified into following ways like natural and synthetic polymers; organic and inorganic polymers; thermoplastic and thermosetting polymers; plastics, elastomers, fibers and liquid resins; atactic, isotactic and syndiotactic polymers.

Polymeric materials are generally insulating or nonconductive materials in nature and normally used in electric and electronic applications as insulators, but polymers are too flexible and too weak to be used in various specific applications. [1-2]. Since the increasing demand for lighter, economic, chemically resistive, conductive materials created a need for new materials often called composite materials.

A composite material composed by material in which two or more distinct structurally complementary substances are combined to produce structural or functional properties not present in either of the individual components. In the world of high tech engineering and materials science, composites are more easily explained by mixtures of chemically different materials that are insoluble in each other and are thus represented by distinct phases: usually a continuous phase (matrix) and a discontinuous phase (may be filler).

1.1 Classification of composites:

Composites may be classified into different types by the way of reinforcement and matrix used in materials.

1.1.1 Classification based on reinforcements:

Composites can be classified as particle-reinforced composites in which particles used as reinforced phase and fiber-reinforced composites where reinforcing phase is in the form of fiber [3]. The particle-reinforced composites can be further classified into large-particle composites and dispersion-strengthened composites based on particle size. Based on fiber alignment and length, the fiber reinforced composites can be classified further into three categories [4],

1. Continuous and aligned
2. Discontinuous and aligned
3. Discontinuous and randomly oriented

1.1.2. Classification Based on Matrix

Based on the matrix used in materials can be mainly classified as [5]

1. Polymer Matrix Composites (PMC)

In polymer matrix composites, the matrix phase is polymer and the reinforcing phase may be metals, fibers or ceramic particles. They are being used in various medical applications and sensing applications.

2. Metal Matrix Composites (MMC)

For metal matrix composites, the matrix is a ductile metal or alloy and the reinforcing medium is continuous like fibers of carbon, silicon carbide, boron and alumina or any others. Also disadvantages of metals used as matrix include corrosion, high density, high stiffness, release of metal ions may cause allergic reactions and not cost effective. Therefore, metal matrix composites are more expensive than polymer matrix composites [6, 7].

3. Ceramic Matrix Composites (CMC)

In ceramic matrix composites, particulates, fibers or whiskers of one ceramic material are embedded into the matrix of another ceramic material. Ceramic composite materials are meant for high temperature applications like heat shield of re-entry spacecrafts.

1.2 Classification of polymer composites:

The polymer composites can be classified into three categories:

1. Macro composites: Polymer macro-composites are heterogeneous composites of polymers and macro sized fillers. The macroscopic characteristics of the composite often reflect its own microstructure.

2. Micro composites: Composites employing micron size fibers with high aspect ratio or fine hollow spheres or fibers as reinforcement are called micro composites. The matrix may be any polymer. The reinforcing phase will be a continuous fiber or short fiber or micron sized fillers such as metal particles. The main advantage of using fibers is to improve strength, stiffness, and thermal stability of composites.

3. Nano composites: Polymer nanocomposites are usually comprised of the composites of polymers with dispersed inorganic nanofillers. The nanofiller can be an insulator, a semiconductor or a metal, and can have spherical, cylindrical, or flake shapes. The polymer (matrix) can be conductive or non-conductive in nature.

Polymer nanocomposites have recently received significant attention because of the new and superior properties (*e.g.* electrical, thermal and mechanical) to conventional composites of these materials and may be synthesized using surprisingly simple and inexpensive techniques [8, 9]. Various aspects can control the physicochemical properties of nanocomposites such as the particle separation, the interphase interactions, the character of the polymer molecular structure, the method of the nanocomposite preparation and so on [10-13]. However we have used nanocomposites in the present work.

1.2.1 Promising Applications of polymer composites/nanocomposites:

Polymers play important role in human life. Other naturally occurring polymers like wood, rubber, leather and silk are serving the humankind for many centuries now. Modern scientific tools revolutionized the processing of polymers thus available synthetic polymers like useful plastics, rubbers and fiber materials.

Commercial and industrial applications of polymer composites/nanocompsoties are so varied that it is impossible to list them all. Only the major structural applications areas is highlighted here which include packaging industry, gas sensing application, oil industry, aircraft, space, automotive, furniture, sporting goods, marine, infrastructure, in electronics, building construction, power industry, medical industry (e.g., bone plates, implants), and in many other industrial products [14].

The progress in doing things much smaller, lighter and faster than before them already been existed has already been going on for many years. This enhanced exactness could facilitate existing products and processes to be more effective/cost effective, hence require less raw materials and energy. This is especially true in the most of fields like IT, electronic and energy industry, space, medical, military and security fields [15].

1.2.1.1 Focussed or Novel application:

(1) Gas sensing:

Polymer nanocomposites have been developed as candidates for different types of sensing applications. The conductive and absorptive properties of insulating polymers doped with conducting materials, and the absorptive properties of insulating polymers with non-conducting fillers are sensitive to exposure to gas vapours. Therefore, they can be used to monitor the existence and concentration of gases in the environment [15, 16].

(2) EMI shielding:

EMI is the kind of environment pollution. Electromagnetic interference (EMI) suppression is another area in which polymer nanocomposites can make great advances. All electronic devices like TV, radios, computers, motors generate and emit radiofrequency waves that can interfere with the operation of electronic components within the same device as well as other electronic devices. Miniaturization of electronic equipment requires components to be packed very close to each other, which increases the problem of electromagnetic interference. When an electromagnetic wave is incident upon a conductive surface, energy is reflected and absorbed. The ability of a material to shield electromagnetic energy, whether it is unwanted energy entering a system or escaping a system, is called its shielding effectiveness (SE) [17, 18]. EMI shielding can be achieved by coating of conductive layer of metal or by making materials from a plastic embedded with metal particles/nanoparticles which is having good conductivity. Metals are more common for shielding because of good conductivity. Also disadvantages with metals used include corrosion, high density, high stiffness, release of metal ions may cause uncertain reactions and not cost effective [6, 7]. Inclusion of metal particles in polymer matrix can solve all the difficulty which is generated with pure metals.

Requirements for shielding:

A material is shielded if the surface of the material is electrically conductive enough to shield against influence from outer fields. Minimum requirements in electric fields as mentioned below

a) Shielding against electrostatic fields

b) Protection against direct charge

c) Static discharge through contact with grounded conductors: a minimum build-up of electrostatic discharging through friction.

The electromagnetic waves can attenuate by shielding materials by three ways of mechanism [19]

a) By reflection at the surface: Reflection requires mobile charge carriers like electrons or holes which interact with electromagnetic radiation. This requirement can be achieved by doping of metal particles in a polymer.

b) By absorption due to thickness of the shield: For absorption, electric and magnetic dipoles require which interact with the field. The electric dipoles may be provided by materials having high dielectric constant or magnetic dipoles by magnetic nanoparticles. Polymers having dielectric constant (> 8) can fulfil the requirement.

c) By multiple reflections: This refers to the multiple reflections at the various surfaces or interfaces in the shield. This can be done by adding nanoparticles or nanoscales so that large surface area or interface area exists in the shield [20].

So the composite materials composed of insulating or conducting polymers doped with metallic particles/nanoparticles serve good for EMI shielding application.

1.3 Science with Ion Beam Irradiation:

Energetic ion beams play a vital role in the field of research and it has been exploited by researchers in different ways in materials science [21]. Ion beam effect on the materials depends on many factors like ion energy, mass of ions, fluence and ion species. The materials modification can be done by two ways, low energy ion (a few tens of keV to a few MeV) implantation and swift heavy ion irradiation (typically a few tens of MeV and higher). The ions lose energy when they traverse through the material which is either used in displacing atoms (of the sample) by elastic collisions or in exciting or ionizing the atoms by inelastic collision. The former is the dominant process at low energies where the displacement of atoms due to elastic collisions is insignificant [22]. In the inelastic collision (cross-section~10^{-16}cm^2) the energy is transferred from the projectile to the atoms through excitation and ionization of the surrounding electrons. The amount of electronic energy loss in each collision varies from tens of eV to a few keV per Angstrom (Å).

The interaction of charged particles with a target can be analysed by considering independently inelastic interactions with target electrons and elastic interactions with screened target nuclei. The former interaction is responsible of the "electronic stopping", (dE/dx)e, that dominates at high velocities, the latter of the "nuclear or atomic stopping", (dE/dx)n that dominates at low velocities.

1.3.1 Ion solid interaction in materials:

Fundamentals of ion solid interaction:

(i) Ion sources:

The basic requirement in this field is the availability of source of energetic ions. There are many small accelerators available and being used exclusively for ion implantation research (energies up to 2–3 MeV). Swift heavy accelerated ions (up to GeV) depending on the material irradiated, being the capacity to access a large range of lower energies using ‘absorbing’ foils of different thickness and different material.

(ii) Stopping Power:

Once an energetic particle beam strikes matter it immediately begins to transfer energy to the target system. The energy deposition process is commonly described by the ‘stopping power’ (−dE/dx), the energy transfers per unit path length of an ion on its trajectory. It is also convenient to split up the particle stopping into two basic and dominant energy transfer mechanisms. One arises from ‘ballistic’ billiard ball type atomic collisions with the target atoms (‘nuclear’ energy transfer) and the other from excitation and ionization of the target electrons (‘electronic’ energy transfer). Light ions of any energy, and energetic heavy ions with stopping powers in keV/Å range, deliver much more energy via electronic excitation than by nuclear collisions. For low energy heavy ions with stopping powers in eV/Å range, the nuclear energy transfer dominates.

The total stopping power is then the sum of both components whose reciprocal integral defines the total projectile range. Both stopping powers increase with increasing energy, reach a maximum and thereafter fall away as shown in Fig 1.1

If the energy transferred to the primary atom ‘knocked on’ is sufficiently high, there can then be secondary, tertiary and higher order atomic knock-ons all of which, if sufficiently localized, comprise an energetic atomic cascade in the target as shown in Fig. 1.2.

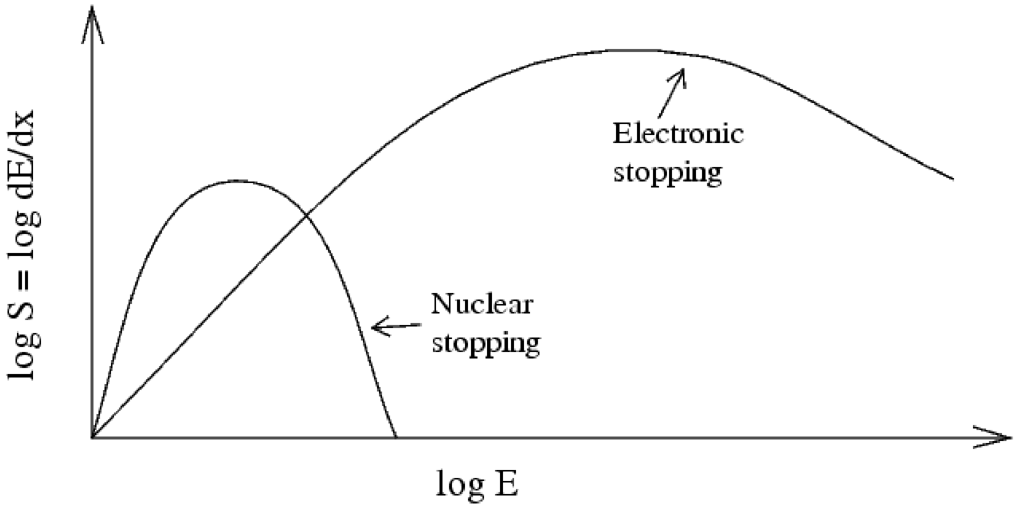

Fig. 1.1 Graph for projectile ion energy versus energy loss

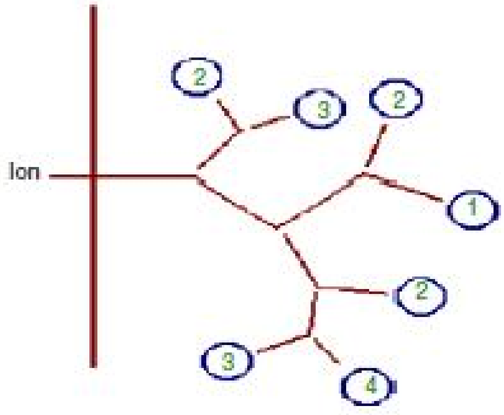

Fig. 1.2 Schematic of ion–solid interaction induced cascade collision

1.3.2 Energy losses:

When an energetic ion passes through a solid, it loses energy through elastic and inelastic scattering processes. The ions lose energy during their passage through the material, which is spent in either displacing atoms by elastic collisions (nuclear stopping) or exciting the atoms by inelastic collisions (electronic stopping). The energy lost due to nuclear stopping is called nuclear energy loss and one due to electronic loss is known as electronic energy loss. Apart from these two events, another mechanism which takes place during slowing down of incident ions is charge exchange process between the ion and the atoms of the solid. This can be expressed as

$$\left(\frac{dE}{dX}\right)_{loss} = \left(\frac{dE}{dX}\right)_{Elect} + \left(\frac{dE}{dX}\right)_{Nucl} + \left(\frac{dE}{dX}\right)_{ChargeExchange}$$

Since charge exchange loss represents a small fraction of total energy loss, which can be neglected.

$$\left(\frac{dE}{dX}\right)_{loss} = \left(\frac{dE}{dX}\right)_{Elect} + \left(\frac{dE}{dX}\right)_{Nucl}$$

$$\cong S_e + S_n$$

Nuclear and electronic energy losses are schematically shown in Fig. 1.1.

1.3.2.1 Nuclear energy loss:

Nuclear energy loss is due to elastic binary collision between a projectile ion and target atoms. This is based on the screened Coulomb potential and impulse approximation. If one knows the form of potential between two atoms, one can calculate value of nuclear stopping power.

1.3.2.2 Electronic energy loss:

The energy loss per unit path length of the ion is known as Specific Energy Loss. This is also termed as stopping power or linear energy transfer (LET). In 1913, Bohr first proposed the theory of electronic energy loss S_e of energetic ions in solids [23]. With electronic stopping one means slowing down due to the inelastic collisions between electrons in the medium and the ion moving through it. The term inelastic is used to signify that the collisions may result in excitations in the electron cloud of the ion; therefore the collision cannot be treated as a classical scattering process between two charged particles. Since the number of collisions an ion experiences with electrons is large, and since the charge state of the ion while traversing in the medium may change frequently, it is very difficult to describe all possible interactions for all possible ion charge states. Instead, the electronic stopping power is given as a simple function of energy Se (E) which is an average taken over all energy loss processes for different charge states. It can be theoretically determined to an accuracy of a few % in the energy range above several hundred keV from theoretical treatments, the best known being the Bethe-Bloch formula [24].

1.3.2.3 Overview of the slowing down process:

Energetic ions entering into material medium, it immediately interacts with many electrons simultaneously. In such encounter, the electron experiences an impulse from the attractive Coulomb force as the projectile ion passes its area. Sometimes this impulse may be sufficient either for excitation or for ionization. The energy, which is transferred to the electron, comes from the energetic ion. So, the velocity of the ion will decrease as a result of the encounter. By the time ion interacts with many electrons, so the net effect is to decrease its velocity continuously until it is stopped.

The swift heavy ions can move a few microns to tens of microns in the target because a single encounter of ions with an electron does not deflect from its path. So, these particles pass a definite range in a given material. In the beginning of the slowing-down process at high energies, the ion slows down mainly by electronic stopping, and moves almost in a straight path. The process is schematically illustrated in Fig. 1.3.

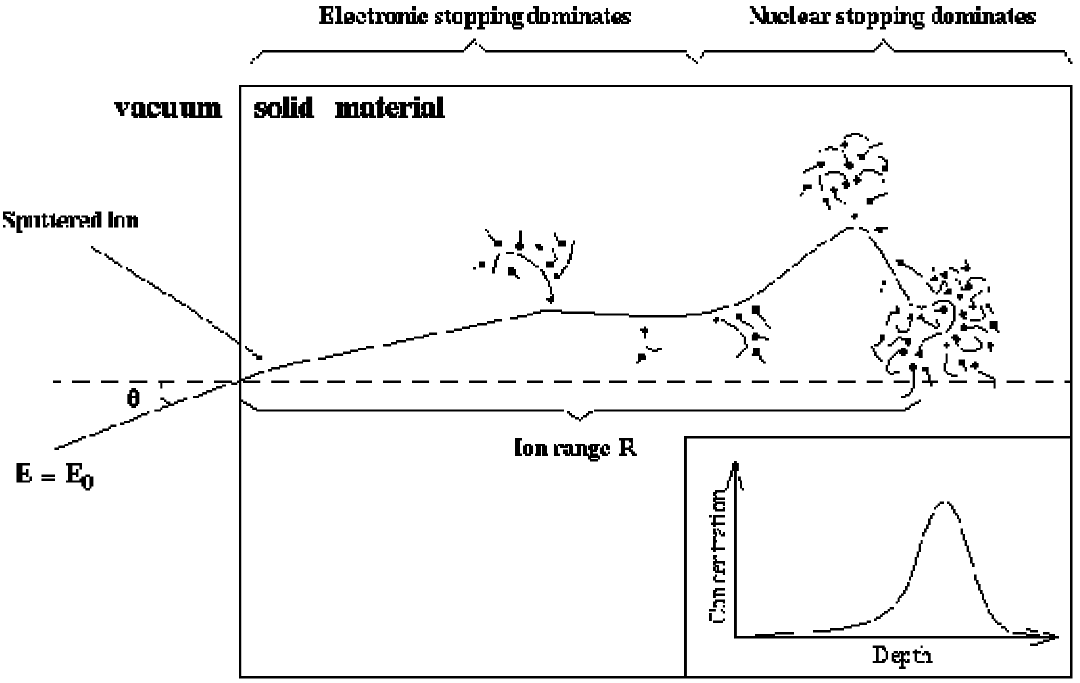

Fig. 1.3 Interaction of ion beam with target material

1.4 Overview on Ion beam induced modification:

1.4.1 Low energy ions:

A study involving ion-solid interactions in the range of eV to few keV is usually called in low energy range. There are two possibilities either materials are made up by ion implantation or low energy ion irradiation.

Low energy ion beam irradiation may have various applications and invariably expose completely new eras in various fields, particularly in materials science and device technology. Low energy accelerators are now standard tools and their exploitation in engineering materials of all kinds of interest: electronic, biological, and metallurgical etc. provide very fruitful activity. Energetic ion beams, when penetrate through the interface of different materials, produce massive atomic transport across the interface which results in many stable, unstable or even thermodynamically non-equilibrium phase formation around the interface. Due to the improved electrical, chemical or optical properties of the ion irradiated materials, ion beam induced mixing of metal/metal or metal/semiconductor systems occupy a major share of the accelerator based materials research.

1.4.2 Swift heavy ions:

In the inelastic collision (cross-section 10^{-16} cm^2) energy is transferred from the projectile to atoms of the matter through excitation and ionization of their surrounding electrons. The amount of electronic energy loss in each collision varies from a few eV/Å to a few keV/Å. For a swift heavy ion (SHI) moving at a velocity comparable to the Bohr velocity of electron, this is the dominant mechanism for transfer of energy to the material causing the modification of its properties. The main difference of materials modification by ion implantation and swift heavy ion irradiation is that in ion implantation the incident low energy ions get embedded in the material cause changes whereas in swift heavy ion irradiation the impinging ions do not get embedded in the materials due to their larger range.

1.5 Ion beam induced modifications in polymeric films:

Polymer/polymer composites materials are scientifically important for research because of their diverse applications like filtration, protective coating, medical science, nanoscale designing, nuclear power plant, space-crafts etc [25, 26]. Studies concerning to the study of the effect of gamma and electron irradiation and swift heavy ions on polymeric materials have been reported in literatures. The modification of polymeric material by irradiation with swift heavy ions has gained considerable interest in the last two decades due to easy access to heavy ion accelerators [27-31]. SHI irradiation of polymers/polymer composites alters the chemico-physical properties considerably. The macroscopic changes are examined in terms of chemical, optical, thermal, magnetic and electrical modifications by means of bond breaking, main-chain scissoning, crosslinking, carbon cluster formation, volatile species liberation, and formation of new chemical bonds [32-34]. Improvement in mechanical, structural and dielectric properties, density, chain length, crystallinity, solubility, and also in the optical transmission properties of the polymers have been reported [34-39]. The nature of changes depends upon properties of polymers, such as the composition and molecular weight, and on the mass and energy of the incident ions and other conditions also.

Polymer nanocomposites with functional metal nanoparticles have much interest due to their cost effectiveness, processibility and high flexibility, rendering possible many applications such as non linear optical switches, magnetic data storage, micro wave absorbers, photovoltaic cells and smart structure [40]. In such kind of applications good adhesion should present between polymer and metal nanoparticles. The interaction between polymer and metal is usually weak but it can be improved or enhanced by means of irradiation. When polymer nanocomposites are irradiated with energetic particles, new adsorption sites might be created which improved polymer-metal adhesion. Irradiation makes possible more prominent polymer-metal bonding and enhances the properties of the nanocomposites [41, 42].

In the present concern, we have used Si^{+11}, C^{+6} ions to study the effect of ion species, energy, fluence on the composites. The effect of ion beam on different properties like dielectric, magnetic, structural and optical properties have been explained in respective sections.

1.5.1. Dielectric properties and improvements due to ion beam irradiation:

The dielectric properties of materials play a fundamental key role in the explanation of physical phenomena in many branches of modern science and engineering. Dielectric spectroscopy a powerful technique provides a linkage between the dynamics of molecular motion of the individual constituents of a complex material and the characterization of its bulk properties. It is important for investigating a variety of dielectric for both electrical and non electrical applications. The dielectric properties are used to describe electrical energy storage, dissipation and energy transfer [43, 44].

There are a number of different dielectric mechanisms, connected to the way a particular medium reacts to the applied field. The electronic polarization occurs in a neutral atom when the electric field displaces the electron density relative to the nucleus it surrounds. Atomic polarization is observed when the electronic cloud is deformed under the force of the applied field, so that the negative and positive charges are formed. Dipole relaxation originates from permanent and induced dipoles aligning to an electric field and heavily dependent on temperature and chemical surrounding. Ionic relaxation comprises ionic conductivity, interfacial and space charge relaxation which predominates at low frequency. Interfacial relaxation occurs when charge carriers are trapped at interfaces of heterogeneous systems. Dielectric relaxation as a whole is the result of the movement of dipoles (dipole relaxation) and electric charges (ionic relaxation) due to an applied alternating field, and is usually observed in the frequency range 10^2-10^{10} Hz [45].

The situation when a constant voltage is applied to a set of juxtaposing capacitor plates. The relation between the amount of free charge, Q, and the voltage drop, V, is $Q = CV$, where C is the capacitance of the capacitor,

$C = \varepsilon_o A/d$, A and d are the cross-sectional area of the plates and thickness between them respectively. ε_o: dielectric permittivity of air = 8.85×10^{-12} F/m.

The relative dielectric constant is then defined as the ratio between the flux density in vacuum and in the dielectric,

$k' = \varepsilon' / \varepsilon_o$

Loss tangent is expressed by,

$\tan \delta = \varepsilon'' / \varepsilon'$

where real part ε‘ defines insulating properties and imaginary part ε“ describes conductive properties of the dielectric material.

There are reports on the effect of ion beam on the dielectric properties of the polymers. There exists few reports on gamma, neutron and electron irradiation of non polymeric materials. These studies provide frame work to some general idea about the effects expected here.

Dielectric loss/constant increases upon irradaition as it is associated with more pronounced electron transitions, the more electron participate in electron hopping phenonmenon created between amorphous zones of destructed polymers [46].

Conductivity by ion beam irradiations of polymers/polymer composites

The results reported that the increase in conductivity value of irradiated samples is increased with increase in radiation dose. The increase in the conductivity due to swift heavy ion irradiation may be attributed to formation of defects and carbonaceous clusters arising due to scission of the polymer chain [47]. The ion beam irradiation leads to charge accumulation at these sites. The increase in crystallinity of the material also contributes to the increase in conductivity after irradiation due to decreased scattering of charge carriers [48]. Frequency dependent conductivity could be attributed to the release of trapped charges in the disordered system. It is observed that with the increase of fluence the AC conductivity of the nanocomposite increases. This may be attributed to release of more trapped charges in the composites, due to huge electronic energy deposition upon SHI irradiation.

Previously, many literatures have been reported on the permanent modifications in electrical properties of both ordinary and conducting polymers by ion beam irradiation [49]. However, we can conclude few reasons for increasing conductivity in brief,

(i) Creation of conjugated double bonds in the back bone chain of the polymer

(ii) Introduction to donor-acceptor complex in the polymer matrix

(iii) Adding conductive fillers such as metallic nanoparticles

(iv) Hopping mechanism

(v) Conversion of the polymeric structure to hydrogen depleted carbon network [50-52].

1.5.2 Structural changes in composite materials:

Ion beams can modify molecular structure in polymers in a controlled way leading to change in behavior. Ionization trail produced by SHI causes bond cleavages and free radicals produced at one site react in a molecular site of a different types from their original site. These are responsible for most of the chemical transformations observed in polymer films: chain scission, crosslinking and double and triple bond formation. Irreversible cleavages of bonds within macromolecule produce volatile species [53-55]. It is known now that ion irradiation of polymers not only leads to the destruction of short range order but also the destruction of long range order. To understand the process of structural modification, in the present study, we have carried out XRD analysis. From the XRD, we can determine changes in crystallite size and percentage (%) crystallinity of the material upon irradiation.

1.5.3 Optical properties of materials upon irradiation:

The promotion of electrons in the σ, π and n orbitals from ground state to the higher energy states which are described by molecular orbitals due to the absorption of light energy by polymeric samples in the UV and visible regions. Many of the optical transitions which occur due to the presence of impurities have energies in the visible region of the spectrum, consequently the defects are referred to as colour centres. The effect of ion beam interaction with polymers produces damage and leads to the generation of new defects and charge states [56, 57]. A shift in the absorption edge towards longer wavelength is also observed upon irradiation. The excitation of π electron requires smaller energy and hence, transition of this type occurs at longer wavelengths. The optical band gap E_g is found from tauc’s equation [58]. From the change in band gap energy upon irradiation makes it clear to understand the change in polymeric materials.

1.5.4 Thermal properties of materials with irradiation:

The important property of the polymer is the glass transition temperature (*T*g), which is defined as the temperature at which the plastic becomes hard and brittle when cooled rapidly after heating. At the glass transition temperature, the weak secondary bonds that stick the polymer chains together are broken, and the macromolecule starts to move. With respect to ion irradiation the change (increase/decrease) in glass transition and melting temperature are observed. So we can confirm the processes of chain scissioning or crosslinking [59].

1.5.5 Changes in Surface morphology:

Ion irradiation of polymers leads in general different mechanisms depending upon ion beam, energy of ion beam, mass and charges. Sometimes it leads to an increase in the surface roughness due to the large sputtering effects [60]. Sometimes it is seen that the surface becomes smoothening upon irradiation because of surface diffusion [61].

1.5.6 Changes in magnetic property:

Zero-Field-Cooled (ZFC)/Field-Cooled (FC) magnetization and magnetic hysteresis measurements were performed using a superconducting quantum interference device (SQUID) magnetometer from 5 K to 300 K to investigate the magnetic properties of the polymer nanocomposites. Magnetization was increased upon irradiation which may be attributed to the creation of free radicals and interaction of particles mediated by the matrix which is also corroborated with the M-H measurements.

1.6 literature survey on selection of filler nanoparticles (Ag, Cu, Ni):

Nobel metal nanoparticles have shown much interest in high-performance catalysts, nanoscale electronic and optoelectronic devices, optical data storage systems, photochemistry, and biological sensors [62]. Nanoparticles particularly of silver reserve important role in the electronic industries.

Over the last decades silver nanoparticles have found applications in catalysis, optics, medical and other areas due to their unique size-dependent optical, electrical and magnetic properties. Currently most of the applications of silver nanoparticles are in biotechnology and bioengineering, textile engineering, water treatment, and silver-based consumer products. There are numerous literatures on the synthesis and characterization on silver polymer nanocomposites [63-66]. X. Huang et al [67] reported that the PVDF/Ag nanocomposites have high dielectric constant and high thermal conductivity and observed no percolation till the loading of 20% of Ag. Igoris Prosyčevas et al [68] observed that nanocomposites (PMMA-PET/ Ag) produced by variation of silver layer thickness shown shifting the plasmon resonance wavelength in the UV-VIS region and looked promising in producing of ultra thin colour filters. Z. H. Mbhele et al [69] investigated an increment in the Young’s modulus and strength of the nanocomposite with an increase in Ag content in the PVA-Ag composites. In-situ formed Ag nanoparticles in the Ag/CB/epoxy composites increased the dielectric constant (K) value due to the pilling of charges at interfaces and decreased the dissipation factor (Df) due to the Coulomb blockade effect as studied by J. Lu et al [70]. P. Gonon [71] et al found that very low percolation threshold obtained (1%) which is believed to be related to a segregated distribution of the fillers (Ag) in the epoxy matrix. Y. Oh [72] observed that the resistivity of the silver/conducting polymer composite was decreased by 83% by the addition of silver-plated single-walled carbon nanotubes. M. K. Abyaneh [73] et al examined that PMMA/Ag composites exhibited a semiconductor-like conductivity at higher temperatures, a rapid metallic conductivity at middle range and nearly temperature independent conductivity at lower temperatures. A. Tang et al [74] fabricated an electrically bistable device using nanocomposite films consisting of silver nanoparticles and a semiconducting polymer by a simple spin-coating method.

Copper nanoparticles are the most abundantly used metal nanoparticles in electronics applications due to its high conductivity and low cost. The development of miniaturized nano devices that integrate electronic, photonic, chemical, and/or biological features is important for electronic and sensing devices [75]. Genaro A. Gelves et al [76] has demonstrated that the electrical percolation of metal nanowires in PS nanocomposites occur at percentage of 0.25–0.75 vol% for Cu nanowires [76]. They also exhibited EMI SE of more than 20 dB for copper nanowire concentrations of only 1.3 vol% and sheet thickness of 0.21 mm [77]. Oleg A. Yeshchenko et al [78] have grown copper nanoparticles on the silica matrix and observed that the efficiency of the luminescence increases appreciably due to decrease of particle size. I.H. Tavman [79] studied the tensile strength, elongation at break and toughness and observed decrease of these properties with increasing copper content which was attributed to the introduction of discontinuities in the structure of PE/Cu composites. G.G. Fedoruk et al [80] investigated conduction mechanism and sensing response of copper phthalocyanine (CuPc)–polymer composites. A.S. Luyt [81] reported the thermal and electrical conductivities of the composites (LDPE/Cu or LLDPE/Cu) were higher than that of the pure polyethylene matrix for both the LDPE and LLDPE and observed percolation concentration at 18.7 vol.% of copper for both polymers. V. Divya et al [82] explained the XRD studies in conjunction with the BJH method and reveals that the composite has crystalline nature with a mesoporous structure with a diameter of 3.5 nm in copper-polyaniline composites. Qing-Bo Wei et al [83] reported the response mechanism of the PAM-g-PVA/Cu films to solvent vapors on the basis of swelling theory, interaction between solvent vapor molecules and nanocomposites as well as the type and strength of interaction that each solvent vapor exhibits on the material. The effect of copper weight percent and surfactants on the conductivity and stability of the composite (PVP/Cu) has been investigated by Long Quoc Pham et al [84].

As an important transition metal, Ni nanoparticles have wide range applications in the fields of permanent magnets, magnetic fluids, magnetic recording media, solar energy absorption, fuel cell electrodes, catalysts etc. So the Ni nanoparticles have fascinated considerable attention [85]. Plenty of reports have been published on the synthesis of nickel nanoparticles by different experimental techniques [86-88]. Carbon–nickel nanocomposite thin films were prepared by ion beam cosputtering a graphite target having a nickel chip attached to its surface and magnetization measurement revealed superparamagnetic nature of composites by F. C. Fonseca et al [89]. The elastic properties showed an improvement with increase in filler (Ni) content but breaking stress and breaking strain were found to decrease in the rubber-nickel nanocomposites as observed by E. Muhammad Abdul Jamal et al [90]. Min Zhi Rong et al studied the interaction between the nanoparticles (Fe, Ni, co) and the grafted polymer (PMMA, PS) by thermal analysis and X-ray photoelectron spectrometry. It was found that there is a strong interfacial interaction in the form of electrostatic bonding in the polymer-grafted nanoparticles [91]. When the inspection frequency of the conductive composite film prepared by carbon fiber/Ni nanoparticles is 1000 MHz, its shielding effectiveness can reach to 28 dB as reported by Ho Chang et al [92]. The size and distribution of the Ni nanoparticles were strongly depend on the heat treatment temperature, indicating that this method allows microstructural tuning of polyimide/Ni nanocomposites as examined by K. Akamatsu et al [93]. D. E. El-

Nashar et al [94] determined the mechanical, electrical, and magnetic properties of natural rubber (NR) composites containing iron or nickel nanoparticles at different percentage varying from 0 to 120 phr (part of magnetic particle per hundred rubber) at room temperature. Jai Prakash et al [95] investigated the synthesis of magnetic nanocomposites by ion beam mixing technique using swift heavy ion irradiation of Ni-Teflon bilayer system and showed that the coercivity of the nanocomposite is found to be 112 Oe at room temperature which is two orders of magnitude larger than that of the bulk Ni (0.87 Oe).

1.7 Reviews on selected polymers (PMMA/PS):

Polymethyl methacrylate (PMMA) belongs to a family of synthetic polymers. It is better known as acrylic. PMMA is a tough, highly transparent material with excellent resistance to ultraviolet radiation and weathering. It can be coloured, moulded, cut, drilled, and formed. These properties make it ideal for many applications including airplane windshields, skylights, automobile taillights, and outdoor signs. PMMA can be further modified by incorporating different additives. These modifications are typically performed to improve specific properties of the polymer. Examples of properties that can be adjusted in this way are impact resistance, chemical resistance, flame retardancy, light diffusion, UV light filtering, or optical effects. S. Agrawal et al [96] studied the UV-Vis measurement and showed red shift in optical absorption and bandgap changed from 4.38–3.60 eV as the irradiation (100 MeV,Si^{+7} ions beam) fluence increased with respect to pristine CdCuS/PMMA nanocomposite polymer film. The study showed that, after the plasma (exposure time 0 to 60 s) treatment, the surface of PMMA film was etched, and oxygen-containing polar groups were introduced into the surface. These two processes can induce a remarkable decrease in water contact and a significant increase in surface energy and the surface properties of PMMA films were improved accordingly as examined by Z. Fang [97]. R. Kumar et al [98] examined the slight shift of peak position and significant changes in peak intensity in the XRD analyses. XRD results showed a decrease of 4.12% in crystallite size of 145 MeV Ne^{6+} ions irradiated sample at the higher fluence of 10^{12} ions/cm^2. Sumit Kumar et al [99] had prepared the multi-walled carbon nanotube (MWCNT) dispersed PMMA composite membranes for hydrogen gas permeation application. Photo-responsive properties of Ag/PMMA nanocomposite films indicate that the conduction paths could be destroyed by illumination and rebuilt in dark condition as observed by C. Chen [100]. It was found that the luminosity of ZnO/PMMA nanocomposite enhanced after irradiation with Ni^{+8} (100 MeV) ions as reported by S. Sharma et al [101]. The mechanical characterization revealed that radiation (50MeV Li^{+3}) significantly modifies the mechanical properties of the PMMA/PC blends [102]. P. Meneghetti et al [103] synthesized a novel polymer gel electrolyte with improved ionic conductivity and stable lithium interfacial resistance, which could be used for battery applications using PMMA/clay nanocomposites. The electrical resistivity and oscillatory shear rheological properties of the composites as a function of MWCNT geometry, functionality, and concentration were measured by C. McClory in PMMA/ MWCNT nanocomposites [104]. Large amounts of material with good antistatic and conductive properties prepared in an inexpensive way using chemically oxidative modification of poly(methyl methacrylate) particles by pyrrole method as investigated by M. Omastova et al [105]. Notwithstanding the remarkable importance of poly(methy1 methacrylate) as a prototype polymer for positive resist (scission rate higher than cross linking rate) the literature studies on the chemical effects induced by energetic beam irradiation on this polymer are relatively scarce [106-110]. The interest for

PMMA is considerable also because it has been reported in literature that beyond a threshold fluence (that in turn depends on the ion) the resist turns negative: i.e. the cross linking rate becomes higher than the scission rate [111]. D. Singh etal [112] studied the temperature dependent dielectric properties and observed that it enhanced with increasing temperature in PMMA/Al composites. Also Singh etal [113] investigated the effect of 120 MeV Ni ions on PMMA/Ni and result showed that surface roughness increased upon irradiation.

Polystyrene is one of the most important polymers of nowadays. Its popularity stems from the fact that it possesses many good properties, such as good processability, rigidity, transparency, low water absorbability, and that it can be produced at low costs. However, polystyrene has some disadvantages, such as sensitivity to chemicals and food materials with high oil content, poor UV-resistance and brittleness, which limit its applications. Polystyrene is mainly used in the packaging industry [114]. Hong et al. [115] carried out surface modification of ZnO nanoparticles by grafting polystyrene to improve their dispersibility, to reduce photocatalytic properties, and to obtain good UV shielding capability to promote their use in cosmetics. V. Komolprasert et al suggested that irradiation did not generate any new chemicals in the PS polymer containing either yellow or blue colorant at a concentration of up to 1% (w/w) from analytical results [116]. M. Pattabi et al reported the effect of 8 MeV electron beam irradiation of polystyrene substrates on the morphology of silver particulate films deposited at 455 K in a vacuum of 8 x 10^{-6} Torr [117]. L.C. Costa et al studied the dc conductivity and the true dielectric response, at low frequencies, of the composites made by dispersing the high conductivity PPy particles in the insulating matrix of PS [118]. S.A. Saqan et al [119] studied the mechanical, thermal, optical and electrical properties of polystyrene/alum composites as a function of alum content and applied field frequency. D. Olmos et al observed neither the cryomilling process nor the presence of BaTiO3 particles (up to 40% wt) seem to alter the structure of the PS polymer [120]. J. Kuljanin-Jakovljevic et al investigated that the higher concentration of CdS (20%) in the (PS/CdS) composite induced acceleration of the thermal degradation, approaching the rate of degradation of the pure polystyrene matrix [121]. Different types of photochromophores and initiators were applied to prepare PS nanocapsules and their effects on the morphology of the capsules were investigated by M. Han [122]. The selectivity permeation results revealed that the MWCNT/PS composite membranes can be used as nanofilter for selective permeation of H_2 gas as observed by S. Kumar [123]. Improvement of the thermal stability of the PS matrix with the usage of the CdS-filler particles in the micrometer size range was demonstrated by J. Kuljanin et al [124]. The dependence of Maxwell–Wagner–Sillars or interfacial polarization of polystyrene–AlN composites on AlN volume fraction has also been studied by S. Yu [125]. E. Balanzat et al [126] proposed that the breaking of the phenyl group, due to multi-ionisation of the ring, could play a major role in the damage process at high electronic stopping power. The relaxation time and the activation energy determined for different composites decrease with increasing temperature as studied by S A Sbeih et al [127].

1.8 Objective of work:

The central intention of the present work is to synthesize the nanocomposites which can defeat some of the tribulations which are not overcome by pure polymer up to now. The injection of material into a target specimen in the form of an accelerated ion beam offers a most valuable tool for altering its physical, chemical, structural, surface and interface properties in a controlled manner and tailoring new materials for basic and applied research for science and technology. On the basis of review carried out on the similar work till this date, ion beam irradiation has proved unique technology for polymer modification. So the physico-chemical properties after ion beam are explained in details. As stated in the previous sections, after taking low and high dielectric material applications in consideration, the fillers are appropriately selected. Synthesis, characterization and processing of low dielectric constant polymer materials are a leading premise for microelectronics, satellite, telecommunication, packaging, biomaterials etc. Rather material with high dielectric constant can be used for EMI shielding application. Therefore taking in mind the drawbacks of pure polymers and metal nanoparticles, nanocomposites have been synthesized to fulfil the requirements. As mentioned above, the dielectric and other physical properties enhanced after doping of the metal nanoparticles. So the different types of conductive nanoparticles were used as filler viz. silver (Ag), nickel (Ni), copper (Cu) are dispersed in poly methyl methacrylate (PMMA) and polystyrene (PS) for making polymer nanocomposites. The irradiation effect on these nanocomposite films was studied with respect to ion specie, energy and fluence. For this purpose 120 MeV Si^{10+}, 85 MeV C^{6+}beams were used. AC electrical, structural, chemical, thermal, magnetic properties and surface morphology of pristine and irradiated nanocomposites are investigated by means of various techniques in the present work.

References:

[1] R. L. Orefice, J. A. C. Discacciati, A. D. Neves, H. S. Mansur, W. C. Jansen, Polymer Testing 22 (2003) 77-81.

[2] R. S. Sethi, M. T. Goosey, Special Polymers for Electronics & Optoelectronics; J. A. Chilton, M. T. Goosey, Eds.; Chapman & Hall: London, (1995) pp 14-46.

[3] T. Richardson**,** “Composites A Design Guide”, Industrial Press Inc, New York (1987).

[4] J. C. Anderson, K. D. Leaver, R. D. Rawlings, J. M. Alexander, Material Science and Engineering, Chapman and Hall India, Madras, India (1990).

[5] D. L. C. Deborah, Composite Materials: Science and Applications Functional Materials for Modern Technologies, Springer, London (2002).

[6] S. Ramakrishna, J. Mayer, E. Wintermantel, K. W. Leing, Biomedical applications of polymer composite materials: a review. Composites Sci. and Tech 61 (2001) 1189.

[7] K. S. Suslick, Sonochemistry Science 247 (4949) (1990) 1439-1445.

[8] B. Lin, G. A. Gelves, J. A. Haber, U. Sundararaj, Ind. Eng. Chem. Res. 46 (2007) 2481–2487.

[9] G. A. Gelves, U. Sundararaj, J. A. Haber, Macromol. Rapid Commun.**,** 26 (2005) 1677–1681.

[10] G. Schmidt, M. M. Malwitz, Curr. Opin. Coll. Interface Sci. 8 (2003) 103–108.

[11] M. B. Muradov, A. Sh. Abdinov, R. H. Hajimamedov, G. M. Eyivazova, Surf. Eng. Appl. Electrochem.**,** 45 (2) (2009)167–170.

[12] S. Stankovich, D. A. Dikin, G. H. B.Dommett, K. M. Kohlhaas, E. J. Zimney, E. A. Stach, R. D. Piner, S. T. Nguyen, R. S. Ruoff, Nature**,** 442 (2006) 282–286.

[13] O. Breuer, U.Sundararaj, Polym. Compos.**,** 25 (2004) 630–645.

[14] S. Wood, R. Jones, A. Geldart, The Social and Economic Challenges of Nanotechnology (No. 0-86226-294-1). Swindon, UK: The Economic and Social Research Council (2003).

[15] J. R. Li, J. R. Xu, M. Q. Zhung, M. Z. Rong, Carbon 41 (2003) 2353-2360.

[16] H. Supriyatno, K. Nakagawa, Y. Sadaoka, Sensors and Actuators B76 (2001) 36-41.

[17] R. Morrison, Solving Interference Problems in Electronics. John Wiley & Sons, Inc.: New York (1995).

[18] D. White, A Handbook on Electromagnetic Shielding Materials and Performance. Don White Consultants, Inc.: Germantown, MD (1975).

[19] F. Rodrigues, C. Cohen, C. K. Ober, L. A. Archer, “ Principles of Polymer Systems” Eds. D. T. Schanck, D. P. Teston, Taylor and Francis, New York, London (2003).

[20] D. D. L. Chung, Carbon, 139 (2001) 279-285.

[21] D. K. Awasthi, Current Science, 78 (11) (2000) 1297-1306.

[22] D. Kanjilal, Current Science, 80 (12) (2001) 1560-1566.

[23] W. Bolse, Mater. Sci. Eng. R 12 (1994) 53.

[24] W. E. Burcham. Elements of nuclear physics. Longman, London and New York, (1979).

[25] Kamlendra Awasthi, Vaibhav Kulshreshtha, B Tripathi, N K Acharya, M Singh and Y K Vijay, Bull. Mater. Sci., 29(3) (2006) 261–264.

[26] Barbari T, Kores W and Paul D *J.* Polym. Phys. 26 **(**1988) 709.

[27] Srivastava, A.; Singh, T.V.; Mule, S.; Rajan, C.R.; Ponrathnam, S., Nucl. Instr. Meth. B,192 (2002) 402.

[28] Hioki, T.; Noda, S.; Sugiura, M.; Kakaeno, M.; Yamada, K.; Kawamoto, J. ,Appl. Phys. Lett., 43 (1983) 30.

[29] Sevil, U.A.; Güven, O.; Kovács, A.; Slezsák, I., Radiation Physics and Chemistry, 67 (2003) 575.

[30] Sonar, P.; Sharma, A.L.; Chandra, A.; Muellen, K.; Srivastava, A. ,Current Applied Physics, 3 (2003) 247.

[31] Alok Srivastava, Virendra Singh, Chetna Dhand, Manindar Kaur , Tejvir Singh, Karin Witte and Ulrich W. Scherer, Sensors, 6 (2006) 262-269.

[32] A. Qureshi, N. L. Singh, Sejal. Shah, P. Kulriya, F. Singh, and D. K. Avasthi, Nucl. Instrum. Methods Phys. Res. B 266 (2009) 1775.

[33] R. Singhal, A. Kumar, Y. K. Mishra, S. Mahopatra, J. C. Pivin, and D. K. Avasthi, Nucl. Instrum. Methods Phys. Res. B 266 (2008) 3257.

[34] D. Fink, M. Mueller, and L. T. Chadderton, Nucl. Instrum. Methods Phys. Res. B 32 (1988) 125.

[35] S. Balanzat, S. Bouffard, A. Le Moe¨l, and N. Betz, Nucl. Instrum. Methods Phys. Res. B 91 (1994) 14.

[36] J. P. Biersack, A. Schmoldt, and D. Fink, Radiat. Eff. Defects Solids 140 (1996) 63.

[37] A. M. P. Hussain and A. Kumar, Eur. Phys. J. Appl. Phys. 36 (2006) 105.

[38] K. R. Nagabhushana, B. N. Lakshminarasappa, G. T. Chandrappa, D. Haranath, and F. Singh, Radiat. Eff. Defects Solids 162 (2007) 325.

[39] S. Sarmah and A. Kumar, Phys. Status Solidi A 207(10) (2010) 2279–2287.

[40] Chaitali Gavade, N. L. Singh, Dolly Singh, Sejal Shah, A. Tripathi, D. K. Avasthi, Integrated Ferroelectrics, 117 (2010) 76–84.

[41] J. Delmonte: Metal/Polymer composites, Van Nostrand Reinhold New York (1990).

[42] A. Heilmann " Polymer films with embedded metal nanoparticles" Eds R. Hull, R. M. Osgood, J. Parisi , Springer, Berlin, Heidelberg, New York, (2003).

[43] F. Kremer, A. Schönhals, Broadband dielectric spectroscopy, Springer, (2003).

[44] A.J. Jonscher, "Dielectric relaxation in solids", Journal of Physics D: Applied Physics, 32(14) (1999) 57-70.

[45] "Dielectrics (physics)". Britannica. (2009) pp. 1(Online).

[46] L. H. Sperling, Introduction To Physical Poly. Sci., John wiley & sons, New York, (1992).

[47] Prerna Aggarwal, Virendra Singh, Arjun Singh, U. W. Scherer, Tejvir Singh, Madan L. Singla, Alok Srivastava, Radiation Physics and Chemistry 81 (2012) 284–289.

[48] S. Sarmah and A. Kumar, Phys. Status Solidi A 207(10) (2010) 2279–2287.

[49] D. Fink (Ed.), Transport Processes in Ion Irradiated Polymers and Applications, Springer Series in Materials Science, Vol. 65, Springer-Verlag, (2004).

[50] A. Harper Charles, Modern Plastics Handbook, McGraw Hill, New York, (1999).

[51] R. O. Ebewele, " Polymer Science and Technology", CRC Press, London, (2000).

[52] Anjum Qureshi, N. L. Singh, Sejal Shah, F. Singh, And D. K. Avasthi, Journal of Macromolecular Science, Part A: Pure and Applied Chemistry 45 (2008) 265–270.

[53] H.W. Choi, H. J. Woo, W. Hong, J.K. Kim, S. K. Lee, C.H. Eum, Applied Surface Science 169-170 (2001) 433-437.

[54] Lakhwant Singh, Ravinder Singh, Nuclear Instruments and Methods in Physics Research B 225 (2004) 478–482.

[55] R. Kumaravel, K.Ramamurthi, Indra Sulania, K. Asokan, D. Kanjilal, D. K. Avasti, P. K. Kulria, Radiation Physics and Chemistry 80 (2011) 435–439.

[56] A. Semwal, A. Negi, R. G. Sonkawade, J. M. S. Rana, R. C. Ramola, Indian J of pure and App Phy 48 (2010) 496-499.

[57] H S Virk, P S Chandi And A K Srivastava, Bull. Mater. Sci. 24(5) (2001) 529–534.

[58] A. Das, S. Dhara and A. Patnaik, Physical Rev B 59 (1999) 11069.

[59] Virendra Singh, Tejvir Singh, Amita Chandra, S.K. Bandyopadhyay, Pintu Sen, K. Witte, U.W. Scherer, Alok Srivastava, Nuclear Instruments and Methods in Physics Research B 244 (2006) 243–247.

[60] N L Singh, Sejal Shah, Anjum Qureshi, A Tripathi, F Singh, D.K.Avasthi, P M Raole, Bull. Mater. Sci., 34(1) (2011) 81–88.

[61] Sejal Shah, Dolly Singh, Anjum Qureshi, N L Singh, K. P. Singh, V. Shrinet, Indian journal of pure and applied physics, 46 (2008) 439-442.

[62] D. Zhang, L. Qi, J. Yang, J. Ma, H. Cheng, and L. Huang, Chem. Mater., 16 (2004) 872.

[63] Jian Xu, Xia Han, Honglai Liu, Ying Hu, Colloids and Surfaces A: Physicochem. Eng. Aspects 273 (2006) 179–183.

[64] B. Raneesh, A. Pragatheeswaran, P. Dhanasekaran, P. Chandrasekaran, Nandakumar Kalarikkal, Journal of Ovonic Research, 6(4) (2010) 187 -191.

[65] A. Sreekumaran Nair, Nadappuram P. Binoy, Seeram Ramakrishna, T. R. R. Kurup, Lai Wah Chan, Cheong Hian Goh, Md. Rafiqul Islam, Thomas Utschig, T. Pradeep, Applied materials and interfaces, 1(11) (2009) 2413–2419.

[66] Osman Eksik, A. Tuncer Erciyes, Yusuf Yagci, Journal of Macromolecular Science, Part A: Pure and Applied Chemistry 45 (2008) 698–704.

[67] Xingyi Huang, Pingkai Jiang, Liyuan Xie, Applied Physics Letters 95 (2009) 242901.

[68] Igoris Prosyčevas, Judita Puišo, Asta Guobienė, Sigitas Tamulevičius, Ramūnas Naujokaitis, Materials Science 13 (2007) 188-192.

[69] Z. H. Mbhele, M. G. Salemane, C. G. C. E. van Sittert, J. M. Nedeljkovic, V. Djokovic, A. S. Luyt, Chem. Mater. 15 (2003) 5019-5024.

[70] Jiongxin Lu, Kyoung-Sik Moon, Jianwen Xu and C. P. Wong, J. Mater. Chem., 16 (2006) 1543–1548.

[71] P. Gonon, A. Boudefel, Journal of Applied Physics 99 (2006) 024308.

[72] Youngseok Oh, Daewoo Suh, Youngjin Kim, Eungsuek Lee, Jee Soo Mok, Jaeboong Choi and Seunghyun Baik, Nanotechnology 19 (2008) 495602 (7pp).

[73] M. Kazemian Abyanehabd, S. Jafarkhani and S.K. Kulkarni, Journal of Experimental Nanoscience 6(2) (2011) 159–173.

[74] Aiwei Tang, Shengchun Qu, Yanbing Hou, Feng Teng, Hairen Tan, Jie Liu, Xingwang Zhang, Yongsheng Wang, and Zhanguo Wang, Journal of Applied Physics 108 (2010) 094320.

[75] George H. Chan, Jing Zhao, Erin M. Hicks, George C. Schatz, and Richard P. Van Duyne, Nano letters, 7(7) (2007) 1947-1952.

[76] Genaro A. Gelves, Bin Lin, Uttandaraman Sundararaj, Joel A. Haber, Adv. Funct. Mater. 16 (2006) 2423–2430.

[77] Genaro A. Gelves, Mohammed H. Al-Saleh and Uttandaraman Sundararaj, J. Mater. Chem. 21 (2011) 829–836.

[78] Oleg A. Yeshchenko, Igor M. Dmitruk, Andriy M. Dmytruk, Alexandr A. Alexeenko, Materials Science and Engineering B 137 (2007) 247–254.

[79] I.H. Tavman, Powder Technology 91 (1997) 63-67.

[80] G.G. Fedoruk, D.I. Sagaidak, A.V. Misevich, A.E. Pochtenny, Sensors and Actuators B 48 (1998) 351–355.

[81] A.S. Luyt, J.A. Molefi, H. Krump, Polymer Degradation and Stability 91 (2006) 1629-1636.

[82] V. Divya, M.V. Sangaranarayanan, European Polymer Journal 48 (2012) 560–568.

[83] Qing-BoWei, Yan-Ling Luo, Chang-Hu Zhang, Li-Hua Fan, Ya-Shao Chen, Sensors and Actuators B 134 (2008) 49–56.

[84] Long Quoc Pham, Jong Hwa Sohn, Chang Woo Kim, Ji Hyun Park, Hyun Suk Kang, Byung Cheol Lee,Young Soo Kang, Journal of Colloid and Interface Science 365 (2012) 103–109.

[85] Huazhi Wang, Xinli Kou, Jie Zhang, Jiangong Li, Bull. Mater. Sci., 31(1) (2008) 97–100.

[86] R S Ningthoujam, N S Gajbhiye, Sachil Sharma, Pramana- J. Phys.72(3) (2009) 577-586.

[87] Xiao-Min Ni, Xiao-Bo Su, Zhi-Ping Yang, Hua-Gui Zheng, Journal of Crystal Growth 252 (2003) 612–617.

[88] Huazhi Wang, Xinli Kou, Jie Zhang, Jiangong Li, Bull. Mater. Sci. 31(1) (2008) 97–100.

[89] F. C. Fonseca, A. S. Ferlauto, F. Alvarez, G. F. Goya and R. F. Jardim, Journal Of Applied Physics 97 (2005) 044313.

[90] E. Muhammad Abdul Jamal, P.A. Joy, Philip Kurian, M.R. Anantharamana, Materials Science and Engineering B 156 (2009) 24–31.

[91] Min Zhi Rong, Ming Qiu Zhang, Hong Bing Wanga, Han Min Zeng, Applied Surface Science 200 (2002) 76–93.

[92] Ho Chang, Yun-Min Yeh, Kouhsiu-David Huang, Materials Transactions, 51(6) (2010) 1145- 1149.

[93] K. Akamatsu, K. Nakahashi, S. Ikeda, H. Nawafune, Eur. Phys. J. D 24(2003) 377–380.

[94] D. E. El-Nashar, S. H. Mansour, E. Girgis, J Mater Sci 41 (2006) 5359–5364.

[95] Jai Prakash, A. Tripathi, J.C. Pivin, Jalaj Tripathi, A.K. Chawla, Ramesh Chandra, S.S. Kim, K. Asokan, D.K. Avasthi, Adv. Mat. Lett. 2(1) (2011) 71-75.

[96] Shweta Agrawal, Subodh Srivastava, Sumit Kumar, S S Sharma, B Tripathi, M Singh, Y K Vijay, Bull. Mater. Sci. 32(6) (2009) 569–573.

[97] Zhi Fang, Yuan Liu, Kun Liu, Tao Shao, Cheng Zhang, Vacuum 86 (2012) 1305-1312.

[98] Rajesh Kumar, S.A. Ali, Paramjit Singh, U. De, H.S. Virk, Rajendra Prasad, Nuclear Instruments and Methods in Physics Research B 269 (2011) 1755–1759.

[99] Sumit Kumara, Anshu Sharma, Balram Tripathi, Subodh Srivastava, Shweta Agrawal, M. Singh, Kamlendra Awasthi, Y.K. Vijay, Micron 41 (2010) 909–914.

[100] Cheng Chen, Junguo Li, Guoqiang Luo, Yuanlu Xiong, Qiang Shen Lianmeng Zhang, Applied Surface Science 258 (2012) 10180– 10184.

[101] Sarla Sharma, Rishi Vyas, Subodh Shrivastava, Y.K. Vijay, Physica B 406 (2011) 3230–3233.

[102] Manasvi Dixit, Deepika, Mahesh Baboo, Kananbala Sharma, N. S. Saxena, D. K. Avasthi, Pawan K. Kulriya, International Journal of Polymeric Materials 59 (2010) 873–890.

[103] Paulo Meneghetti, Syed Qutubuddin, Thermochimica Acta 442 (2006) 74–77.

[104] Caroline McClory, Tony McNally, Mark Baxendale, Petra Pötschke, Werner Blau, Manuel Ruether, European Polymer Journal 46 (2010) 854–868.

[105] Maria Omastova, Juraj Pavlinec, Jurgen Pionteck, Frank Simon, Stanislav Kosina, Polymer 39(25) (1998) 6559–6566.

[106] D. Fink, L.T. Chadderton, F. Hosoi. H. Omichi, T. Sagusa, A. Schmoldt, L. Wang, R. Klett and J. Hillenbrand, Nucl. Instr. and Meth. B 91 (1994) 146.

[107] J. Davenas, P. Thevenard, G. Boiteux, M. Fallavier and X.L. Lu, Nucl. Instr. and Meth. B 46 (1990) 317.

[108] R. Kallweit, U. Roll, P. Eichinger, H. Strack and A. Piker, Mater. Res. Symp. Proc. 268 (1992) 363.

[109] J.C. Corelli, A.J. Steckl, D. Pulver and J.N. Randall, Nucl. Instr. and Meth. B 19/20 (1987) 1009.

[110] I. Adesida, C. Anderson and E.D. Wolf, J. Vat. Sci. Technol. B 1 (1983) 1182.

[111] T. M. Hall, A. Wagner, L P. Thompson, J. Appl. Phys. 53(1982) 3997.

[112] Dolly Singh, N.L. Singh, P. Kulriya, A. Tripathi and D.M. Phase, Journal of Composite Materials, 44 (2010) 3165.

[113] N L Singh, Sejal Shah, Anjum Qureshi, A Tripathi, F Singh, D.k.Avasthi, P M Raole, Bull. Mater. Sci., 34 (2011) 81–88.

[114] Ku P.L., Advances in Polymer Technology, 8(3) (1988) 201-223.

[115] Hong RY, Li JH, Chen LL, Liu DQ, Li HZ, Zheng Y, Powder Technology 189 (2009) 426–432.

[116] V. Komolprasert, Todd Diel, G. Sadler, Radiation Physics and Chemistry 75 (2006) 149–160.

[117] Manjunatha Pattabi, S.C. Gurumurthy, Ganesh Sanjeev, A.B. Gaikwad, Nuclear Instruments and Methods in Physics Research B 269 (2011) 1534–1539.

[118] L.C. Costa, F. Henry, M.A. Valente, S.K. Mendiratta, A.S. Sombra, European Polymer Journal 38 (2002) 1495–1499.

[119] S.A. Saqan, A.S. Ayesh, A.M. Zihlif, E. Martuscelli, G. Ragosta, Polymer Testing 23 (2004) 739–745.

[120] D. Olmos, J.M. Martínez-Tarifa, G. González-Gaitano, J. González-Benito, Polymer Testing 31 (2012) 1121–1130.

[121] J. Kuljanin-Jakovljevic, M. Marinovic Cincovic, Z. Stojanovic, A. Krkljes, N.D. Abazovic, M.I. Comor, Polymer Degradation and Stability 94 (2009) 891–897.

[122] Mijeong Han, Eunha Lee, Eunkyoung Kim, Optical Materials 21 (2002) 579-583.

[123] Sumit Kumar, Subodh Srivastava, Y.K. Vijay, International journal of hydrogen energy 37 (2012) 3914-3921.

[124] J. Kuljanin, M. Vuckovic, M. I. CComor, N. Bibic, V. Djokovic, J.M. Nedeljkovic, European Polymer Journal 38 (2002) 1659–1662.

[125] Suzhu Yu, Peter Hing, Xiao Hu, J. Appl. Phys. 88(1) (2000) 398-404.

[126] E. Balanzat, S. Bouffard, A. Bouquerel, J. Devy, Chr. Gate, Nuclear Instruments and Methods in Physics Research B I 16 (1996) 159- 163.

[127] S A Sbeih and A M Zihlif, J. Phys. D: Appl. Phys. 42 (2009) 145405 (7pp).

Chapter – II

Materials and Experimental Techniques

Abstract

A brief review of the concept of polymer composites and general descriptions of the experimental methods and tools are given in this chapter. The working principles and operation of Pelletron accelerators has been conversed. Different characterization techniques have been used to do off-line analysis of the pristine and irradiated samples in this work. These techniques with their proper specifications and operating principle have been described.

2.0 Introduction

This chapter deals with the detailed description of the material (polymers and fillers) used for the present study, the working principle of Pelletron and different techniques used for the offline measurement of pristine and irradiated samples. Detail explanation of following is considered in this chapter.

- Materials: Properties and preparation methods of Polymer/fillers
- Working principle and details of Pelletron
- Sample preparation and thickness measurement
- Calculation of ion range and its energy loss by SRIM code
- X-ray diffraction
- UV-visible analysis
- Differential Scanning Calorimetry (DSC)
- Scanning electron microscopy (SEM)
- Superconducting Quantum Interference Device (SQUID)
- AC electric response

2.1 Materials

2.1.1 Selected polymers:

(a) Polymethyl methacrylate (PMMA)

PMMA (polymethyl methacrylate) is a versatile polymeric material that is well suited for many imaging and non-imaging microelectronic applications. PMMA is most commonly used as a high resolution positive resist for direct write e-beam as well as x-ray and deep UV micro lithographic processes. PMMA is also used as a protective coating for wafer thinning, as a bonding adhesive and as a sacrificial layer [1, 2].

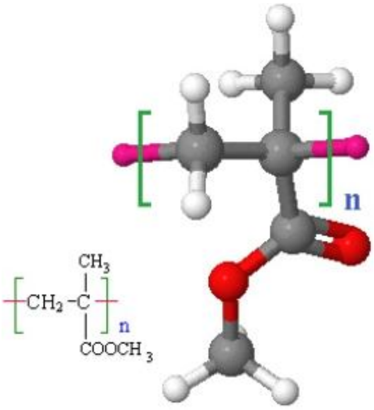

IUPAC name: Poly (methyl 2-methylpropenoate)

Molecular formula: $(C_5O_2H_8)_n$

PMMA is an amorphous, linear polymer valued for its hardness, rigidity, transparency and weathering resistance. But modified PMMA was even more outstanding performance edge. They are widely used in optical instruments, construction areas, can be used as medical devices, such as additional limbs, dentures, medical optical basic raw material. It is still used as a glass substitute for aerospace equipment, light cover, surface cover plates, car and motorcycle windshields [3,4].

(b) Polystyrene (PS)

Polystyrene is a "polymer of styrene." Polymers are large molecules consisting of adjoined identical molecules, and styrene is a colorless, oily liquid. When polystyrene is made, its structure is that of a rigid transparent thermoplastic. It is one of the most common types of plastic, and it can be found in the home, in the office, at industrial sites, and just about any other place you would find plastics. Businesses rely on polystyrene for a number of uses, including manufacturing, packaging, and construction.

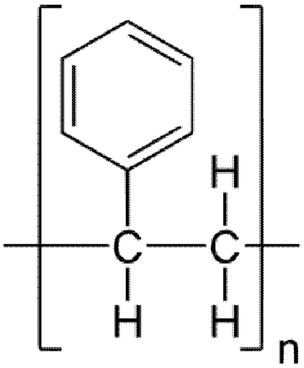

IUPAC name: Poly(1-phenylethane-1,2-diyl)

Molecular formula: $(C_8H_8)_n$

Polystyrene is a hard, crystal clear, amorphous solid at room temperature that exhibits high stiffness, good dimensional stability, moderately high heat deflection temperature and excellent electrical insulating properties. It retains its stiffness to about 20-25°C below glass transition temperature (Tg). However, polystyrene will become softer as it getting closer to its Tg. Above Tg, polystyrene behaves under stress as a viscous fluid. When the temperature is further raised, it will become rubbery and highly extensible. Polystyrene is a very important one due to its easy processibility, low density, low price, good optical transparency, and acceptable thermal insulation and damping properties. However, it is brittle under impact and the resistance towards surfactants and solvent is very poor [5, 6].

2.1.2 Fillers:

(a) Silver nanoparticles (Ag)

Appearance: Grey

Silver nanoparticles have unique optical, electrical, and thermal properties and are being incorporated into products that range from photovoltaics to biological and chemical sensors. Examples include conductive inks, pastes and fillers which utilize silver nanoparticles for their high electrical conductivity, stability, and low sintering temperatures [7]. Additional applications include molecular diagnostics and photonic devices, which take advantage of the novel optical properties of these nanomaterials. An increasingly common application is the use of silver nanoparticles for antimicrobial coatings, and many textiles, keyboards, wound dressings, and biomedical devices [8].

(b) Nickel nanoparticles (Ni)

Appearance: Black

As an important transition metal, Ni nanoparticles have wide ranging applications in the fields of permanent magnets, magnetic fluids, magnetic recording media, solar energy absorption, fuel cell electrodes, catalysts etc. So the synthesis of Ni nanoparticles has attracted considerable attention. The magnetic fluid made of nickel nanoparticles provides excellent properties. It is widely used for sealants, shock absorption materials, medical equipment, and optical displays. Due to its large surface and high activity, nickel nanoparticles are efficient catalysts for chemical reactions such as hydrogenation and treatment of exhaust to reduce harmful chemicals. Conductive paste is commonly used for wiring and packaging. In the microelectronics industry, it plays an important role in the miniturization of electronic devices and circuits. They can be made into electrodes with a large surface area to considerably improve energy density [9-12].

(c) Copper nanoparticles (Cu)

Appearance: Dark red (brown)

Copper is an essential trace element in animals and plants, but in excess copper is toxic. Due to its high electrical conductivity, large amounts of copper are used by the electrical industry for wire. Recent research reveals that diluted magnetic semiconductors can be produced using Copper. Copper is also resistant to corrosion caused by moisture, making it a widely used material in pipes, coins, and jewellery. The key applications of copper nanoparticles are listed here: Acts as an anti-biotic, anti-microbial, and anti-fungal agent when added to plastics, coatings, and textiles, Copper diet supplements with efficient delivery characteristics, High strength metals and alloys, EMI shielding, Heat sinks and highly thermal conductive materials, Efficient catalyst for chemical reactions and for the synthesis of methanol and glycol, electronics, displays, and transmissive conductive thin film applications. Copper nanoparticles application research is ongoing to discover their potential dielectric, magnetic, electrical, optical, imaging, catalytic, biomedical and bioscience properties [13, 14].

2.1.3 Polymer nanocomposites:

Polymer composites were prepared by doping different concentrations i.e. 5, 10, 15 wt. % of silver, nickel, copper nanoparticles in PMMA and PS with THF (Tetra hydro furan) and toluene as a solvent. The mixture of filler and polymers was stirred for 2-3 hours and sonicate for few minutes to get dispersion in matrix and then pour into petri dishes. Thus the composite films were prepared by casting method.

2.1.4. Thickness measurement of the composite films:

The thickness of as synthesized composites was measured by a sensitive digital instrument. Sensitivity of the instrument was 0.001mm. The thickness of polymers was measured at 8-10 places randomly chosen and average of it was taken. The calculated thickness was listed in Table 2.1.

Table 2.1 Thickness of the polymers

Sample	Thickness
Pure PMMA films	**110 µm**
PMMA + Ag	**110 µm**
PMMA + Ni	**120 µm**
PMMA + Cu	**120 µm**
Pure PS films	**110 µm**
PS + Ag	**120 µm**
PS + Ni	**120 µm**
PS + Cu	**110 µm**

2.2 Ion beam irradiation

Energetic ions for polymer irradiation can be produced in several ways. Nowadays the common approach is the use of ion implanters and ion accelerators. The basic difference between both is, the available energy range and the ion beam currents delivered from both the machines. Ion implanters usually work in the range of 10 to several 100 keV energy interval delivering high currents that can go from tens of µA to few tens of mA. Ion accelerators work in the MeV energy region but with lower currents. The present work delivers the high energetic particle accelerator.

2.2.1 The Pelletron accelerator:

A high energy Pelletron accelerator, tandem Van de Graaff type accelerator, for basic and applied research in nuclear physics, atomic physics, materials science, biosciences and other allied fields is running at IUAC. This Linear accelerator is planned as a booster accelerator. A 15UD Pelletron accelerator is capable of delivering any ion from proton to uranium up to energy of a few hundred MeV depending upon the nature of ion. It has been installed at IUAC, New Delhi by the Electrostatic International Inc., USA. This is a tandem Van de Graaff accelerator, in which the charge carrier belt is replaced by a chain of pellets. The digit 15 stands for 15 MV terminal voltage and UD stands for Unit Double. The whole machine is mounted vertically; a schematic of the machine is shown in Fig 2.1.

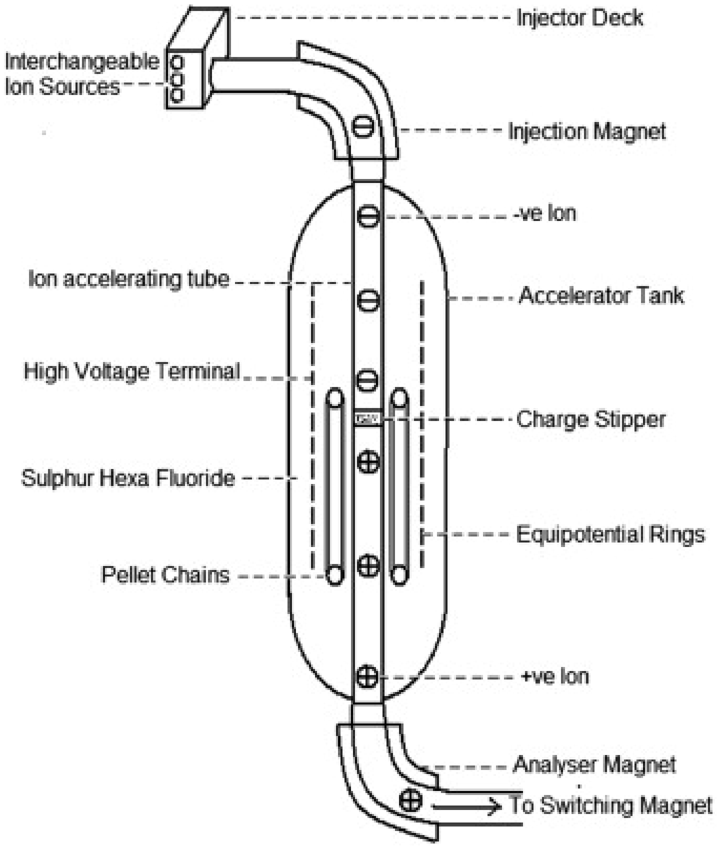

Fig. 2.1 Schematic of Pelletron accelerator

The Pelletron accelerator has an insulating steel tank of height 26.57 and width 5.5 m. In order to attain insulation (to prevent sparking/discharging) the tank is filled with sulfur hexafluoride (SF6) gas at a pressure of 4.0 Torr. The SNICS (Source of Negative Ion by Cesium Sputtering) ion source acts as a source of negative ions that are momentum analyzed by the injector magnets. A high voltage terminal with 1.52 mm diameter and 3.81 mm length at the middle of the tank can be charged by a high potential varied from 4 to 15 MV using an electrostatic charge transfer device. This terminal is connected to the tank vertically through ceramic titanium tubes known as the accelerating tubes. A potential gradient is maintained with the help of these tubes.

Negative ions from the ion source are injected towards the terminal and are stripped off a few electrons through stripper foils. The yield is converted into positive ions.

These ions are further accelerated as they proceed to the bottom of the tank at ground potential. As a result the ions from the accelerator gain energy, given by Eq. (1.1) as,

$$E = V_{\pi} (q + 1) \text{ MeV} \qquad (2.1.1)$$

where V_{π} is terminal potential and q is the number of positive charges (charge states) on the ions after stripping.

Thus a heavy ion of charge state q will attain a final kinetic energy equal to (q + 1) × 15 MeV. Thus protons accelerated to a full terminal voltage would have energy of 30 MeV. By using appropriate magnets with respect to the charge states and energies, the high energetic ions are analyzed and are bent at 90° with respect to vertical position by using analyzer magnet. These redirected ions are directed to the desired experimental area in the beam hall with the help of multi-port switching magnet. Fig. 2.2 shows that the materials science chamber for ion beam irradiation.

Fig.2.2 Materials Science Chamber for Irradiation

Irradiation procedure

The irradiation process for materials generally carried out at the materials science beam line facility of IUAC New Delhi. This beam line is at 15° angle with respect to the direction of the unswitched direct beam. The beam line is maintained at ultra-low pressure of the order of 10^{-9} Torr and the irradiation is carried out in high vacuum target chamber (HVC). It is fixed in Material Science beam line of Pelletron (Fig 2.2). It has arrangement of temperature control from low temperature to high temperature, dose control which includes positive bias to the target for secondary electron suppression (Faraday cup) and proper mechanical support and alignment. The vacuum in the target chamber is generally maintained below 10^{-6} Torr. A large number of samples can be mounted on all the four sides of a specially designed ladder, which is 10 cm long copper block of rectangular cross-section. Each sample was fixed on the ladder with the help of silver paste. Conducting path was provided by using a line of silver paste from the top surface of the sample to the copper block. The target ladder is inserted in the HVC from the top. Keeping beam current constant, irradiation is carried out at room temperature. By using magnetic quadruple and a steerer the beam is focused on the target. For attaining uniform irradiation the beam is scanned in a desired cm^2 area with the help of a magnetic scanner. The ion fluence is estimated using the ladder current and the current integrator.

2.2.2 Calculation of range and energy loss by SRIM code:

Stopping and Range of Ions in Matter (SRIM) is a group of computer programs which calculate interaction of ions with matter; the core of SRIM is a program. SRIM is based on a Monte Carlo simulation method, namely the binary collision approximation with a random selection of the impact parameter of the next colliding ion. As the input parameters, it needs the ion type and energy (in the range 10 eV – 2

GeV) and the material of one or several target layers. SRIM uses several different stopping theories to evaluate the accuracy of experimental stopping powers. Specifically, calculations are made for all ions in individual targets (which eliminates common difficulties with target dependent quantities such as shell corrections and mean ionization potentials.). Calculations are also made of one heavy ion in all solids, which eliminates some of the difficulties with ion dependent quantities such as the degree of ion stripping. Also, calculations are made from fundamental theories like the Brandt–Kitagawa theory and LSS theory [15].

This is very efficient calculation made up by statistical algorithms which allow the ions to jumps between calculated collisions and then averaging the collision over the applied range. During the collisions, the ion and atom have a screened Coulomb collision, including exchange and correlation between the overlapping electron shells. The ion has long range interactions creating electron excitations and plasmons within the target. These are described by including description of target’s collective electronic structure and inter atomic bond structure when the calculation is set up. The charge state of ion within the target is described using the concept of effective charge which depends on velocity of ion and cloud of electrons in the long range screening. The particle losses its energy after each collision by the so called nuclear energy loss which transfer the momentum to the target during collision. Like this it is stopped at or on the surface of the target material.

The SRIM code can be used to compute the ion distribution, detailed calculation for damage cascades, calculation of surface sputtering, electron/neutron/photon cascades, various ion angle/energy/positions, stopping power for ions in gases and compounds.

In the present work, we have estimated the projected range, nuclear stopping power and electronic stopping power of 85 MeV C ions and 120 MeV Si ions in PMMA and PS using SRIM-2003[16].

Results obtained by SRIM-2003 code:

When energetic charged ion strikes on polymeric materials, it loses its energy by two mechanisms known as electronic stopping and nuclear stopping. The projected range , electronic stopping power, nuclear stopping power for 85 MeV C beam and 120 MeV Si beam in PMMA and PS composites was mentioned in Table 2.2.

Table 2.2 Projected ranges for Polymer composites

Sample name	C-ion		
	Projected range µm	Electronic loss eV/Å	Nuclear loss eV/Å
PMMA film	105	$4.90\text{x } 10^{1}$	$2.79\text{x } 10^{-2}$
PMMA+Ag	112	$4.90\text{x } 10^{1}$	$2.79\text{x } 10^{-2}$
PMMA+Ni	99.31	$5.60\text{x } 10^{1}$	$3.10\text{x } 10^{-2}$
PMMA+Cu	105	$5.16\text{x } 10^{1}$	$2.89\text{x } 10^{-2}$
PS film	104	$5.32\text{x } 10^{1}$	$2.89\text{x } 10^{-2}$
PS+Ag	109	$5.31\text{x } 10^{1}$	$2.89\text{x } 10^{-2}$
PS+Ni	98.12	$5.98\text{x } 10^{1}$	$3.19\text{x } 10^{-2}$
PS+Cu	99	$5.38\text{x } 10^{1}$	$2.90\text{x } 10^{-2}$

Sample name	Si-ion		
	Projected range	Electronic loss	Nuclear loss
PMMA film	32	2.81×10^{2}	2.65×10^{-1}
PMMA+Ag	36.8	2.81×10^{2}	2.65×10^{-1}
PMMA+Ni	31.72	3.19×10^{2}	2.49×10^{-1}
PMMA+Cu	33.75	3.01×10^{2}	2.32×10^{-1}
PS film	33	3.04×10^{2}	2.33×10^{-1}
PS+Ag	35	3.08×10^{2}	2.93×10^{-1}
PS+Ni	32	3.18×10^{2}	2.43×10^{-1}
PS+Cu	34	3.10×10^{2}	2.33×10^{-1}

In all the cases, maximum energy of the ion beam was lost by electronic interactions. The thickness of polymer sample is larger than the projected range of the beam in the polymer. Hence the beam was stopped in the polymer and maximum dissipation of heat took place at the end. The composites show a lower projected range due to increase in density after doping of filler. This implies that the most of energy loss was due to the electronic energy loss.

2.2.3 Irradiations:

The composite films of different concentrations of metal nanoparticles powder in PMMA and PS were prepared by casting method in which THF and toluene is used as a solvent respectively. These films were irradiated with 85 MeV C- ions and 120 MeV Si-ions at fluence of 1 x 10^{11}, 1 x10^{12} ions/cm^2 at IUAC, New Delhi, India. The ion beam was defocused using a scanning system, so that an area of 1.0 x 1.0 cm^2 was uniformly irradiated. The beam current was kept low (0.5 pnA) to suppress thermal decomposition and was monitored intermittently with a Faraday cup. The details of irradiation upon samples are shown below in Table2.3.

Table 2.3 Irradiation details of the samples

Sr No	Sample	Fluence (ions/cm^2)	Energy and ions
1.	Pure PMMA	1 x10^{11}, 1 x 10^{12}	85 MeV Carbon, 120 MeV Silicon
	PMMA+5% Ag	1 x10^{11}, 1 x 10^{12}	85 MeV Carbon, 120 MeV Silicon
	PMMA+10% Ag	1 x10^{11}, 1 x 10^{12}	85 MeV Carbon, 120 MeV Silicon
	PMMA+15% Ag	1 x10^{11}, 1 x 10^{12}	85 MeV Carbon, 120 MeV Silicon
2.	PMMA+5% Ni	1 x10^{11}, 1 x 10^{12}	85 MeV Carbon, 120 MeV Silicon
	PMMA+10% Ni	1 x10^{11}, 1 x 10^{12}	85 MeV Carbon, 120 MeV Silicon
	PMMA+15% Ni	1 x10^{11}, 1 x 10^{12}	85 MeV Carbon, 120 MeV Silicon
3.	PMMA+5% Cu	1 x10^{11}, 1 x 10^{12}	85 MeV Carbon, 120 MeV Silicon
	PMMA+10% Cu	1 x10^{11}, 1 x 10^{12}	85 MeV Carbon, 120 MeV Silicon
	PMMA+15% Cu	1 x10^{11}, 1 x 10^{12}	85 MeV Carbon, 120 MeV Silicon
4.	Pure PS	1 x10^{11}, 1 x 10^{12}	85 MeV Carbon, 120 MeV Silicon
	PS+ 5% Ag	1 x10^{11}, 1 x 10^{12}	85 MeV Carbon, 120 MeV Silicon
	PS+ 10% Ag	1 x10^{11}, 1 x 10^{12}	85 MeV Carbon, 120 MeV Silicon
	PS+ 15% Ag	1 x10^{11}, 1 x 10^{12}	85 MeV Carbon, 120 MeV Silicon
5.	PS+ 5% Ni	1 x10^{11}, 1 x 10^{12}	85 MeV Carbon, 120 MeV Silicon
	PS+ 10%Ni	1 x10^{11}, 1 x 10^{12}	85 MeV Carbon, 120 MeV Silicon
	PS+ 15% Ni	1 x10^{11}, 1 x 10^{12}	85 MeV Carbon, 120 MeV Silicon
6.	PS+ 5% Cu	1 x10^{11}, 1 x 10^{12}	85 MeV Carbon, 120 MeV Silicon

	PS+ 10% Cu	1 x10^{11}, 1 x 10^{12}	85 MeV Carbon, 120 MeV Silicon
	PS+ 15% Cu	1 x10^{11}, 1 x 10^{12}	85 MeV Carbon, 120 MeV Silicon

2.3 Experimental characterization techniques

2.3.1 X-ray Diffraction (XRD):

X-ray diffraction (XRD) is a non-destructive analytical technique for identification and quantitative determination of long-range order in various crystalline compounds and also reveals information regarding chemical composition and physical properties. X-rays are electromagnetic radiation which generated by electrons of high energy strike on heavy metal target. When electrons hit the material, some of the electrons will approach the nucleus of the metal atoms where they are deflected because of their opposite charges. This deflection causes the energy of the electron to decrease, and this decrease in energy which resulting an x-ray.

X-rays interact with electrons in atoms. When x-rays collide with electrons, some x-rays from the incident beam are deflected away from the incident direction. If the wavelengths of these scattered x-rays remain unchanged, the process is called an elastic scattering (Thompson Scattering) in that only momentum is transferred during collision [17]. These are the x-rays that are measured in diffraction experiments. They carry information about the electron distribution in materials. On the other hand, during inelastic collision (Compton Scattering), x-rays transfer some of their energy to the electrons and so the scattered x-rays will have different wavelength than the incident x-rays.

Diffraction phenomenon is the consequence of x-ray radiation being scattered by atoms regularly arranged in a lattice possessing interatomic distances of a magnitude comparable to the wave length of the incident radiation. X-rays diffracted from different atoms interfere with each other. If the atoms are arranged in a periodic fashion, as in the case of crystals, the peaks in the interference pattern will correspond to the distribution of atoms. The peaks in an x-ray diffraction pattern are directly related to the atomic distances by Bragg's law [18].

$$n\lambda = 2d\sin\theta \tag{2.2.2}$$

where, λ is the wavelength of x-ray, d is the inter-planar distance, θ is the scattering angle and n an integer representing the order of the diffraction peak, as shown in Fig. 2.3.

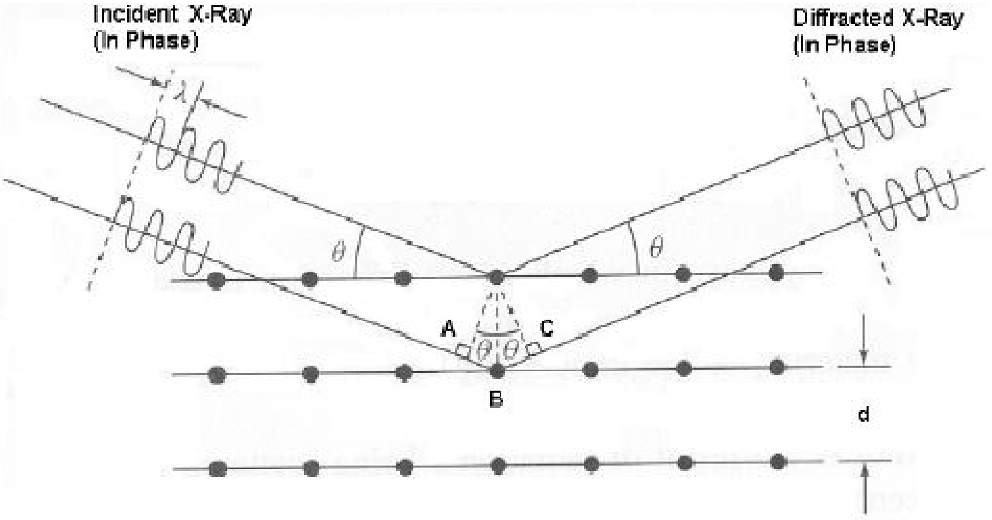

Fig. 2.3 Schematic of Bragg's law

X-ray diffraction data can be collected by using either reflection or transmission geometry as shown in Fig. 2.4(a, b). In the reflection mode, x-rays scattered or reflected from the sample are detected as shown in Fig. 2.4 (a). The reflected x-rays interfere with each other such that in the diffractogram, intense peaks are obtained at corresponding d values, according to the Bragg's law.

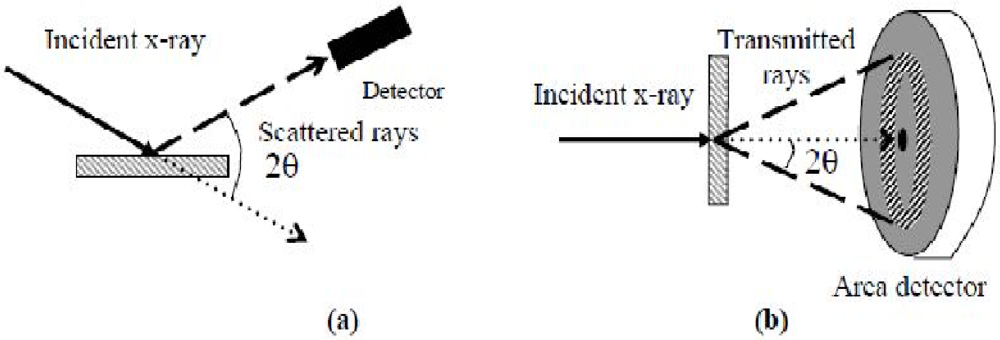

Fig. 2.4 Schematic of x-ray diffraction geometries (a) reflection mode (b) transmission mode

The peak position, intensity, and shape provide important information about the long-range order in the material. For example, the apparent crystal size (L) can be quantitatively calculated by Scherrer's formula [19]

$$b = K\lambda / L\cos\theta \qquad (2.2.3)$$

Where b is FWHM in radians, λ is the wavelength of X-ray beam (1.5418 Å), L is the crystallite size in Å, K is a constant which varies from 0.89 to 1.39, but for most of the cases it is close to 1.

In the transmission mode, an area detector detects the x-rays transmitted through the sample. A circular cone of transmitted rays is incident on the detector, giving a circular ring like pattern as shown in the Fig. 2.3 (b). The radius of the circular ring corresponds to the inter-planar distance. X-Ray Diffraction (XRD) uses the "fingerprint" of a crystalline material to allow identification of unknown phases in a mixture. It is commonly used in the engineering, geological and materials sciences for applications such as corrosion studies, material fabrication, analysis of combustion products, mineral identification and determination of lattice parameters.

In the present study, the structural studies were carried out by X-ray powder diffractometer (Bruker AXS D8 Advance) with Cu K_α radiation (1.5418 Å) in a wide range of Bragg angles ($10^\circ \leq 2\theta \leq 80^\circ$).

2.3.2 Differential Scanning Calorimetry (DSC):

DSC, is a thermo analytical technique in which the difference in the amount of heat required to increase the temperature of a sample and reference are measured as a function of temperature. Both the sample and reference are maintained at nearly the same temperature throughout the experiment. Generally, the temperature program for a DSC analysis is designed such that the sample holder temperature increases linearly as a function of time. A sample of known mass is heated or cooled and the changes in its heat capacity are tracked as changes in the heat flow. This allows the detection of transitions like melts, glass transitions, phase changes, and curing. Because of this flexibility, DSC is used in many industries including pharmaceuticals, polymers, food, paper, printing, manufacturing, agriculture, semiconductors, and electronics as most materials exhibit some sort of transitions.

A solid material can be amorphous, crystalline, or a combination of the two. Using Differential Scanning Calorimetry (DSC), one can better understand phase transitions and reactions in materials, and how they contribute to the properties and characteristics of the material.

One of the most widely used techniques to measure T_g and T_m is differential scanning-calorimetry (DSC) [20-22]. The signal in a DSC experiment is related to the difference between the “thermal response” of a small (10 to 30 mg) polymer sample and reference cell (empty) in two separate aluminium pans. The two are heated and cooled at the same rate or maintained at a constant temperature, as illustrated in Fig.2.4. Thermocouple junctions just underneath each position monitor both the temperature of the sample side T_s, and the difference between the temperature of sample side and the temperature of reference, $\Delta T = T_r - T_s$. If the cell is empty and thermally symmetric, the temperature of the reference side will always be the same as the temperature of the sample side irrespective of heating and cooling. The values of specific heat, C_p, may be obtained from the recorded heat-flow rate by calibration with a pure compound such as sapphire for which C_p is known precisely at different temperatures from calorimetry measurements.

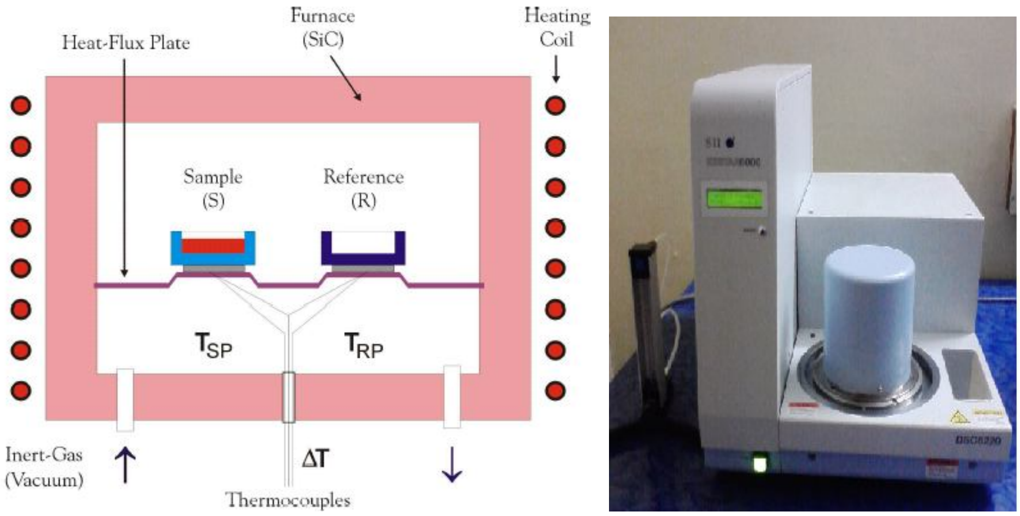

Fig. 2.5 Schematic of DSC

A discontinuity in C_p (i.e., $\Delta C_p = C_p^{\,l} - C_p^{\,g}$), characteristic of a second-order transition, is observed at the polymer T_g that is often identified as the temperature at the midpoint of the step change in C_p (i.e., at $\Delta C_p/2$).

For many amorphous polymers, T_g (K) and ΔC_p (J g^{-1} K^{-1}) are related by the approximate relationship that $\Delta C_p \times T_g$ [21]. During heating of a semicrystalline polymer, additional crystallisation may occur at temperatures between T_g and T_m. At T_m, which may be defined as the extrapolated temperature of the initial slope of the melt endotherm, the crystallites begin to melt over a wide range of temperatures. The breadth of the endotherm is much larger than typically observed for pure low-molecular-weight compounds as a consequence of the lower order of perfection of polymer crystallites. By calibration with a low-molecular-weight standard such as benzoic acid, the heat of fusion (ΔQ) of a semicrystalline polymer can be determined from measurement of the area under the melt endotherm recorded by DSC.

The thermal analysis was performed with differential scanning calorimetry (S II EXSTAR 6000, DSC 6220) with the heating rate of 5^{o}C min^{-1} in the present study.

2.3.3 UV-visible spectroscopy:

Ultraviolet spectrometry is based on absorption of light in visible or ultraviolet regionby an analyte, and is used for measuring its concentration in a solution. Asenergy in the form of ultraviolet or visible light is absorbed by a molecule containing π-electrons or non-bonding electrons, these electrons are excited to higher anti-bonding molecular orbitals. Therefore this technique is appropriate for transition metal ions, highly conjugated organic compounds and biological macromolecules as analytes. Energy carried by a photon is inversely proportional to its wavelength; therefore, lower the energy gap between the highest occupied molecular orbital and lowest unoccupied molecular orbital**,** the longer the wavelength of light a molecule can absorb. The energy gaps between ground and excited states depend on the chemical nature of the molecule of interest and therefore the wavelength of the light is chosen accordingly for absorption by that molecule.

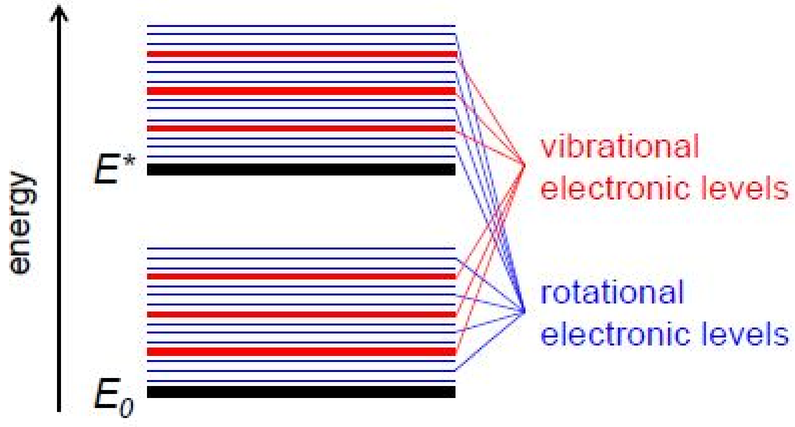

Fig. 2.6 Energy levels diagram

The concentration, c, of the absorbing species and the path length, b, through the solution affect absorbance directly. This relationship can be expressed with Beer's law as A=εbc, where ε is molar absorptivity, which depends on temperature, pressure and molecular nature of the analyte. Absorbance (A) is the log of ratio of Po is the radiant power of incident beam to the power of transmitted beam P. Po generally corresponds to compensate the attenuation of a beam due to scattering by large molecules, absorption by the solvent or container, and/or reflection.

In ultraviolet or visible radiation absorption, the wavelengths of absorption peaks can be correlated with the types of bonds that exist in the species that is analysed. For this reason, while UV-VIS absorption spectroscopy is used mostly for quantitative determination of compounds containing absorbing groups, molecular absorption spectroscopy is also valuable for identifying functional groups in a molecule. Calibration yielding absorbance vs. concentration relationship is ordinarily made using the absorbance values at a wavelength corresponding to an absorption peak, because the change in absorbance per unit of concentration is greatest at this point, and thus the maximum sensitivity is realized, where good adherence to Beer's law can be expected.

Instrumentation

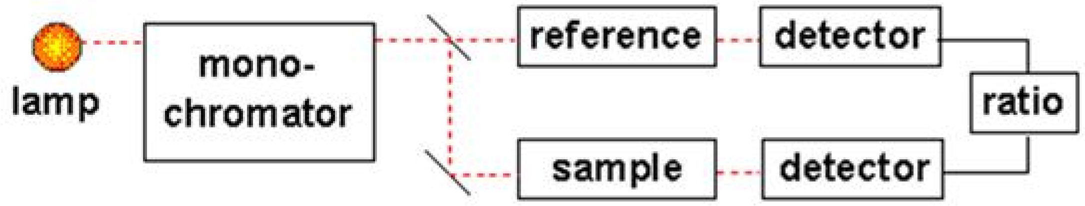

Fig. 2.7 Instrumentation of UV-vis spectrometer

A UV-visible spectrophotometer consists of a light source, a monochromator, sample cell and a detector. Among the light sources, most common are tungsten filament (300-2500nm), deuterium arc lamp (190-400nm) or xenon arc lamp (160-2000nm) or LED for visible wavelengths. Monochromator provides a continuous spectrum using the light coming from the source so that light beam at a specific wavelength can be selected and sent to the solution inside the sample cell. Detector measures the intensities of the light coming from both the blank sample and analyte solution. Hence the absorbance values are calculated for each solution [23-25].

Determinations of band gap

The change in optical properties has been studied by Perkin- Elmer 25 Lambda UV-Visible spectrophotometer in the frequency range 200-800 cm^{-1}. The optical band gap E_g is obtained by Tauc's equation [26]:

$$\omega\varepsilon(\lambda)=(\hbar\omega-E_g)^2 \qquad (2.2.4)$$

where $\varepsilon(\lambda)$ is the optical absorbance and λ is the wavelength. The intersection of the extrapolated spectrum with the abscissa of the plot $\varepsilon^{1/2}/\lambda$ versus $1/\lambda$ yields the gap wavelength λ_g from which the energy gap is derived as $E_g = hc/\lambda_g$.

The number of carbon atoms per cluster (N) can be calculated by following the relation [27]

$$Eg=34.3/\sqrt{N}eV \qquad (2.2.5)$$

where N is the number of carbon atoms per cluster and Eg is the energy band gap.

The number of carbon hexagon rings in the cluster (M) is then found from the relation [27]

$$Eg \approx 2\,|\beta|/\sqrt{M} \qquad (2.2.6)$$

2.3.4 Scanning Electron Microscope (SEM):

A scanning electron microscope (SEM) enables the investigation of specimens with a resolution down to the nanometer scale. It is a type of electron microscope that produces images of a sample surface by scanning it with a high energy beam of electrons in a raster scan pattern. The electrons interact with atoms that make up the sample producing various signals that contain information about the sample's surface topography and composition and other properties such as electrical conductivity.

The main signals which are generated by the interaction of the primary electrons (PE) of the electron beam and the specimen´s bulk are secondary electrons (SE) and backscattered electrons (BSE) and furthermore X rays. They come from an interaction volume in the specimen which differs in diameter according to different energies of the primary electrons (typically between 200 eV and 30 keV). The SE come from a small layer on the surface and yield the best resolution, which can be realized with a scanning electron microscope. The well known topographical contrast delivers micrographs which resemble on conventional light optical images. The BSE come from deeper regions of the investigated material thus giving a lower resolution. As a byproduct of the image giving signals X-rays are produced. They result from ionization processes of inner shells of the atom leading to electromagnetic radiation. The characteristic X-rays give information about the chemical composition of the material. The methods energy dispersive X-ray spectroscopy (EDS) and wavelength dispersive X-ray spectroscopy (WDS) enable the detection of chemical elements from Boron to Uranium in a qualitative and even quantitative manner.

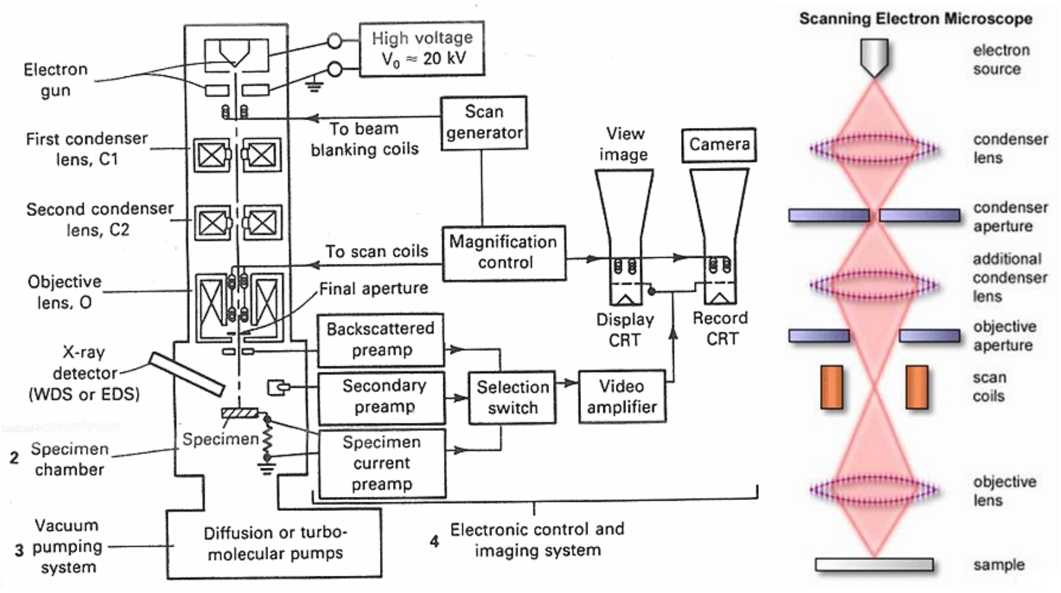

Fig. 2.8 Schematic and working of SEM

Working of SEM:

The schematic of SEM is shown in Fig. 2.8. The Virtual Source at the top represents the electron gun, producing a stream of monochromatic electrons. The stream is condensed by the first condenser lens. This lens is used to both form the beam and limit the amount of current in the beam. It works in conjunction with the condenser aperture to eliminate the high-angle electrons from the beam. The beam is then constricted by the condenser aperture, eliminating some high-angle electrons. The second condenser lens forms the electrons into a thin, tight, coherent beam and is usually controlled by the ‘‘fine probe current knob’’. A user selectable objective aperture further eliminates high-angle electrons from the beam. A set of coils then ‘‘scan’’ or ‘‘sweep’’ the beam in a grid fashion, dwelling on points for a period of time determined by the scan speed. The final lens, the Objective, focuses the scanning beam onto the part of the specimen desired. When the beam strikes the sample interactions occur inside the sample and are detected with various instruments. Before the beam moves to its next dwell point these instruments count the number of interactions and display a pixel on a CRT whose intensity is determined by this number. This process is repeated until the grid scan is finished and then repeated, the entire pattern can be scanned 30 times per second.

SEM can examine the following information in the samples:

Topography: The surface features of an object or ‘‘how it looks’’, its texture; detectable features limited to a few nanometers.

Morphology: The shape, size and arrangement of the particles making up the object that are lying on the surface of the sample or have been exposed by grinding or chemical etching; detectable features limited to a few nanometers.

Composition: The elements and compounds that the object is composed of and the relative amounts of them.

Crystallographic Information: How the atoms are arranged in the object; direct relation between these arrangements and materials.

2.3.5 Quantum Interference Device (SQUID):

Superconducting Quantum Interference Devices (SQUID) are very sensitive magnetometers capable of measuring extremely small magnetic fields typically of the order of 10^{-17} T [28]. They are based on superconducting loops containing Josephson junctions. Their noise levels in a SQUID are extremely low. A Josephson junction is made up of two superconductors, separated by an insulating layer so thin that electrons can pass through it. A SQUID consists of tiny loops of superconductors employing Josephson junctions to achieve superposition: each electron moves simultaneously in both directions. Because the current is moving in two opposite directions, the electrons have the ability to perform as qubits (that theoretically could be used to enable quantum computing). SQUIDs have been used for a variety of testing purposes that demand extreme sensitivity, including engineering, medical, and geological equipment. Because they measure changes in a magnetic field with such sensitivity, they do not have to come in contact with a system that they are testing.

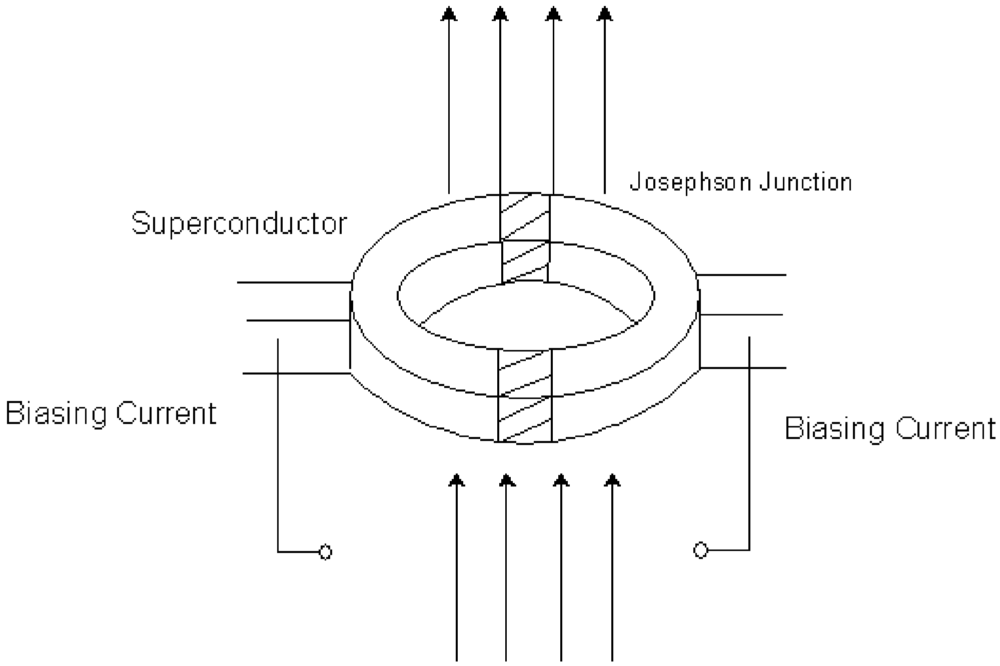

Fig. 2.9 Basic of SQUID

Design of SQUID

SQUID consists of two Josephson junctions connected in parallel. When the SQUID is biased with a current greater than the critical current, the voltage across the SQUID is modulated with the flux treading the SQUID at a period of one flux quantum,

$\Phi_0 \equiv h/2e$ (2.2.7)

Therefore, the SQUID is a flux-to-voltage transducer. This special flux-to-voltage characteristic has enabled researchers to use the device to detect small magnetic field, current, voltage, inductance and magnetic susceptibility. SQUIDs are the most sensitive devices in detecting the magnetic flux. Low-To SQUID has been used in a wide range of applications, including biomagnetism, susceptometers, nondestructive evaluation, geophysic s scanning SQUID microscope, and nuclear magnetic resonance [28].

2.3.6 Dielectric properties (Impedance phase-gain analyzer):

The evaluation of dielectric parameters namely dielectric permittivity and dielectric loss provide insight into the polarization process that takes place in materials.

Dielectric behavior of a material is arising from the dielectric polarization when the material is under the influence of an external electric field. When an electric field is applied across the sample, there is a shift of charges and electric dipoles are formed inside the material. This shift of charges inside the material causes a net charge to accumulate on the electrodes introducing a capacitance in the system.

When the applied electric field is removed the net dielectric dipole moment formed in the material is supposed to vanish immediately. But this will not happen in reality. Depending on the material there is a delay in coming back to the zero dipole moment state. This delay is due to the various frictional or dissipative forces present in the material. These damping forces cause a power loss and this is termed as the dielectric loss. When a sinusoidally changing electric field is applied across the sample the resulting polarization in the material is lagged by a fixed phase angle due to the dielectric loss. This gives rise to two components of polarization inside the material, these two components can be considered the real and imaginary components of the polarization when represented in a complex plane. Accordingly there are two components for the dielectric permittivity of the material when a sinusoidally varying electric field is applied [29].

Fig. 2.10 shows the Impedance gain phase analyzer/ LCR meter, available at M. S. University of Baroda, Vadodara. This Impedance gain phase analyzer (Solartron-1260) uses powerful microprocessor-controlled digital and analogue techniques to provide a comprehensive range of impedance and frequency response measuring facility. It can be operated for the frequency range from 100 Hz to 10 MHz. Dielectric loss, capacitance and resistance were obtained directly from LCR meter. Using these values conductivity also was calculated.

Fig. 2.10 Impedance phase gain analyzer (Solartron 1260)

(a) AC electrical conductivity:

Electrical conductivity is ability of a material to conduct electric current. An electrical potential difference is applied in a material and its movable charges tend to flow and cause a raise in the electric current. The electrical conductivity is defined as the inverse of the resistivity. In the case of polymers, free electrons which are not attached to the macromolecular chain of polymers, contribute to the conductivity of polymer. Therefore the conductivity of thermoplastic polymers like PMMA, PS, PVC etc are found to be less. There are many methods to improve the conductivity of polymers. In the present study we have reported two effective techniques to get better improvement in conductivity by several orders (a) by doping of metal nanoparticles: which depends upon filler size, shape, orientations and amount of the filler (b) by ion beam irradiation: which depends upon ion species, fluence and energy of ion.

To determine the conductivity the composite materials inserted between the electrodes as shown in figure 2.9.

The a.c. conductivity has been formulated as follows, Electrical conductivity is defined as the quantity of electrical charge that is transferred per unit of time over a unit of cross sectional area under a unit potential difference gradient;

$$\sigma = \frac{\left(\frac{dq}{dt}\right)}{A\left(\frac{dV}{dx}\right)} \tag{2.2.8}$$

Ohms law describes an equivalent definition as the ratio of the current density to electric field;

$$\sigma = \frac{J}{E} \tag{2.2.9}$$

Where, J is the current density, E is the electric field strength vector which is E=D/ε; where D is the displacement vector of the dipole charges and ε is the complex permittivity of the material. For the parallel plate capacitors, the electric field intensity is the ratio of the potential difference between the plates to the interplate distance (t) so

$E=V/t$ (2.2.10)

Since $Q/A=V\,\varepsilon/t$ and $J=dq/dt$, $Q/A=q$

So $J= d/dT(V\,\varepsilon/t) = (\varepsilon/ t)\,(dV/dT) = (\varepsilon/ d)Vj\,\omega$ (2.2.11)

Substituting for E and J in equation

$\sigma_{\text{a.c.}} = J/E = \varepsilon j\omega =(\varepsilon- j\varepsilon'')j\omega= \varepsilon j\omega + \varepsilon''\omega$ (2.2.12)

For the a.c. conductivity to be a real so must neglect j

$\sigma_{\text{a.c.}} = \omega\varepsilon''$ (2.2.13)

When the applied electric field is removed the net dielectric dipole moment formed in the material is supposed to vanish immediately. But this will not happen in reality.

Depending on the material there is a delay in coming back to the zero dipole moment state. This delay is due to the various frictional or dissipative forces present in the material. These damping forces cause a power loss and this is termed as the dielectric loss. When a sinusoidally changing electric field is applied across the sample the resulting polarization in the material is lagged by a fixed phase angle due to the dielectric loss. This gives rise to two components of polarization inside the material, one is in phase and the other is 90° out of phase. These two components can be considered the real and imaginary components of the polarization when represented in a complex plane. Accordingly there are two components for the dielectric permittivity of the material when a sinusoidally varying electric field is applied.

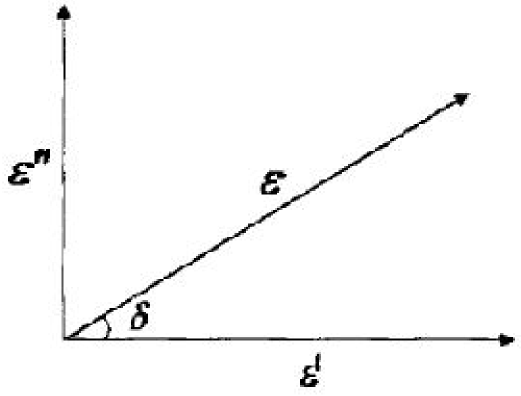

Fig. 2.11 Representation of complex permittivity

$\varepsilon' = \varepsilon \cos\delta$ (2.2.14)

$\varepsilon'' = \varepsilon \sin\delta$ (2.2.15)

$\tan\delta = \varepsilon''/\varepsilon'$ (2.2.16)

substituting the value in (2.2.13) and we get

$\sigma_{ac} = \omega\varepsilon \tan\delta$ (2.2.17)

Where, $\omega = 2\pi f$ and $\varepsilon = \varepsilon_0\varepsilon_r$ (ε_r is the relative permittivity and ε_0 is permittivity of free space).

$\sigma_{ac} = 2\pi f \tan\delta\ \varepsilon_0\varepsilon_r$ (2.2.18)

The dielectric constant can be calculated by

$\varepsilon_r = C_p \text{ x } t/ \varepsilon_0 A$ (2.2.19)

From the relation (2.2.18) and (2.2.19) we can get the final expression

$\sigma_{ac} = 2\pi f \tan\delta \, C_p \, t/A = 2\pi f D \, C_p \, t/ A$ (2.2.20)

To calculate the ac conductivity of polymer we have used this relation.

Where, D = tanδ which is directly measured from LCR meter, C_p is the capacitance of the material, A and t are the area of electrode and thickness of sample respectively.

(b) Dielectric constant:

In the electronic and electrical industry, capacitor represents one of the most fundamental devices. It serves the purpose of filtering unwanted signals, of allowing alternating current (AC) signals to pass while blocking direct current (DC). It can act as a battery or as a power source. In general the capacitor is a very versatile device, and as such, it has many properties based on the application where it is used.

The defining characteristic of a capacitor is its ability to store electric charge. This ability is called its capacitance C, and is defined by the following relationship:

$C=Q/V$ (2.2.21)

Where, Q is the stored charge and *V* is the potential difference connected across the electrodes. The SI unit of capacitance is the farad, which is 1 coulomb per volt. The capacitance of a capacitor with flat, parallel electrodes separated by vacuum is directly proportional to the active electrode area A and inversely proportional to the separation d as described by the following equation:

$C=\mathcal{E}_0 A/\mathrm{t}$ (2.2.22)

where $\mathcal{E}_0$ is a universal constant having the value of 8.85×10^{-12} F/m.

When two parallel electrodes are separated by a distance *t* with dielectric materials, the capacitance can be expressed as:

$C=\mathcal{E}_0\mathcal{E}rA/t$ (2.2.23)

where $\mathcal{E}r$ is the relative permittivity.

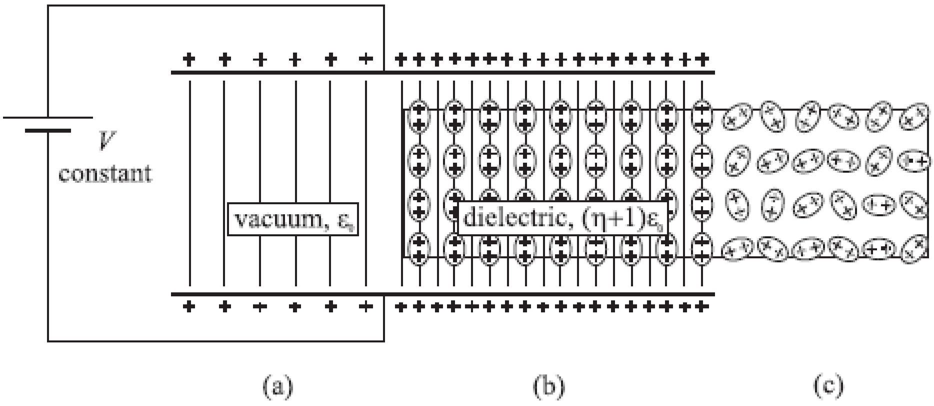

Fig. 2.12 Polarization in Dielectric (a) vacuum capacitor, (b) polarised dipoles in the dielectric inserted between the capacitor plates, (c) random dipoles when no electric field is applied.

From the equation (2.2.23) we can see how effective a capacitor to store energy depends on the material used for the dielectric. And each material has unique dielectric permittivity and dielectric strength, which is the maximum voltage that can be applied across the electrodes without breakdown. If breakdown occurs, current will flow between the electrodes.

(c) Dielectric Loss:

The dielectric loss is a measure of energy loss in the dielectric during AC operation, which is a material property and does not depend on the geometry of capacitor. Usually the dielectric loss, expressed as the loss tangent (tan δ) or dissipation factor (Df) can be defined as

$\tan\delta = \mathcal{E}''/\mathcal{E}'$ (2.2.16)

In general, dielectric loss of the dielectric material is resulted from distortional, dipolar, interfacial, and conduction loss. The distortional loss is related with electronic and ionic polarization mechanisms. The interfacial loss originates from the excessive polarized interface induced by the fillers and specifically the movement or rotation of the atoms or molecules in an alternating electric field. The conduction loss is attributed to the dc electrical conductivity of the materials, representing the flow of actual charge through the dielectric materials [30, 31].

References:

[1] Brydson, Plastics Materials, Butterworths (1989).

[2] Campo, E. Alfredo, the Complete Part Design Handbook, Hanser (2006).

[3] Osswald, et al, International Plastics Handbook, Hanser (2006).

[4] Strong, Plastics Materials and Processing, Prentice Hall (2000).

[5] Rajesh Kumar Srivastava, T. N. Narayanan, A. P. Reena Mary, M. R. Anantharaman, Anchal Srivastava, Robert Vajtai, Pulickel M. Ajayan, Appl. Phys. Lett., 99 (2011) 113116.

[6] L.C. Costa, F. Henry, M.A. Valente, S.K. Mendiratta, A.S. Sombra, European Polymer Journal 38 (2002) 1495–1499.

[7] Pranay Jain, Vibor Aggarwal, International Journal of Nano and Material Sciences, 1(2) (2012) 108-120.

[8] R. C. Doty, T. R. Tshikhudo, M. Brust, D. G. Ferning, Chem. Mater. 17 (2005) 4630.

[9] P S Guo, Z Sun, Y W Chen, Z H Zheng, Mater. Lett. 60 (2006) 966.

[10] Zh S Luo, Ch L Chen, D J Zhao, Sh L Luo and Zh Ch Li, Chem. Phys. Lett. 421 (2006) 584.

[11] Huazhi Wang, Xinli Kou, Jie Zhang, Jiangong Li, Bull. Mater. Sci., Vol. 31 (2008) 97.

[12] Xiao-Min Ni, Xiao-Bo Su, Zhi-Ping Yang, Hua-Gui Zheng, Journal of Crystal Growth 252 (2003) 612.

[13] Yeh, M.S.; Yang, Y.S.; Lee, Y.P.; Lee, H.F.; Yeh, Y.H.; Yeh, C.S. J. Phys. Chem. B R., 103 (1999) 6851.

[14] George H. Chan, Jing Zhao, Erin M. Hicks, George C. Schatz, Richard P. Van Duyne, Nano letters, 7 (2007) 1947.

[15] J. Lindhard, M. Scharff, H.E. Schiott, Kgl. Danske Vid. Sels. Mat.-Fys. Medd. 33 (1963) 1.

[16] J. F. Ziegler, code SRIM 2006, The stopping range of ions in matter (IBM research), New York, USA (2006).

[17] Klugg, H. P.; Alexander, L. E. X-ray diffraction procedures; John Wiley & Sons: USA (1974).

[18] Bragg, W.L. (1913). "The Diffraction of Short Electromagnetic Waves by a Crystal". *Proceedings of the Cambridge Philosophical Society* 17: 43–57.

[19] Scherrer, P. Gott. Nachar, 2 (1918) 98–100.

[20] P. J. Haines, "Thermal Methods of Analysis", Blackie Academic and Professional, 1995, p.63. ,

[21] J. R. Fried, "Polymer Science and Technology", Prentice Hall PTR, 1995, p.153.

[22] M. P. Stevens, "Polymer Chemistry", Oxford University Press, 1999, p.149.

[23] Skoog, A.D., Leary J. J., “Principles of Instrumental Analysis”, 4th ed., pp. 123-173.

[24] Ewing, W.Galen, “Instrumental Methods of Chemical Analysis”, 4th ed., pp. 34-42, 63-74.

[25] Willar, Merritt, Dean, Settle, “Instrumental Methods of Analysis”, 6th ed., pp.66-78.

[26] A. K. Srivastava, H. S. Virk, J. Polym. Mater. 17 (2000) 325-328.

[27] A. Das, S. Dhara and A. Patnaik, Physical Rev B 59 (1999) 11069

[28] Hong-Chang Yang et aI, Tamkang Journal of Science and Engineering, 6, No. 1, (2003) 9-18.

[29] B. Tareev, Physics of Dielectrics Materials, MlR Publishers (1975), Moscow

[30] J. Lu, K. S. Moon and C. P. Wong, Proceedings of 11th International Symposium on Advanced Packaging Materials, pp. 88-92 (2006).

[31] J. Lu, K. S. Moon, J. Xu and C. P. Wong, 231st American Chemical Society Meeting, Atlanta, GA, March 26-30 (2006).

Chapter - III

Effect of swift heavy ions on physical properties of PMMA/Ag and PS/Ag nanocomposites

----

Abstract

In this chapter swift heavy ions (120 MeV Si ions, 85 MeV C ions) induced modifications of Silver nanoparticles dispersed PMMA and PS nanocomposites films at the fluences of 1 x 10^{11}, 1 x 10^{12} ions/cm^2 were studied. 120 MeV Si swift heavy ions induced more prominent effects on the physico-chemical properties of polymer nanocomposites compared to those of C-ions. An XRD analysis reveals that the crystallite size of the composites decreased after ion beam irradiation which is also corroborated by the DSC analysis due to the chain scissioning upon irradiation in PMMA nanocomposites. In PS nanocomposites, we observed cross linking upon irradiation. It was observed from the UV- visible spectroscopy analysis that the band gap value moved to the lower energy on doping with metal nanoparticles, as well as upon irradiation. SEM images showed damages upon ion beam irradiation. The dielectric constant of the composites increased with the increase of metal content and also upon ion beam irrdaition. These phenomena could be interpreted from interfacial polarization of heterogeneous systems.

3.0 Introduction:

Polymer reinforced with fillers is a common way to achieve improved properties in the fabrication of modern plastics due to their synergistic and hybrid properties derived from several components. Polymer nanocomposites have recently received significant attention because of the new and superior properties (e.g., electrical, thermal, and mechanical) to conventional composites of these materials and may be synthesized using surprisingly simple and inexpensive techniques [1, 2].

Swift heavy ion (SHI) irradiation is a unique post-deposition treatment in view of its ability to modify the polymers properties which are associated with the collisions of penetrating high energy ions with the target atoms and the formation of defects [3]. The defects lead to the change in the structural, optical and electrical transport properties of the materials. These changes are strongly dependent on mass of the incident ions, irradiation energy and fluences. The irradiation may cause ionization or excitation, and possibly displacement of atoms from their sites in the lattice of the materials. Different studies of effect of ion beam irradiation on polymers/polymer composites expose a variety of changes in structural and chemical composition, main-chain scissioning, intermolecular cross-linking, creation of unsaturated bonds, formation of volatile fragments and creation of carbonaceous clusters etc. [4, 5, 6]

So far not much work have been reported which deals with the SHI effect on the nanocomposites. The aim for this work is to produce composites with high dielectric constant and low dielectric loss which is required for telecommunications, microelectronic devices, EMI shielding etc. For that purpose, we have synthesized following polymer nanocomposites and studied the effect of 120 MeV Si ions and 85 MeV C ions on these composites.

(i) PMMA + Ag [7]

(ii) PS + Ag [8]

Properties and preparation methods of composites have been discussed in chapter 2. All the films were irradiated with 120 MeV Si- ions and 85 MeV C- ions at the fluences of 1 x 10^{11}, 1 x 10^{12} ions/cm^2 at Inter University Accelerator Centre (IUAC), New Delhi, India. We have studied changes in the optical, structural, dielectric and thermal properties of composites due to swift heavy ions irradiation by means of UV–visible spectroscopy, X-ray diffraction, impedance gain phase analyzer and differential scanning calorimetry.

3.1 Effect of swift heavy ions irradiation on PMMA + Ag nanocomposites:

3.1.1 X-ray diffraction analysis:

The diffraction patterns of the pristine and irradiated polymer composites films are shown in Fig. 3.1(a-f). The diffraction peaks of Ag/PMMA composites showed four well defined crystalline peaks at 2θ = 38.4, 44.3, 64.7 and 77.6^0, corresponding to the (111), (200), (220) and (311) planes of the face-centered cubic (fcc) Ag phase compared with the standard powder diffraction card of Joint Committee on Powder Diffraction Standards (JCPDS), and silver file No. is 04–0783. The broad peak at 2 θ = 14.79 in the diffraction pattern of the pristine film indicates that the polymer is amorphous in nature. Because of influence of silver nanoparticles in PMMA matrix, it shows semi-crystalline diffraction pattern. It is observed from figure that intensity of diffraction peak varies after both irradiation. The crystallite size has been calculated before and after irradiation using Scherrer’s formula (2.2.3) [9] as discussed in chapter 2 in section 2.3.1.

$b=K\lambda/L\cos\theta$

where b is FWHM in radians, λ is the wavelength of X-ray beam (1.5418 Å), L is the crystallite size in Å, K is a constant which varies from 0.89 to 1.39, but for most of the cases it is close to 1.

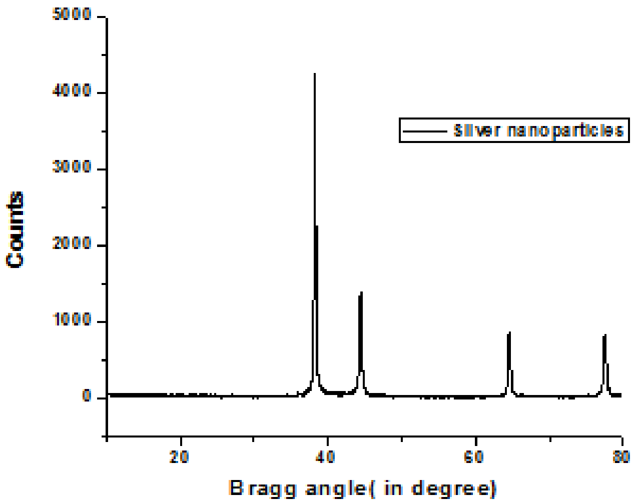

(a)

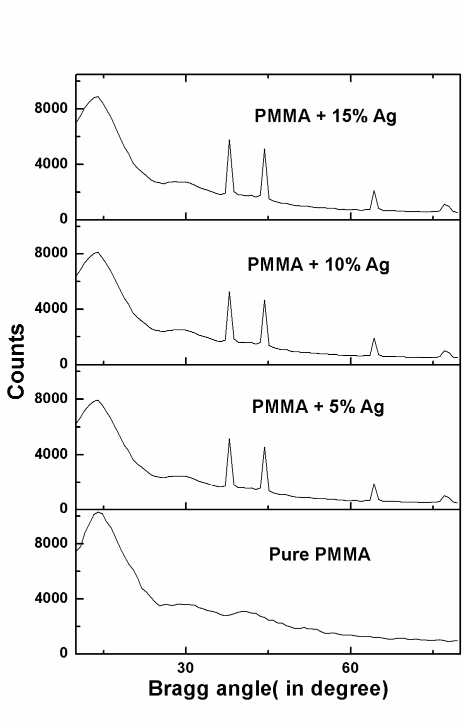

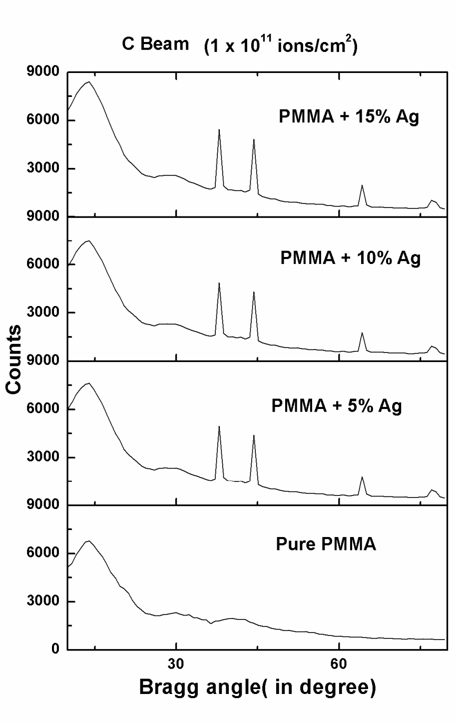

(b) (C)

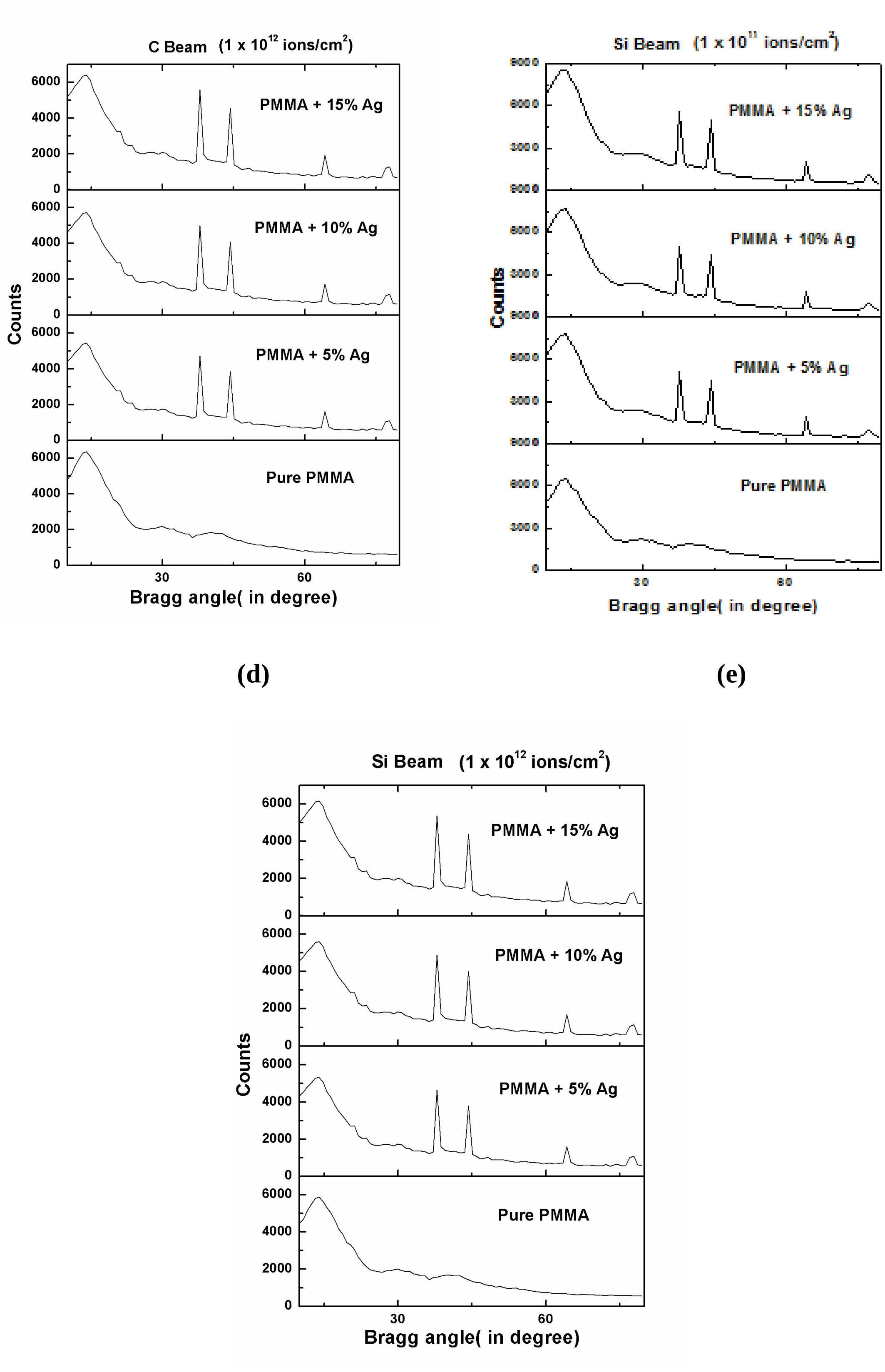

(d) **(e)**

(f)

Fig. 3.1 X-ray diffraction patterns of (a) silver nanoparticles, (b) PMMA+ Ag (pristine) (C) C beam (1 x 10^{11} ions/cm^2) (d) C beam (1 x 10^{12} ions/cm^2) (e) Si beam (1 x 10^{11} ions/cm^2) (f) Si beam (1 x 10^{12} ions/cm^2)

The appearance of sharp peak in composite indicates some degree of crystallinity. Results show that crystallite size of fillers decreases slightly upon both ion beams irradiations. It is also observed that the intensity of the peak decreases and to some extent broadening of the peak after irradiation offers confirmation of decrease in crystallinity. Since no significant change in the peak position is observed, this reveals that lattice parameters do not change significantly in both irradiations. The broadening of peak suggests an evolution of the polymer towards a more disordered state [10]. The crystallite size was calculated from the relation 2.2.3 as discussed in chapter 2 corresponding to the peak of the pristine and irradiated samples and the results are listed in Table 3.1

Table 3.1 Crystallite size of pristine and irradiated samples

Sample	Pristine		C Beam		Si Beam	
	2θ	Crystallite size (nm)	Crystallite size (nm) ($1x10^{11}$) ions/cm^2	Crystallite size (nm) ($1x10^{12}$) ions/cm^2	Crystallite size (nm) ($1x10^{11}$) ions/cm^2	Crystallite size (nm) ($1x10^{12}$) ions/cm^2
PMMA+ 5%Ag	38.07	32.64	31.61	30.14	31.20	29.98
	44.24	33.17	32.18	30.67	30.34	29.34
	64.23	32.44	30.11	29.10	29.23	28.54
	Average	32.75	31.30	29.97	30.26	29.28
PMMA + 10%Ag	38.05	32.89	31.11	30.34	31.56	29.88
	44.21	33.98	30.21	29.11	29.56	29.34
	64.19	34.23	32.67	31.33	29.33	29.58
	Average	33.70	31.33	30.26	30.15	29.60
PMMA + 15%Ag	38.01	34.24	33.25	31.22	32.89	30.69
	44.18	36.12	34.12	32.78	31.78	30.31
	64.15	38.45	36.78	33.67	30.14	29.45
	Average	36.27	34.72	32.56	31.60	30.15

Results show that the ion beam irradiation causes large amount of energy deposition in the material which leads to decrease in crystallite size. It may be attributed to splitting of crystalline grains due to absorption of large amount of energy and it also reflects the formation of disorder system. The irradiation may induce chain scissioning, which is also corroborated by DSC analysis, assumed to be responsible for the reduction in crystallinity of the composite [10].

3.1.2 Thermal response (Differencial scanning calorimetry (DSC)):

The important property of the polymer is the glass transition temperature (*T*g), which is defined as the temperature at which the plastic becomes hard and brittle when cooled rapidly after heating. At the glass transition temperature, the weak secondary bonds that stick the polymer chains together are broken, and the macromolecule starts to move. The influence of silver nanoparticles and irradiation on the glass transition behavior of polymer matrix (PMMA) was investigated with dynamic DSC technique. The values of Tg were taken as the midpoint of the glass transition event and

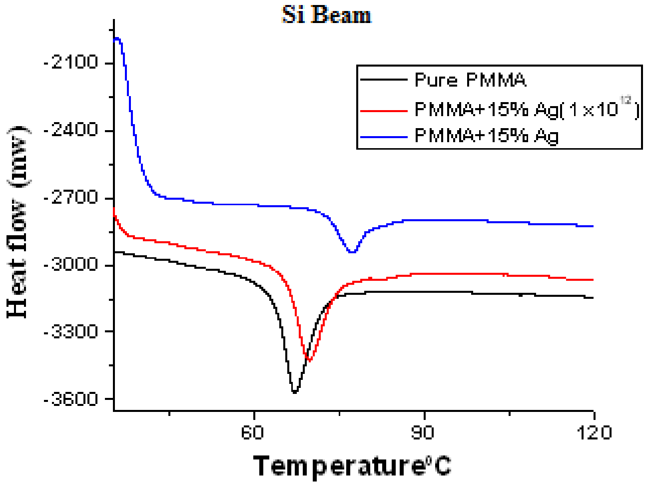

(a)

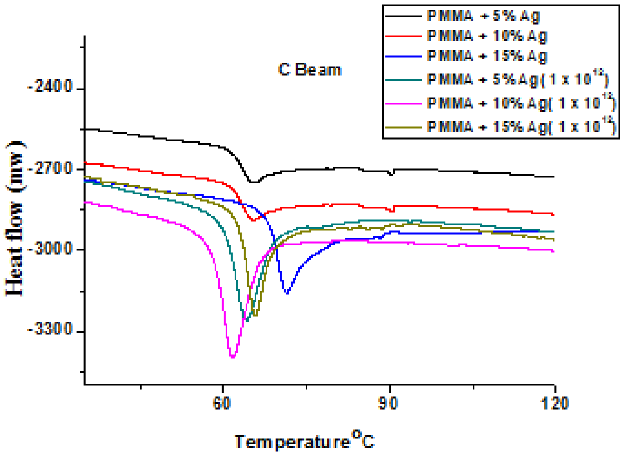

(b)

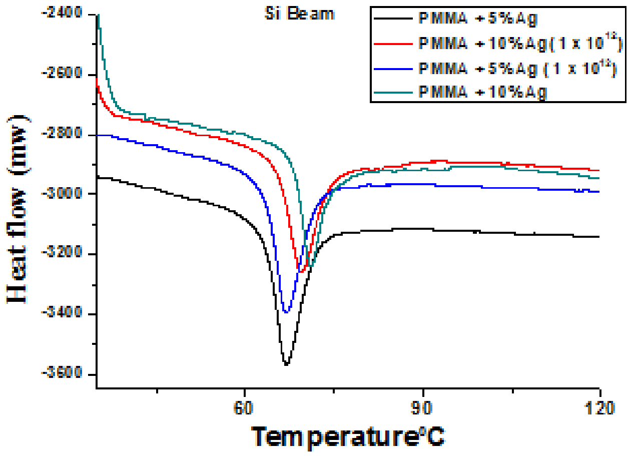

(c)

Fig. 3.2 DSC thermo grams for (a) Pure and composites, (b) Composites for C beam, (c) Composites for Si beam

collected as shown in Fig. 3.2(a, b, c). The pure PMMA has a Tg value of 64.60^{o}C, while tendency of increase of Tg value after inclusion of silver nanoparticles was observed for Ag/PMMA nanocomposites. The interaction of polymer chains and nanoparticles surface can alter the chain kinetics by decreasing or increasing glass transition temperature of the polymer [11]. We found the value of Tg, for pristine and irradiated samples is listed in Table 3.2 for highest fluence of C beam and Si beam.

Table 3.2 Values of glass transition for pristine and irradiated composites

Sample name	Tg (Pristine)	Tg (C beam)	Tg (Si beam)
PMMA + 5 %Ag	65.8	64.1	63.1
PMMA + 10 %Ag	66.1	64.8	63.2
PMMA + 15 %Ag	71.4	65.8	64.2

Ash et al [12] explained the decrease of Tg values in terms of thin film model. When the inter-particles distance is small enough, then the polymer between two particles can be considered as a thin film. Assuming that there is small or no interfacial interaction between the filler and matrix exists and then Tg decreases.

3.1.3 Optical response:

Ultraviolet-visible spectroscopy provides an idea about the optical band-gap energy (*E*g), and thus a significant tool for investigation. The absorption of light energy by polymeric materials in the ultraviolet and visible regions involves promotion of electrons in σ, π and n orbitals from the ground state to higher energy states which are explained by molecular orbitals [13]. The following types of electronic transitions $\sigma \rightarrow \sigma^*$, $n \rightarrow \sigma^*$, $n \rightarrow \pi^*$, and $\pi \rightarrow \pi^*$ are involved in the ultraviolet and visible regions. Many of the optical transitions which resulted due to the presence of impurities have energies in the visible part of the spectrum; consequently the defects are referred to as colour centres [14]. The decrease in energy band gap of the composites upon irradiation which leads to the formation of new defects and new charge states, due to breakage of bonds and formation of free radicals, unsaturation etc [15].

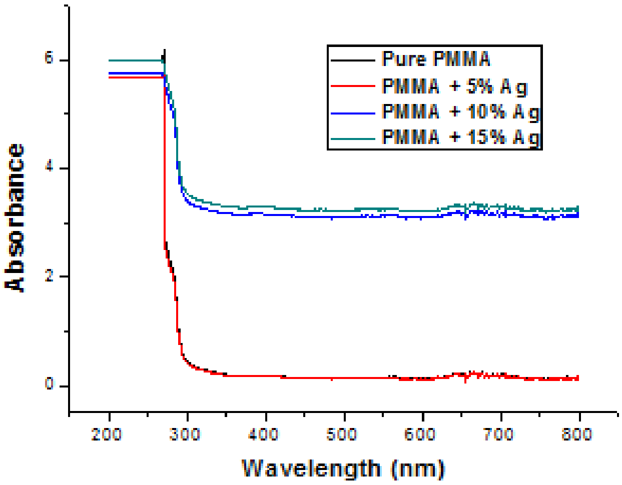
Absorbance
Wavelength (nm)
0
2
4
6
200
300
400
500
600
700
800
Pure PMMA
PMMA + 5% Ag
PMMA + 10% Ag
PMMA + 15% Ag

(a)

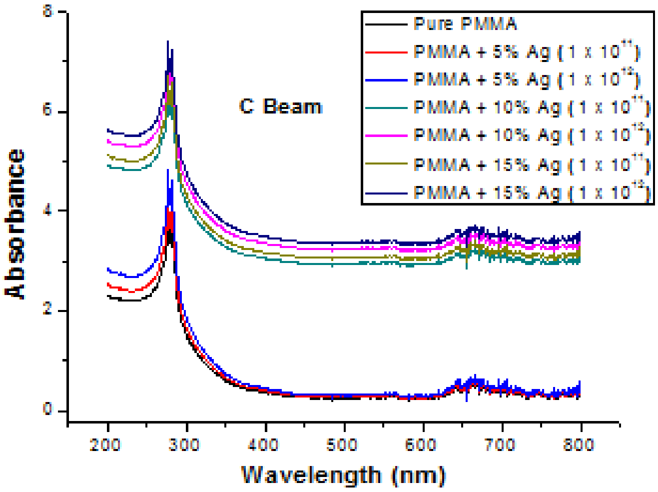
Absorbance
Wavelength (nm)
C Beam
0
2
4
6
8
200
300
400
500
600
700
800
Pure PMMA
PMMA + 5% Ag (1 x 10^{11})
PMMA + 5% Ag (1 x 10^{12})
PMMA + 10% Ag (1 x 10^{11})
PMMA + 10% Ag (1 x 10^{12})
PMMA + 15% Ag (1 x 10^{11})
PMMA + 15% Ag (1 x 10^{12})

(b)

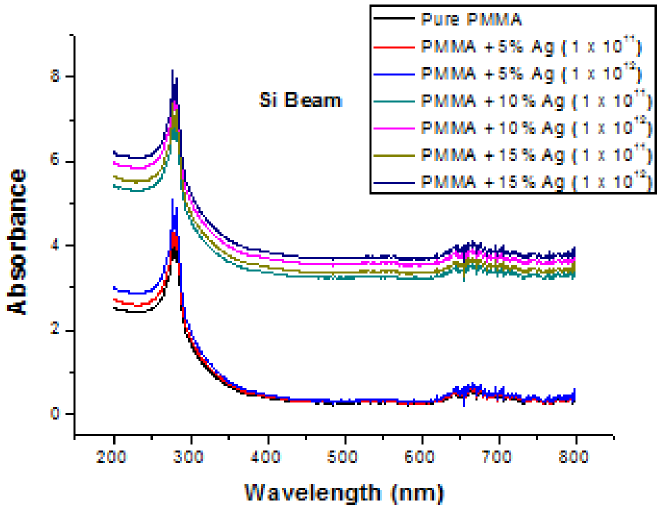

(c)

Fig. 3.3 Absorbance spectra for (a) pristine (b) irradiated by C-beam (c) irradiated by Si- beam

Determinations of band gap

Optical feature of the pristine and irradiated samples have been studied by Perkin-Elmer 25 Lambda UV-Visible spectroscope in the frequency range 200-800 cm^{-1} as illustrated in Fig.3.3 (a, b, c). The optical band gap E_g is obtained by tauc's equation [16] as discussed in chapter 2 in the section 2.3.3 by the relation 2.2.4.

i. e.

$$\omega\varepsilon(\lambda) = (\hbar\omega - E_g)^2$$

Where $\varepsilon(\lambda)$ is the optical absorbance and λ is the wavelength. The intersection of the extrapolated spectrum with the abscissa of the plot $\varepsilon^{1/2}/\lambda$ versus $1/\lambda$ yields the gap wavelength λ_g from which the energy gap is derived as $E_g = hc/\lambda_g$. It is noticed that the band gap (energy gap) value shifted to lower energy from 4.58 eV upto 3.21 eV due to doping of silver nanoparticles and also upon irradiation. This is because of the scissioning of polymer chain and as a result, creation of free radicals, unsaturation etc. and thus a capability of increasing the conductivity of the composites [17].

The number of carbon atoms per cluster can be calculated by and shown in Table 3.3[14] from the relation 2.2.5 as explained in chapter 2.

$E_g = 34.3/\sqrt{N}$ eV

Where, N is the number of carbon atoms per cluster and Eg is the energy band gap.

Table 3.3 Band gap (B.G) and no. of carbon atoms (N) of pristine and irradiated samples

Sample	Pristine	C Beam		Si Beam	
	B.G eV	B.G eV 1 x 10^{11} ions/cm^2	B.G eV 1 x 10^{12} ions/cm^2	B.G eV 1 x 10^{11} ions/cm^2	B.G eV 1 x 10^{12} ions/cm^2
Pure PMMA	4.58	4.50	4.38	4.36	4.26
PMMA + 5%Ag	4.28	4.21	4.10	4.05	3.87
PMMA + 10%Ag	4.10	4.01	3.89	3.80	3.52
PMMA + 15%Ag	3.82	3.75	3.65	3.61	3.21

Sample	Pristine	C Beam		Si Beam	
	No. of carbon atoms(N)	No. of carbon atoms(N) 1 x 10^{11} ions/cm^2	No. Of carbon atoms(N) 1 x 10^{12} ions/cm^2	No. of carbon atoms(N) 1 x 10^{11} ions/cm^2	No. Of carbon atoms(N) 1 x 10^{12} ions/cm^2
Pure PMMA	56	58	61	62	65
PMMA + 5%Ag	64	66	70	72	78
PMMA + 10%Ag	70	73	77	81	95
PMMA + 15%Ag	80	84	88	90	114

3.1.4 Surface morphology:

Fig. 3.4(a–f) shows the SEM images of pristine, composites and irradiated (1 x 10^{12} ions/cm^2) composite films with magnification of X250. The analysis shows that the filled particles are distributed randomly in the matrix which display continuous contact between themselves and formed conducting paths. The surface roughness is observed to increase upon irradiation. The increase in roughness with Ag-nanoparticles may be attributed to the increase in density and size of metal particles on the surfaces of the films, which is also responsible for decrease in crystallinity of the material as indicated by XRD analysis [18].

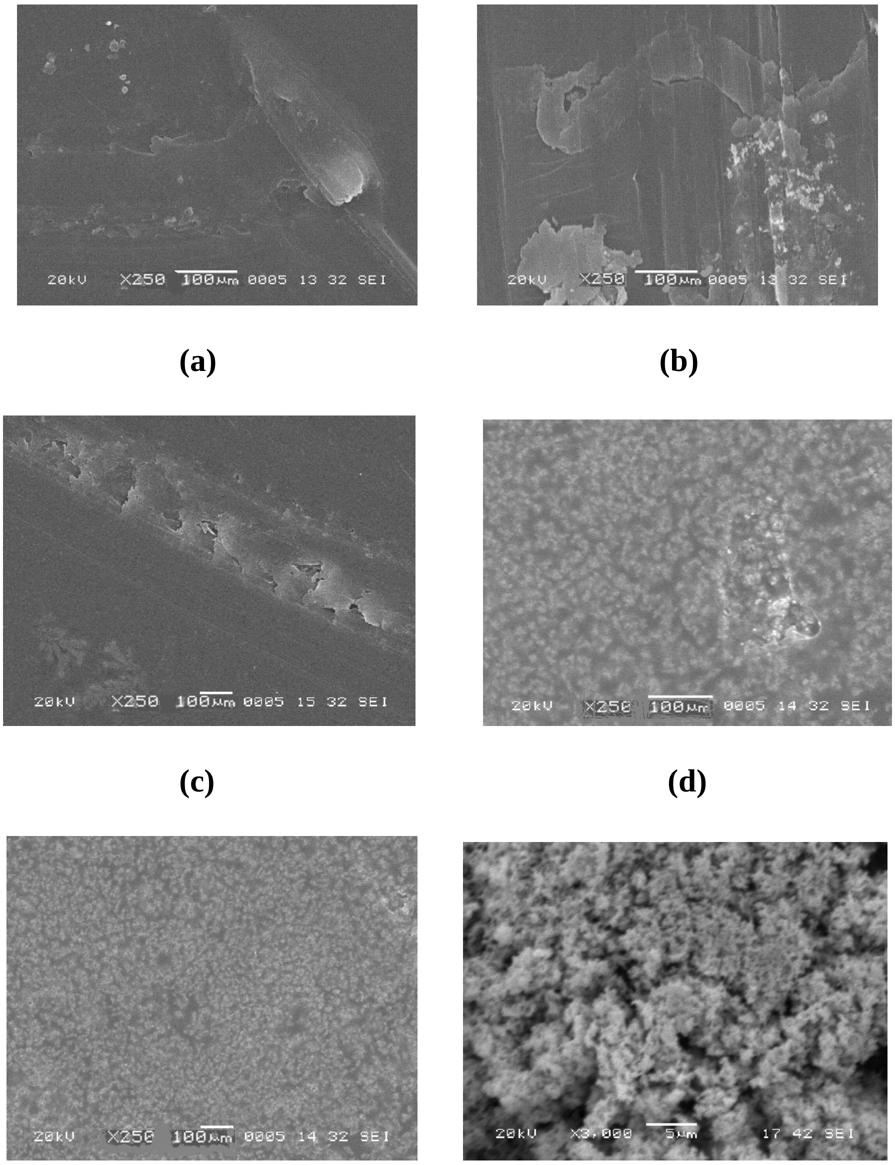

(a) **(b)**

(c) **(d)**

(e) **(f)**

Fig. 3.4 SEM Images for (a) Pure PMMA (b) PMMA irradited (C beam) (c) PMMA+15% Ag (d) PMMA+15% Ag (C Beam) (e) PMMA+15% Ag (Si beam) (f) Ag nanoparticles

3.1.5 AC Electrical Frequency Response:

Conductivity: AC electrical measurement was carried out for pristine and irradiated samples. The conductivity was calculated by relation (2.2.20) as discussed in chapter 2 in section (2.3.6(a)). Fig. 3.5 (a-e) shows the variation of conductivity with log of frequency for the pristine and irradiated samples at different silver nanoparticles concentrations. I

t was revealed that the conductivity increases with increasing concentration of dispersed nanoparticles and also with irradiation fluences. The increase in conductivity with different concentrations of silver nanoparticles for pristine samples may be attributed to the conductive phase formed by dispersed nanoparticles in polymer matrix. It is known that electrical conductivity of such composites depends on the type and concentration of the dispersed compound [19, 20]. It is also observed that the conductivity increases upon irradiation. Irradiation is expected to promote the metal to polymer bonding and convert the polymeric structure in to a hydrogen depleted carbon network. It is this carbon network that is believed to make the polymers more conductive [18].

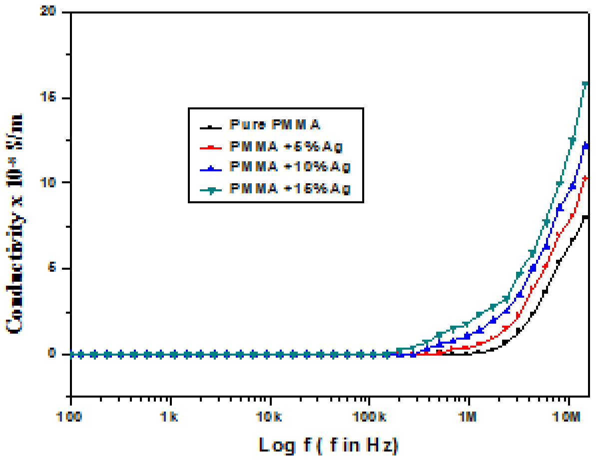

(a)

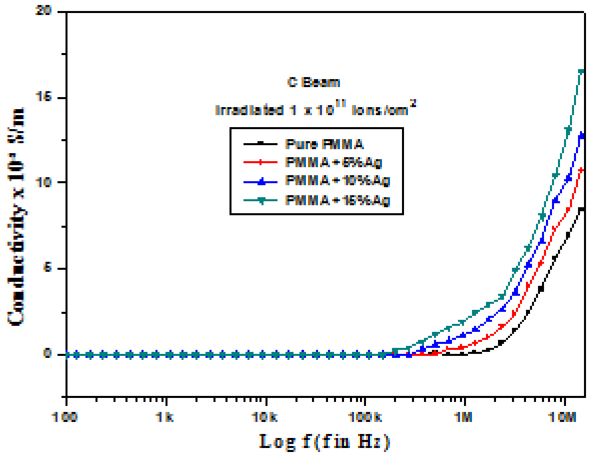
C Beam
Irradiated 1 x 10^{11} Ions/cm^2
Pure PMMA
PMMA+5%Ag
PMMA+10%Ag
PMMA+15%Ag
Conductivity x 10^{-4} S/m
20
15
10
5
0
100
1k
10k
100k
1M
10M
Log f(f in Hz)

(b)

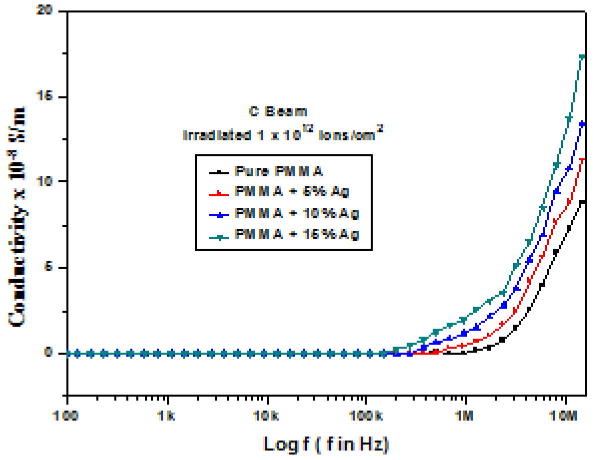
C Beam
Irradiated 1 x 10^{12} Ions/cm^2
Pure PMMA
PMMA + 5% Ag
PMMA + 10% Ag
PMMA + 15% Ag
Conductivity x 10^{-4} S/m
20
15
10
5
0
100
1k
10k
100k
1M
10M
Log f (f in Hz)

(c)

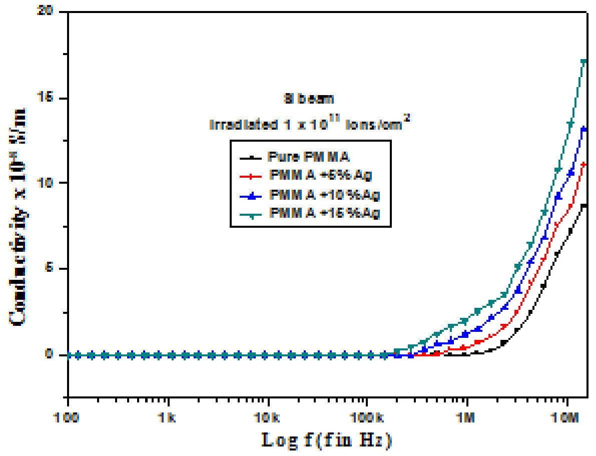
Si beam
Irradiated 1 x 10^{11} Ions/cm^2
Pure PMMA
PMMA +5% Ag
PMMA +10% Ag
PMMA +15% Ag
Conductivity x 10^{-4} S/m
20
15
10
5
0
100
1k
10k
100k
1M
10M
Log f(f in Hz)

(d)

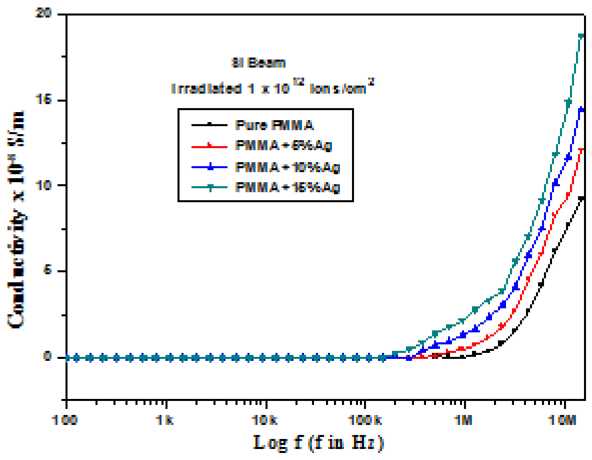

(e)

Fig. 3.5 Conductivity Vs Log f for (a) pristine (b) C beam (1 x 10^{11} ions/cm^2) (c) C beam (1 x 10^{12} ions/cm^2) (d) Si beam (1 x 10^{11} ions/cm^2) (e) Si beam (1 x 10^{12} ions/cm^2)

Dielectric properties of composites:

The variation of dielectric constant with respect to frequency for the PMMA/ silver nano particles composites at different filler concentrations are shown in Figure 3.6 (a-e). The effective dielectric constant in nanocomposites is determined by dielectric polarization i.e. interfacial polarization between polymer and particles [21]. It is well recognized that nanocomposites have a huge volume fraction of interfaces where interfacial polarizations are most likely to occur. When the fillers are dispersed in the insulating polymer, the dielectric constant of composites increases with concentration of fillers [22].

As apparent from Fig. 3.6, the dielectric constant remains almost constant up to 100 kHz. At these frequencies, the motion of free charge carriers may be assumed constant through the polymer matrix**.** Ion migration in solids is assumed to be dependent on the hoping rate *i.e.* the jumping frequency of the ions, which has a unique value for an ion. Therefore, the nearly constant value of dielectric constant may be due to the presence of some ionic species in excess amount [23]. It is also

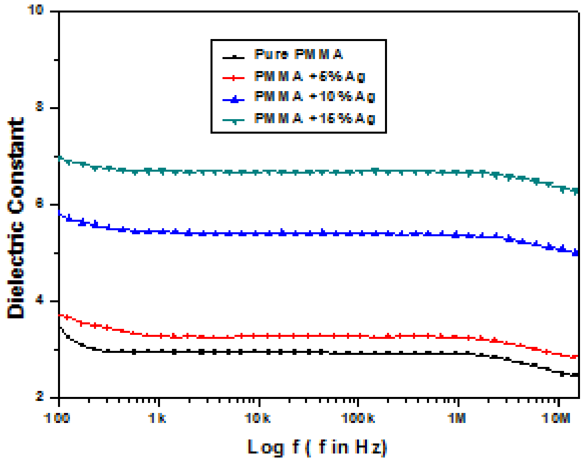
Dielectric Constant
10
8
6
4
2
100
1k
10k
100k
1M
10M
Log f (f in Hz)
Pure PMMA
PMMA +5% Ag
PMMA +10% Ag
PMMA +15% Ag

(a)

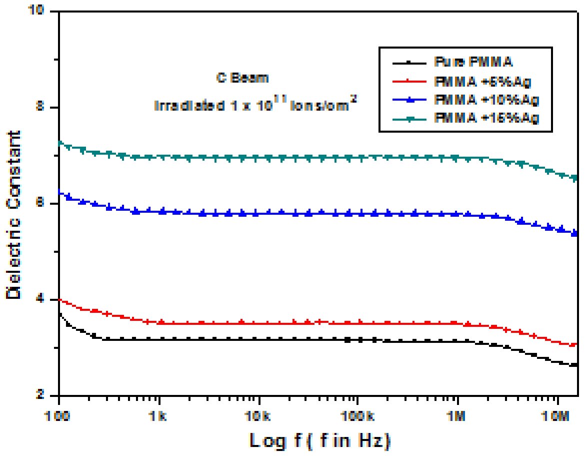
Dielectric Constant
10
8
6
4
2
100
1k
10k
100k
1M
10M
Log f (f in Hz)
C Beam
Irradiated 1 x 10^11 Ions/cm^2
Pure PMMA
PMMA +5%Ag
PMMA +10%Ag
PMMA +15%Ag

(b)

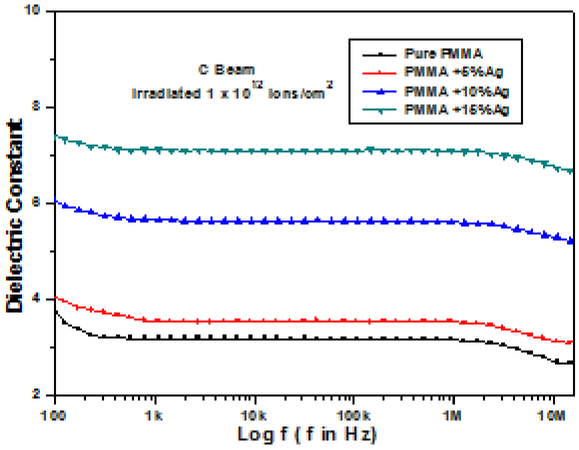
Dielectric Constant
10
8
6
4
2
100
1k
10k
100k
1M
10M
Log f (f in Hz)
C Beam
Irradiated 1 x 10^12 Ions/cm^2
Pure PMMA
PMMA +5%Ag
PMMA +10%Ag
PMMA +15%Ag

(c)

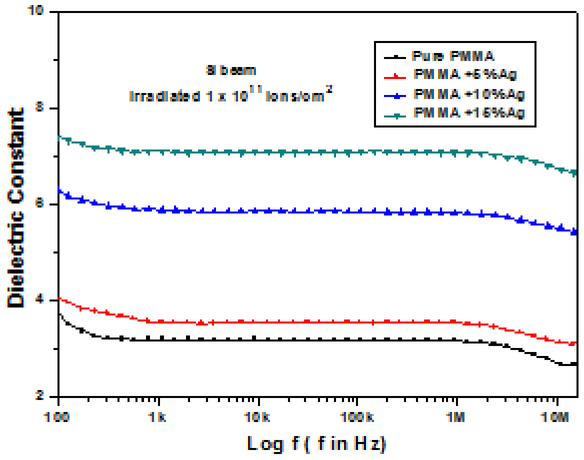

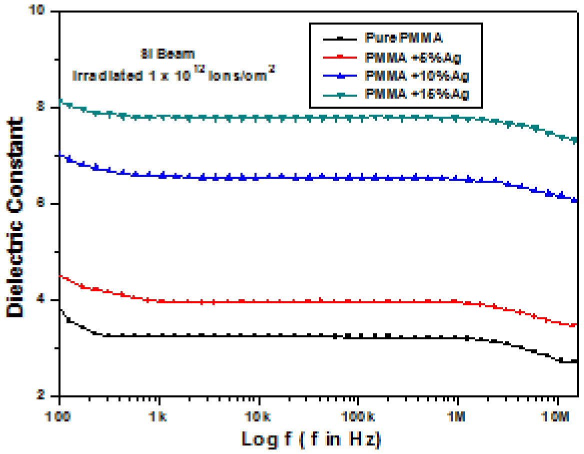

(e)

Fig. 3.6 Dielectric constant Vs Log f for (a) pristine (b) C beam (1 x 10^{11} ions/cm^2) (c) C beam (1 x 10^{12} ions/cm^2) (d) Si beam (1 x 10^{11} ions/cm^2) (e) Si beam (1 x 10^{12} ions/cm^2)

observed that dielectric constant increases for irradiated films. The increase in dielectric constant may be attributed to the chain scission and as a result the increase in the number of free radicals, unsaturation etc. As frequency increases further (i.e., beyond 100 kHz), the charge carriers migrate through the dielectric and get trapped against a defect sites and induced an opposite charge in its vicinity. At these frequencies, the polarization of trapped and bound charges cannot take place and hence the dielectric constant decreases [24]. The observed nature of the fluence dependence of dielectric constant in studied frequency range can be explained by the prevailing influence of the enhanced free carriers due to irradiation [25].

Fig. 3.7 (a-e) shows the variation of dielectric loss with log frequency for pristine and irradiated samples of pure PMMA and silver nanoparticles dispersed PMMA films at different concentrations. In general, the dielectric loss of the dielectric material causes from distortional, dipolar, interfacial, and conduction loss. The distortional loss is related to electronic and ionic polarization mechanisms. The interfacial loss created from the excessive polarized interface induced by the fillers and specifically the movement or rotation of the atoms or molecules in an alternating electric field. The conduction loss is featured to the dc electrical conductivity of the materials, representing the flow of actual charge through the dielectric materials [26].

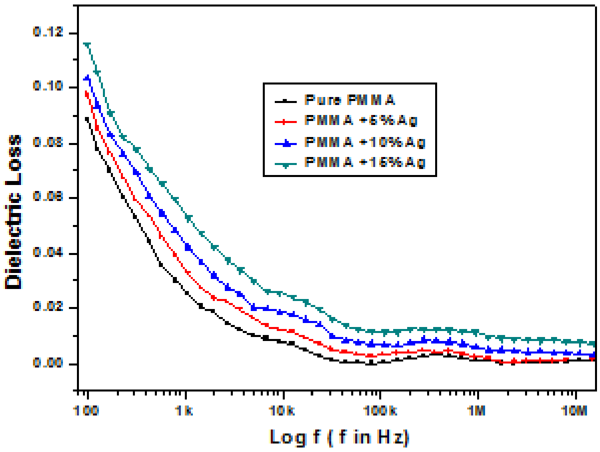

(a)

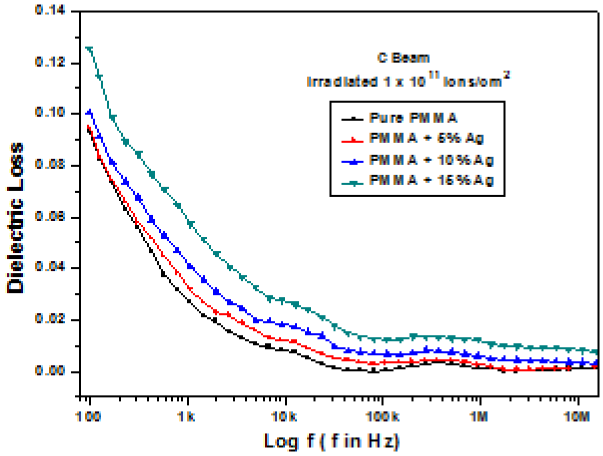
C Beam
Irradiated 1 x 10^{11} Ions/cm^2
Pure PMMA
PMMA + 5% Ag
PMMA + 10% Ag
PMMA + 15% Ag
Dielectric Loss
0.14
0.12
0.10
0.08
0.06
0.04
0.02
0.00
100
1k
10k
100k
1M
10M
Log f (f in Hz)

(b)

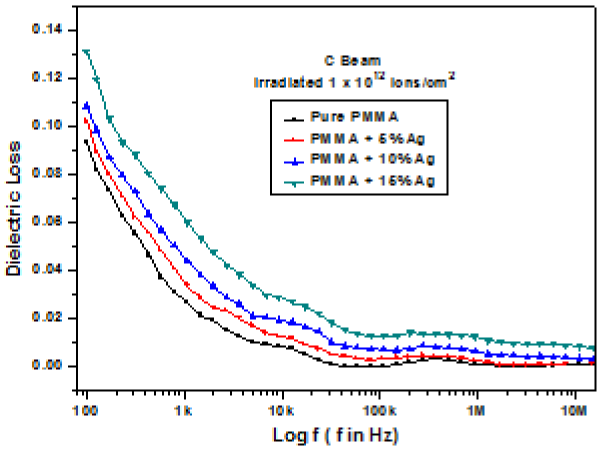
C Beam
Irradiated 1 x 10^{12} Ions/cm^2
Pure PMMA
PMMA + 5% Ag
PMMA + 10% Ag
PMMA + 15% Ag
Dielectric Loss
0.14
0.12
0.10
0.08
0.06
0.04
0.02
0.00
100
1k
10k
100k
1M
10M
Log f (f in Hz)

(c)

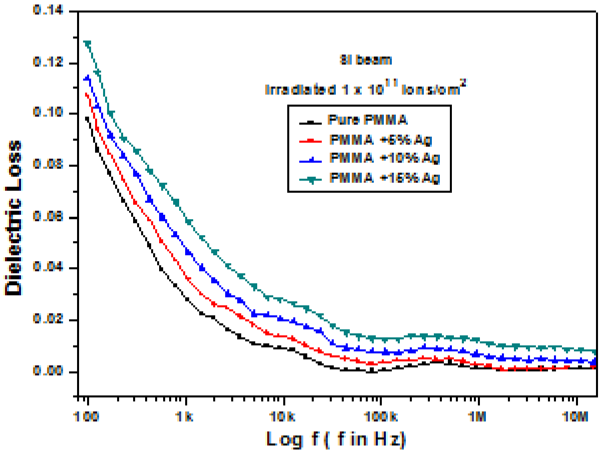
Si beam
Irradiated 1 x 10^{11} Ions/cm^2
Pure PMMA
PMMA +5% Ag
PMMA +10% Ag
PMMA +15% Ag
Dielectric Loss
0.14
0.12
0.10
0.08
0.06
0.04
0.02
0.00
100
1k
10k
100k
1M
10M
Log f (f in Hz)

(d)

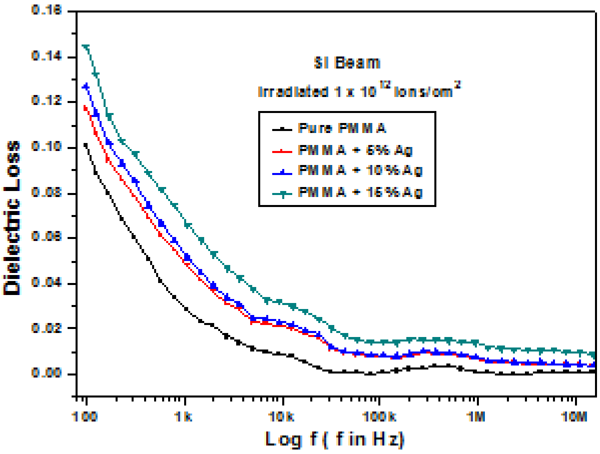

(e)

Fig. 3.7 Dielectric loss Vs Log f for (a) pristine (b) C beam (1 x 10^{11} ions/cm^2) (c) C beam (1 x 10^{12} ions/cm^2) (d) Si beam (1 x 10^{11} ions/cm^2) (e) Si beam (1 x 10^{12} ions/cm^2)

The dielectric loss decreases exponentially with the increase of log frequency. It is noticed that dielectric loss increases moderately with the concentration of filler and also with upon both ion beams irradiations which may be attributed to the interfacial polarization mechanism of the heterogeneous system [26].

Conclusion:

Dispersion of silver nanoparticles in PMMA films has enhanced the properties of the pure polymer significantly. The increase in dielectric properties with different concentrations may be pointed to the conductive phase formed by dispersed nanoparticles in polymer matrix. Ion beam irradiation also has been shown to significantly enhance the dielectric properties which may be due to conversion of the polymeric structure into a hydrogen-depleted carbon network. It was found that the band gap value moved to lower energy (from 4.58 eV upto 3.21 eV) on doping with silver nanoparticles as well as upon irradiation from the UV- visible spectroscopy analysis. An XRD analysis reveals that the crystallite size of the samples decreased after ion beam irradiation which is also corroborated with the DSC analysis due to the chain scissioning upon irradiation. So we have concluded that effect of Si-beam is more effective than that of the C-beam because of large energy loss of heavy ion.

3.2 Effect of swift heavy ions irradiation on PS + Ag nanocomposites:

3.2.1 X-ray diffraction analysis:

The XRD patterns of composites are shown in Fig. 3.8(a-e). The figure clearly indicates that silver is crystalline, but the polymer is amorphous in nature and its composites show a semi-crystalline behavior. The diffraction patterns of the irradiated samples exhibited an increase in the peak intensity and a decrease in the full width at half-maximum (FWHM) corresponding to all observed peaks of silver. The average crystallite size *(t)* for pristine and irradiated samples was calculated using Scherrer's formula [9] as discussed in chapter 2 in section 2.3.1 from relation 2.2.3.

$b=K\lambda/L\cos\theta$

where b is FWHM in radians, λ is the wavelength of X-ray beam (1.5418 Å), L is the crystallite size in Å, K is a constant which varies from 0.89 to 1.39, but for most of the cases it is close to 1.

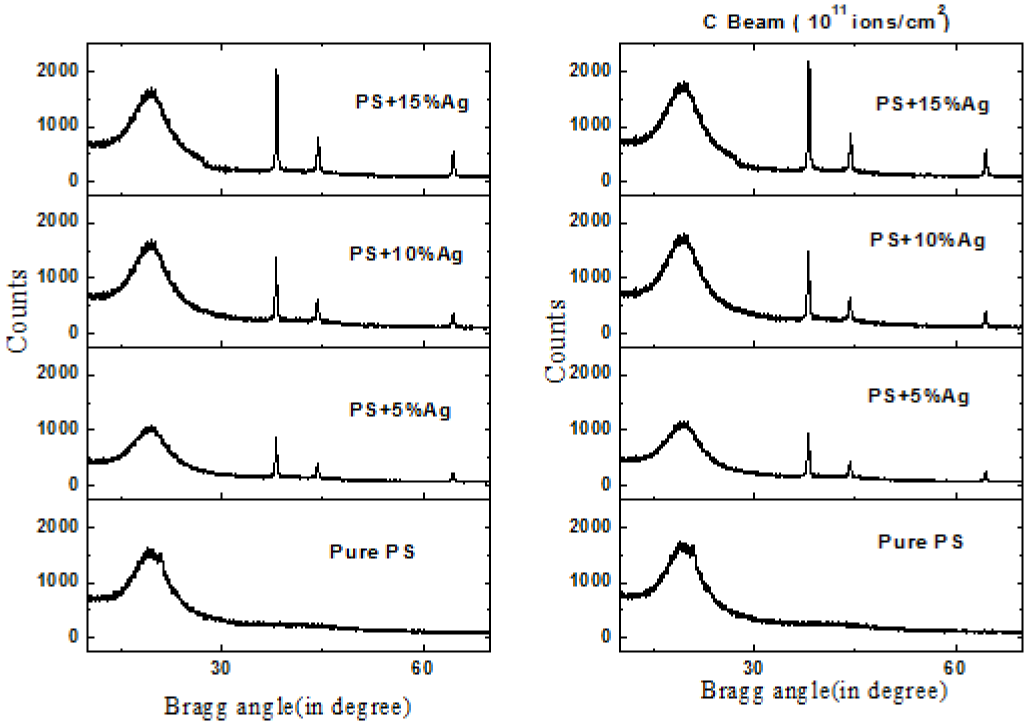

(a) (b)

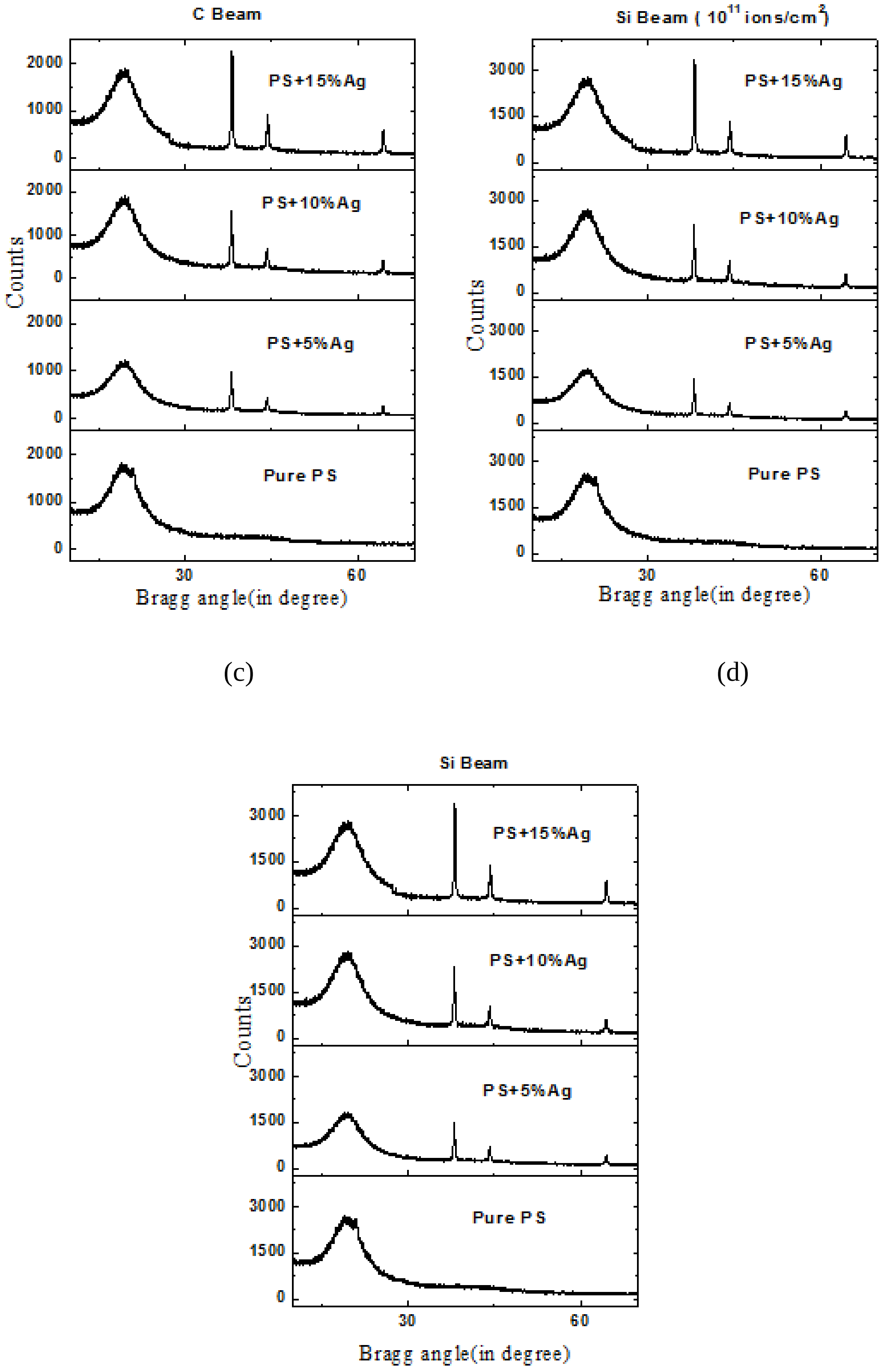

(c) (d)

(e)

Fig. 3.8 X-ray diffraction patterns of (a) PS+ Ag (pristine) (b) C beam (1 x 10^{11} ions/cm^2) (c) C beam (1 x 10^{12} ions/cm^2) (d) Si beam (1 x 10^{11} ions/cm^2) (e) Si beam (1 x 10^{12} ions/cm^2)

Table 3.4 Crystallite size of pristine and irradiated samples

Sample	Pristine		C Beam		Si Beam	
	2θ	Crystallite size (nm)	Crystallite size (nm) (1x10^{11}) ions/cm^2	Crystallite size (nm) (1x10^{12}) ions/cm^2	Crystallite size (nm) (1x10^{11}) ions/cm^2	Crystallite size (nm) (1x10^{12}) ions/cm^2
PS + 5%Ag	38.04	38.79	38.86	38.98	39.11	39.67
	44.22	36.95	37.18	37.95	37.89	38.19
	64.38	35.12	36.11	38.75	37.43	39.54
	Average	36.95	37.38	38.56	38.14	39.13
PS + 10%Ag	38.05	36.19	37.11	37.94	38.43	38.97
	44.21	38.13	38.21	38.54	38.45	39.58
	64.14	40.14	40.67	40.92	41.76	42.31
	Average	38.15	38.66	39.13	39.27	40.28
PS + 15%Ag	37.87	37.98	38.25	38.51	38.46	38.88
	44.11	37.87	38.01	38.19	38.34	38.90
	64.01	41.92	42.28	43.12	43.11	44.67
	Average	39.26	39.51	39.94	39.97	40.82

The crystallite size was calculated corresponding to the peak of the pristine and irradiated samples, and the results are listed in Table 3.4 [27]. It is observed that crystallite size increasing with filler concentrations and with irradiation fluence. The increase in crystallite size may be attributed to the cross linking phenomenon.

3.2.2. Thermal response (Differential scanning calorimetry (DSC)):

Fig.3.9 shows the influence of different concentrations of silver nanoparticles on the glass transition behavior of the polymer matrix. At the glass transition temperature, the weak secondary bonds that stick the polymer chains together are broken, and the macromolecule starts to move. The interaction of polymer chains and nanoparticle

Table 3.5 Values of glass transition for pristine and irradiated composites

Sample name	Tg (Pristine)	Tg (C beam)	Tg (Si beam)
PS + 5 %Ag	65.2	65.7	66.2
PS + 10 %Ag	70.8	71.4	72.1
PS + 15 %Ag	71.9	72.7	73.2

surfaces can alter the chain kinetics by decreasing or increasing the glass transition temperature of the polymer. *T*g of pure PS is observed at 66.5°C. The Tg of pristine composite samples increased with filler contents and it further increased upon both ion beams irradiations to the higher temperature side as shown in Fig. 3.9 (a, b, c). This behavior probably arises due to branching (cross-linking effect) when islands of nanoparticles are bonded with polymeric chains. This lowers the mobility of the chains, and as a result, the glass transition temperature increases in the nanocomposites [28].

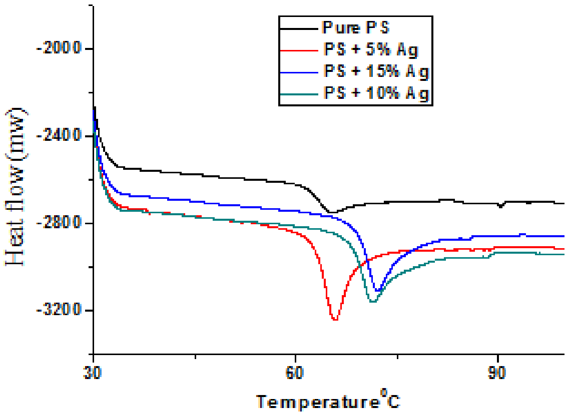

(a)

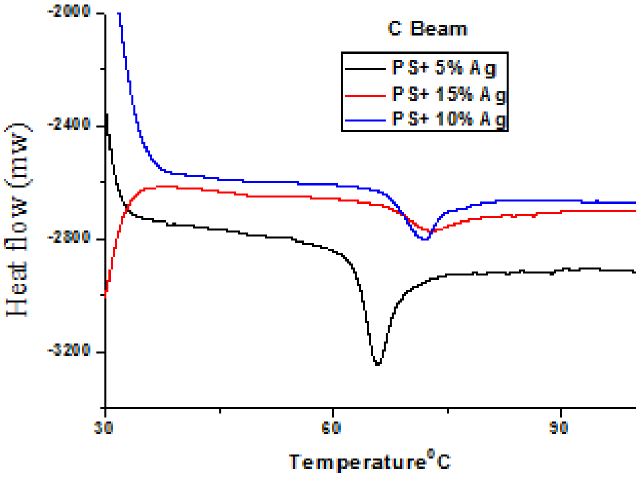

(b)

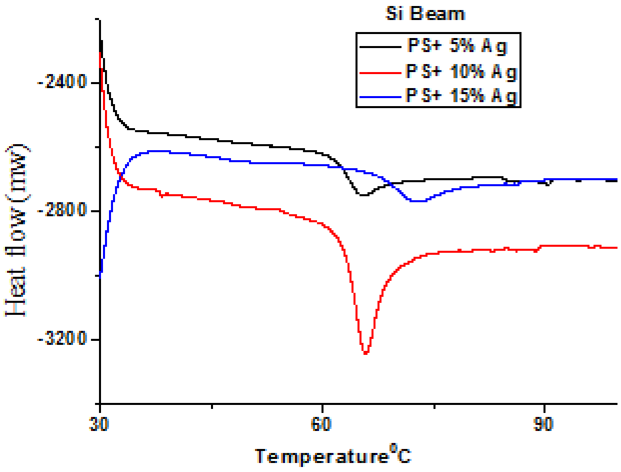

(c)

Fig. 3.9 DSC thermo grams for (a) pristine (b) Irradiated by C beam (1 x 10^{12} ions/cm^2) (C) Irradiated by Si beam (1 x 10^{12} ions/cm^2)

3.2.3 Optical response:

UV–vis spectroscopy is an important tool to investigate the value of optical band gap energy (Eg). The electronic transitions (→) that are involved in the ultraviolet and visible regions are of the following type σ → σ *, n → π*, and π → π* [29]. The absorbance edge of the UV-vis spectra of pristine nanocomposites and irradiated by C ions and Si ions as shown in Fig.3.10. The absorbance in aromatic compounds is due to the π to π* transition. This is very sensitive to the change in the environment around the phenyl ring [30]. It is observed that optical absorption increases with increasing energy loss and this absorption shifts from UV–vis towards the visible region for all irradiated nanocomposite samples. With increase of electronic energy loss the nanocomposites become gradually opaque to the visible light and the absorption edge shifts from UV to visible region. This is consistent with the observation that the material changes from transparent to opaque with increase of energy deposition. The increase in absorption with irradiation may be attributed to the formation of a conjugated system of bonds due to bond cleavage and reconstruction [31]. The shifting of absorption edge towards visible is generally considered to result from carbonization of the material under irradiation [32] which is also corroborated with the dielectric results.

Determination of optical band gap:

Optical feature of the pristine and irradiated samples have been studied by Perkin-Elmer 25 Lambda UV-Visible spectroscope in the frequency range 200-800 cm^{-1} as illustrated in Fig. 3.10(a-e). The optical band gap E_g is obtained by tauc's equation [16] as discussed in chapter 2 in the section 2.3.3 by the relation 2.2.4.

i. e. $\omega\varepsilon(\lambda) = (\hbar\omega - E_g)^2$

Where ε(λ) is the optical absorbance and λ is the wavelength. The intersection of the extrapolated spectrum with the abscissa of the plot $\varepsilon^{1/2}/\lambda$ versus $1/\lambda$, yields the gap wavelength λ_g from which the energy gap is derived as $E_g = hc/\lambda_g$. It is noticed that the band gap (energy gap) value shifted to lower energy from 4.38 eV upto 3.30 eV due to doping of silver nanoparticles and also upon irradiation by both ions beams. The decrease of the optical gap of ion-irradiated samples can be explained by the model of Robertson and O Reilly [33, 34]. They explained that the decrease in the band gap might be attributed to the transformation from separated aromatic rings to a structure similar to graphite with increasing fluences.

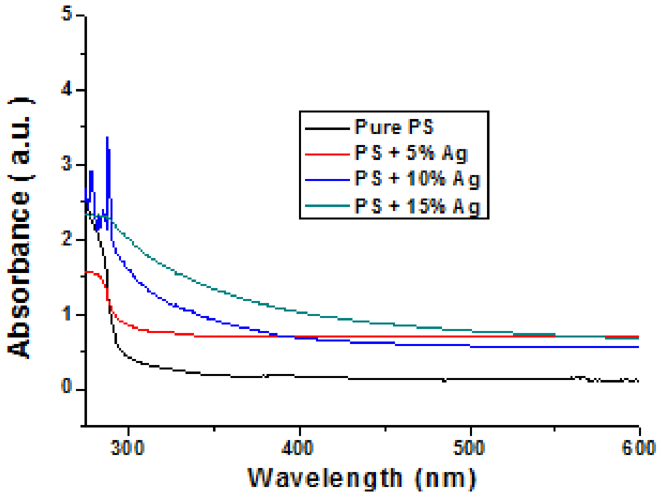

(a)

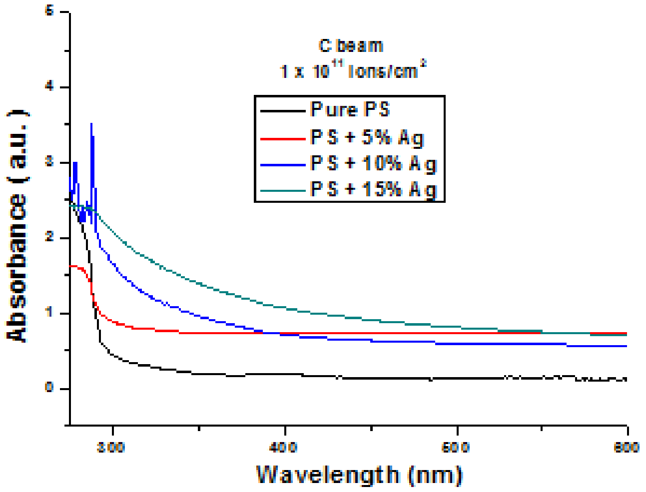

(b)

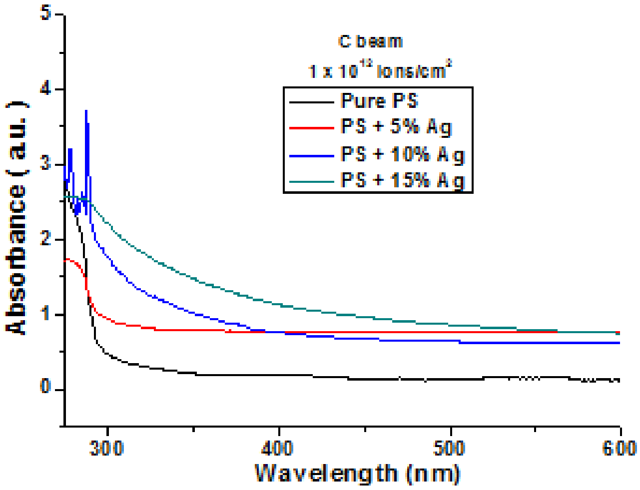
C beam
1 x 10^12 Ions/cm^2
Pure PS
PS + 5% Ag
PS + 10% Ag
PS + 15% Ag
Absorbance (a.u.)
0
1
2
3
4
5
300
400
500
600
Wavelength (nm)

(c)

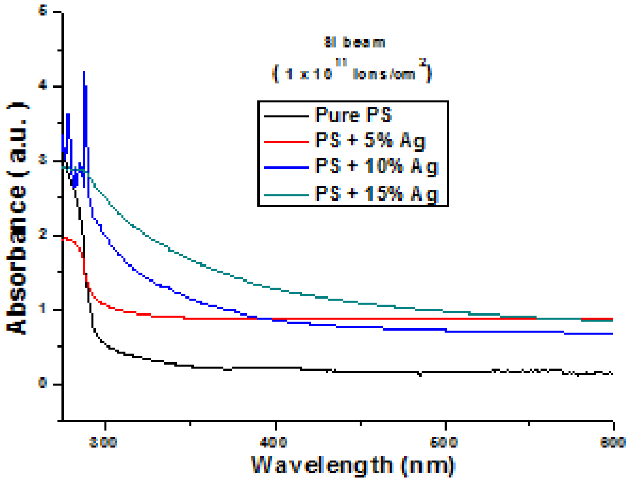
SI beam
(1 x 10^11 Ions/cm^2)
Pure PS
PS + 5% Ag
PS + 10% Ag
PS + 15% Ag
Absorbance (a.u.)
0
1
2
3
4
5
300
400
500
600
Wavelength (nm)

(d)

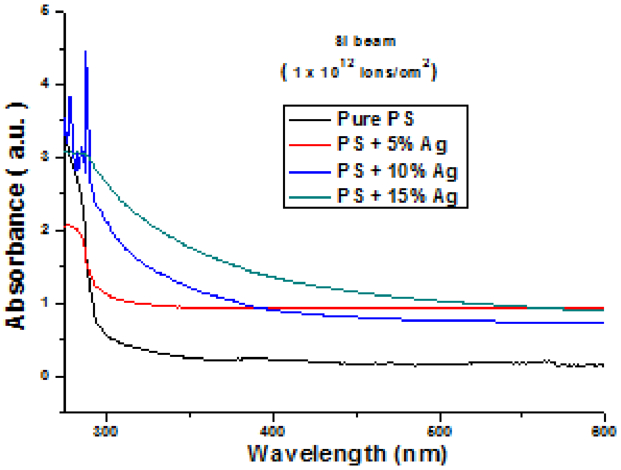

(e)

Fig. 3.10 Absorbance spectra of (a) Pristine (b) Irradiated by C beam (1 x 10^{11} ions/cm^2) (c) Irradiated by C beam (1 x 10^{12} ions/cm^2) (d) Irradiated by Si beam (1 x 10^{11} ions/cm^2) (e) Irradiated by Si beam (1 x 10^{12} ions/cm^2)

The number of carbon hexagon rings [33] in the cluster (M) is then found from the relation 2.2.6 as explained in chapter 2 in section 2.3.3.

$$Eg \approx 2\,|\beta| / \sqrt{M}$$

Where, |β| is a bond integral that represents the interaction energy of two π atomic orbitals. A theoretical value for |β| proposed by Robertson and O Reilly is 2.9 eV, which according to Compagnini et al. [34] is an overestimation of the true value. So, the best-fit value of |β| given by them is 2.2 eV. In the present study on the aromatic polymer, given equation has been used to calculate the value of M and its behaviour with different ions is summarized in Table 3.6. The number of rings (M) remains constant with the filler and upon irradiation except for Si-ions at a fluence of 1 x 10^{12} ions/cm^2.

Table 3.6 Band gap by direct allowed transitions, number of carbon atoms in pure PS, composites and irradiated films.

Sample	Pristine		C Beam		Si Beam	
	Band gap in eV	No. of carbon hexagon rings	Band gap in eV	No. of carbon hexagon rings	Band gap in eV	No. of carbon hexagon rings
Pure PS	4.38	~1	4.21	~1	3.89	~1
PS + 5%Ag (1 x 10^{11} ions/cm^2)	4.33	~1	4.11	~1	3.89	~1
PS + 5%Ag (1 x 10^{12} ions/cm^2)	4.28	~1	3.90	~1	3.87	~1
PS + 10%Ag (1 x 10^{11} ions/cm^2)	4.21	~1	3.88	~1	3.70	~1
PS + 10%Ag(1 x 10^{12} ions/cm^2)	4.15	~1	3.78	~1	3.50	~1
PS + 15%Ag (1 x 10^{11} ions/cm^2)	4.10	~1	3.70	~1	3.44	~1
PS + 15%Ag(1 x 10^{12} ions/cm^2)	3.90	~1	3.60	~1	3.30	~2

3.2.4 Surface morphology:

Fig. 3.11(a–e) shows the SEM images of pristine, composites and irradiated composite films with magnification of X250. The analysis shows that the filled partilces are distributed randomly in the matrix which display continuous contact between themselves and formed conducting paths. The surface becomes smoothen upon irradiation.The decrease in roughness with Ag-nanoparticles may be attributed to the decrease in density of metal particles on the surfaces of the films, which is also responsible for increase in crystallinity of the material as indicated by XRD analysis.

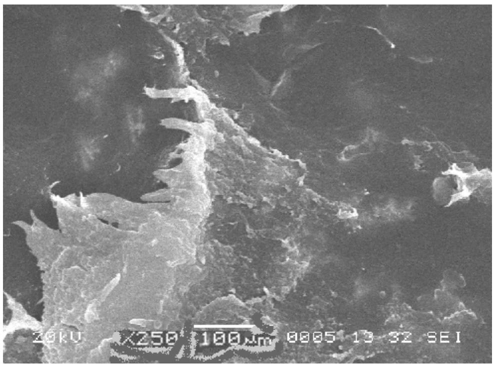

(a)

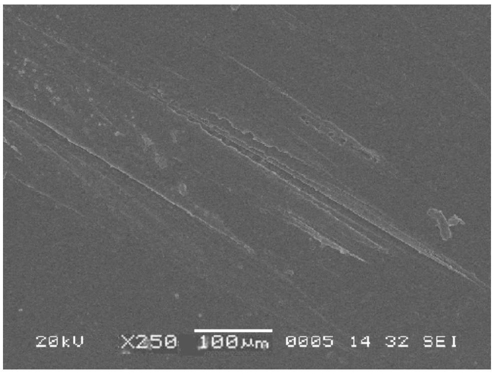

(b)

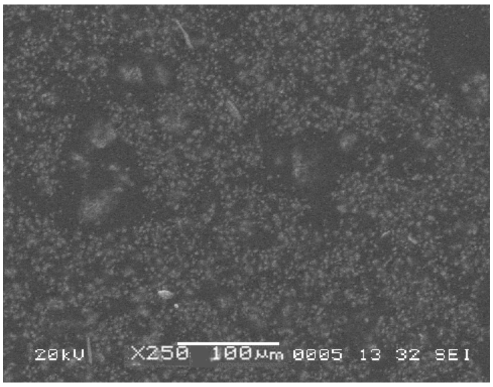

(c)

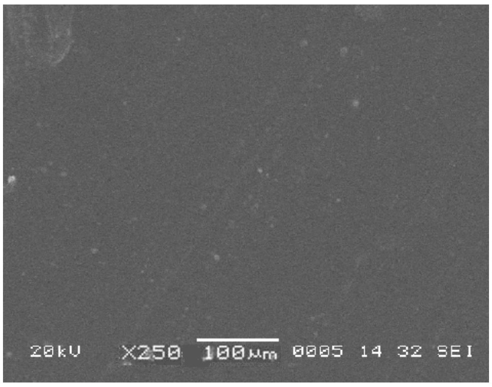

(d)

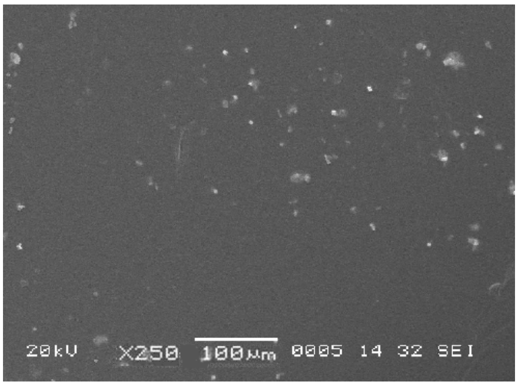

(e)

Fig. 3.11 SEM Images for (a) Pure PS (b) PS irradited (C beam) (c) PS+15% Ag (d) PS+15% Ag (C Beam) (e) PS+15% Ag (Si beam)

3.2.5 AC electrical frequency response:

Conductivity: Fig. 3.12(a-e) shows the frequency dependent ac electrical conductivity of pristine and irradiated composites. The increase in conductivity with silver nanoparticles concentration for pristine samples may be attributed to the conductive phase formed by dispersed metal nanoparticles in polymer matrix. It is known that electrical conductivity of such composites depends on the type and concentration of the dispersed compound [20, 21]. The increase in conductivity is related to a possible increase in the number of conduction paths created between the filler particles aggregates in the composite and as a consequence electrical path in the polymer matrix in addition to a decrease in the width of the potential barriers within the bulk region of high conductivity. Therefore more charge carriers may be able to ‘hop’ by tunneling, resulting in the increase in the bulk conductivity and it also increases with increasing filler concentration [19]. Conductivity is further observed to increase upon irradiation. Irradiation is expected to promote the metal to polymer bonding and convert polymeric structure into hydrogen depleted carbon network. It is this carbon network that is believed to make the polymer more conductive [27].

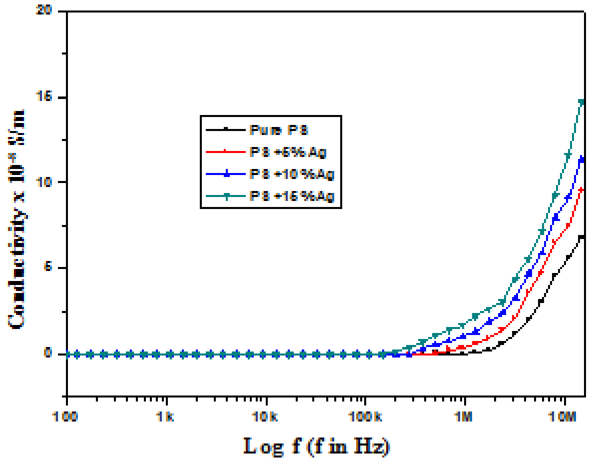
20
15
10
5
0
Conductivity x 10-8 S/m
Pure PS
PS +5% Ag
PS +10 % Ag
PS +15 % Ag
100
1k
10k
100k
1M
10M
Log f (f in Hz)

(a)

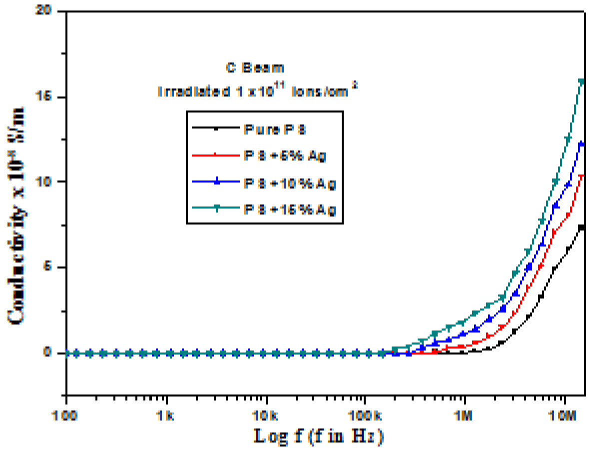
20
15
10
5
0
Conductivity x 10-8 S/m
C Beam
Irradiated 1 x 10^{11} ions/cm^{2}
Pure PS
PS +5% Ag
PS +10 % Ag
PS +15 % Ag
100
1k
10k
100k
1M
10M
Log f (f in Hz)

(b)

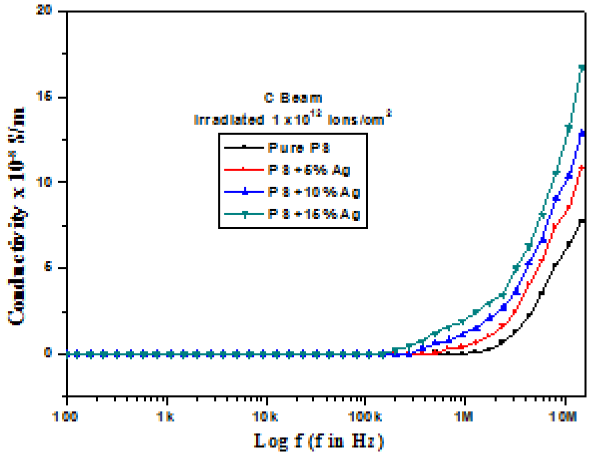
20
15
10
5
0
Conductivity x 10-8 S/m
C Beam
Irradiated 1 x 10^{12} ions/cm^{2}
Pure PS
PS +5% Ag
PS +10 % Ag
PS +15 % Ag
100
1k
10k
100k
1M
10M
Log f (f in Hz)

(c)

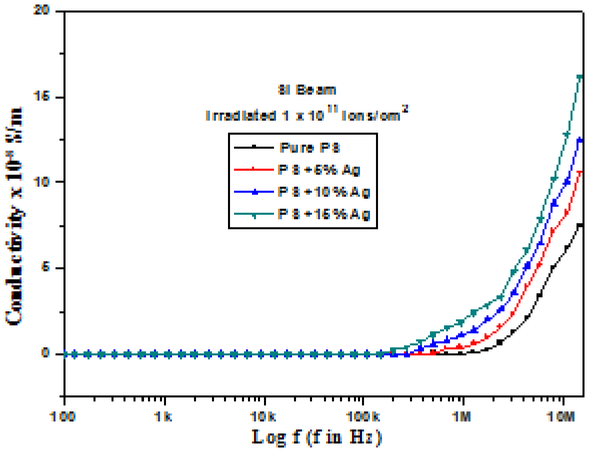

(d)

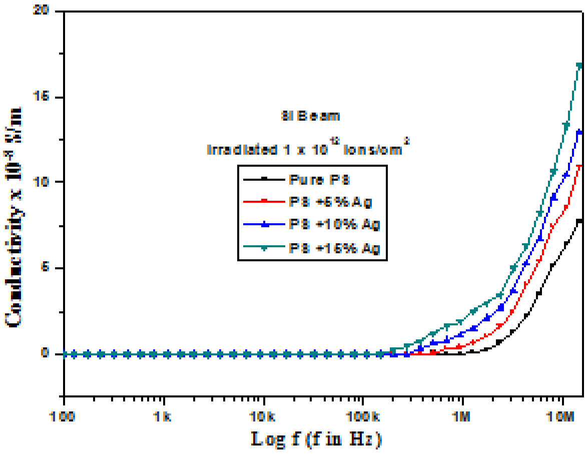

(e)

Fig. 3.12 Conductivity Vs Log f for (a) pristine (b) C beam (1 x 10^{11} ions/cm^2) (c) C beam (1 x 10^{12} ions/cm^2) (d) Si beam (1 x 10^{11} ions/cm^2) (e) Si beam (1 x 10^{12} ions/cm^2)

Dielectric property of composites:

Fig. 3.13 (a-e) shows the dependence of the dielectric constant on the frequency of the applied field at different filler concentrations and irradiation fluences. It is observed that the dielectric constant decreases at high frequency; this is thought to be caused by the slow dielectric relaxation of the matrix and the interface of the composite [33]. At these frequencies, the charge carriers roam through the dielectric and get trapped against a defect site, inducing an opposite charge in their vicinity, and as a result, the motion of charge carriers is slowed down and the value of the dielectric constant decreases. According to the Dissado and Hill theory, in intra-

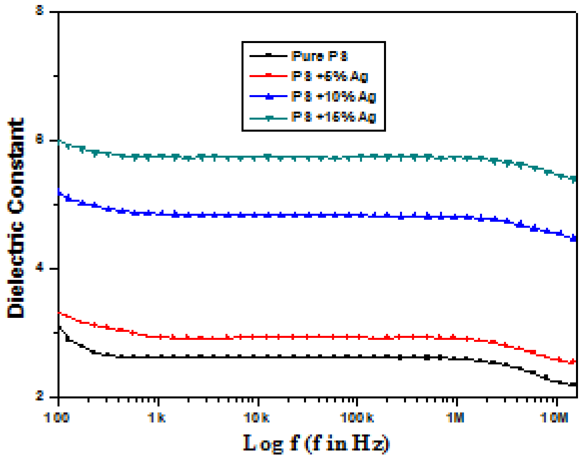

(a)

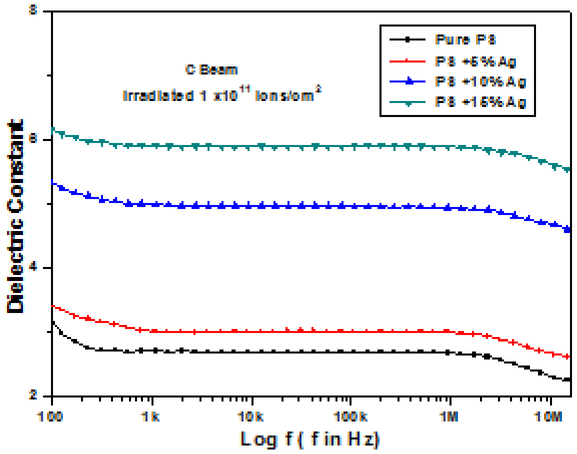

(b)

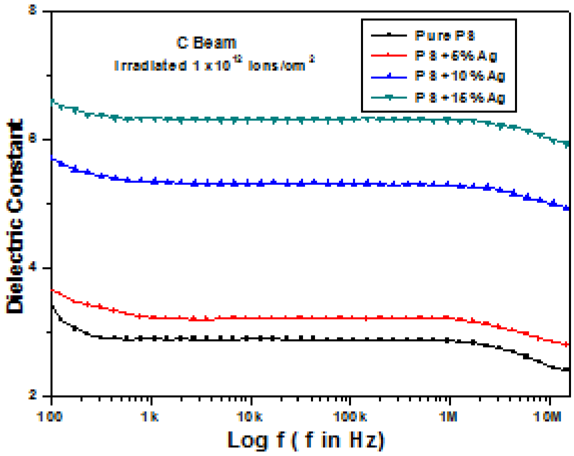
C Beam
Irradiated 1 x10^12 Ions/cm^2
Pure PS
PS+5%Ag
PS+10%Ag
PS+15%Ag
Dielectric Constant
Log f (f in Hz)
2
4
6
8
100
1k
10k
100k
1M
10M

(c)

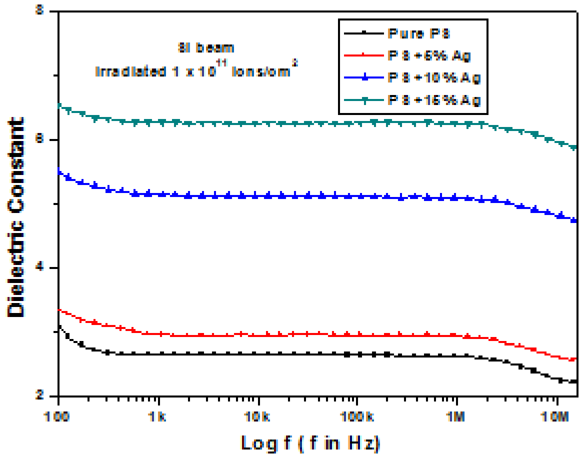
Si beam
Irradiated 1 x 10^11 Ions/cm^2
Pure PS
PS+5% Ag
PS+10% Ag
PS+15% Ag
Dielectric Constant
Log f (f in Hz)
2
4
6
8
100
1k
10k
100k
1M
10M

(d)

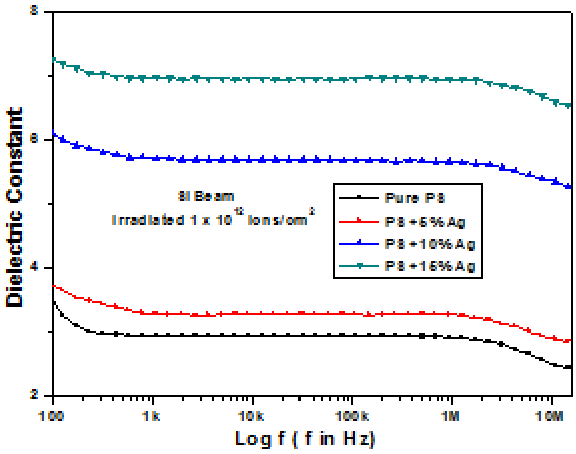
Si Beam
Irradiated 1 x 10^12 Ions/cm^2
Pure PS
PS+5%Ag
PS+10%Ag
PS+15%Ag
Dielectric Constant
Log f (f in Hz)
2
4
6
8
100
1k
10k
100k
1M
10M

(e)

Fig. 3.13 Dielectric Constant Vs Log f for (a) pristine (b) C beam (1 x 10^{11} ions/cm^2) (c) C beam (1 x 10^{12} ions/cm^2) (d) Si beam (1 x 10^{11} ions/cm^2) (e) Si beam (1 x 10^{12} ions/cm^2)

cluster motions, the relaxation of a dipole will produce a ‘chain’ response in its neighboring dipoles and the reaction of the neighboring dipoles will, in turn, affect the first dipole, so the overall effect will be seen as a single-cluster dipole moment relaxation. This reduces the dielectric constant at these frequencies [35]. There is an increase in the dielectric permittivity with metal concentrations as the quantity of accumulated charges increases because of the polarization of polymer/metal at the interfaces. The polarization makes an additional contribution to the charge quantity. The increase in the dielectric constant upon irradiation may be attributed to the chain scission, which results in an increase in free radicals, unsaturation, etc., when compared with the pristine samples [36].

The dielectric loss decreases exponentially first, then becomes less dependent on the frequency. This is because the induced charges gradually fail to follow the reversing field, causing a reduction in the electronic oscillations as the frequency is increased. The dielectric loss also increases moderately with filler contents and with irradiation fluence also, as shown in Fig. 3.14 (a-e) [37]. The increase in the dielectric loss may be attributed to the interfacial polarization mechanism of the heterogeneous system.

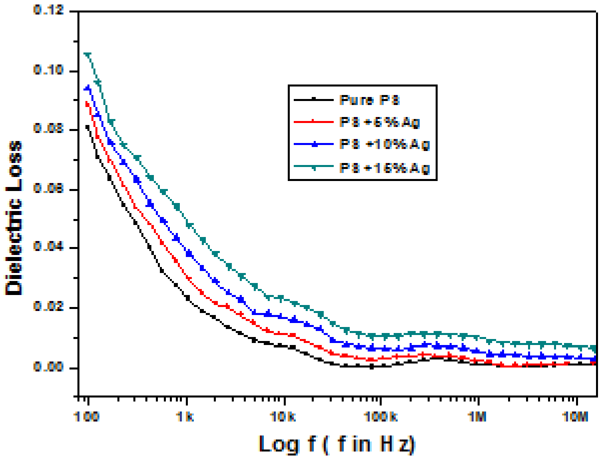
Dielectric Loss
0.12
0.10
0.08
0.06
0.04
0.02
0.00
100
1k
10k
100k
1M
10M
Log f (f in Hz)
Pure PS
PS +5% Ag
PS +10% Ag
PS +15% Ag

(a)

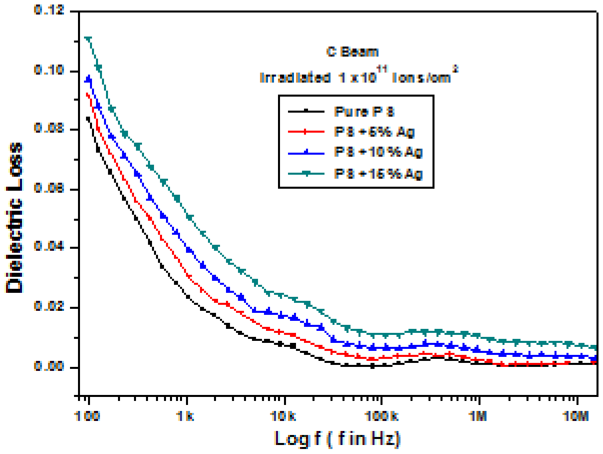
Dielectric Loss
0.12
0.10
0.08
0.06
0.04
0.02
0.00
100
1k
10k
100k
1M
10M
Log f (f in Hz)
C Beam
Irradiated 1 x 10^{11} ions/cm^{2}
Pure PS
PS +5% Ag
PS +10% Ag
PS +15% Ag

(b)

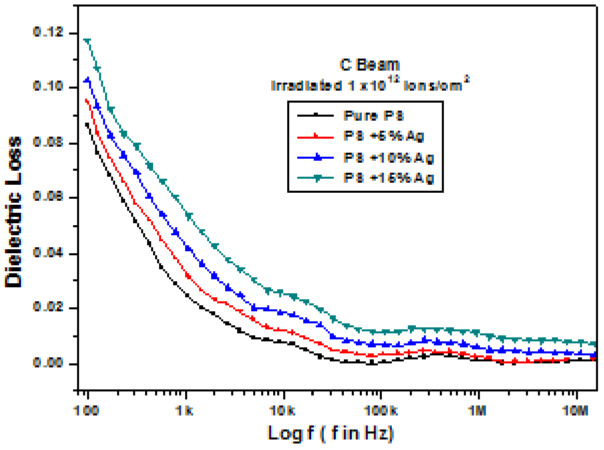
Dielectric Loss
0.12
0.10
0.08
0.06
0.04
0.02
0.00
100
1k
10k
100k
1M
10M
Log f (f in Hz)
C Beam
Irradiated 1 x 10^{12} ions/cm^{2}
Pure PS
PS +5% Ag
PS +10% Ag
PS +15% Ag

(c)

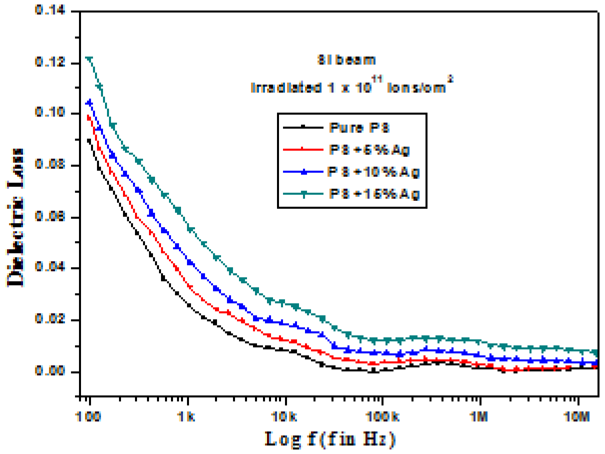

(d)

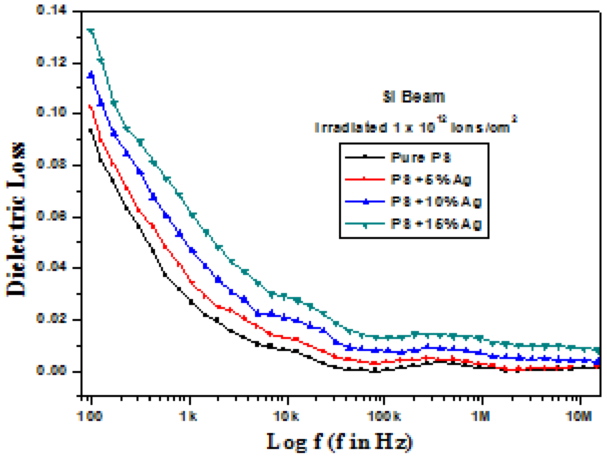

Figure 3.14 Dielectric loss Vs Log f for (a) pristine (b) C beam (1 x 10^{11} ions/cm^2) (c) C beam (1 x 10^{12} ions/cm^2) (d) Si beam (1 x 10^{11} ions/cm^2) (e) Si beam (1 x 10^{12} ions/cm^2)

Conclusion:

Dispersion of silver nanoparticles in PS films has enhanced the properties of the pure polymer significantly. The increase in dielectric properties with different concentrations may be pointed to the conductive phase formed by dispersed nanoparticles in polymer matrix. Ion beam irradiation also has been shown to significantly enhance the dielectric properties may be due to conversion of the polymeric structure into a hydrogen-depleted carbon network. It was found that the band gap value moved to lower energy (from 4.38 eV upto 3.30 eV) on doping with silver nanoparticles as well as upon irradiation as revealed from the UV- visible spectroscopy analysis. An XRD analysis reveals that the crystallite size of the samples increased after ion beam irradiation which is also corroborated with the DSC analysis due to the crosslinking upon irradiation.

3.3 Summary

Two different composites have been studied using two different ion beams (C and Si) irradiations. Structural, optical, electrical properties and surface morphology have been examined by different characterization techniques.

The XRD analysis, results show that the crystallite size of fillers decreases slightly upon both ion beams irradiations in PMMA nanocomposites. It is also observed that the intensity of the peak decreases and to some extent broadening of the peak after irradiation offers confirmation of decrease in crystallinity. Since no significant change in the peak position is observed, this reveals that lattice parameters do not change significantly in both irradiations. Rather in the case of PS nanocomposites, crystallite size of fillers increases upon both ion beams irradiations which may be attributed to cross linking effect.

The DSC thermograms analysis reveals that the Tg value decreases upon irradiations in PMMA nanocomposites and increases upon irradiations in PS nanocomposites. This behavior probably arises due to branching (cross-linking effect) when islands of nanoparticles are bonded with polymeric chains. This lowers the mobility of the chains, and as a result, the glass transition temperature increases in the nanocomposites. Decrease in Tg was explained by thin film model. When the inter-particles distance is small enough, then the polymer between two particles can be considered as a thin film. Assuming that there is small or no interfacial interaction between the filler and matrix exists and then Tg decreases.

The band gap values for both composites were increased upon concentration of fillers and both ions irradiations. It was observed from the UV- visible spectroscopy analysis that the band gap value moved to the lower energy.

SEM images showed that increase in density in PMMA nanocomposites and decrease in density in PS nanocomposites upon irradiations.

Ac electrical conductivity of all pristine and irradiated samples at different filler concentrations is shown in Fig.3.15. The increase in conductivity with silver nanoparticles concentration for pristine samples may be attributed to the conductive phase formed by dispersed metal nanoparticles in polymer matrix. The increase in conductivity is related to a possible increase in the number of conduction paths created between the filler particles aggregates in the composite and as a consequence electrical path in the polymer matrix in addition to a decrease in the width of the potential barriers within the bulk region of high conductivity. Therefore more charge carriers may be able to ‘hop’ by tunneling, resulting an increase in the bulk conductivity and it also increases with increasing filler concentration. Conductivity is further observed to increase upon irradiation. Irradiation is expected to promote the metal to polymer bonding and convert polymeric structure into hydrogen depleted carbon network. It is this carbon network that is believed to make the polymer more conductive. Fig 3.15 shows comparison of conductivity of all composites before and after irradiation. For the sake of comparison filler concentration (5, 10, 15 wt%) at a fluence of 1 x 10^{12} ions/cm^2 for C and Si ions beams at a frequency of 10 MHz have considered. In Fig 3.16, similar comparison has also been made for dielectric constant of all composites.

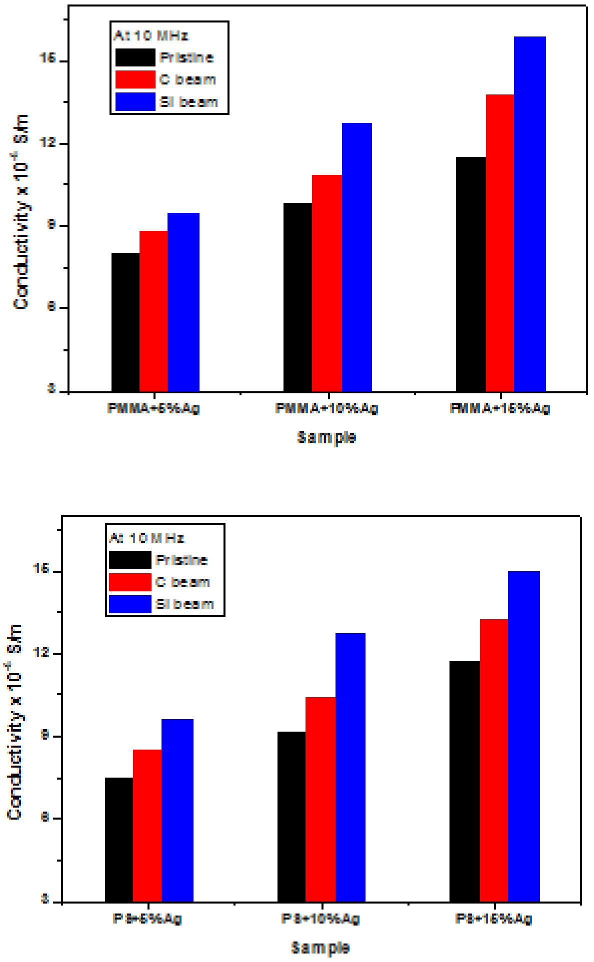

Fig. 3.15 Comparison of conductivity of pristine and irradiated samples at 10 MHz

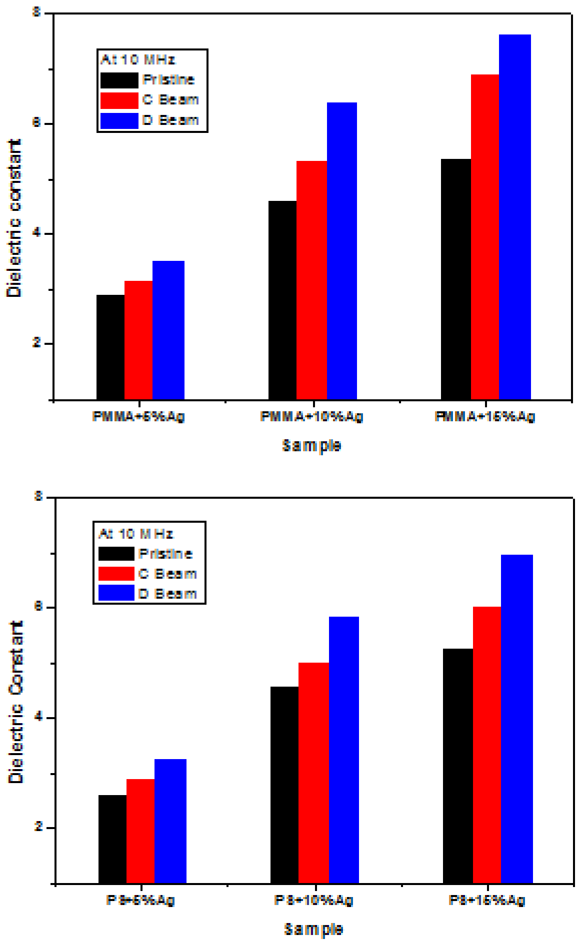

Fig. 3.16 Comparison of dielectric constant of pristine and irradiated samples at 10 MHz

Fig. 3.16 shows the dependence of the dielectric constant on the frequency of the applied field at different filler concentrations and irradiation fluences.

In all the cases, it reveals that dielectric loss is positive and signifies inductive behaviour of the material.

References:

[1] Lin Bin, A. Gelves Genaro, A. Haber Joel, and Sundararaj Uttandaraman, Ind. Eng. Chem. Res., 46 (2007) 2481-2487.

[2] A. Gelves Genaro, Sundararaj Uttandaraman, A. Haber Joel, Macromol. Rapid Commun., 26 (2005)1677–1681.

[3] K. Singh Samra, S. Thakur, L. Singh, Nuclear Instruments and Methods in Physics Research B 269 (2011) 550–554.

[4] Kawaljeet Singh Samra, Sonika Thakur, Lakhwant Singh, Nuclear Instruments and Methods in Physics Research B, 269 (2011) 550–554.

[5] Chaitali Gavade, N. L. Singh, D. K. Avasthi, Alok Banerjee, Nuclear Instruments and Methods in Physics Research B,268(2010) 3127–3131.

[6] R. Kumaravel, K. Ramamurthi, Indra Sulania, K. Asokan, D. Kanjilal, D. K. Avasti, P. K.Kulria, Radiation Physics and Chemistry, 80 (2011) 435–439.

[7] Chaitali Gavade, N. L. Singh, P. K. Khanna, Journal of Nanoscience and Nanotechnology, 14 (2014)1.

[8] Chaitali Gavade, N. L. Singh, Anita Sharma, P. K. Khanna, Fouran Singh, Radiation Effects & Defects in Solids,166 (2011) 585–591.

[9] P. Scherrer, Gott Nachar**,** 2 (1918) 98–100.

[10] R. Kumar, U. De, R. Prasad, Nucl. Instrum. Methods B 248 (2006) 279-283.

[11] V.V. Vodnik , D.K. Bozanic, E. Dzunuzovic, J. Vukovic, J.M. Nedeljkovic, European Polymer Journal 46 (2010) 137.

[12] B. J. Ash, L. S. Schadler, R. W. Siegel, Mater Lett 55 (1–2) (2002) 83.

[13] D. L. Pavia, G.M. Lampman, G.S. Kriz, Introduction to Spectroscopy, Harcourt College Publishers, Philadelphia (2001).

[14] A. K. Srivastava, H. S. Virk, J. Polym. Mater. 17 (2000) 325.

[15] H S Virk , P S Chandi And A K Srivastava, Bull. Mater. Sci. 24(5) (2001) 529.

[16] A. Das, S. Dhara and A. Patnaik Physical Rev B 59 (1999) 11069.

[17] Anjum Qureshi , Dolly Singh , N.L. Singh, S. Ataoglu , Arif N. Gulluoglu , Ambuj Tripathi ,D.K. Avasthi, Nuclear Instruments and Methods in Physics Research B 267 (2009) 3456.

[18] S. Shah, N.L. Singh, A. Qureshi, D. Singh, K.P. Singh, V. Shrinet, A. Tripathi, Nucl. Instrum. Methods B 226 (2008) 1768-1774.

[19] M. Abu-Abdeen, G. M. Nasr, H. M. Osman, A. I. Abound, Egypt J. Sol. 25 (2002) 275-294.

[20] Ye. P. Mamunya, V. V. Davydenko, P. Pissis, E. V. Lebedev, Eur. Polymer Journal 38 (2002) 1887-1897.

[21] Santanu Singha, M. Joy Thomas, IEEE Transactions on Dielectrics and Electrical Insulation 15(1) (2008) 2-11.

[22] Rajesh Kumar, S Asad Ali, Udayan De, D K Avasthi and Rajendra Prasad, Indian J. Phys. 83 (7) (2009) 963-968.

[23] A.K. Jonscher, Dielectric Relaxation in Solids; Chesla Dielectric Press: London, 1983.

[24] T. Phukan, D. Kanjilal, T. D. Goswami, Nucl. Instr. And Meth. B 234 (2005) 520-524.

[25] Jiongxin Lu, Kyoung-Sik Moon, Jianwen Xu, C. P. Wong, J. Mater. Chem.16 (2006) 1543-1548.

[26] N. L. Singh, Sejal Shah , Anjum Qureshi , K. P. Singh , V. Shrinet , P. K. Kulriya , A. Tripathi Radiation Effects & Defects in Solids 163(2) (2008) 169-177.

[27] D. Singh, N.L. Singh, A. Qureshi, P. Kulriya, A. Tripathi, D.K. Avasthi, A.N. Gulluoglu, J. Non-Cryst. Solids, 356 (2010) 856–863.

[28] X. Yan, T. Xu, S. Xu, S. Wang, Nanotechnology, 15 (2004) 1759–1762.

[29] Rajesh Kumar, S. Asad Ali, A.K. Mahur, H.S. Virk, F. Singh, S.A. Khan, D.K. Avasthi, Rajendra Prasad, Nuclear Instruments and Methods in Physics Research B 266 (2008) 1788–1792.

[30] S. Saravanana, M.R. Anantharaman, S. Venkatachalam, D.K. Avasthi, Vacuum 82 (2008) 56–60.

[31] L.S. Farenza, R.M. Papaleo, A. Hallen, M.A. Araujo, R.P. Livi, B.U.R. Sundqvist, Nucl. Instr. and Meth. B 105 (1995) 134.

[32] Zhiyong Zhu, Yunfan Jin, Changlong Liu, Youmei Sun, Mingdong Hou, Chonghong Zhang, Zhiguang Wang, Jie Liu, Xiaoxi Chen, Baoquan Li, Yanbin Wang, Nuclear Instruments and Methods in Physics Research B 169 (2000) 83-88.

[33] A. Das, S. Dhara and A. Patnaik Physical Rev B 59 (1999) 11069.

[34] J. Robertson, E.P. O Reilly, Phys. Rev. B 35 (1987) 2946.

[35] G. Sui, S. Jana, W. H. Zhong, M. A. Fuqua, C. A. Ulven, Acta Mater., 56 (2008) 2381–2388.

[36] N. L. Singh, S.Shah, A. Qureshi, K. P. Singh, V. Shrinet, A. Tripathi, Radiat. Eff. Def. Solids (163)(2) (2008) 169–177.

[37] A. Qureshi, N. L. Singh, S. Shah, F. Singh, D.K. Avasthi, J. Macromol. Sci. (45) (2008) 265–270.

[38] S. Shah, D. Singh, A. Qureshi, N. L. Singh, K. P. Singh, V. Shrinet, Indian J. Pure Appl. Phys. (46) (2008) 439–442.

Chapter - IV

Effect of swift heavy ions on physical properties of PMMA/Cu and PS/Cu nanocomposites

----

Abstract

Effect of swift heavy ions (120 MeV Si ions, 85 MeV C ions) induced modifications of Copper nanoparticles dispersed PMMA and PS nanocomposites films at different fluences were studied. 120 MeV Si swift heavy ions induced more prominent effects on the physico-chemical properties of polymer nanocomposites compared to those of C-ions. An XRD analysis reveals that the crystallite size of the composites decreased after ion beam irradiation which is also corroborated by the DSC analysis due to the chain scissioning upon irradiation in PMMA nanocomposites. In PS nanocompsoites, we observed cross linking upon irradiation. It was observed from the UV- visible spectroscopy analysis that the band gap value moved to the lower energy on doping with metal nanoparticles, as well as upon irradiation. SEM images showed damages upon ion beam irradiation. The dielectric constant of the composites increased with the increase of metal content. These phenomena could be interpreted from interfacial polarization of heterogeneous systems.

4.0 Introduction:

Polymers have traditionally been considered as excellent host matrices for composite materials. Several advanced polymer composites have been synthesized with a wide variety of inclusions like metals, semiconductors, carbon nanotubes and magnetic nanoparticles [1–3]. Many attractive properties of polymers like non-corrosiveness, light weight, mechanical strength and dielectric tenability can be utilized along with magnetic and optical properties of nanoparticles to make multifunctional materials. Inclusion of nanoparticles exhibit novel properties that significantly differ from those of corresponding bulk solid state owing to the different effects in terms of the small size effect, surface effect, quantum size effect and macroscopic quantum tunnel effect [4–6]. Copper nanoparticles have potential applications as fillers in polymers in many electronic devices. The progress in miniaturized nano devices that integrate electronic, photonic, chemical, and/or biological features is important for electronic as well as sensing devices [7].

Ion beam irradiation of polymeric materials can induce irreversible changes in their macroscopic properties, such as, electrical, thermal and surface related mechanical properties. These changes are responsible to fundamental events like electronic excitation, ionization, chain scission and cross-linking as well as mass loss, which take place due to ion beam irradiation [8].

In this chapter we are dealt with polymer nanocomposites and effect of irradiation upon

(i) PMMA + Cu [9]

(ii) PS + Cu [10]

Properties and preparation methods of nanocomposites have been discussed in chapter 2. All the films were irradiated with 120 MeV Si- ions and 85 MeV C- ions at the fluences of 1 x 10^{11}, 1 x 10^{12} ions/cm^2 at Inter University Accelerator Centre (IUAC), New Delhi, India. We have studied changes in the optical, structural, dielectric and thermal properties of composites due to swift heavy ion irradiation by means of X-ray diffraction, UV–visible spectroscopy, impedance gain phase analyzer and differential scanning calorimetry.

4.1 Effect of swift heavy ions irradiation on PMMA + Cu nanocomposites:

4.1.1 X-ray diffraction analysis:

Fig. 4.1(a-g) shows XRD spectra of the copper nanocomposite films, which illustrate the amorphous nature of PMMA and the crystalline behavior of copper nanoparticles. The average particle size of the copper nanoparticles was obtained around 10.81 nm. The diffraction patterns of the irradiated samples by 85 MeV C ions and 120 MeV Si ions exhibited decrease in the peak intensity and an increase in the full width at half maximum (FWHM) corresponding to all observed peaks of copper. This behavior may be attributed to chain scissioning taking place, which may results in the alignment of the polymeric chains. The average crystallite size (t) for pristine and irradiated samples was calculated using Scherrer's formula [11] as dicussed in chapter 2 in section 2.3.1 from the realtion 2.2.3.

$b = K\lambda / L\cos\theta$

where b is FWHM in radians, λ is the wavelength of X-ray beam (1.5418 Å), L is the crystallite size in Å, θ is the angle between the atomic plane and both the incident and reflected planes, K is a constant which varies from 0.89 to 1.39, but for most of the cases it is close to 1.

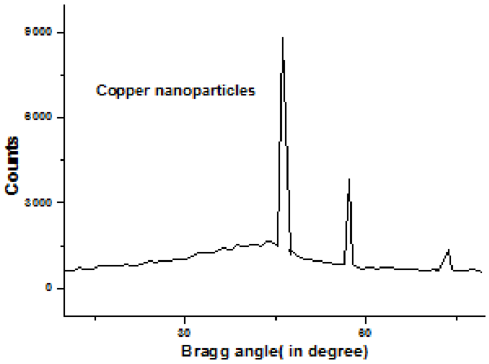
Copper nanoparticles
Counts
9000
6000
3000
0
30
60
Bragg angle(in degree)

(a)

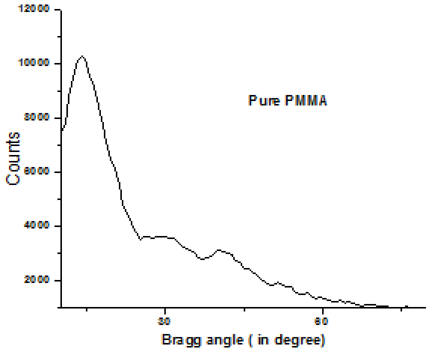
Pure PMMA
Counts
12000
10000
8000
6000
4000
2000
30
60
Bragg angle (in degree)

(b)

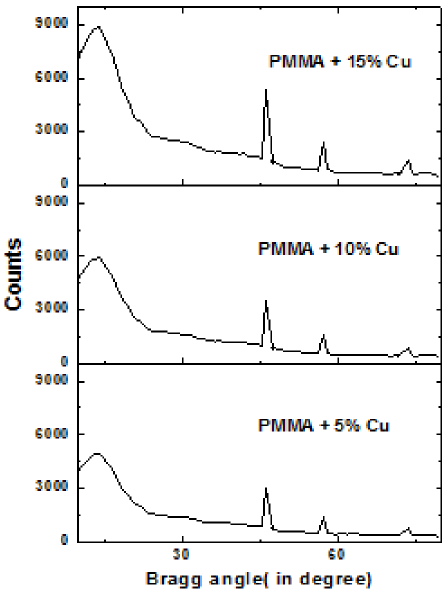
PMMA + 15% Cu
PMMA + 10% Cu
PMMA + 5% Cu
Counts
9000
6000
3000
0
30
60
Bragg angle(in degree)

(c)

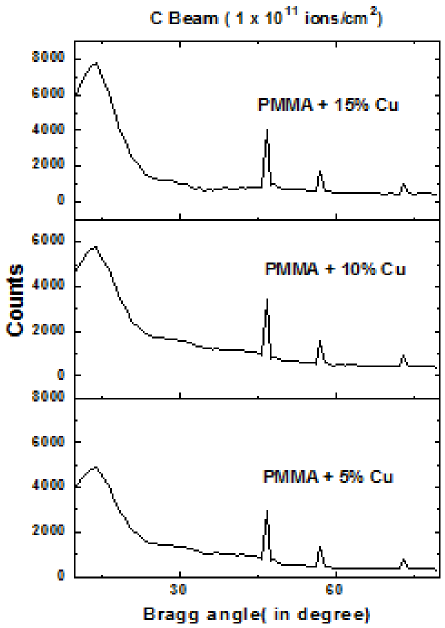
C Beam (1 x 10¹¹ ions/cm²)
PMMA + 15% Cu
PMMA + 10% Cu
PMMA + 5% Cu
Counts
8000
6000
4000
2000
0
30
60
Bragg angle(in degree)

(d)

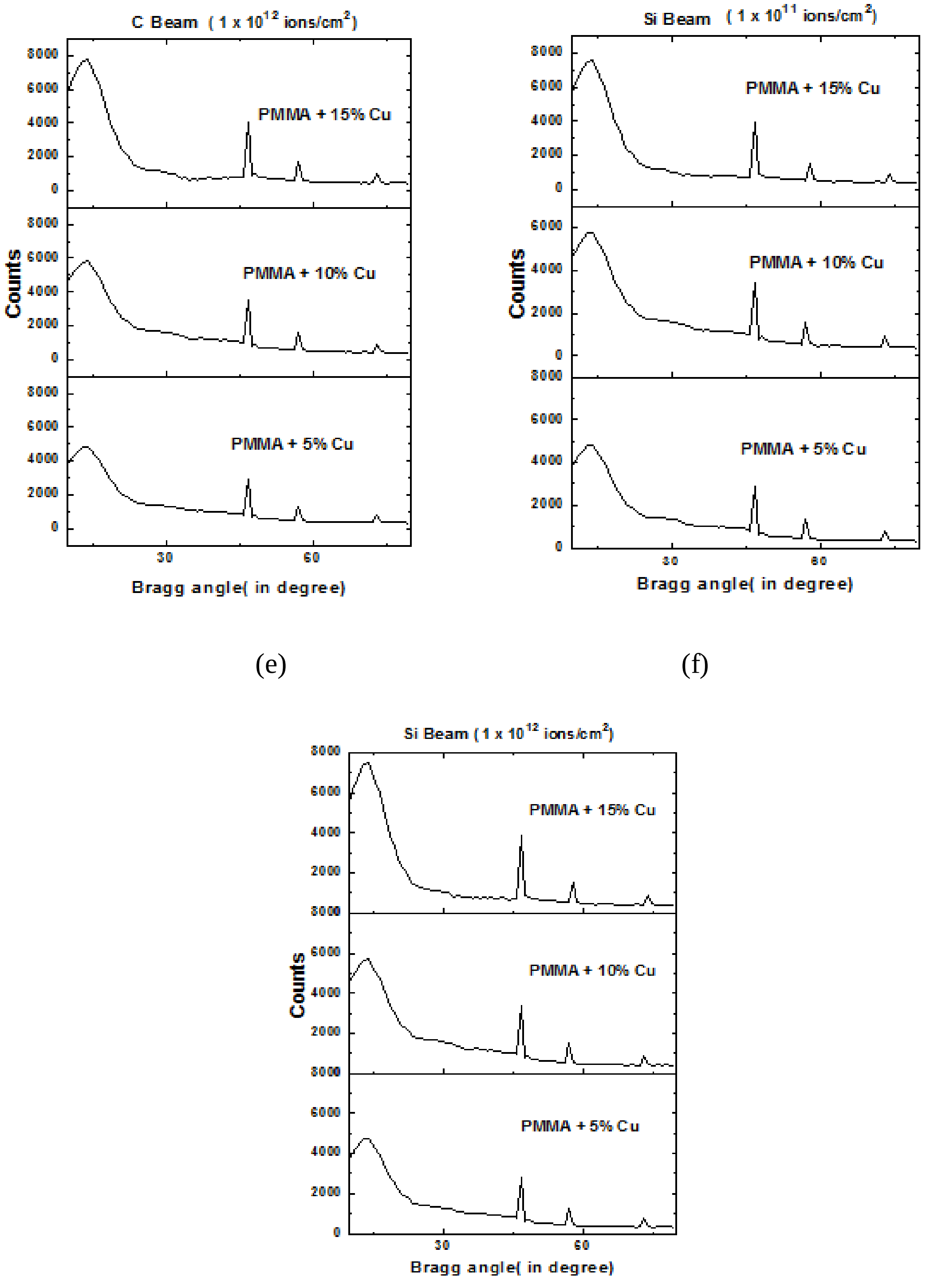

(e) (f)

(g)

Fig. 4.1 X-ray diffraction patterns of (a) copper nanoparticles (b) pure PMMA (c) PMMA+ Cu(pristine) (d) C beam (1 x 10^{11} ions/cm^2) (e) C beam (1 x 10^{12} ions/cm^2) (f) Si beam (1 x 10^{11} ions/cm^2) (g) Si beam (1 x 10^{12} ions/cm^2)

The crystallite size was calculated corresponding to the peak of the pristine and irradiated samples and the results are listed in Table 4.1 [12]. Irradiation deposited large amount of energy in material and leads to decrease in crystallite size. This may be attributed to splitting of crystalline grains. The decrease in crystallite size suggested the chain scissioning mechanism.

Table 4.1 Crystallite size of pristine and irradiated samples

Sample	Pristine		C Beam		Si Beam	
	2θ	Crystallite size (nm)	Crystallite size (nm) $(1x10^{11})$ ions/cm^2	Crystallite size (nm) $(1x10^{12})$ ions/cm^2	Crystallite size (nm) $(1x10^{11})$ ions/cm^2	Crystallite size (nm) $(1x10^{12})$ ions/cm^2
PMMA+ 5%Cu	46.73	12.16	11.64	11.26	11.56	11.21
	58.05	12.64	11.61	11.14	11.20	11.08
	Average	12.40	11.63	11.2	11.38	11.15
PMMA + 10%Cu	46.56	12.23	11.78	11.56	11.48	10.86
	58.05	12.89	11.51	11.34	11.16	10.58
	Average	12.56	11.65	11.45	11.32	10.72
PMMA + 15%Cu	46.39	12.36	11.81	11.68	11.11	10.54
	58.01	12.24	11.25	11.22	10.89	10.39
	Average	12.30	11.53	11.45	11.00	10.47

4.1.2 *Thermal response (Differential scanning calorimetry (DSC)):*

A differential scanning calorimetry experiment was performed using a reference material, and a predetermined heating (or cooling) rate was imposed to the system with a temperature excursion. The sample followed the temperature of the reference, and the heating power difference between the sample and reference was recorded. The values of *T*g were taken as the midpoint of the glass transition event and collected as shown in Fig. 4.2. The pure PMMA has a *T*g value of 64.60◦C, while the tendency of increase in *T*g value after insertion of copper nanoparticles was observed for Cu/PMMA nanocomposites. We found the value of *T*g for pristine and irradiated samples at 71.89◦C and 61.8◦C, respectively, for the highest concentration of copper.

The value of Tg for highest fluence is listed in Table 4.4. The results reveal that the glass transition temperature increases for the composites as compared with the pure PMMA and may be due to the interactions of the filler nanoparticles and PMMA in a more ordered state and resulting in the cross-linking of the polymer and nanoparticles. After irradiation, it was found that *T*g shifted to lower temperature. It reveals that the ion irradiation leads to polymer chain scissioning and a subsequent reduction in the molecular weight. As a result, the system moved toward the more disordered state, which is also corroborated with XRD results [13].

Table 4.2 Values of glass transition for pristine and irradiated composites

Sample name	Tg (Pristine)	Tg (C beam)	Tg (Si beam)
PMMA + 10 %Cu	70.2	65.7	64.2
PMMA + 15 %Cu	71.9	61.8	61.5

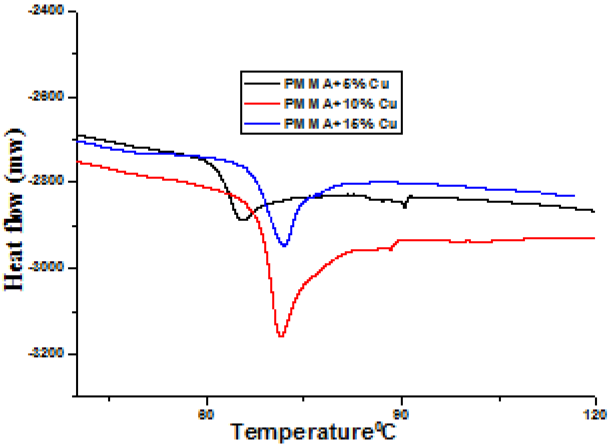

(a)

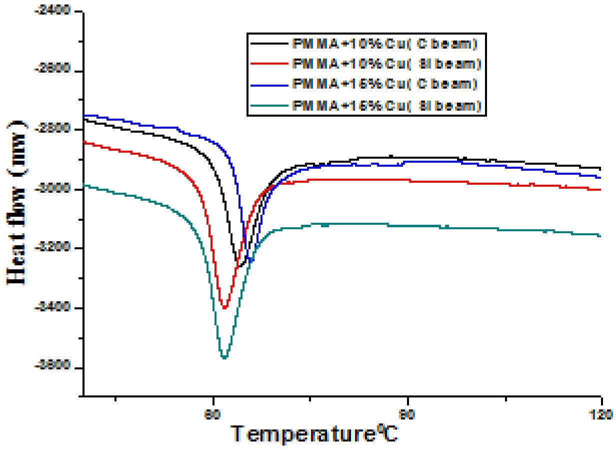

(b)

Fig. 4.2 DSC spectra of (a) composites (b) irradiated films (1 x 10^{12} ions/cm^2)

4.1.3 Optical response:

The promotion of electrons in the σ, π and n orbitals from ground state to the higher energy states which are described by molecular orbitals due to the absorption of light energy by polymeric samples in the UV and visible regions. Many of the optical transitions which occur due to the presence of impurities have energies in the visible region of the spectrum, consequently the defects are referred to as colour centres. The effect of ion beam interaction with polymers produces damage and leads to the generation of new defects and charge states [14, 15]. A shift in the absorption edge towards longer wavelength is observed for irradiated samples. This behaviour is generally interpreted as caused by the formation of extended systems of conjugated bonds, i.e. possible formation of carbon clusters. In the investigated range of wavelengths the absorption bands are associated to the π–π* electronic transitions. These types of transitions occur in the unsaturated centers of the molecules, i.e. in compounds containing double or triple bonds and also in aromatics. The excitation of π electron requires smaller energy and hence, transition of this type occurs at longer wavelengths [16].

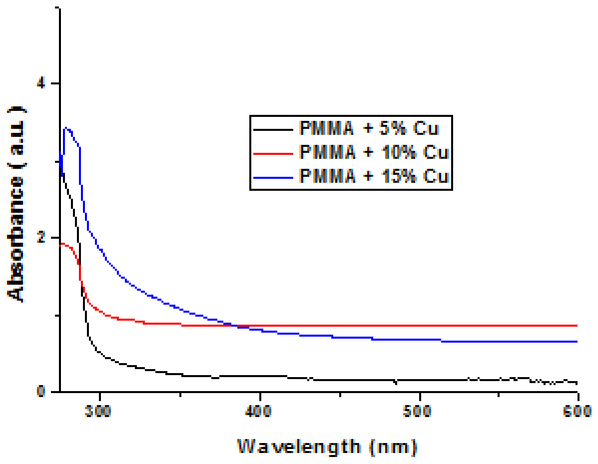
PMMA + 5% Cu
PMMA + 10% Cu
PMMA + 15% Cu
Absorbance (a.u.)
0
2
4
300
400
500
600
Wavelength (nm)

(a)

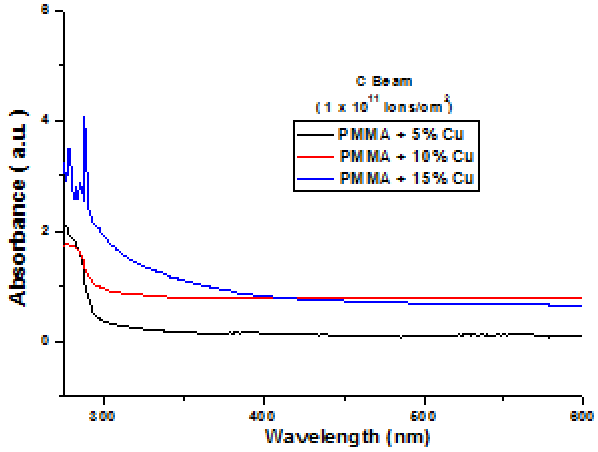
C Beam
(1 x 10^11 Ions/cm^2)
PMMA + 5% Cu
PMMA + 10% Cu
PMMA + 15% Cu
Absorbance (a.u.)
0
2
4
6
300
400
500
600
Wavelength (nm)

(b)

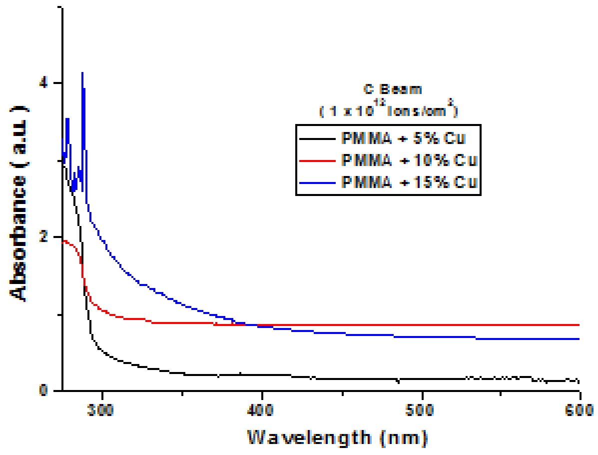
C Beam
(1 x 10^12 Ions/cm^2)
PMMA + 5% Cu
PMMA + 10% Cu
PMMA + 15% Cu
Absorbance (a.u.)
0
2
4
300
400
500
600
Wavelength (nm)

(C)

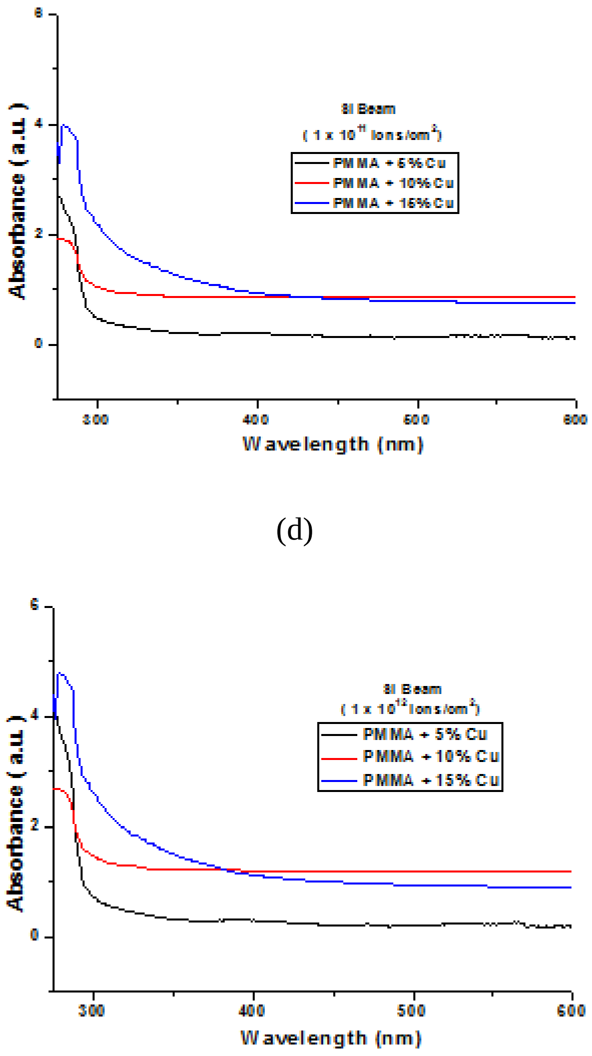

(d)

(e)

Fig. 4.3 Absorbance spectra for (a) PMMA+ Cu(pristine) (b) C beam (1 x 10^{11} ions/cm^2) (c) C beam (1 x 10^{12} ions/cm^2) (d) Si beam (1 x 10^{11} ions/cm^2) (e) Si beam (1 x 10^{12} ions/cm^2)

Determinations of band gap:

The change in optical properties has been studied by Perkin- Elmer 25 Lambda UV-Visible spectrophotometer for the pristine and irradiated samples in the frequency range 200-800 cm^{-1}. The optical band gap E_g is obtained by Tauc's equation [17] as explained in chapter 2 in section 2.3.3 by relation 2.2.4.

$\omega\varepsilon(\lambda)=(\hbar\omega-E_g)^2$

where ε(λ) is the optical absorbance and λ is the wavelength. The intersection of the extrapolated spectrum with the abscissa of the plot $\varepsilon^{1/2}/\lambda$ versus $1/\lambda$ yields the gap wavelength λ_g from which the energy gap is derived as $E_g = hc/\lambda_g$. It is noticed that the band gap (energy gap) value shifted to lower energy from 4.30 eV upto 3.22 eV due to doping of copper nanoparticles and also upon irradiation. This is because of the scissioning of polymer chain and as a result, creation of free radicals, unsaturation etc. and thus a capability of increasing the conductivity of the composites [18].

Table 4.3 Band gap (B.G) and no. of carbon atoms (N) of pristine and irradiated samples

Sample	Pristine	C Beam		Si Beam	
	B.G eV	B.G eV 1 x 10^{11} ions/cm^2	B.G eV 1 x 10^{12} ions/cm^2	B.G eV 1 x 10^{11} ions/cm^2	B.G eV 1 x 10^{12} ions/cm^2
PMMA + 5%Cu	4.30	4.24	4.13	4.12	4.10
PMMA + 10%Cu	4.11	4.05	3.95	3.80	3.62
PMMA + 15%Cu	3.78	3.65	3.55	3.40	3.22

Sample	Pristine	C Beam		Si Beam	
	No. of carbon atoms(N)	No. of carbon atoms(N) 1 x 10^{11} ions/cm^2	No. Of carbon atoms(N) 1 x 10^{12} ions/cm^2	No. of carbon atoms(N) 1 x 10^{11} ions/cm^2	No. Of carbon atoms(N) 1 x 10^{12} ions/cm^2
PMMA + 5%Cu	67	68	69	69	70
PMMA + 10%Cu	72	73	75	84	90
PMMA + 15%Cu	82	85	90	93	113

The number of carbon atoms per cluster (N) can be calculated by following the relation 2.2.5 [12] given in chapter 2; the values of are listed in Table 4.3.

$E_g=34.3/\sqrt{N}$ eV

where N is the number of carbon atoms per cluster and Eg is the energy band gap.

4.1.4 Surface morphology:

Fig. 4.4(a–d) shows the SEM images of pristine, composites and irradiated composite films at a fluence of 1 x 10^{12} ions/cm^2 with magnification of X250. The analysis shows that the filled partilces are distributed randomly in the matrix which display continuous contact between themselves and formed conducting paths. After irradiation, significant changes in surface morphology were observed. Considerable damage in the polymeric structure was observed after irradiation, which is also responsible for decrease in crystallinity of the material as indicated by XRD analysis [19].

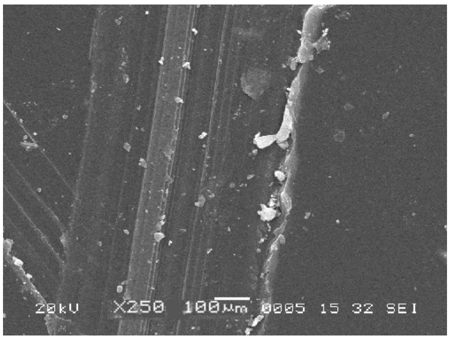

(a)

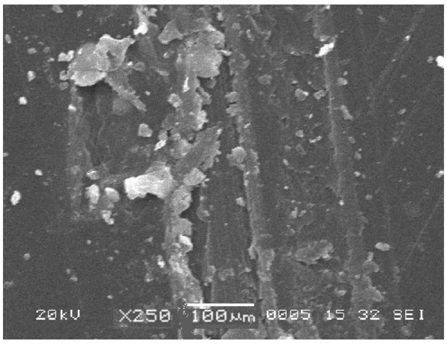

(b)

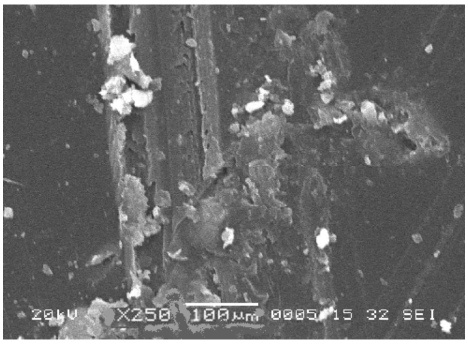

(c)

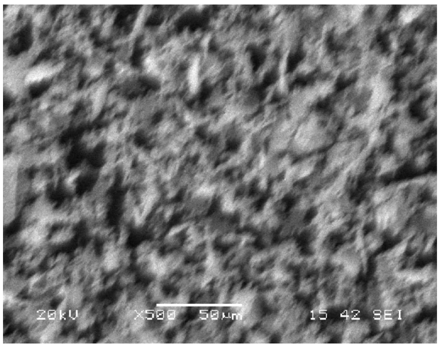

(d)

Fig. 4.4 SEM images of (a) PMMA+ 15 % Cu (pristine) (b) PMMA + 15 % Cu (C beam) (c) PMMA + 15 % Cu (Si beam) and (d) Copper nanoparticles

4.1.5 AC Electrical Frequency Response:

Conductivity: AC electrical measurement was carried out for pristine and irradiated samples. Fig. 4.5 (a-e) shows the variation of conductivity with log of frequency for the pristine and irradiated samples at different copper nanoparticles concentrations. The increase in conductivity with copper nanoparticles concentration for pristine samples may be attributed to the conductive phase formed by dispersed copper nanoparticles in polymer matrix [20–22]. As shown in Fig. 4.5(a-e), we observed two behaviors (i) the frequency independent conductivity in the region of 100 Hz to 1 MHz which is due to free charge carriers available in the composite system and (ii) the frequency dependent conductivity in the region of 1–10 MHz because of trapped charges, which are active at higher frequency only and it contributed to sudden rise in conductivity [23]. The electrical conduction in pure PMMA may occur by the electron jumping (hopping or tunnelling) between filled and empty sites localized in the energy band gap due to the presence of carbonyl group (C=O) in PMMA which may be acted as an electron donor group at higher frequency range [24]. The increase in conductivity is related to a possible increase in the number of conduction paths created between the filler (copper nanoparticles) particles aggregates in the composite and as a consequence electrical path in the polymer matrix due to a decrease in the width of the potential barriers within the bulk region of composites. Therefore, more charge carriers may be able to ‘hop’ by tunnelling, resulting in the increase in the bulk conductivity and it also increases with increasing filler concentrations [25]. Irradiation is expected to promote the metal to polymer bonding and convert polymeric structure into hydrogen depleted carbon network that is believed to make the polymer more conductive [26].

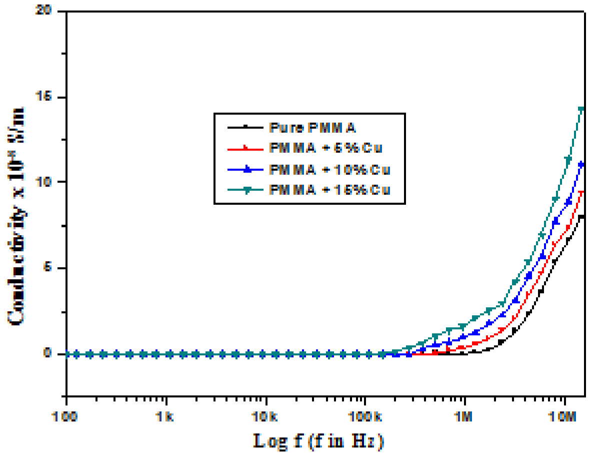

(a)

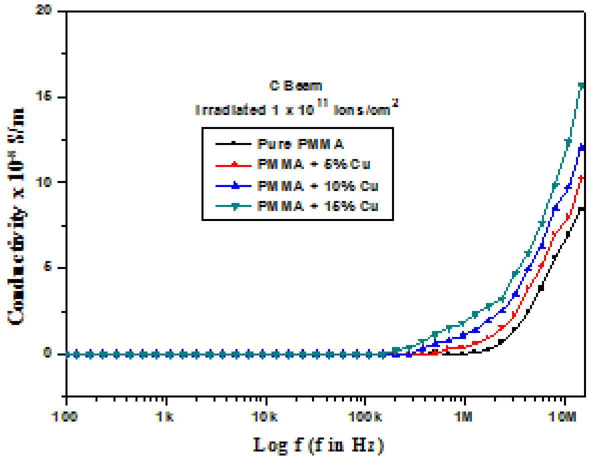

(b)

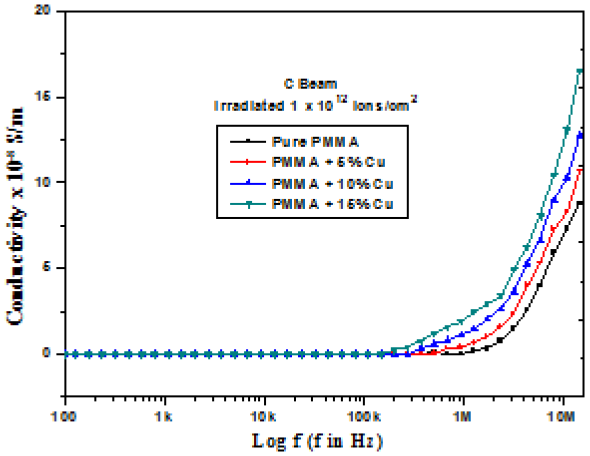
C Beam
Irradiated 1 x 10^12 Ions/cm^2
Pure PMMA
PMMA + 5% Cu
PMMA + 10% Cu
PMMA + 15% Cu
Conductivity x 10^-8 S/m
Log f (f in Hz)
0
5
10
15
20
100
1k
10k
100k
1M
10M

(c)

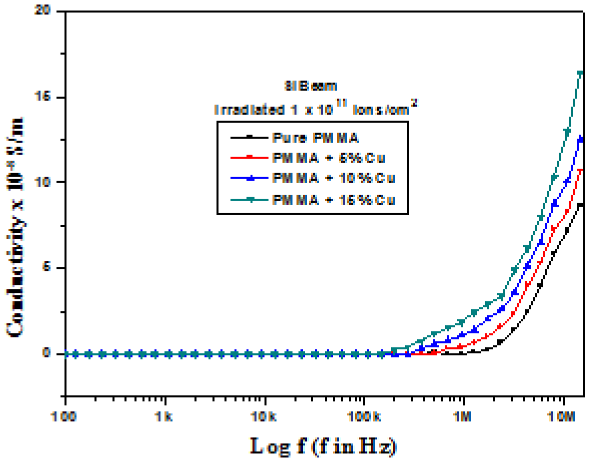
SI Beam
Irradiated 1 x 10^11 Ions/cm^2
Pure PMMA
PMMA + 5% Cu
PMMA + 10% Cu
PMMA + 15% Cu
Conductivity x 10^-8 S/m
Log f (f in Hz)
0
5
10
15
20
100
1k
10k
100k
1M
10M

(d)

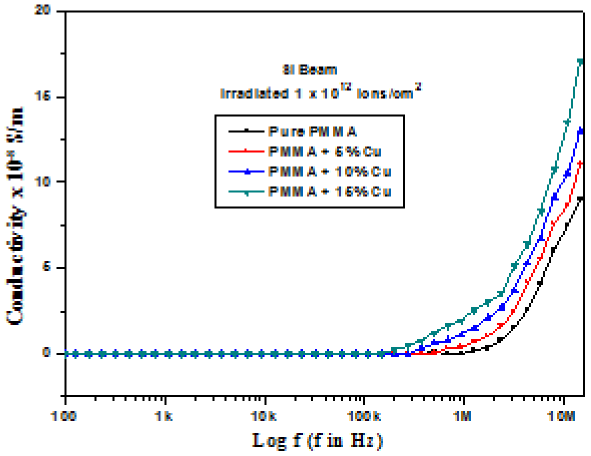
SI Beam
Irradiated 1 x 10^12 Ions/cm^2
Pure PMMA
PMMA + 5% Cu
PMMA + 10% Cu
PMMA + 15% Cu
Conductivity x 10^-8 S/m
Log f (f in Hz)
0
5
10
15
20
100
1k
10k
100k
1M
10M

(e)

Fig. 4.5 Conductivity Vs Log f for (a) pristine (b) C beam (1 x 10^{11} ions/cm^2) (c) C beam (1 x 10^{12} ions/cm^2) (d) Si beam (1 x 10^{11} ions/cm^2) (e) Si beam (1 x 10^{12} ions/cm^2)

Dielectric properties of composites:

The variation of dielectric constant with respect to frequency for the PMMA/ copper nano composites at different filler concentrations are shown in Figure 4.6 (a -e). The dielectric constant depends on the filler concentration and irradiation fluence. Due to doping of copper nanoparticles, the quantity of the accumulated charge increases because of polarization of the polymer/metal at interfaces. The polarization makes an additional contribution to the charge quantity. From this point of view, the dielectric constant of the composites will be higher than the pure polymer. Permittivity is a frequency dependent parameter in polymer/polymer composites systems. All the free dipolar functional groups in the polymer chain can orient themselves resulting in a higher permittivity value at lower frequencies. The slow migration of the active species may be the cause of decrease in the dispersion at higher frequencies. Commonly at low frequency region, the variation of dielectric constant with frequency suggests the presence of higher space charge polarizability of the material. The dielectric constant is found to decrease with increasing frequency. In the direction of applied field, the electronic exchange of the number of ions provides local displacements of electrons which produce the polarization in the polymeric composites. This gradually decreasing dielectric constant with increased frequency is thought to be caused by the slow dielectric relaxation of the matrix and the interface of the composite [27-29].

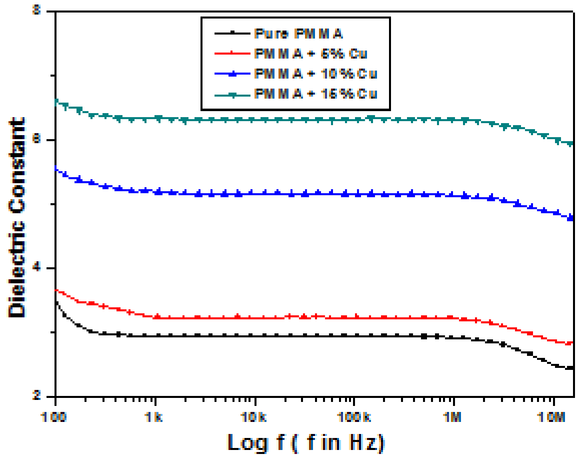
Pure PMMA
PMMA + 5% Cu
PMMA + 10% Cu
PMMA + 15% Cu
Dielectric Constant
Log f (f in Hz)
2
4
6
8
100
1k
10k
100k
1M
10M

(a)

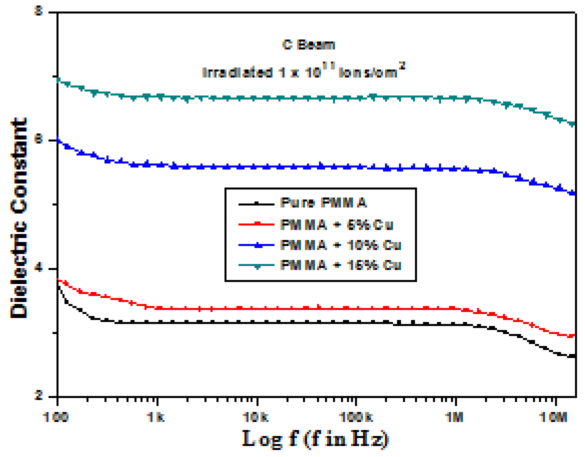
C Beam
Irradiated 1 x 10^11 Ions/cm^2
Pure PMMA
PMMA + 5% Cu
PMMA + 10% Cu
PMMA + 15% Cu
Dielectric Constant
Log f (f in Hz)
2
4
6
8
100
1k
10k
100k
1M
10M

(b)

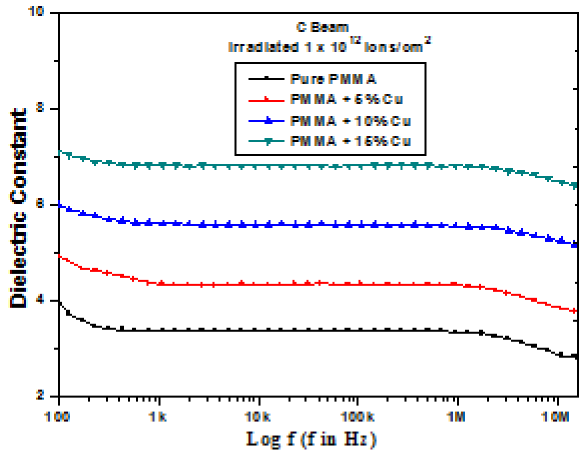
C Beam
Irradiated 1 x 10^12 Ions/cm^2
Pure PMMA
PMMA + 5% Cu
PMMA + 10% Cu
PMMA + 15% Cu
Dielectric Constant
Log f (f in Hz)
2
4
6
8
10
100
1k
10k
100k
1M
10M

(c)

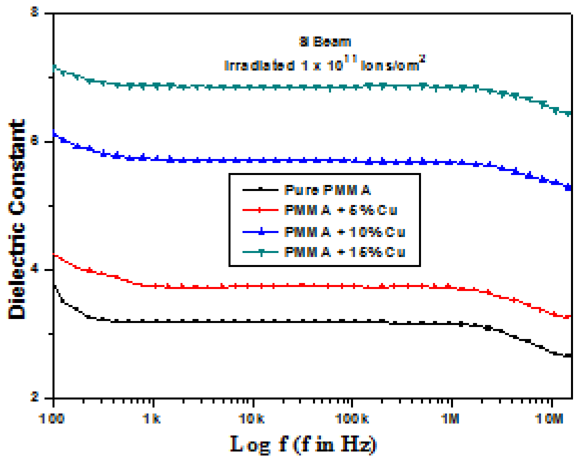

(d)

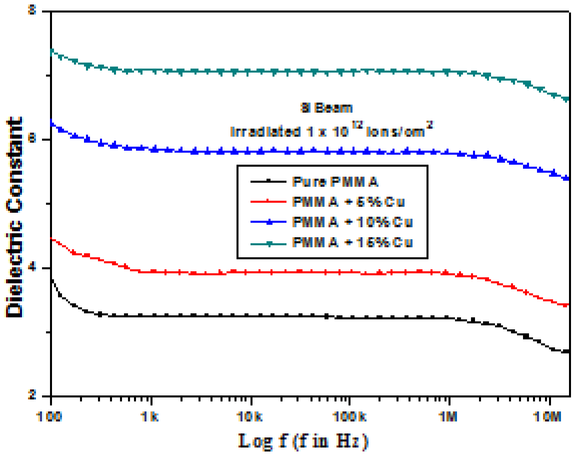

(e)

Fig. 4.6 Dielectric constant Vs Log f for (a) pristine (b) C beam (1 x 10^{11} ions/cm^2) (c) C beam (1 x 10^{12} ions/cm^2) (d) Si beam (1 x 10^{11} ions/cm^2) (e) Si beam (1 x 10^{12} ions/cm^2)

Fig. 4.7 (a -e) shows frequency dependence of the dielectric loss of the PMMA/Cu nano composites for pristine and irradiated samples. The dielectric loss decreased exponentially at low frequency and then became less dependent on frequency. This is because the induced charges gradually fail to follow the reversing field causing a reduction in the electronic oscillations as the frequency increased. It is noticed that dielectric loss increases moderately with the concentration of filler and also with the fluence which may be attributed to the interfacial polarization mechanism of the heterogeneous system [30, 31].

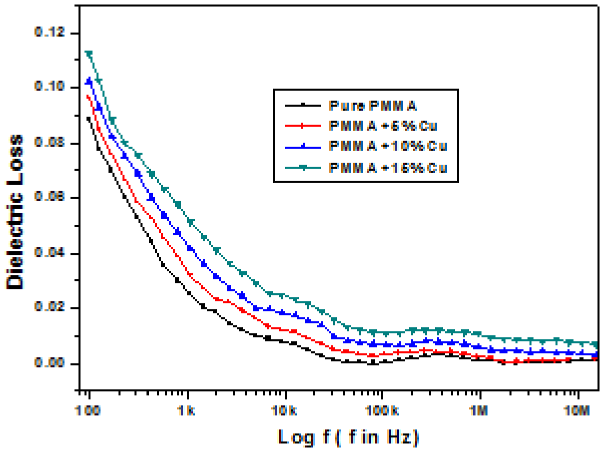

(a)

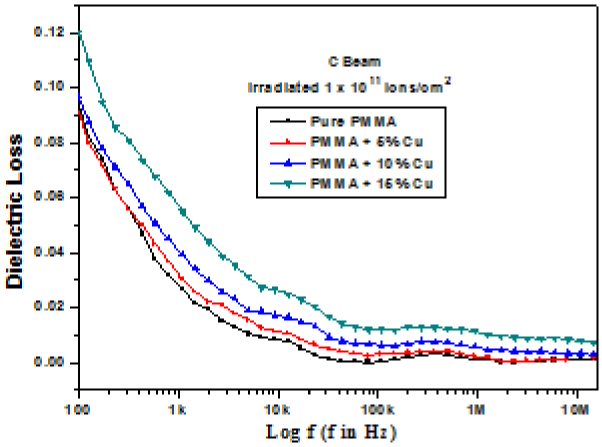

(b)

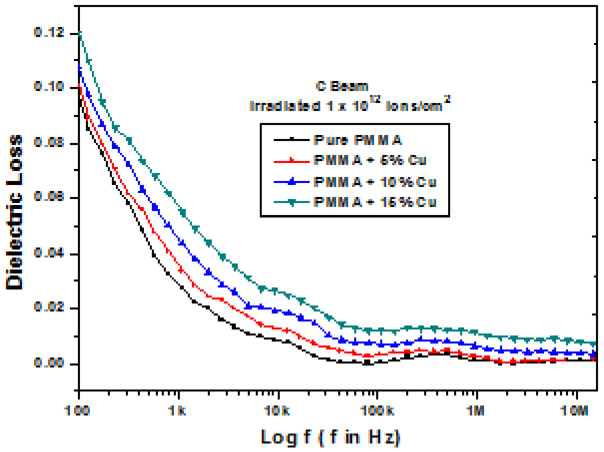
C Beam
Irradiated 1 x 10^{12} Ions/cm^2
Pure PMMA
PMMA + 5% Cu
PMMA + 10% Cu
PMMA + 15% Cu
Dielectric Loss
0.12
0.10
0.08
0.06
0.04
0.02
0.00
100
1k
10k
100k
1M
10M
Log f (f in Hz)

(c)

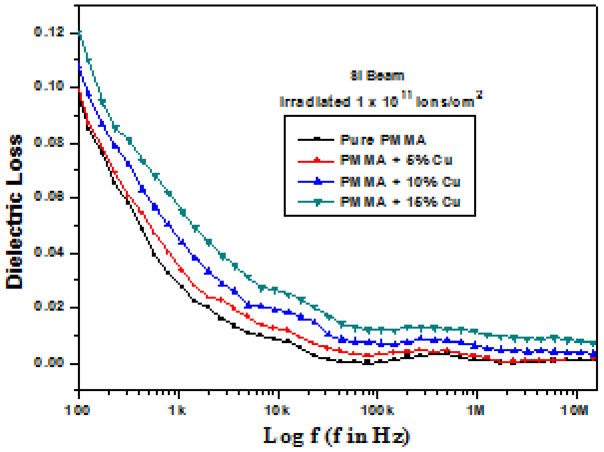
Si Beam
Irradiated 1 x 10^{11} Ions/cm^2
Pure PMMA
PMMA + 5% Cu
PMMA + 10% Cu
PMMA + 15% Cu
Dielectric Loss
0.12
0.10
0.08
0.06
0.04
0.02
0.00
100
1k
10k
100k
1M
10M
Log f (f in Hz)

(d)

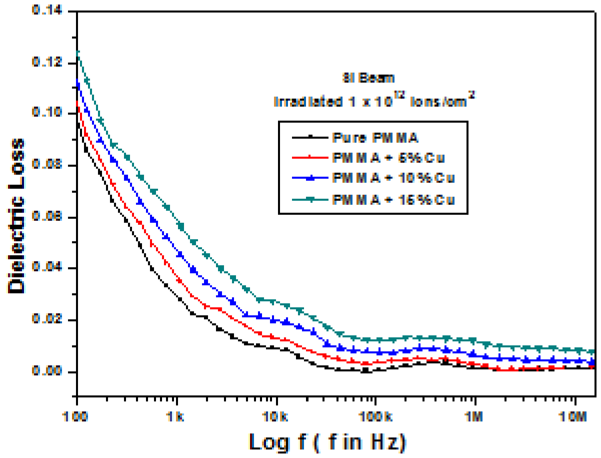
Si Beam
Irradiated 1 x 10^{12} Ions/cm^2
Pure PMMA
PMMA + 5% Cu
PMMA + 10% Cu
PMMA + 15% Cu
Dielectric Loss
0.14
0.12
0.10
0.08
0.06
0.04
0.02
0.00
100
1k
10k
100k
1M
10M
Log f (f in Hz)

(e)

Fig. 4.7 Dielectric loss Vs Log f for (a) pristine (b) C beam (1 x 10^{11} ions/cm^{2}) (c) C beam (1 x 10^{12} ions/cm^{2}) (d) Si beam (1 x 10^{11} ions/cm^{2}) (e) Si beam (1 x 10^{12} ions/cm^{2})

Conclusion:

Dispersion of copper nanoparticles in PMMA films has enhanced the properties of the pure polymer significantly. The increase in dielectric properties with different concentrations may be pointed to the conductive phase formed by dispersed nanoparticles in polymer matrix. Ion beam irradiation also has been shown to significantly enhance the dielectric properties may be due to conversion of the polymeric structure into a hydrogen-depleted carbon network. It was found that the band gap value moved to lower energy (from 4.30 eV upto 3.22 eV) on doping with copper nanoparticles as well as upon irradiation as observed from the UV- visible spectroscopy analysis. An XRD analysis reveals that the crystallite size of the samples decreased after ion beam irradiation which is also corroborated with the DSC analysis due to the chain scissioning upon irradiation.

4.2 Effect of swift heavy ions irradiation on PS + Cu nanocomposites:

4.2.1 X-ray diffraction analysis:

The X-ray diffraction patterns of pristine and irradiated Cu nanocomposites are shown in Fig. 4.8. It clearly indicates that copper is a crystalline but polymer is amorphous in nature and its composites show semi-crystalline behaviour. The diffraction patterns of the irradiated samples by 85 MeV C ions and 120 MeV Si ions which exhibited an increase in the peak intensity and a decrease in the full width at half maximum (FWHM) corresponding to all observed peaks of copper. This behavior may be attributed to cross-linking effect, which may results in the alignment of the polymeric chains.

Table 4.4 Crystallite size of pristine and irradiated samples

Sample	Pristine		C Beam		Si Beam	
	2θ	Crystallite size (nm)	Crystallite size (nm) ($1x10^{11}$) ions/cm^2	Crystallite size (nm) ($1x10^{12}$) ions/cm^2	Crystallite size (nm) ($1x10^{11}$) ions/cm^2	Crystallite size (nm) ($1x10^{12}$) ions/cm^2
PS+ 5%Cu	46.13	11.67	11.74	11.86	12.06	12.21
	57.22	11.94	12.07	12.14	12.20	12.38
	Average	11.80	11.90	12.00	12.13	12.29
PS + 10%Cu	46.16	11.78	11.88	11.96	12.08	12.36
	57.25	12.02	12.11	12.34	12.16	12.58
	Average	11.90	11.99	12.15	12.12	12.47
PS + 15%Cu	46.18	11.89	11.98	12.98	13.21	13.52
	57.23	12.06	12.25	13.11	13.29	13.78
	Average	11.97	12.11	13.05	13.25	13.65

The average crystallite size (t) for pristine and irradiated samples was calculated using Scherrer's formula [11] as given in the chapter 2 in section 2.3.1 by relation 2.2.3.

$b=K\lambda/L\cos\theta$

where b is FWHM in radians, λ is the wavelength of X-ray beam (1.5418 Å), L is the crystallite size in Å, K is a constant which varies from 0.89 to 1.39, but for most of the cases it is close to 1.

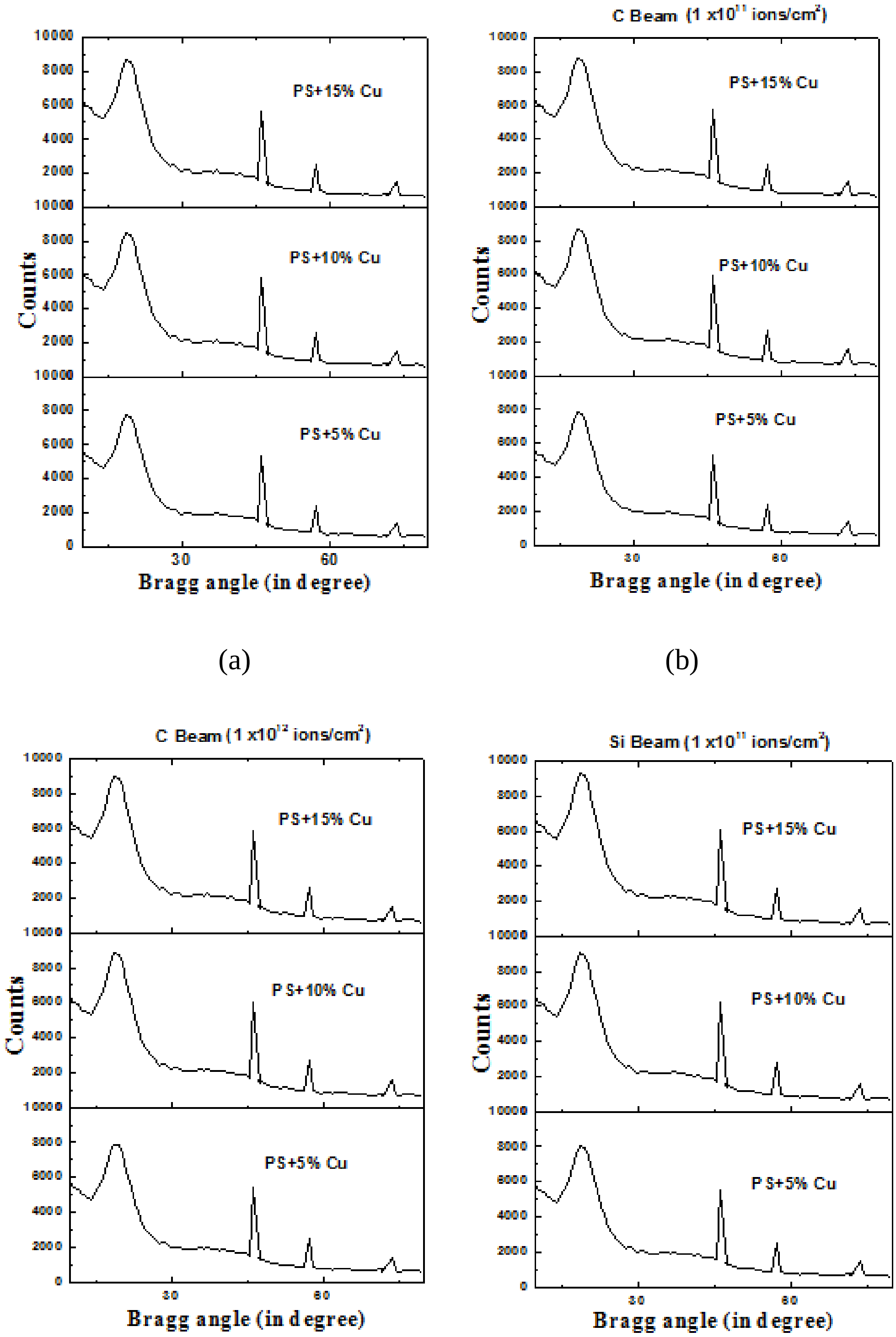

(a) (b)

(c) (d)

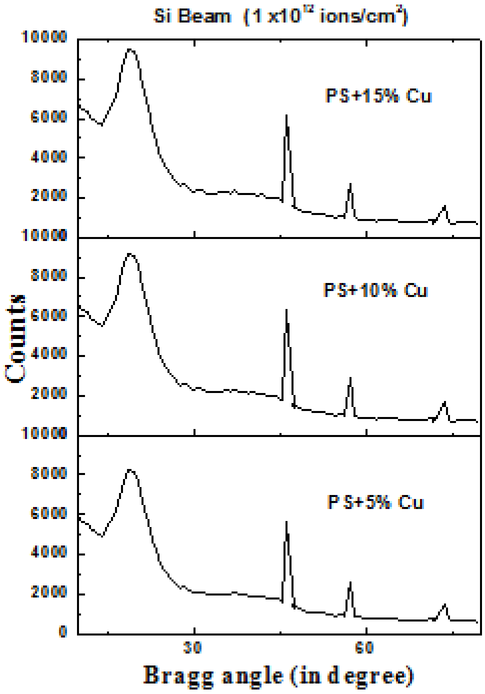

(e)

Fig 4.8 X-ray diffraction patterns of (a) PS+ Cu (pristine) (b) C beam (1 x 10^{11} ions/cm^2) (c) C beam (1 x 10^{12} ions/cm^2) (d) Si beam (1 x 10^{11} ions/cm^2) (e) Si beam (1 x 10^{12} ions/cm^2)

The crystallite size was calculated corresponding to the peak of the pristine and irradiated samples and the results are listed in Table 4.4. The increase in crystallite size suggested the cross linking mechanism [32].

4.2.2 Thermal response (Differential scanning calorimetry (DSC)):

The glass transition temperature (Tg) is an important physical parameter to characterize the structural property of an amorphous polymer in terms of chain rigidity and intermolecular forces [30]. The interaction of polymer chains and nanoparticles surfaces can alter the chain kinetics by decreasing or increasing glass transition temperature of the polymer. Tg of the pure PS is observed at 66.2 ^{o}C and of that compositess are ahown in Fig 4.9. The value of Tg at highest fluence is listed in Table 4.5. Also, it should be pointed out that increase of

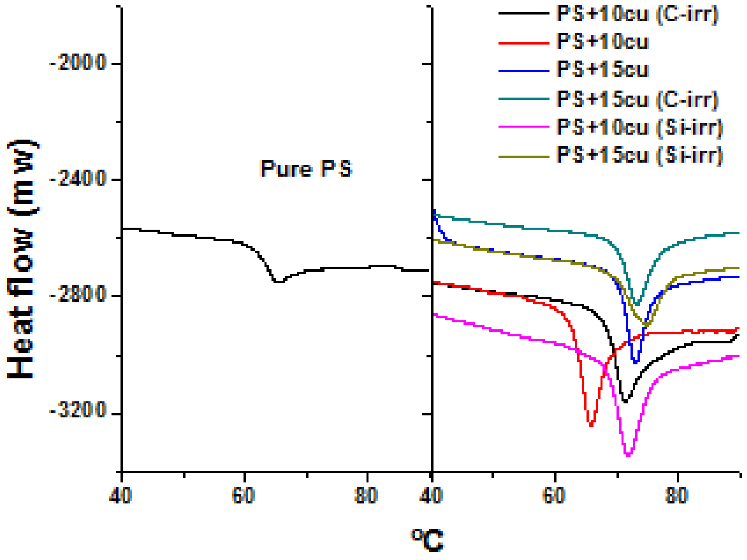

Fig. 4.9 DSC spectra of pure, composites and irradiated (1 x 10^{12} ions/cm^2) films

Table 4.5 Values of glass transition for pristine and irradiated composites

Sample name	Tg (Pristine)	Tg (C beam)	Tg (Si beam)
PS + 10 %Cu	65.9	71.4	72.2
PS + 15 %Cu	72.9	73.3	74.8

Tg with the increase of energy loss as well as with filler content indicates that the mobility of the matrix is altered due to decrease of the interparticle distances. This result is in agreement with previous DSC measurements of Bergeret and Alberola [33]. So after irradiation with ions, glass transition temperature is shifted further towards higher temperature, this further reveals cross linking between nanoparticles and polymer matrix which is also corroborated with XRD results. This behavior probably arises due to branching formed (cross linking effect) when islands of nanoparticles are bonded with polymeric chains. This lowers the mobility of the chains, and as a result the glass transition temperature increases in the nanocomposites [34].

4.2.3 Optical response:

UV–vis spectroscopy is an important tool to investigate the value of optical band gap energy (Eg). The electronic transitions (→) that are involved in the ultraviolet and visible regions are of the following type σ → σ *, n → π*, and π → π* [35]. The absorbance edge of the UV-vis spectra of pristine nanocomposites and irradiated by C ions and Si ions shown in Fig 4.10 (a-e). The absorbance in aromatic compounds is due to the π to π* transition. This is very sensitive to the change in the environment around the phenyl ring [36]. It is observed that optical absorption increases with increasing energy loss and this absorption shifts from UV–vis to the visible region for all irradiated nanocomposite samples. With increase of electronic energy loss, the nanocomposites become gradually opaque to the visible light and the absorption edge shifted from UV to the visible. This is consistent with the observation that the material changes from transparent to opaque with increase of energy deposition. The increase in absorption with irradiation may be attributed to the formation of a conjugated system of bonds due to bond cleavage and reconstruction [37]. The shifting of absorption edge towards visible is generally considered to result from carbonization of the material under irradiation [38] which is also corroborated with dielectric results.

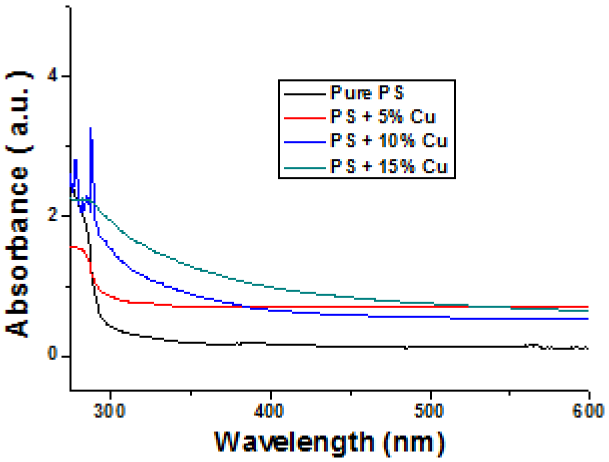
Pure PS
PS + 5% Cu
PS + 10% Cu
PS + 15% Cu
Absorbance (a.u.)
0
2
4
300
400
500
600
Wavelength (nm)

(a)

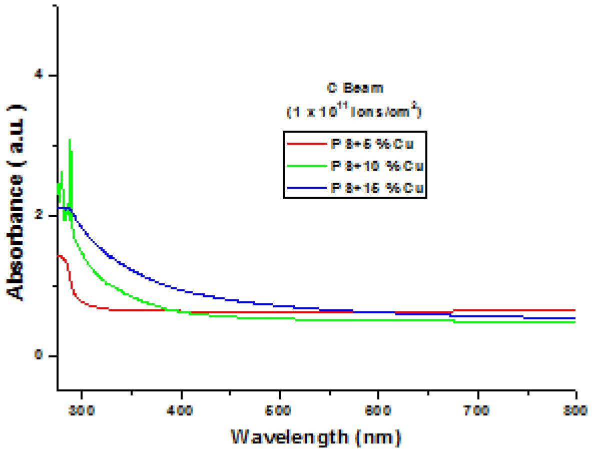
C Beam
(1 x 10^11 Ions/cm^2)
PS+5 %Cu
PS+10 %Cu
PS+15 %Cu
Absorbance (a.u.)
0
2
4
300
400
500
600
700
800
Wavelength (nm)

(b)

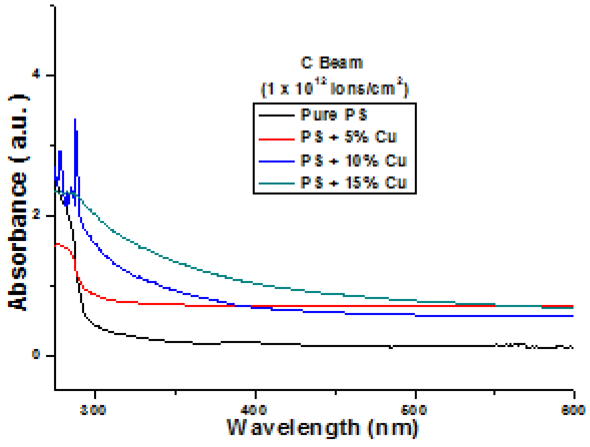
C Beam
(1 x 10^12 Ions/cm^2)
Pure PS
PS + 5% Cu
PS + 10% Cu
PS + 15% Cu
Absorbance (a.u.)
0
2
4
300
400
500
600
Wavelength (nm)

(c)

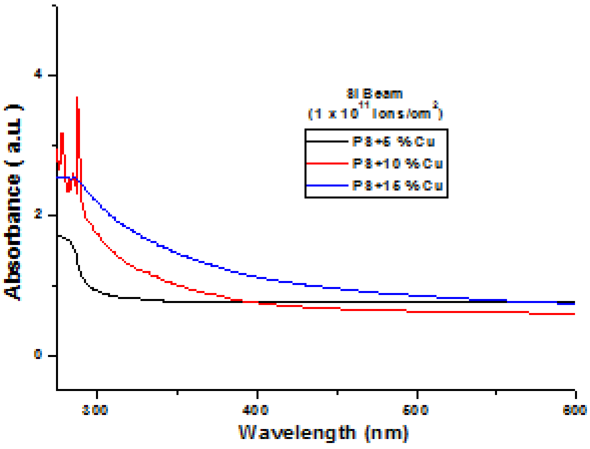

(d)

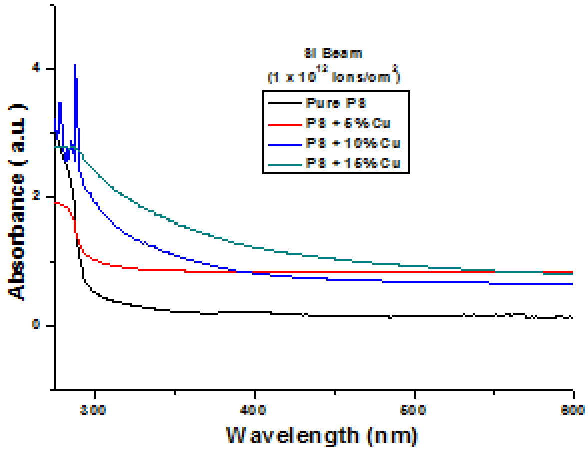

(e)

Fig. 4.10 Absorbance spectra for (a) PS+ Cu(pristine), (b) C beam (1 x 10^{11} ions/cm^2) (c) C beam (1 x 10^{12} ions/cm^2) (d) Si beam (1 x 10^{11} ions/cm^2) (e) Si beam (1 x 10^{12} ions/cm^2)

Determination of optical band gap:

Optical feature of the pristine and irradiated samples have been studied by Perkin-Elmer 25 Lambda UV-Visible spectroscope in the frequency range 200-800 cm^{-1} as illustrated in Fig. 4.10(a-e). The optical band gap E_g is obtained by tauc's equation [17].

i. e. $\omega\varepsilon(\lambda) = (\hbar\omega - E_g)^2$

Where $\varepsilon(\lambda)$ is the optical absorbance and λ is the wavelength. The intersection of the extrapolated spectrum with the abscissa of the plot $\varepsilon^{1/2}/\lambda$ versus $1/\lambda$ yields the gap wavelength λ_g from which the energy gap is derived as $E_g = hc/\lambda_g$. It is noticed that the band gap (energy gap) value shifted to lower energy from 4.33 eV upto 3.40 eV due to doping of copper nanoparticles and also upon irradiation of both ions. This behavior of the optical gap of ion-irradiated samples can be explained following the model of Robertson and O Reilly [39, 40].

The number of carbon hexagon rings in the cluster (M) is then found from the relation [40]

$Eg \approx 2\ |\beta|\ \sqrt{M}$

Where, $|\beta|$ is a bond integral that represents the interaction energy of two π atomic orbitals. A theoretical value for $|\beta|$ proposed by Robertson and O Reilly is 2.9 eV, which according to Compagnini et al. [28] is an overestimation of the true value. So, the best-fit value of $|\beta|$ given by them is 2.2 eV. In the present study on the aromatic polymer, given equation has been used to calculate the value of M and its behaviour with different ions is summarized in Table 4.6. The number of rings (M) remains constant with the filler and upon irradiation except for Si-ions at a fluence of 1×10^{12} ions/cm^2.

Table 4.6 Band gap by direct allowed transitions, number of carbon atoms in pure PS, composites and irradiated films.

Sample	Pristine		C Beam		Si Beam	
	Band gap in eV	No. of carbon hexagon rings	Band gap in eV	No. of carbon hexagon rings	Band gap in eV	No. of carbon hexagon rings
PS + 5%Cu (1 x 10^{11} ions/cm^2)	4.33	~1	4.28	~1	4.04	~1
PS + 5%Cu (1 x 10^{12} ions/cm^2)	4.30	~1	3.94	~1	3.88	~1
PS + 10%Cu (1 x 10^{11} ions/cm^2)	4.24	~1	3.90	~1	3.78	~1
PS + 10%Cu(1 x 10^{12} ions/cm^2)	4.17	~1	3.82	~1	3.60	~1
PS + 15%Cu (1 x 10^{11} ions/cm^2)	4.10	~1	3.75	~1	3.50	~1
PS + 15%Cu(1 x 10^{12} ions/cm^2)	3.98	~1	3.65	~1	3.40	~2

4.2.4 Surface morphology:

Fig. 4.11(a–c) shows the SEM images of pristine, composites and irradiated composite films with magnification of X250. The analysis shows that the filled partilces are distributed randomly in the matrix which display continuous contact between themselves and formed conducting paths. The surface becomes smoothen upon irradiation.The decrease in roughness with Cu-nanoparticles may be attributed to the decrease in density of metal particles on the surfaces of the films, which is also responsible for increase in crystallinity of the material as indicated by XRD analysis.

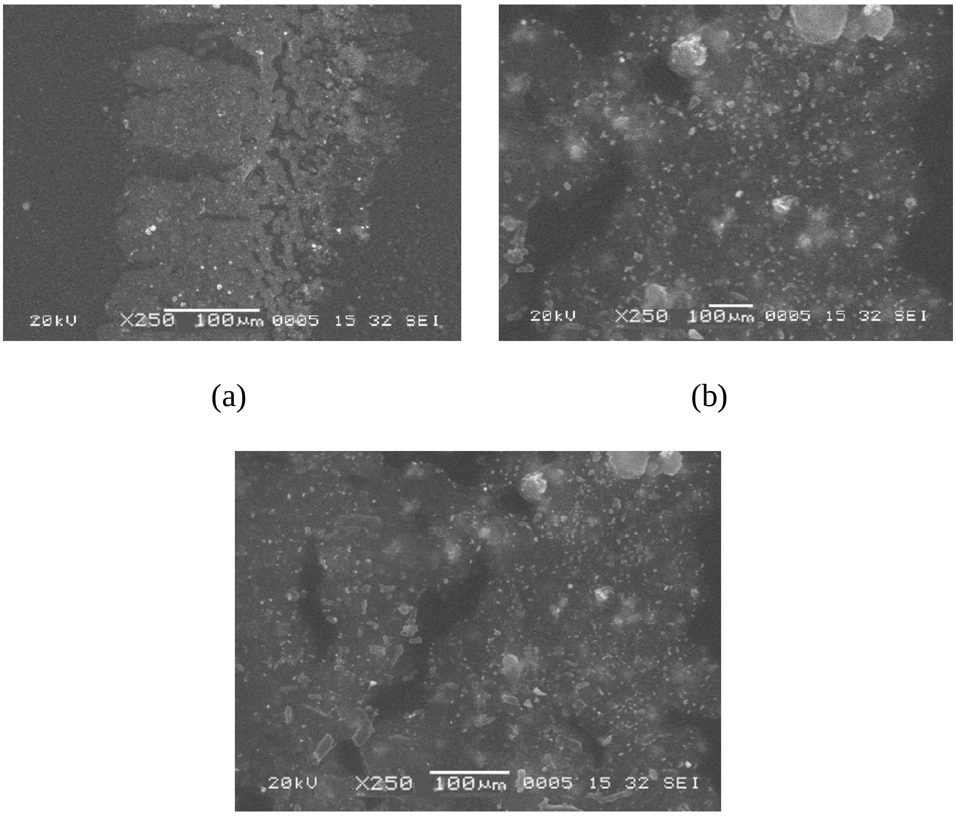

(a) (b)

(c)

Fig. 4.11 SEM images of (a) PS+ 15 % Cu (pristine) (b) PS + 15 % Cu (C beam- 1 x 10^{12}) (c) PS + 15 % Cu (Si beam- 1 x 10^{12})

4.2.5 AC electrical frequency response:

Conductivity: The ac conductivity of the composites as a function of the frequency is shown in the Fig.4.12 (a-e). The conductivity of composite was studied with respect to irradiation fluence and filler concentration. The conductivity of composite was increased with concentration of filler that is possibly due to the electronic interaction process taking place in the composites and therefore resulted composites show more conductive with the increase of the filler content [41]. It is known that the electrical conductivity of such composites depends on the type and concentration of the fillers. Irradiation is expected to promote the metal to polymer bonding and convert the polymeric structure into a hydrogen depleted carbon network due to emission of hydrogen and/or other volatile gases. It is this carbon network that is believed to make the polymer more conductive [32].

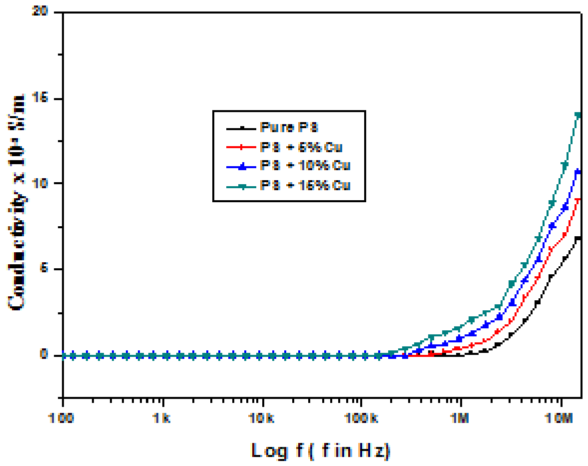

(a)

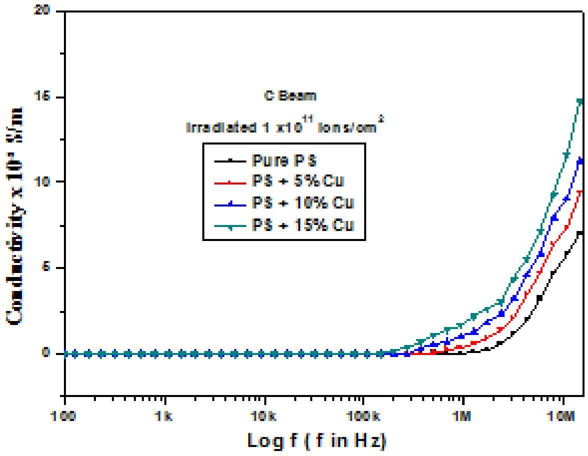

(b)

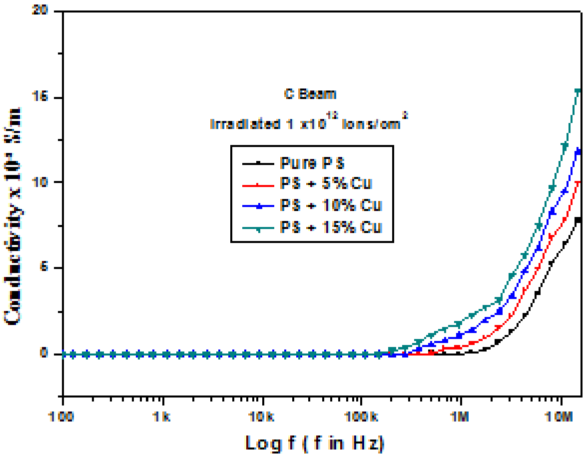
C Beam
Irradiated 1 x10^{12} Ions/cm^{2}
Pure PS
PS + 5% Cu
PS + 10% Cu
PS + 15% Cu
Conductivity x 10^{-3} S/m
20
15
10
5
0
100
1k
10k
100k
1M
10M
Log f (f in Hz)

(c)

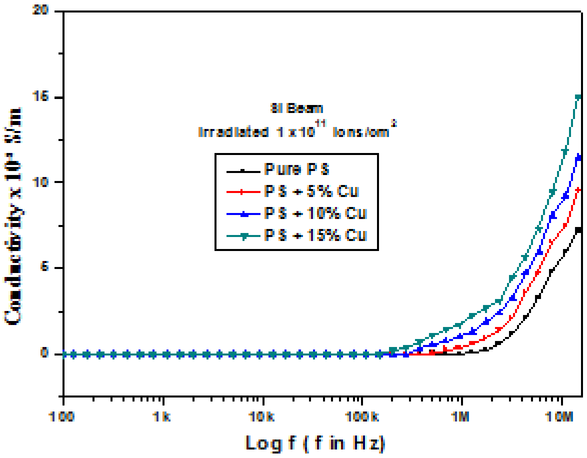
SI Beam
Irradiated 1 x10^{11} Ions/cm^{2}
Pure PS
PS + 5% Cu
PS + 10% Cu
PS + 15% Cu
Conductivity x 10^{-3} S/m
20
15
10
5
0
100
1k
10k
100k
1M
10M
Log f (f in Hz)

(d)

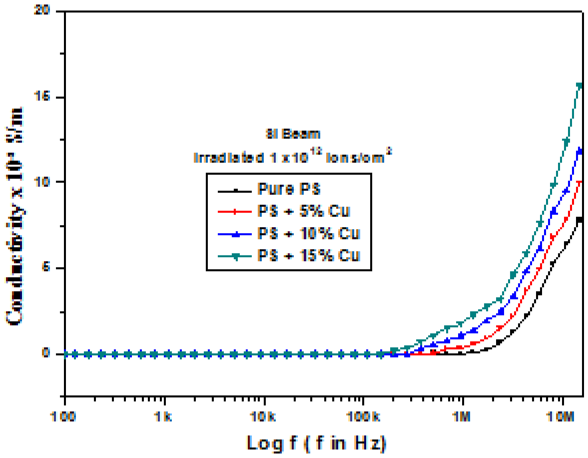
SI Beam
Irradiated 1 x10^{12} Ions/cm^{2}
Pure PS
PS + 5% Cu
PS + 10% Cu
PS + 15% Cu
Conductivity x 10^{-3} S/m
20
15
10
5
0
100
1k
10k
100k
1M
10M
Log f (f in Hz)

(e)

Fig. 4.12 Conductivity Vs Log f for (a) pristine (b) C beam (1 x 10^{11} ions/cm^2) (c) C beam (1 x 10^{12} ions/cm^2) (d) Si beam (1 x 10^{11} ions/cm^2) (e) Si beam (1 x 10^{12} ions/cm^2)

Dielectric properties of composites:

Fig. 4.13 (a-e) shows the variation of dielectric constant of pristine and irradiated PS/Cu nanocomposites at different concentrations (5%, 10%, 15%) of Cu nanoparticles as a function of frequency with C-ions and Si-ions respectively. The increase in the dielectric content with filler content is a direct consequence of interfacial polarization effect between polymer and the filler particles [42, 43]. It is observed that dielectric permittivity remains almost constant up to 100 kHz, because the motion of charge carriers is almost constant at these frequencies. As frequency increases further the polarization of trapped and bound charges cannot take place due to the charge carriers migrate through the dielectric and get trapped against defect sites and induces an opposite charge in its vicinity and hence the dielectric constant

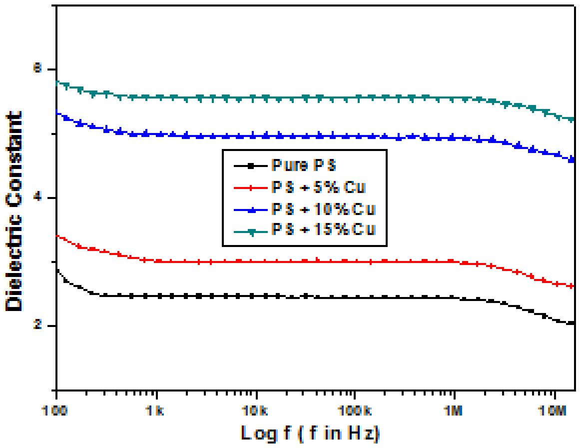

(a)

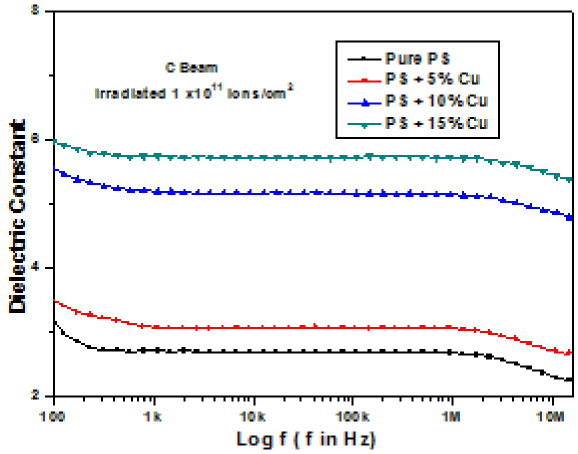
C Beam
Irradiated 1 x10^{11} Ions/cm^2
Pure PS
PS + 5% Cu
PS + 10% Cu
PS + 15% Cu
Dielectric Constant
2
4
6
8
100
1k
10k
100k
1M
10M
Log f (f in Hz)

(b)

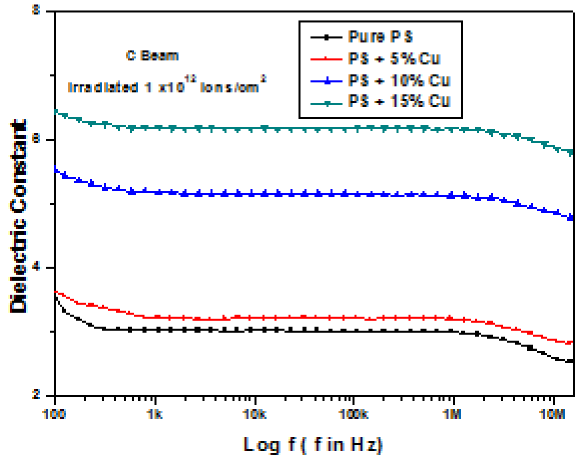
C Beam
Irradiated 1 x10^{12} Ions/cm^2
Pure PS
PS + 5% Cu
PS + 10% Cu
PS + 15% Cu
Dielectric Constant
2
4
6
8
100
1k
10k
100k
1M
10M
Log f (f in Hz)

(c)

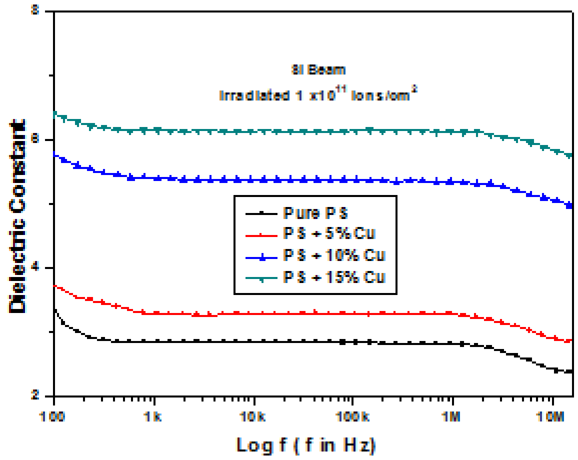
Si Beam
Irradiated 1 x10^{11} Ions/cm^2
Pure PS
PS + 5% Cu
PS + 10% Cu
PS + 15% Cu
Dielectric Constant
2
4
6
8
100
1k
10k
100k
1M
10M
Log f (f in Hz)

(d)

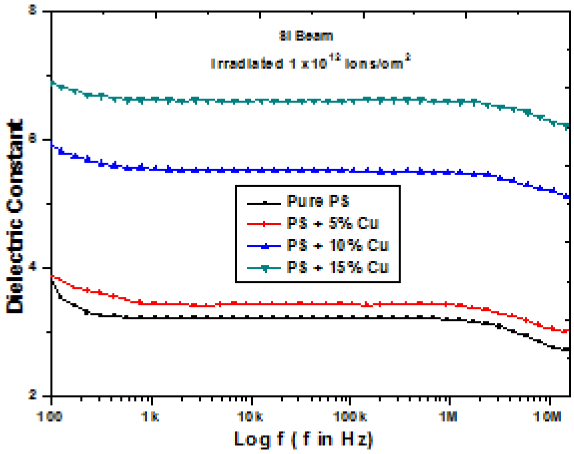

(e)

Fig. 4.13 Dielectric Constant Vs Log f for (a) pristine (b) C beam (1 x 10^{11} ions/cm^2) (c) C beam (1 x 10^{12} ions/cm^2) (d) Si beam (1 x 10^{11} ions/cm^2) (e) Si beam (1 x 10^{12} ions/cm^2)

decreases. Also according to Dissado and Hill theory at high frequency, intra-cluster motions are dominant. In intra-cluster motions, the relaxation of a dipole will produce a ‘chain’ response in its neighboring dipoles and the reaction of the neighboring dipoles will, in turn, affect the first dipole, so the overall effect will be seen as a single cluster dipole moment relaxation [30, 44]. This reduces the dielectric constant at these frequencies. It was also observed that dielectric constant increases after ion beam irradiation by both ions (C and Si) which may be attributed to chain scission and the resulting an increase in free radicals, unsaturation etc.

The increase in dielectric loss with increasing filler contents may be attributed to the interfacial polarization mechanism of the heterogeneous system. Fig. 4.14 (a-e) shows the variation of dielectric loss with frequency of pristine and irradiated with C-ion and Si-ion respectively. The dielectric loss decreases exponentially and then becomes less dependent on frequency. This is because the induced charges gradually fail to follow the reversing field, causing a reduction in the electronic oscillations as frequency increases [30].

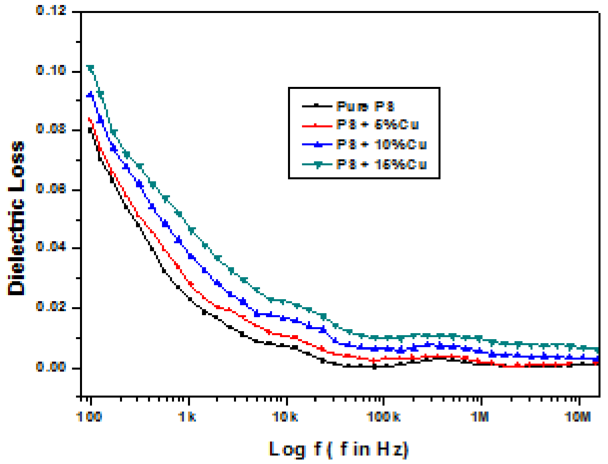
Dielectric Loss
0.12
0.10
0.08
0.06
0.04
0.02
0.00
100
1k
10k
100k
1M
10M
Log f (f in Hz)
Pure PS
PS + 5%Cu
PS + 10%Cu
PS + 15%Cu

(a)

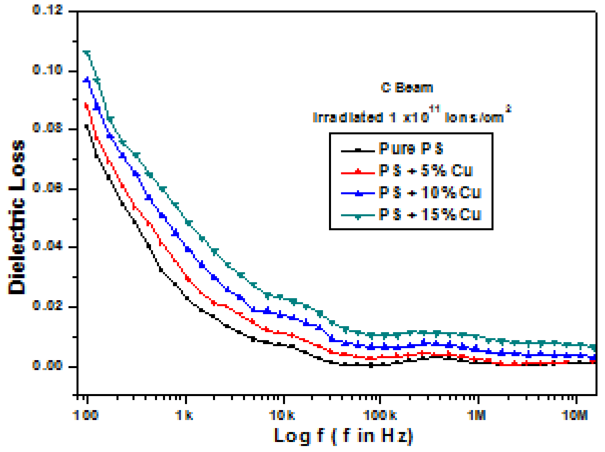
Dielectric Loss
0.12
0.10
0.08
0.06
0.04
0.02
0.00
100
1k
10k
100k
1M
10M
Log f (f in Hz)
C Beam
Irradiated 1 x10^11 Ions/cm^2
Pure PS
PS + 5% Cu
PS + 10% Cu
PS + 15% Cu

(b)

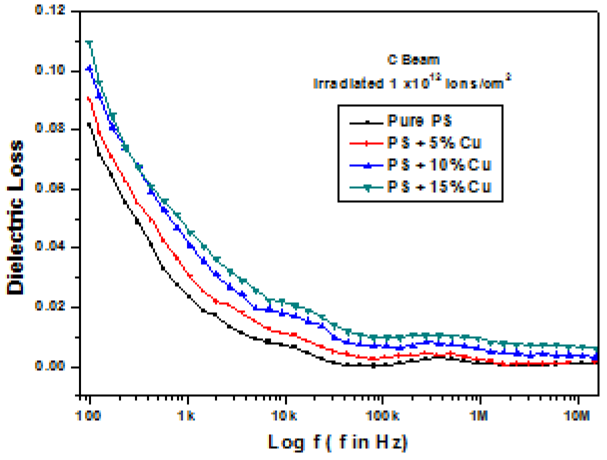
Dielectric Loss
0.12
0.10
0.08
0.06
0.04
0.02
0.00
100
1k
10k
100k
1M
10M
Log f (f in Hz)
C Beam
Irradiated 1 x10^12 Ions/cm^2
Pure PS
PS + 5% Cu
PS + 10% Cu
PS + 15% Cu

(c)

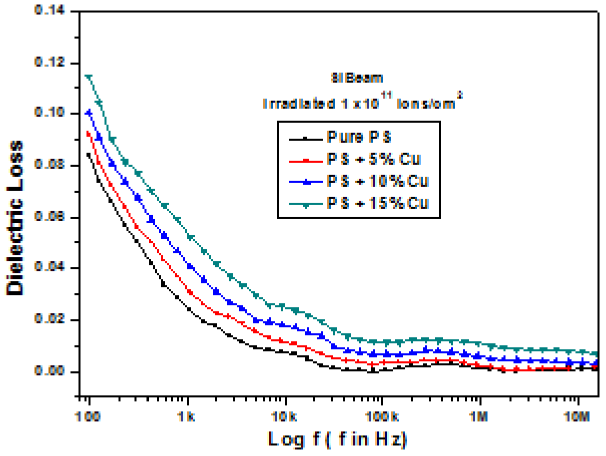

(d)

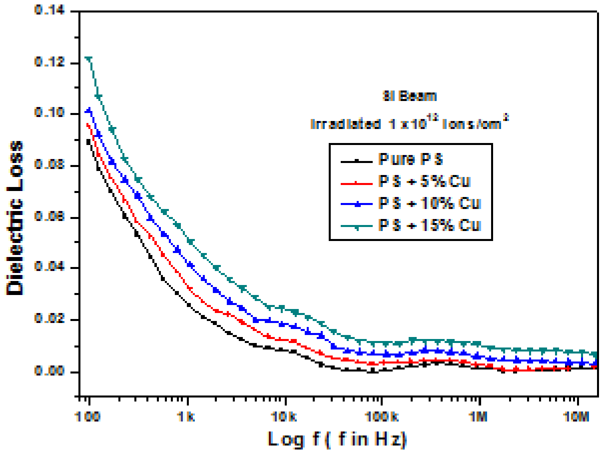

(e)

Fig. 4.15 Dielectric loss Vs Log f for (a) pristine (b) C beam (1 x 10^{11} ions/cm^2) (c) C beam (1 x 10^{12} ions/cm^2) (d) Si beam (1 x 10^{11} ions/cm^2) (e) Si beam (1 x 10^{12} ions/cm^2)

Conclusion:

Dispersion of copper nanoparticles in PS films has enhanced the properties of the pure polymer significantly. An XRD analysis reveals that the crystallite size of the samples increased after ion beam irradiation which is also corroborated with the DSC analysis due to the cross linking effect upon irradiation. It is found that the band gap value moved to lower energy (from 4.33 eV upto 3.40 eV) on doping with copper nanoparticles as well as upon irradiation as observed from the UV- visible spectroscopy analysis. The increase in dielectric properties with different concentrations may be pointed to the conductive phase formed by dispersed nanoparticles in polymer matrix. Ion beam irradiation also has been shown to significantly enhance the dielectric properties may be due to conversion of the polymeric structure into a hydrogen-depleted carbon network. So we have concluded that effect of Si-beam is more effective than that of the C-beam in the present study because of large energy loss of heavy ion.

4.3 Summary

In this chapter, two different nano composites i.e (PMMA/Cu, PS/Cu) have been studied using two different ions beams (C and Si) irradiations. Structural, optical, thermal, electrical properties and surface morphology have been examined by different characterization techniques.

In PMMA/Cu nanocomposites, results show that the crystallite size of fillers decreases slightly upon both ions beams irradiations as observed from XRD analysis. It is also observed that the intensity of the peak decreases and to some extent broadening of the peak after irradiation offers confirmation of decrease in crystallinity. Since no significant change in the peak position is observed, this reveals that lattice parameters do not change significantly in both ions irradiations. Whereas in the case of PS nanocomposites, crystallite size of fillers increases upon both ions irradiations which may be attributed to cross linking phenomenon.

In DSC thermograms, the Tg value decreases upon irradiations in PMMA nanocomposites and increases upon irradiations in PS composites. This behavior probably arises due to branching (cross-linking effect) when islands of nanoparticles are bonded with polymeric chains. This lowers the mobility of the chains, and as a result, the glass transition temperature increases in the nanocomposites.

The band gap values for both composites were increased upon concentration of fillers and both ions irradiations. It was observed from the UV- visible spectroscopy analysis that the band gap value moved to the lower energy.

SEM images showed that increase in density in PMMA nanocomposites and decrease in density in PS nanocomposites upon irradiations.

Ac electrical conductivity of all pristine and irradiated samples at different filler concentrations is shown in Fig.4.16. The increase in conductivity with copper nanoparticles concentration for pristine samples may be attributed to the conductive phase formed by dispersed metal nanoparticles in polymer matrix. The conductivity of composite was studied with respect to irradiation fluence and filler concentration. The conductivity of composite was increased with concentration of filler that is possibly due to the electronic interaction process taking place in the composites and therefore resulted composites show more conductive with the increase of the filler content. It is known that the electrical conductivity of such composites depends on the type and concentration of the fillers. Irradiation is expected to promote the metal to polymer bonding and convert the polymeric structure into a hydrogen depleted carbon network due to emission of hydrogen and/or other volatile gases. It is this carbon network that is believed to make the polymer more conductive Fig 4.16 shows comparison of conductivity of all composites before and after irradiation. For the sake of comparison filler concentration (5, 10, 15 wt%) at a fluence of 1 x 10^{12} ions/cm^2 for C and Si ions beam at a frequency 10 MHz have considered. In Fig 4.17, shows similar comparison for dielectric constant of all composites.

Fig.4.17 shows the dependence of the dielectric constant on the frequency of the applied field at different filler concentrations and irradiation fluences.

In all the cases, it reveals that dielectric loss is positive and signifies inductive behaviour of the material.

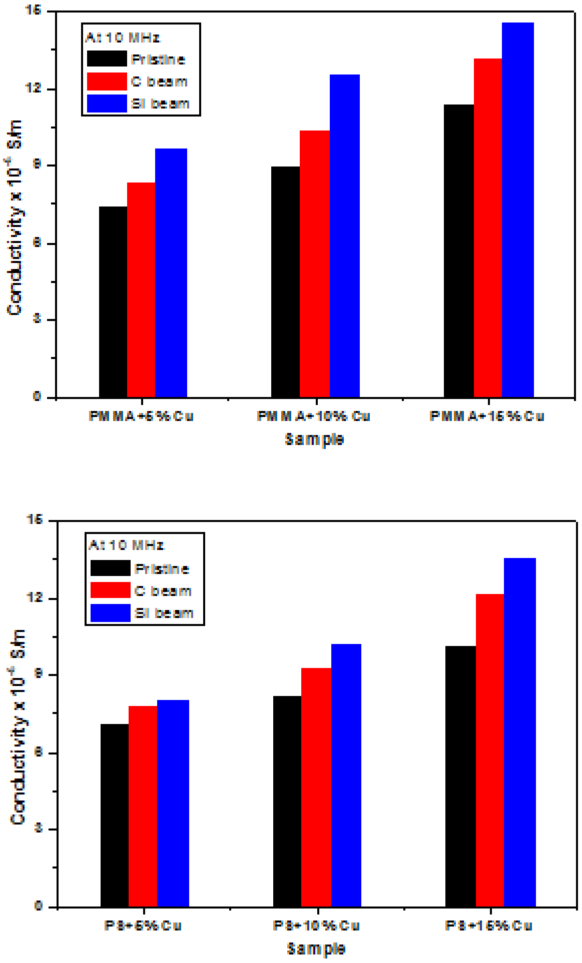

Fig. 4.16 Comparison of Conductivity of pristine and irradiated samples at 10 MHz

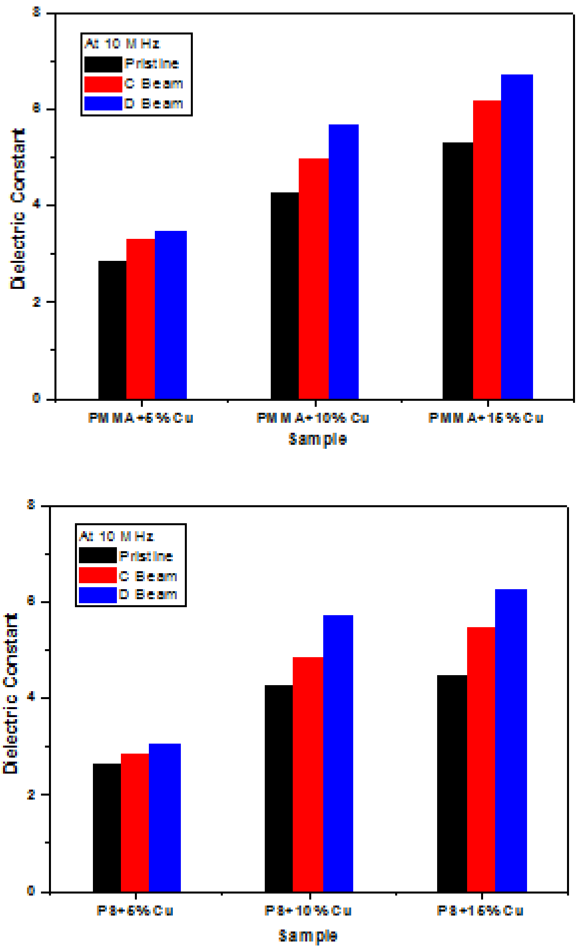

Fig. 4.17 Comparison of Dielectric constant of pristine and irradiated samples at 10 MHz

References:

[1] J.L. Wilson, P. Poddar, N.A. Frey, H. Srikanth, K. Mohomed, J.P. Harmon, S. Kotha, J. Wachsmuth, J. Appl. Phys. 95 (2004) 1934.

[2] A. Heilmann, Polymer Films with Embedded Metal Nanoparticle, Springer, New York, 2003.

[3] P. O' Rourke Muisener, L. Clayton, J. D' Angelo, J.P. Harmon, J. Mater. Res. 17 (2002) 2507.

[4] H. Qiao, Z. Wei, H. Yang, L. Zhu, X. Yan, J. Nanomater. 2009 (2009) 795928.

[5] H. Gleiter, Progr. Mater. Sci. 33 (1990) 223.

[6] Z.L. Wang, Y. Liu, Z. Zhang, Handbook of Nanophase and Nanostructured Materials, Tsinghua University Press, Beijing, China, 2002.

[7] G. H. Chan, J. Zhao, E. M. Hicks, G. C. Schatz, R. P. V. Duyne, *Nano letters* 7(7) (2007) 1947.

[8] Z. Zhu, C. Liu, Y. Sun, J. Liu, Y. Yang, Y. Jin, J. Du, Nucl. Instrum. Methods B 191 (2002) 723.

[9] Chaitali Gavade, Sangeeta Kishorea, N.L. Singh, P.K. Khanna, Radiation Effects and Defects in Solids, 168 (2013) 504.

[10] Chaitali Gavade, N. L. Singh, P. K. Khanna , Sunil Shah, Jounrnal of nanoscience and nanotechnology. (communicated)

[11] P. Scherrer, Gott Nachar 2 (1918**)** 98–100.

[12] A. K. Srivastava, H. S. Virk, J. Polym. Mater. 17 (2000) 325.

[13] N. L. Singh, D. Singh, A. Qureshi, Radiation Effects & Defects in Solids 66(8-9) (2011) 640–647.

[14] A. Semwal, A. Negi, R. G. Sonkawade, J. M. S. Rana, R. C. Ramola, Indian J of pure and App Phy 48 (2010) 496-499.

[15] H S Virk , P S Chandi And A K Srivastava, Bull. Mater. Sci. 24(5) (2001) 529.

[16] L. Singh, K. Singh Samra, Radiation Physics and Chemistry 77 (2008) 252–258.

[17] A. Das, S. Dhara and A. Patnaik Physical Rev B 59 (1999) 11069.

[18] Anjum Qureshi , Dolly Singh , N.L. Singh, S. Ataoglu , Arif N. Gulluoglu , Ambuj Tripathi ,D.K. Avasthi, Nuclear Instruments and Methods in Physics Research B 267 (2009) 3456.

[19] S. Shah, N.L. Singh, A. Qureshi, D. Singh, K.P. Singh, V. Shrinet, A. Tripathi, Nucl. Instrum. Methods B 226 (2008) 1768.

[20] N. L. Singh, A. Qureshi, A. K. Rakshit, D. K. Avasthi, Bull. Mater. Sci.,29 (2006) 605-609.

[21] M. Abu-Abdeen, G. M. Nasr, H. M. Osman, A. I. Abound, Egypt. J. Sol., 25 (2002) 275-294.

[22] Y. P. Mamunya, V. V. Davyadenko, P. Pissis, E. V. Lebedev, Eur. Polym. J.,28 (2002) 1887-1897.

[23] D. Singh, N. L. Singh, A. Qureshi, P. Kulriya, A. Tripathi, D. K. Avasthi, A. N. Gulluoglu, J. Non-Cryst. Solids, 356 (2010) 856-863.

[24] S. M. Reda, Dyes and Pigments,75 (2007) 526-532.

[25] S. Shah, N. L. Singh, A. Qureshi, D. Singh, K. P. Singh, V. Shrinet, A. Tripathi, Nucl. Instrum. Methods B 226 (2008) 1768-1774.

[26] Y. Q. Wang, M. Curry, E. Tavenner, N. Dobson, R. E. Giedd, Nucl. Instrum.

Methods B 219 (2004) 798-803.

[27] S. Prasher, M. Kumar, S. Singh, Asian Journal of Chemistry, 21(10) (2009) S043-S046.

[28] S. Singh, M. Thomas Joy, IEEE Transactions on Dielectrics and Electrical Insulation, 2008, 15(1).

[29] G. Sui, S. Jana, W. H. Zhong, M.A. Fuqua, C. A. Ulven, Acta Materialia, 56 (2008) 2381–2388.

[30] N. L. Singh, S. Shah, A. Qureshi, K. P. Singh, V. Shrinet, P. K. Kulriya, A. Tripathi, Radiation Effects & Defects in Solids,163(2) (2008) 169-177.

[31] N. L. Singh, S. Shah, A. Qureshi, A. Tripathi, F. Singh, D. K. Avasthi, P. M. Raole, Bull. Mater. Sci.,34(1) (2011) 81–88.

[32] D. Singh, N.L. Singh, A. Qureshi, P. Kulriya, A. Tripathi, D.K. Avasthi, A.N. Gulluoglu, J. Non-Cryst. Solids, 356 (2010) 856–863.

[33] A. Qureshi, N. L. Singh, S. Shah, F. Singh, D.K. Avasthi, J. Macromol. Sci., 45 (2008) 265–270.

[34] S. Shah, D. Singh, A. Qureshi, N. L. Singh, K. P. Singh, V. Shrinet, Indian J. Pure Appl. Phys., 46 (2008) 439–442.

[35] Rajesh Kumar, S. Asad Ali, A.K. Mahur, H.S. Virk, F. Singh, S.A. Khan, D.K. Avasthi, Rajendra Prasad, Nuclear Instruments and Methods in Physics Research B 266 (2008) 1788–1792.

[36] S. Saravanana, M.R. Anantharaman, S. Venkatachalam, D.K. Avasthi, Vacuum 82 (2008) 56–60.

[37] L.S. Farenza, R.M. Papaleo, A. Hallen, M.A. Araujo, R.P. Livi, B.U.R. Sundqvist, Nucl. Instr. and Meth. B 105 (1995) 134.

[38] Zhiyong Zhu, Yunfan Jin, Changlong Liu, Youmei Sun, Mingdong Hou, Chonghong Zhang, Zhiguang Wang, Jie Liu, Xiaoxi Chen, Baoquan Li, Yanbin Wang, Nuclear Instruments and Methods in Physics Research B 169 (2000) 83-88.

[39] J. Robertson, E.P. O Reilly, Phys. Rev. B 35 (1987) 2946.

[40] Lakhwant Singh, Kawaljeet Singh Samra, Ravinder Singh, Nuclear Instruments and Methods in Physics Research B 255 (2007) 350–356.

[41] Z. Elimat, J. Phys. D: Appl. Phys., 39 (2006) 2824-2828.

[42] Anjum Qureshi, Ayhan Mergen, Mehmet S. Erog Lu, N. L. Singh, Arif Gu Llu Og Lu, Journal of Macromolecular Science, Part A: Pure and Applied Chemistry 45 (2008) 462–469.

[43] G.C. Psarras, E.Manolakaki, G.M. Tsangarris, Composites A 33 (2002) 375-384.

[44] L.A. Dissado and R.M. Hill, Proc. Roy. Soc. London 390 (1983) 131.

Chapter - V

Effect of swift heavy ions on physical properties of PMMA/Ni and PS/Ni nanocomposites

---

Abstract

In this chapter swift heavy ions (120 MeV Si ions, 85 MeV C ions) induced modifications of Nickel nanoparticles dispersed PMMA and PS composites films at the fluences of 1 x 10^{11}, 1 x 10^{12} ions/cm^2 were studied. 120 MeV Si swift heavy ions induced more prominent effects on the physicochemical properties of polymer nanocomposites compared to those of C-ions. An XRD analysis reveals that the crystallite size of the composites decreased after ion beam irradiation which is also corroborated by the DSC analysis due to the chain scissioning upon irradiation in PMMA nanocomposites. In PS nanocomposites, we observed cross linking upon irradiation. It was observed from the UV- visible spectroscopy analysis that the band gap value moved to the lower energy on doping with metal nanoparticles, as well as upon irradiation. SEM images showed damages upon ion beam irradiation. Magnetic properties enhanced after irradiation which may be attributed to the exchange dipole interaction of particles in the matrix and generation of free radicals.The dielectric constant of the composites increased with the increase of metal content and also upon ion beam irradiation. These phenomena could be interpreted from interfacial polarization of heterogeneous systems.

5.0 Introduction:

Nanoscale materials promise to be important in the development of various current and future focused applications. New behavior at nanoscale not only arises due to the order of magnitude reduction in size but also the appearance of new characteristics like size confinement, interfacial phenomena, quantum mechanics, Coulomb blockade etc [1]. Nanoparticles are characterized by an extremely large surface to volume ratio, and their properties are determined mainly by the behavior of their surface [2]. Nanosize particles (NPs) of ferromagnetic metals such as Fe, Co, and Ni have been extensively studied due to the richness of their novel physical properties and the broad range of potential applications. As an important transition metal, Ni nanoparticles have wide range of applications in the fields of permanent magnets, magnetic fluids, magnetic recording media, solar energy absorption, fuel cell electrodes, catalysts etc [3]. Metal nanoparticles dispersed in polymer matrices have recently been the subjects of intense study for the development of nano electronics devices [4]. The thermoplastic polymers used as the hosts are the potential lead for manufacture of the nanocomposites because the size and distribution of dispersed metal nanoparticles can be readily organized.

The ion irradiated polymers exhibited enhanced oxidation resistance and improved electrical conductivity. Irradiation effects in inorganic materials are manifested as changes in physical properties such as refractive index, magnetization and hardness [5]. The fundamental processes associated with these changes are defect formation through electronic and nuclear interactions of radiation and the subsequent chemical interaction between the defects and elements in the materials. Study of radiation induced defects in inorganic compounds is important for their role in device fabrication [6, 7]. The chemical changes brought about by ion beam in polymers underline that the physical modifications are limited to a few basic processes: gas evolution, cross linking and degradation. The chemical changes are more dramatic in polymers because of the macromolecular structure of these materials. The kind of changes, which predominate, depends on the polymer type and radiation dosage.

In this chapter we are dealing with polymer nanocomposites and effect of irradiation upon

(i) PMMA + Ni [8]

(ii) PS + Ni [9]

Properties and preparation methods of nanocomposites have been discussed in chapter 2. All the films were irradiated with 120 MeV Si- ions and 85 MeV C- ions at the fluences of 1 x 10^{11}, 1 x 10^{12} ions/cm^2 at Inter University Accelerator Centre (IUAC), New Delhi, India. We have studied changes in the optical, structural, dielectric thermal and magnetic properties of composites due to swift heavy ion irradiation by means of UV–visible spectroscopy, X-ray diffraction, impedance gain phase analyzer and differential scanning calorimetry and SQUID magnetometer.

5.1 Effect of swift heavy ions irradiation on PMMA + Ni nanocomposites:

5.1.1 X-ray diffraction analysis:

X-ray diffraction spectra as shown in Fig. 5.1(a-g) reveal the amorphous nature of pure PMMA and crystalline behaviour of Ni powder. The appearance of sharp peak in composite indicates some degree of crystallinity, although the decrease in intensity of the diffraction peak and a slight broadening of the peak after irradiation gives evidence of decrease in crystallinity. However, no considerable change in the peak position is observed, which reveals that the lattice parameters do not change significantly [10]. The crystallite size has been calculated before and after irradiations using Scherrer's formula [11] as dicussed in chapter 2 in section 2.3.1 from the realtion 2.2.3.

$b = K\lambda / L\cos\theta$

where b is FWHM in radians, λ is the wavelength of X-ray beam (1.5418 Å), L is the crystallite size in Å, K is a constant which varies from 0.89 to 1.39, but for most of the cases it is close to 1.

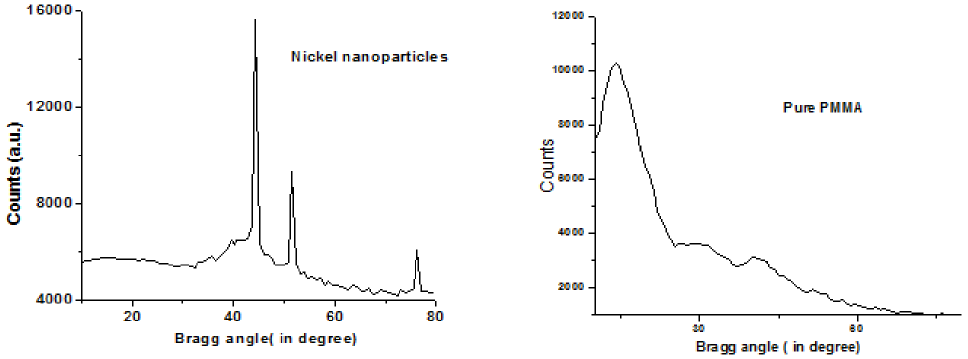

(a) (b)

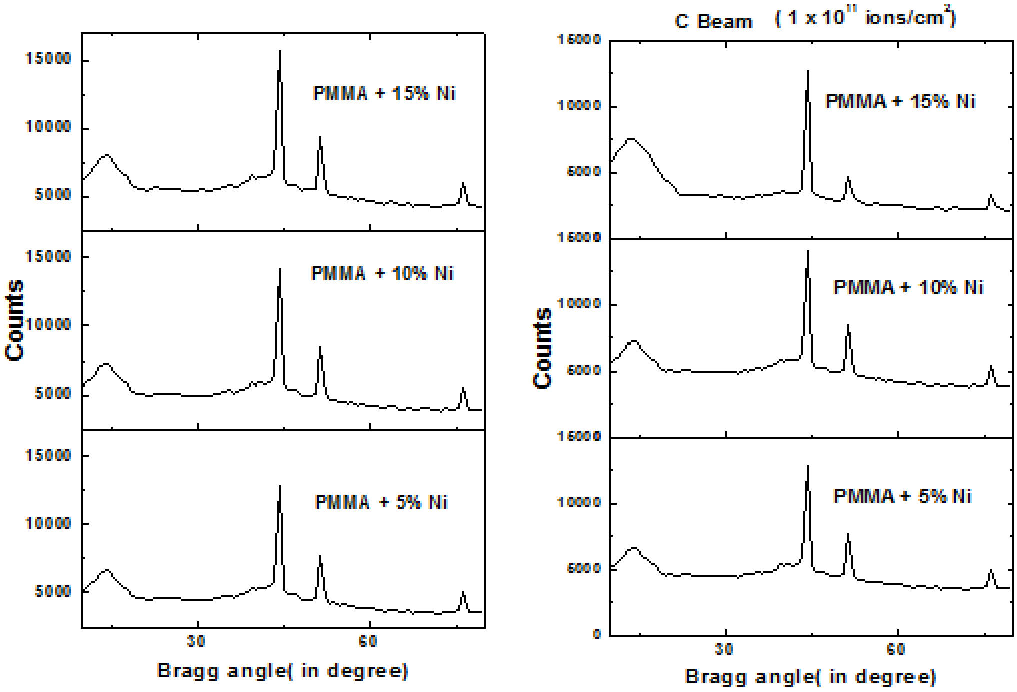

(c) (d)

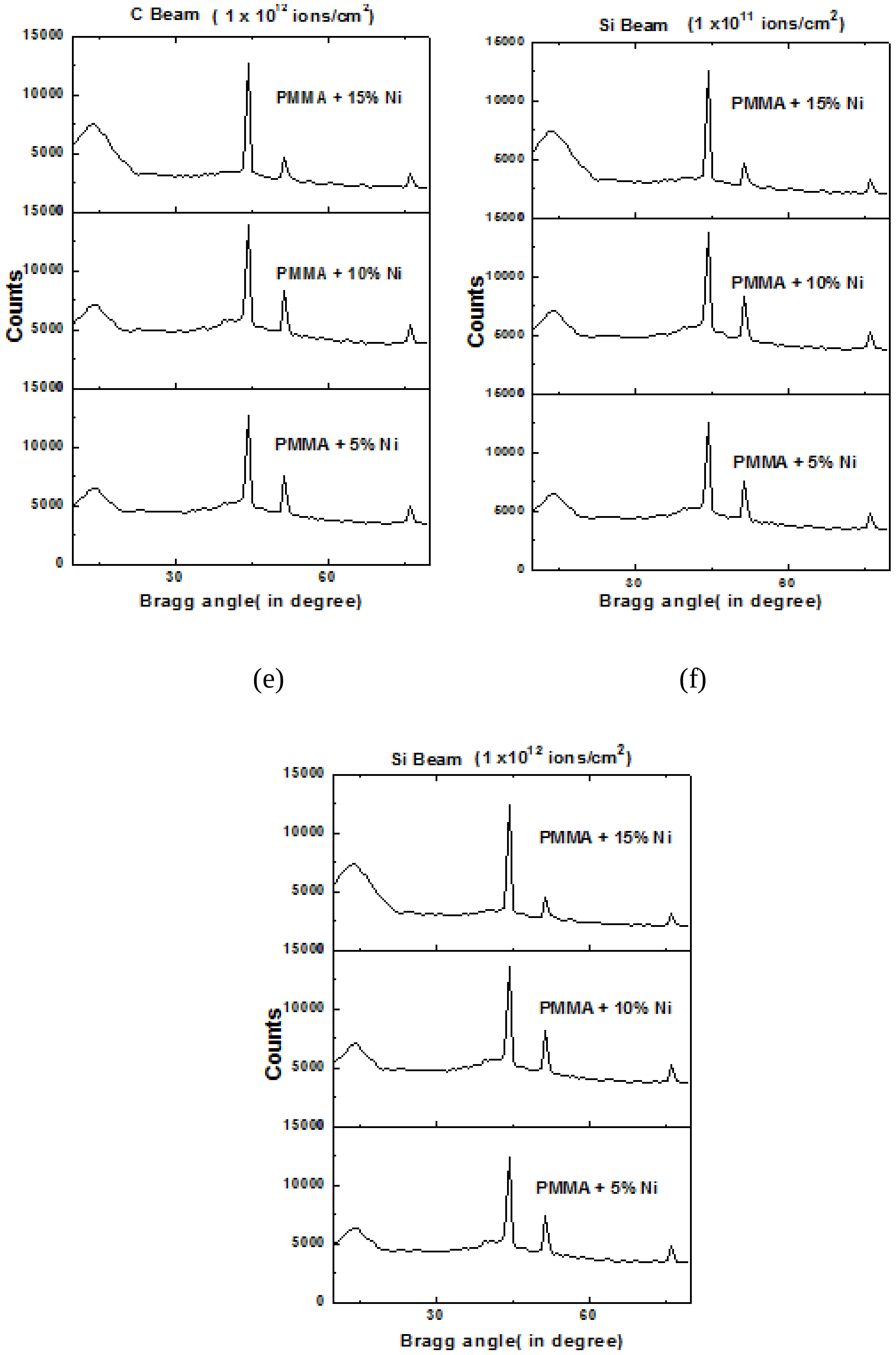

(e)

(f)

(g)

Fig. 5.1 X-ray diffraction patterns of (a) nickel nanoparticles (b) pure PMMA (c) PMMA+ Ni(pristine), (d) C beam (1 x 10^{11} ions/cm^2) (e) C beam (1 x 10^{12} ions/cm^2) (f) Si beam (1 x 10^{11} ions/cm^2) (g) Si beam (1 x 10^{12} ions/cm^2)

The crystallite sizes of the pristine and irradiated samples are listed in Table 5.1. The irradiation may induce chain scissioning, which is also corroborated by DSC analysis, assumed to be responsible for the reduction in crystallinity of the composite because of large amount of energy deposition in the material [10].

Table 5.1 Crystallite size of pristine and irradiated samples

Sample	Pristine		C Beam		Si Beam	
	2θ	Crystallite size (nm)	Crystallite size (nm) $(1x10^{11})$ ions/cm^2	Crystallite size (nm) $(1x10^{12})$ ions/cm^2	Crystallite size (nm) $(1x10^{11})$ ions/cm^2	Crystallite size (nm) $(1x10^{12})$ ions/cm^2
PMMA+ 5%Ni	44.58	14.65	14.21	13.78	13.65	13.53
	51.58	12.82	12.35	11.21	11.02	10.37
	Average	13.74	13.28	12.50	12.34	11.95
PMMA + 10%Ni	44.35	14.20	13.51	12.50	12.05	11.87
	51.40	11.90	11.45	11.03	10.80	10.20
	Average	13.05	12.48	11.77	11.43	11.04
PMMA + 15%Ni	44.28	12.54	11.10	11.05	10.98	10.67
	51.37	10.50	10.32	10.21	10.04	9.58
	Average	11.52	10.71	10.63	10.51	10.13

5.1.2 Thermal response (Differential Scanning Calorimetery (DSC)):

The glass transition temperature (*T*g) is the important property of the polymer, The glass transition is defined to be the reversible change in amorphous materials between a hard, brittle state into a rubbery molten state. At the glass transition temperature, the weak secondary bonds that stick the polymer chains together are broken, and the macromolecule starts to move. A differential scanning calorimetry (DSC) experiment was performed using a reference and a predetermined heating (or cooling) rate was imposed to the system with a temperature excursion. If a temperature difference develops between the sample and reference, the power is adjusted to remove the difference and DSC measures the heating power difference between the sample and reference and it was recorded as shown in Fig. 5.2. The pure PMMA has a Tg value of about 64.60 ^{o}C, while tendency of increasing Tg value after insertion of nanoparticles was observed for Ni/PMMA nanocomposites. We found that the value of Tg, for pristine and irradiated samples is observed at about 78.74^{o}C and 76.33^{o}C, respectively, for highest concentration of Ni nanoparticles due to Si ion irradaition. After irradiations, it was found that Tg shifted to lower temperature. It reveals that the ion irradiation leads to polymer chain scissioning and subsequently reduction in molecular weight. As a result, the system moved towards the more disordered state, which is also corroborated by XRD results [12]. The value of Tg for highest fluence is listed in Table5.2.

Table 5.2 Values of glass transition for pristine and irradiated composites

Sample name	Tg (Pristine)	Tg (C beam)	Tg (Si beam)
PMMA + 5 %Ni	67.1	66.5	65.1
PMMA + 10 %Ni	71.2	69.5	66.9
PMMA + 15 %Ni	77.8	76.8	72.8

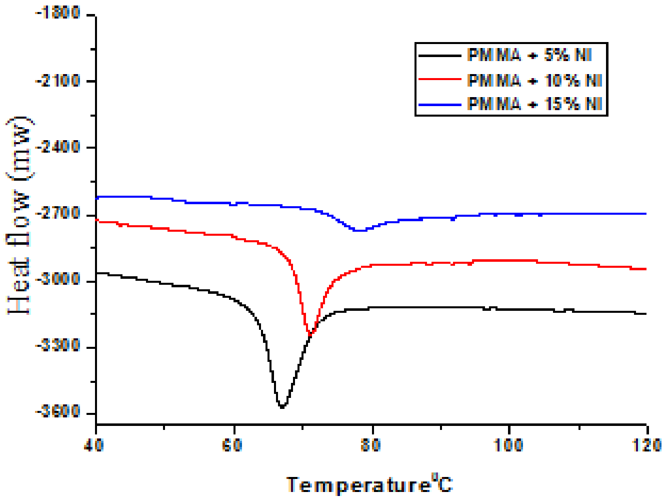

(a)

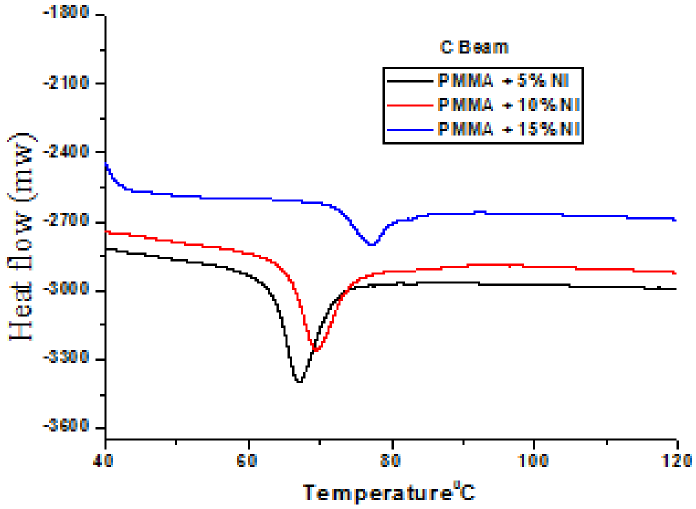

(b)

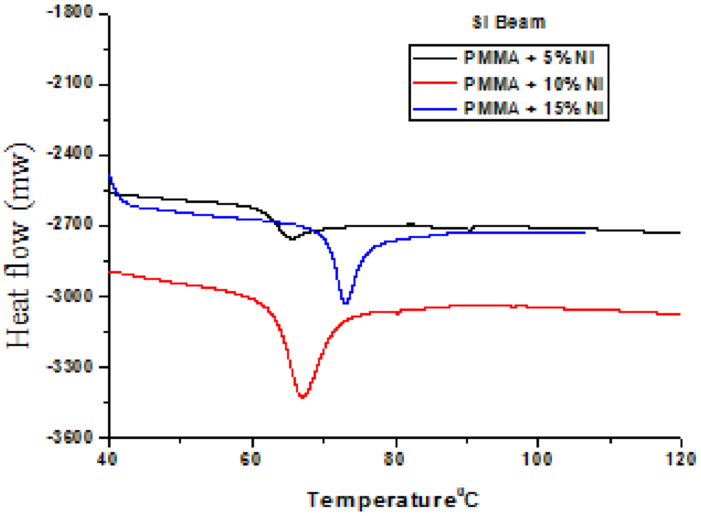

(c)

Fig. 5.2 DSC curves for pristine and irradiated (1 x10^{12} ions/cm^2) samples

5.1.3 Optical response:

The promotion of electrons in the σ, π and n orbitals from ground state to the higher energy states which are described by molecular orbitals due to the absorption of light energy by polymeric samples in the UV and visible regions. Many of the optical transitions which occur due to the presence of impurities have energies in the visible region of the spectrum, consequently the defects are referred to as colour centres. The effect of ion beam interaction with polymers produces damage and leads to the generation of new defects and charge states [13, 14]. A shift in the absorption edge towards longer wavelength is observed for irradiated samples as shown in Fig. 5.3(a-e). This behaviour is generally interpreted as caused by the formation of extended systems of conjugated bonds, i.e. possible formation of carbon clusters. In the investigated range of wavelengths the absorption bands are associated to the π–π* electronic transitions. These types of transitions occur in the unsaturated centers of the molecules, i.e. in compounds containing double or triple bonds and also in aromatics. The excitation of π electron requires smaller energy and hence, transition of this type occurs at longer wavelengths [15].

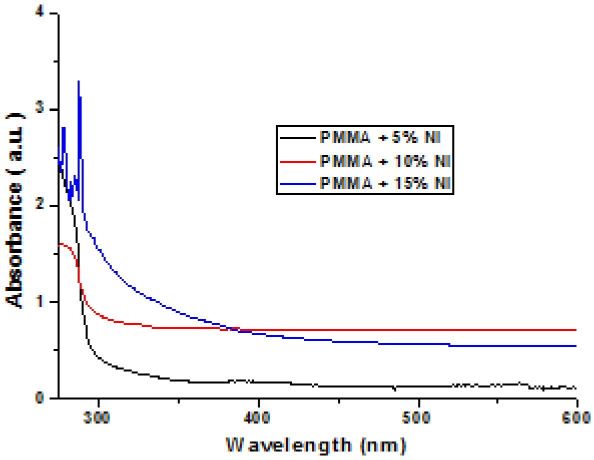

(a)

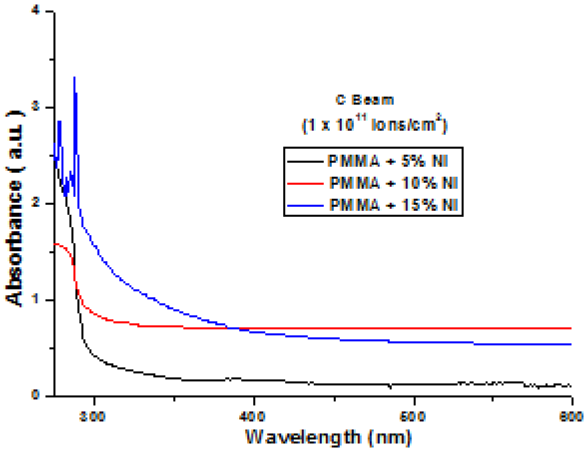

C Beam
(1 x 10^{11} Ions/cm^2)
PMMA + 5% Ni
PMMA + 10% Ni
PMMA + 15% Ni
Absorbance (a.u.)
0
1
2
3
4
300
400
500
600
Wavelength (nm)

(b)

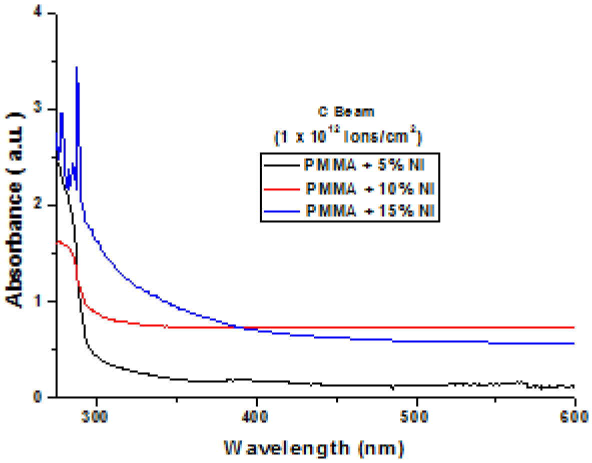

C Beam
(1 x 10^{12} Ions/cm^2)
PMMA + 5% Ni
PMMA + 10% Ni
PMMA + 15% Ni
Absorbance (a.u.)
0
1
2
3
4
300
400
500
600
Wavelength (nm)

(c)

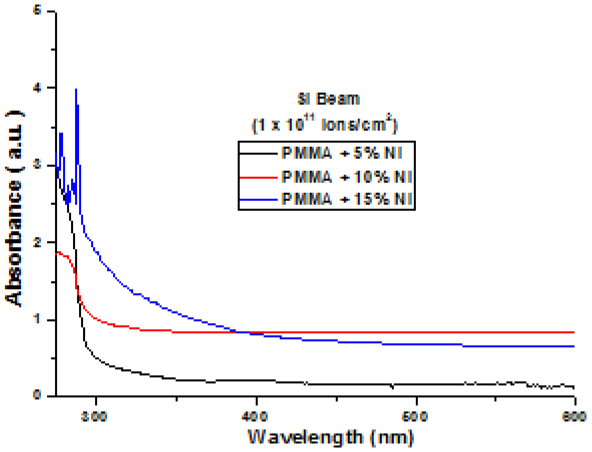

Si Beam
(1 x 10^{11} Ions/cm^2)
PMMA + 5% Ni
PMMA + 10% Ni
PMMA + 15% Ni
Absorbance (a.u.)
0
1
2
3
4
5
300
400
500
600
Wavelength (nm)

(d)

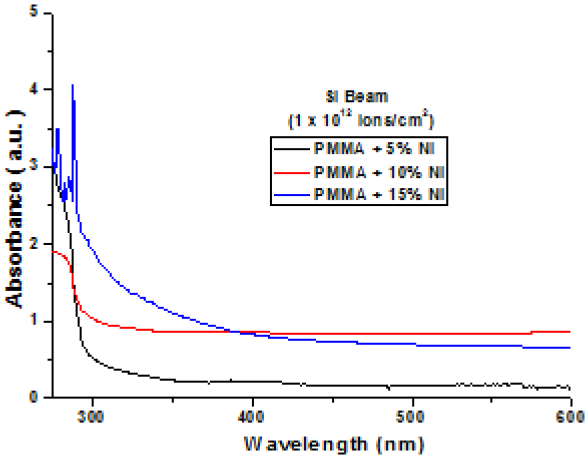

(e)

Fig. 5.3 Absorbance spectra for (a) PMMA+ Ni (pristine) (b) C beam (1 x 10^{11} ions/cm^2) (c) C beam (1 x 10^{12} ions/cm^2) (d) Si beam (1 x 10^{11} ions/cm^2) (e) Si beam (1 x 10^{12} ions/cm^2)

Determination of band gap:

The change in optical properties have been studied by Perkin- Elmer 25 Lambda UV-Visible spectrophotometer for the pristine and irradiated samples in the frequency range 200-600 cm^{-1} as illustrated in Fig. 5.3. The optical band gap E_g is obtained by Tauc's equation [16] as described in chapter 2 in section 2.3.3 by relation 2.2.4.

$\omega\varepsilon(\lambda)=(\hbar\omega-E_g)^2$

where $\varepsilon(\lambda)$ is the optical absorbance and λ is the wavelength. The intersection of the extrapolated spectrum with the abscissa of the plot $\varepsilon^{1/2}/\lambda$ versus $1/\lambda$ yields the gap wavelength λ_g from which the energy gap is derived as $E_g = hc/\lambda_g$. It is noticed that the band gap (energy gap) value shifted to lower energy from 4.37 eV to 3.43 eV due to doping of nickel nanoparticles and also upon irradiation. This is because of the scissioning of polymer chain and as a result, creation of free radicals, unsaturation etc. and thus a capability of increasing the conductivity of the composites [17].

The number of carbon atoms per cluster (N) can be calculated by following the relation 2.2.5 [18] as discussed in chapter 2 in section 2.3.3; the values are listed in Table 5.3.

$Eg=34.3/\sqrt{N}eV$

where N is the number of carbon atoms per cluster and Eg is the energy band gap.

Table 5.3 Band gap by direct allowed transitions, number of carbon atoms in pristine and irradiated composites films.

Sample	Pristine	C Beam		Si Beam	
	B.G eV	B.G eV 1×10^{11} ions/cm^2	B.G eV 1×10^{12} ions/cm^2	B.G eV 1×10^{11} ions/cm^2	B.G eV 1×10^{12} ions/cm^2
PMMA + 5%Ni	4.37	4.28	4.18	4.15	3.95
PMMA + 10%Ni	4.16	4.10	3.92	3.86	3.74
PMMA + 15%Ni	3.84	3.75	3.55	3.48	3.43

Sample	Pristine	C Beam		Si Beam	
	No. of carbon atoms(N)	No. of carbon atoms(N) 1×10^{11} ions/cm^2	No. Of carbon atoms(N) 1×10^{12} ions/cm^2	No. of carbon atoms(N) 1×10^{11} ions/cm^2	No. Of carbon atoms(N) 1×10^{12} ions/cm^2
PMMA + 5%Ni	62	64	67	68	75
PMMA + 10%Ni	68	72	77	80	84
PMMA + 15%Ni	80	83	90	97	100

5.1.4 Surface Morphology:

Fig. 5.4(a–d) shows the SEM images of pristine, composites and irradiated composite films with magnification of X250. The analysis shows that the filled partilces are distributed randomly in the matrix which display continuous contact between themselves and formed conducting paths. After irradiation, significant changes in surface morphology were observed. Considerable damage in the polymeric structure was observed after irradiation, which is also responsible for decrease in crystallinity of the material as indicated by XRD analysis [19].

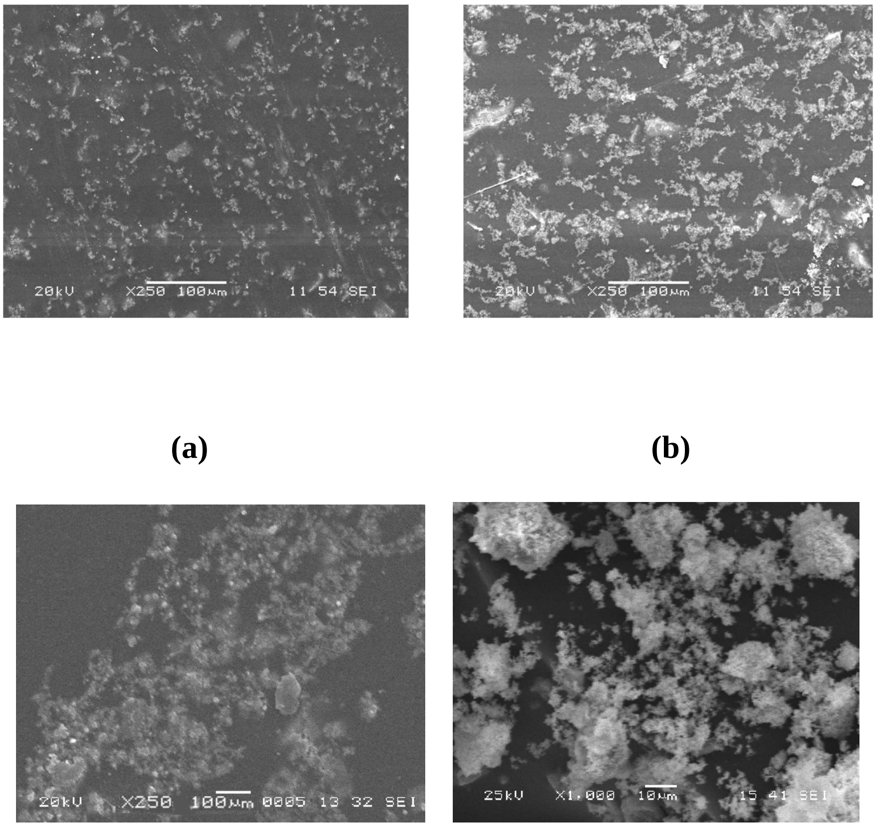

(a) **(b)**

(c) **(d)**

Fig. 5.4 SEM images of (a) PMMA+ 15 % Ni (pristine) (b) PMMA + 15 % Ni (C beam) (c) PMMA + 15 % Ni (Si beam) and (d) Nickel nanoparticles

5.1.5 Magnetic Properties:

The temperature (T) and magnetic field (H) variations of the magnetization (M) were measured with a SQUID (superconducting quantum interference device) magnetometer. The temperature variations of M for the zero field- cooled (ZFC) and the field-cooled (FC) cases were measured from 5-300 K at applied field, H = 500 Oe. Hysteresis measurements were carried out at 300 K with magnetic field swept from 50 kOe to -50 kOe.

Nickel is known to be one of the important magnetic materials. The magnetic measurement of Ni/PMMA nanocomposites having Ni concentration of 15% by weight is discussed here. Figure 5.5(a, b, c) shows the M-H curves for the pristine and irradiated samples. The magnetic parameters extracted from the measurements are listed as saturation magnetization (M_S) ~ 0.085 emu/gm, coercive field (H_C) ~ 138 Oe, remnant magnetization (M_R) ~ 0.015 emu/gm for pristine and M_S ~ 0.107 emu/gm, H_C ~147 Oe, M_R ~ 0.020 emu/gm and M_S ~ 0.120 emu/gm, H_C ~150 Oe, M_R ~ 0.022 emu/gm for C and Si ions irradiated composites, respectively. For the sake of comparison, we note that the saturation magnetization and the coercive field for commercial bulk nickel powder at 300 K are about 57.5 emu/g and 100 Oe, respectively. Kumar et al.[20] showed that M_S ~ 30.1 emu/gm for nickel nanoparticles in the polystyrene matrix is smaller than that of commercial bulk nickel powder; the magnetization of the nickel nanoparticles in the polystyrene matrix at 1.6 Tesla did not reach full saturation and shows a very weak hysteresis. This deviation is undoubtedly a result of the nanostructure of the sample. The saturation magnetization in nanoparticle system is generally lower than that of the bulk materials and is strongly influenced by the supporting matrix. The increase in values of M_S and H_C after irradiation may be attributed to the change in exchange and dipolar interactions mediated by the matrix.

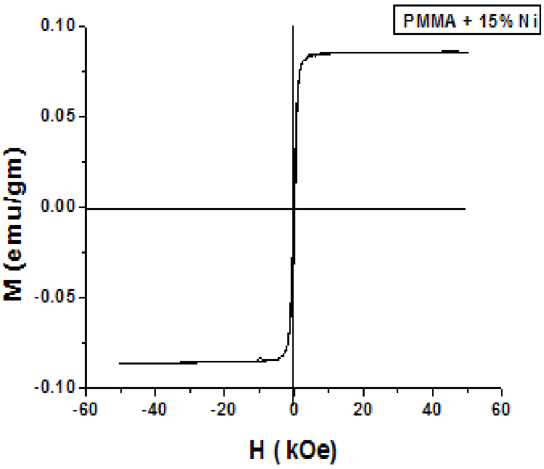
PMMA + 15% Ni
0.10
0.05
0.00
-0.05
-0.10
M (emu/gm)
-60
-40
-20
0
20
40
60
H (kOe)

(a)

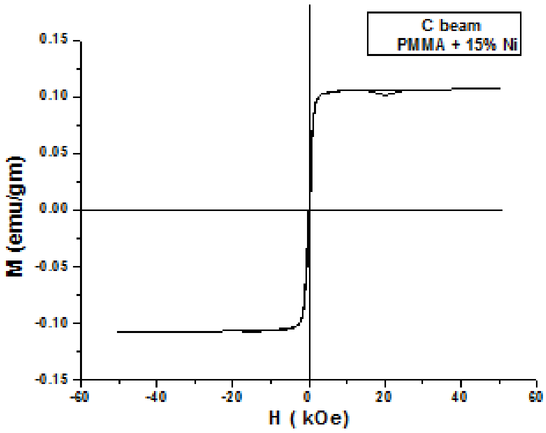
C beam
PMMA + 15% Ni
0.15
0.10
0.05
0.00
-0.05
-0.10
-0.15
M (emu/gm)
-60
-40
-20
0
20
40
60
H (kOe)

(b)

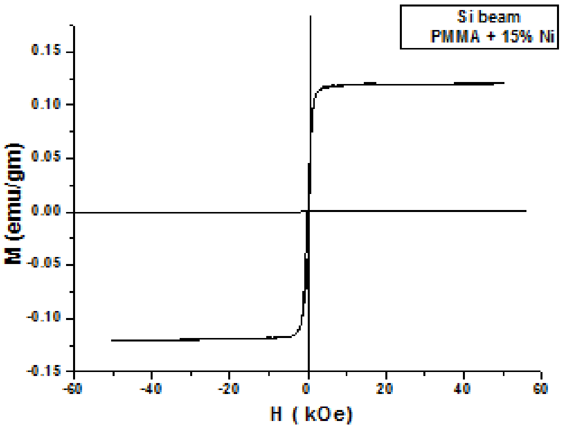
Si beam
PMMA + 15% Ni
0.15
0.10
0.05
0.00
-0.05
-0.10
-0.15
M (emu/gm)
-60
-40
-20
0
20
40
60
H (kOe)

(c)

Fig. 5.5 M-H loop for pristine and irradiated samples

Fig. 5.6 shows the comparison of FC-ZFC curves for nanocomposites. For the zero-field-cooled (ZFC) measurements, the sample was cooled down from room temperature to 5 K in the absence of an external magnetic field and the magnetic data were acquired during the warming run in a constant external field. In the field-cooled (FC) measurements, the samples were initially cooled down to 5 K in the presence of a magnetic field and the FC data were recorded during the warm up cycle in the same magnetic field.

FC magnetization decreases continuously with the increase of temperature. Such characteristic behavior of FC magnetization data is attributed to ferromagnetism in material [21]. None of these curves show any characteristic sharp change in magnetization associated with the well established ferromagnetic to super paramagnetic transition in single domain nanoparticles. This indicates that the particles (mostly in clusters) in the polymer matrix are predominantly ferromagnetic [22].

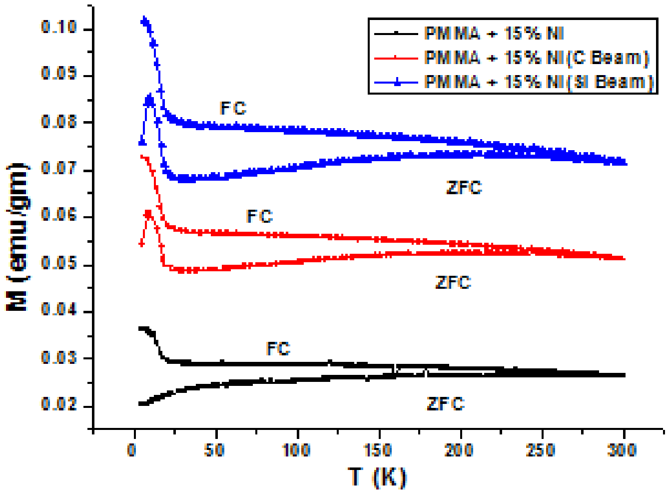

Fig. 5.6 FC- ZFC magnetization for pristine and irradited samples

5.1.6 AC Electrical Frequency Response:

Conductivity: Fig. 5.7(a-e) shows the frequency dependence of AC electrical conductivity of pristine and irradiated nanocomposites. The increase in conductivity with nickel concentration for pristine samples may be attributed to the conductive phase formed by dispersed metal nano particles in the polymer matrix. It is known that electrical conductivity of such composites depends on the type and concentration of the dispersed materials [23, 24]. An AC field applied to the metal–polymer–metal structure may cause a net polarization which is out of phase at sufficiently high frequency with the field. This may result in an increased AC conductivity which appears at frequencies greater than that at which traps are filled or emptied [25]. It is also observed that conductivity increases on increasing fluence. This increase in conductivity is probably due to the generation of large number of charged and active chemical species, cations, anions, and radicals [26].

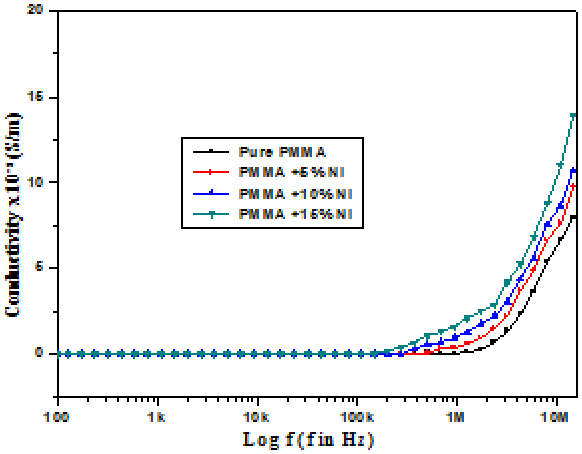

(a)

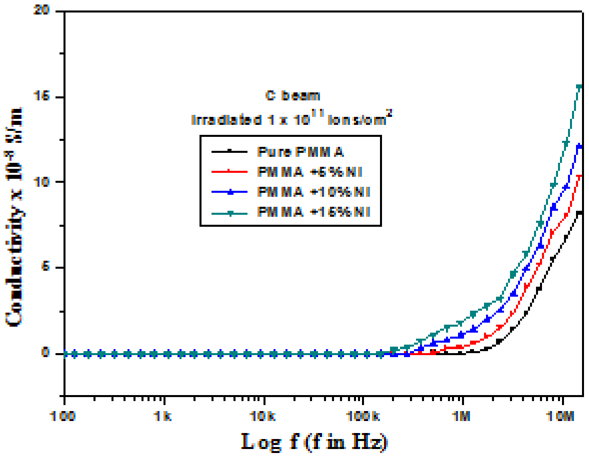
C beam
Irradiated 1 x 10^{11} ions/cm^2
Pure PMMA
PMMA +5% Ni
PMMA +10% Ni
PMMA +15% Ni
Conductivity x 10^{-8} S/m
0
5
10
15
20
100
1k
10k
100k
1M
10M
Log f (f in Hz)

(b)

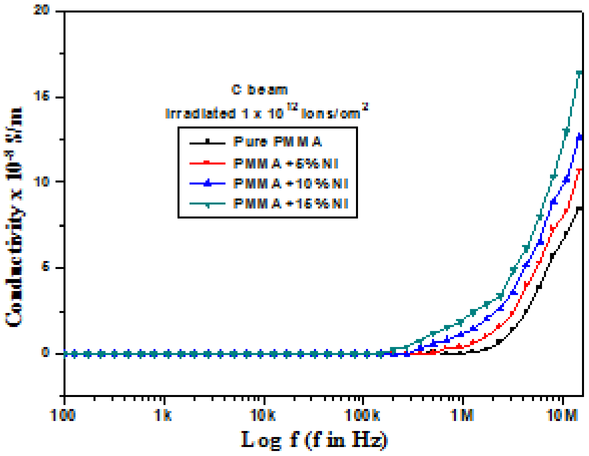
C beam
Irradiated 1 x 10^{12} ions/cm^2
Pure PMMA
PMMA +5% Ni
PMMA +10% Ni
PMMA +15% Ni
Conductivity x 10^{-8} S/m
0
5
10
15
20
100
1k
10k
100k
1M
10M
Log f (f in Hz)

(c)

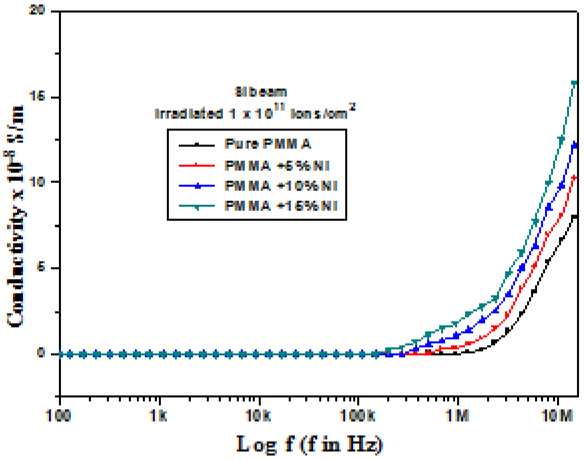
Si beam
Irradiated 1 x 10^{11} ions/cm^2
Pure PMMA
PMMA +5% Ni
PMMA +10% Ni
PMMA +15% Ni
Conductivity x 10^{-8} S/m
0
5
10
15
20
100
1k
10k
100k
1M
10M
Log f (f in Hz)

(d)

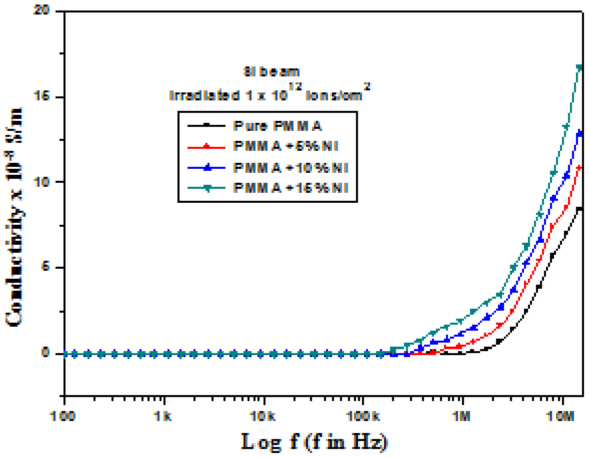

(e)

Fig. 5.7 Conductivity Vs Log f for (a) pristine (b) C beam (1 x 10^{11} ions/cm^2) (c) C beam (1 x 10^{12} ions/cm^2) (d) Si beam (1 x 10^{11} ions/cm^2) (e) Si beam (1 x 10^{12} ions/cm^2)

Dielectric properties of composites:

The dielectric constant showed the ability of a material to store electric potential energy under the influence of an alternative electric field. The effect of nickel concentrations and irradiation on the dielectric constant under various applied sweep frequencies is shown in Fig. 5.8(a-e). The variation in dielectric constant with frequency indicated the presence of an interfacial polarization in the PMMA matrix. This gradually decreasing dielectric constant with increased frequency is thought to be caused by the slow dielectric relaxation of the matrix and the interface of the composite [23]. At higher frequencies, the periodic reversal of the electric field occurs so fast that there is no excess ion diffusion in the direction of the field. Hence dielectric constant decreases with increasing frequency. The observed behaviour of the fluence dependence of dielectric constant in studied frequency range can be explained by the enhanced free carriers due to irradiation [24].

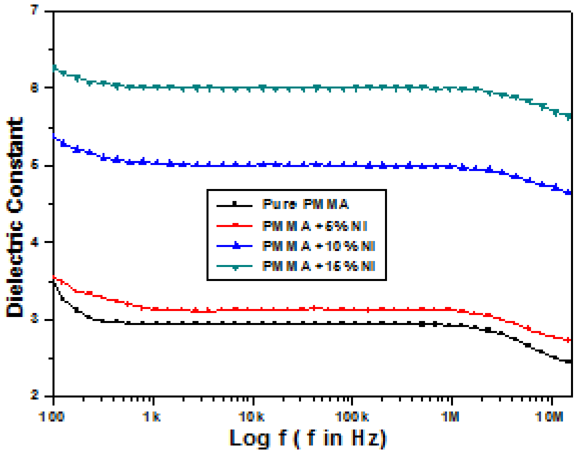
Dielectric Constant
7
6
5
4
3
2
100
1k
10k
100k
1M
10M
Log f (f in Hz)
Pure PMMA
PMMA +5% Ni
PMMA +10% Ni
PMMA +15% Ni

(a)

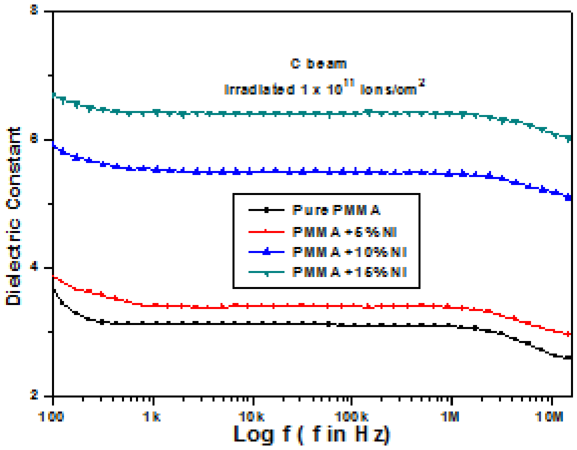
C beam
Irradiated 1 x 10^11 ions/cm^2
Dielectric Constant
8
6
4
2
100
1k
10k
100k
1M
10M
Log f (f in Hz)
Pure PMMA
PMMA +5% Ni
PMMA +10% Ni
PMMA +15% Ni

(b)

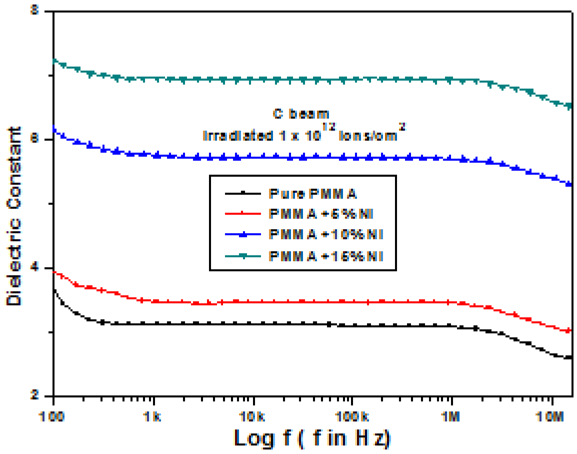
C beam
Irradiated 1 x 10^12 ions/cm^2
Dielectric Constant
8
6
4
2
100
1k
10k
100k
1M
10M
Log f (f in Hz)
Pure PMMA
PMMA +5% Ni
PMMA +10% Ni
PMMA +15% Ni

(c)

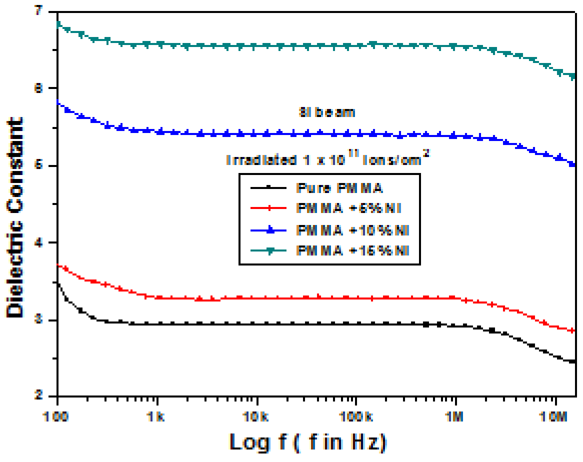

(d)

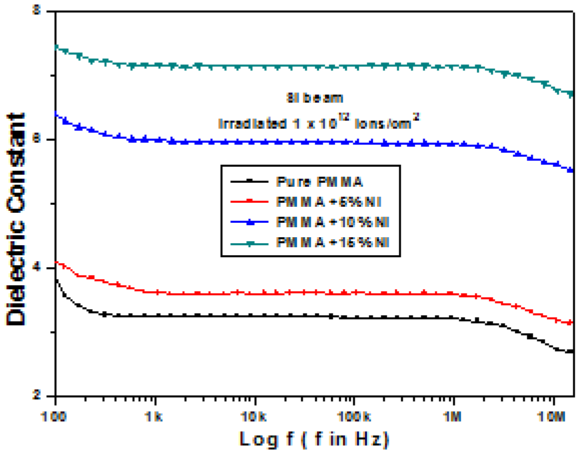

(e)

Fig. 5.8 Dielectric constant Vs Log f for (a) pristine (b) C beam (1 x 10^{11} ions/cm^2) (c) C beam (1 x 10^{12} ions/cm^2) (d) Si beam (1 x 10^{11} ions/cm^2) (e) Si beam (1 x 10^{12} ions/cm^2)

Fig. 5.9(a-e) shows the variation of dielectric loss with log frequency. The dielectric loss decreases exponentially and then became less dependent on frequency. As the frequency increased further, the charge accumulation decreases so the dipole polarization effects reduced, and the value of the loss factor declined accordingly [25]. The increase in dielectric loss with increasing filler contents may be attributed to the interfacial polarization mechanism of the heterogeneous system. Further, moderate increase in loss occurs due to irradiation. The growth in dielectric loss and thus increase in conductivity is brought by an increase in the conduction of residual current and the conduction of absorption current [23].

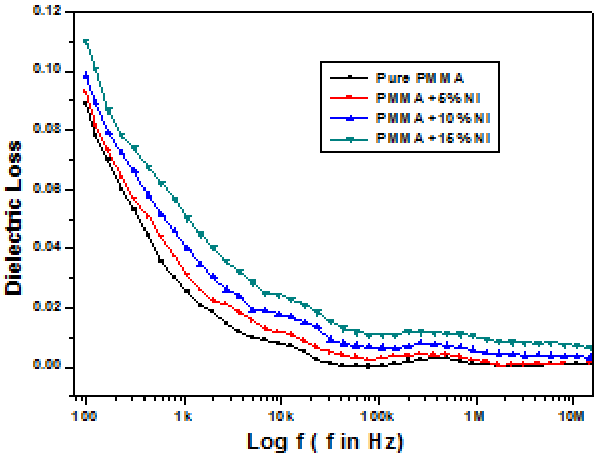

(a)

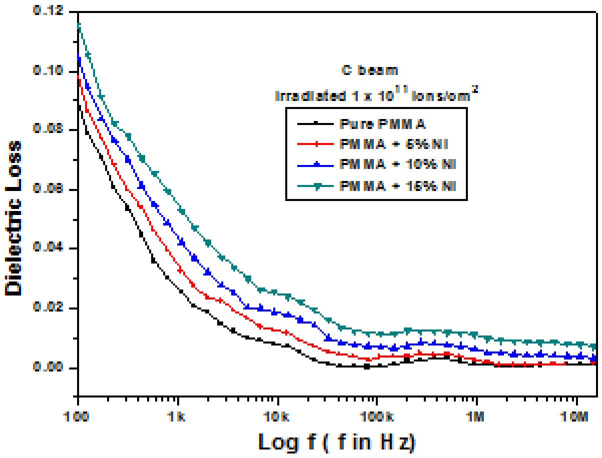

(b)

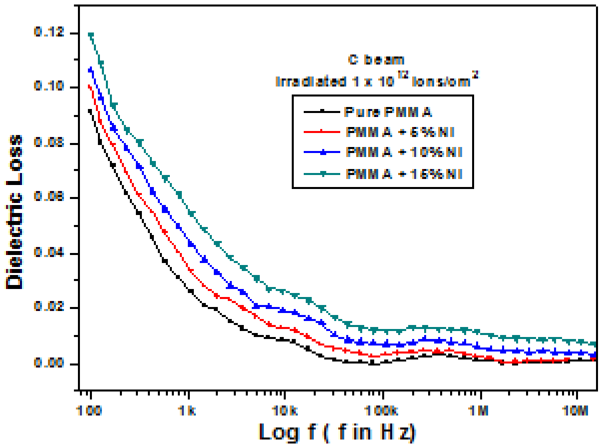
C beam
Irradiated 1 x 10^{12} Ions/cm^2
Pure PMMA
PMMA + 5% Ni
PMMA + 10% Ni
PMMA + 15% Ni
Dielectric Loss
0.12
0.10
0.08
0.06
0.04
0.02
0.00
100
1k
10k
100k
1M
10M
Log f (f in Hz)

(c)

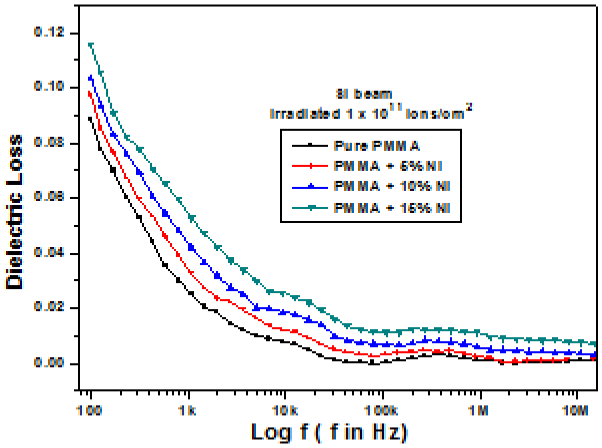
Si beam
Irradiated 1 x 10^{11} Ions/cm^2
Pure PMMA
PMMA + 5% Ni
PMMA + 10% Ni
PMMA + 15% Ni
Dielectric Loss
0.12
0.10
0.08
0.06
0.04
0.02
0.00
100
1k
10k
100k
1M
10M
Log f (f in Hz)

(d)

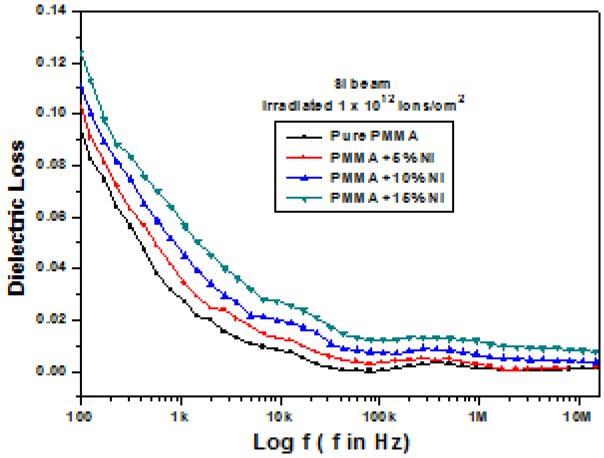
Si beam
Irradiated 1 x 10^{12} Ions/cm^2
Pure PMMA
PMMA + 5% Ni
PMMA + 10% Ni
PMMA + 15% Ni
Dielectric Loss
0.14
0.12
0.10
0.08
0.06
0.04
0.02
0.00
100
1k
10k
100k
1M
10M
Log f (f in Hz)

(e)

Fig. 5.9 Dielectric loss Vs Log f for (a) pristine (b) C beam (1 x 10^{11} ions/cm^2) (c) C beam (1 x 10^{12} ions/cm^2) (d) Si beam (1 x 10^{11} ions/cm^2) (e) Si beam (1 x 10^{12} ions/cm^2)

Conclusion:

It was observed from the UV- visible spectroscopy analysis that the band gap value moved to the lower energy (from 4.37 eV upto 3.43 eV) on doping with nickel nanoparticles, as well as upon irradiation. An XRD analysis reveals that the crystallite size of the composites decreased after ion beam irradiation which is also corroborated by the DSC analysis due to the chain scissioning upon irradiation. SEM images showed damages upon ion beam irradiation. The ion beam irradiation of polymer nanocomposites leads to chain scission and cross linking. As a result of that there are changes in magnetic and dielectric properties. The magnetic properties enhanced after irradiation which may be attributed to the exchange dipolar interaction of particles in the matrix and generation of free radicals. AC electrical and dielectric properties of PMMA/Ni nanocomposites were studied over a wide range of frequency as a function of filler concentration. Both the dielectric constant and the electrical conductivity of the composites increased with the increase of Ni content. These phenomena could be interpreted from interfacial polarization of heterogeneous systems. From the changes observed in composites due to ion beam irradiation, we conclude that the effect of Si-beam is more effective than that of the C-beam because of large energy loss due to heavy ion.

5.2 Effect of swift heavy ions irradiation on PS + Ni nanocomposites:

5.2.1 X-ray diffraction analysis:

The X-ray diffraction patterns of pure Ni (Fig 5.1(a)) and nanocomposites are shown in Fig 5.10. It clearly indicates that nickel is a crystalline but polymer is amorphous in nature and its composite shows semi-crystalline behaviour. The diffraction patterns of the irradiated samples by 85 MeV C ions and 120 MeV Si ions, which exhibited an increase in the peak intensity and a decrease in the full width at half maximum (FWHM) corresponding to all observed peaks of nickel. This behavior may be attributed to cross-linking effect, which may results in the alignment of the polymeric chains. The average crystallite size (t) for pristine and irradiated samples was calculated using Scherrer’s formula [11] as dicussed in chapter 2 in section 2.3.1 from the realtion 2.2.3.

$b=K\lambda/L\cos\theta$

where b is FWHM in radians, λ is the wavelength of X-ray beam (1.5418 Å), L is the crystallite size in Å, K is a constant which varies from 0.89 to 1.39, but for most of the cases it is close to 1.

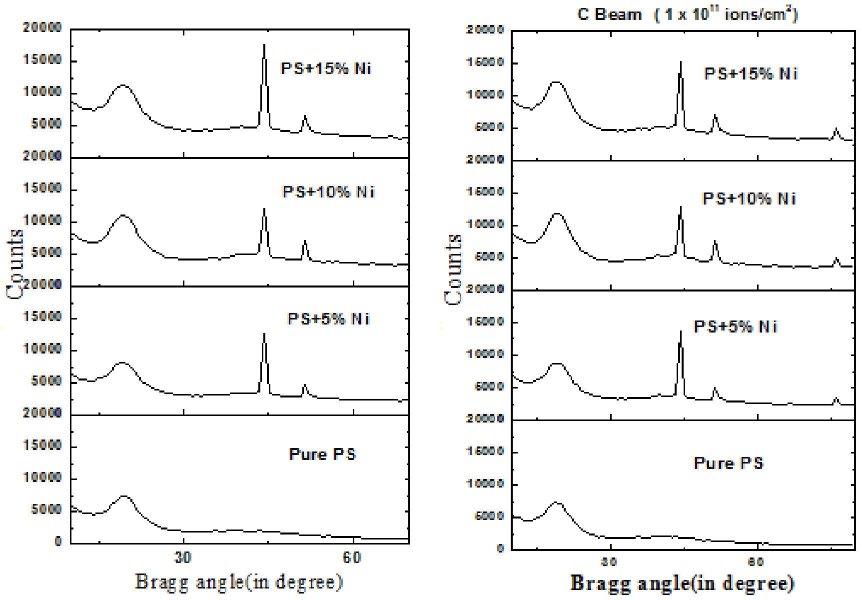

(a) (b)

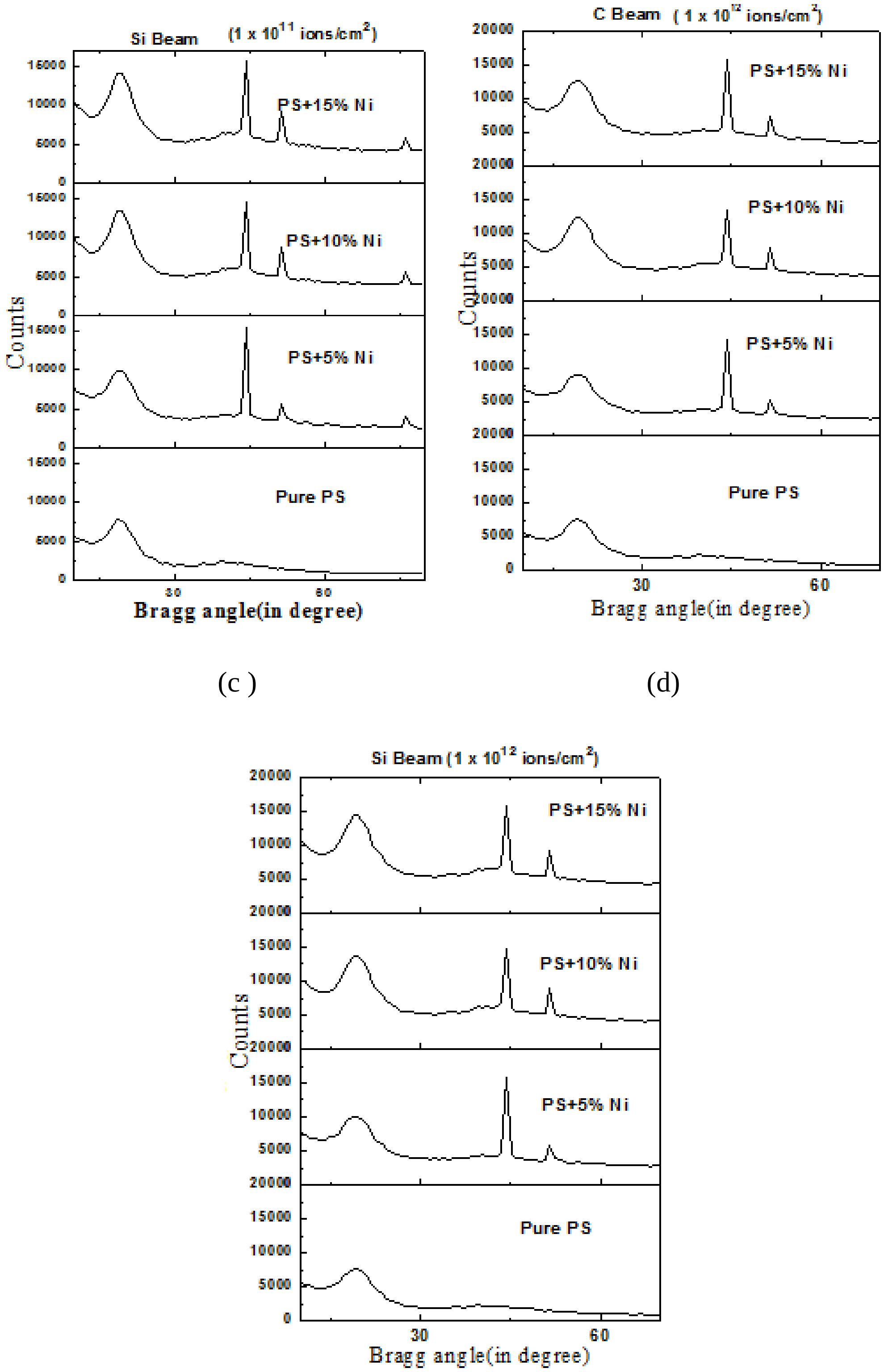

(c) (d)

(e)

Fig 5.10 X-ray diffraction patterns of (a) PS+ Ni (pristine) (b) C beam (1 x 10^{11} ions/cm^2) (c) C beam (1 x 10^{12} ions/cm^2) (d) Si beam (1 x 10^{11} ions/cm^2) (e) Si beam (1 x 10^{12} ions/cm^2)

The crystallite size was calculated corresponding to the peak of the pristine and irradiated samples and the results are listed in Table 5.4 [26]. The increase in crystallite size suggested the cross linking mechanism.

Table 5.4 Crystallite size of pristine and irradiated samples

Sample	Pristine		C Beam		Si Beam	
	2θ	Crystallite size (nm)	Crystallite size (nm) ($1x10^{11}$) ions/cm^2	Crystallite size (nm) ($1x10^{12}$) ions/cm^2	Crystallite size (nm) ($1x10^{11}$) ions/cm^2	Crystallite size (nm) ($1x10^{12}$) ions/cm^2
PS+ 5%Ni	44.54	10.21	10.53	10.78	10.98	11.13
	51.24	10.82	10.90	11.02	11.10	11.15
	Average	10.52	10.72	10.89	11.04	11.14
PS + 10%Ni	44.56	10.28	10.67	10.89	11.52	11.87
	51.25	10.89	11.01	11.10	11.67	11.98
	Average	10.58	10.84	10.99	11.60	11.92
PS + 15%Ni	44.60	10.40	10.80	11.50	11.76	11.88
	51.27	11.10	11.56	11.75	12.02	12.24
	Average	10.75	11.18	11.62	11.89	12.06

5.2.2 Thermal response (Differential Scanning Calorimetery (DSC)):

Fig. 5.11 shows the glass transition behavior of polymer matrix and composites. The important property of the glass transition (Tg) of polymer at which, the weak secondary bonds that stick the polymer chains together are broken, and the macromolecule starts to move. The interaction of polymer chains and nanoparticles surface can alter the chain kinetics by decreasing or increasing glass transition temperature of the polymer. Tg of the pure PS is observed at 65.2 ^{o}C and those of composite, pristine and irradiated samples at 66.2 ^{o}C and 72.5^{o}C respectively with 85 MeV C-ions. Further with 120 MeV Si-ions, we observed that the Tg of irradiated sample is around 75.68 °C. The value of Tg for highest fluence is listed in Table 5.5. This behavior probably arises due to branching formed (cross linking

Table 5.5 Values of glass transition for pristine and irradiated composites

Sample name	Tg (Pristine)	Tg (C beam)	Tg (Si beam)
PS + 5 %Ni	65.8	71.9	73.1
PS + 10 %Ni	67.1	73.3	74.5
PS + 15 %Ni	71.5	73.7	75.7

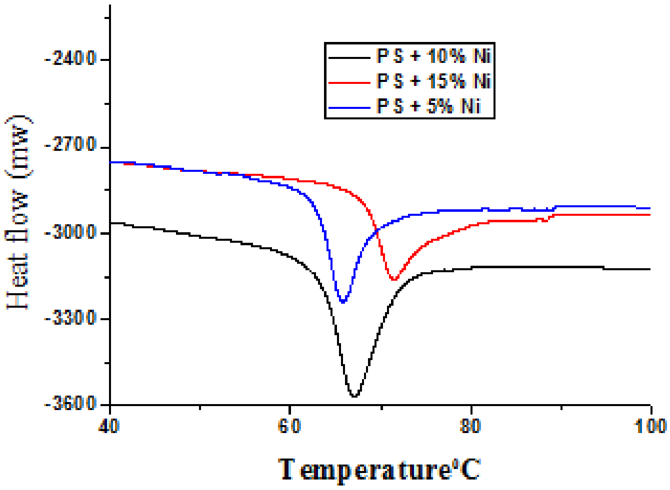

(a)

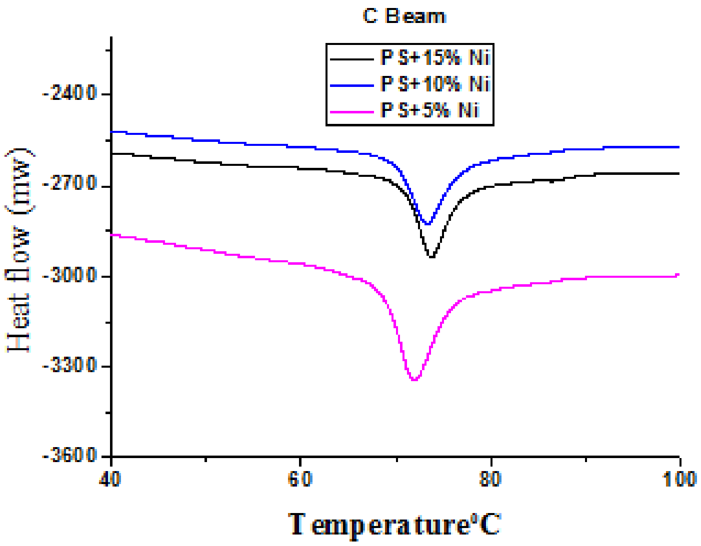

(b)

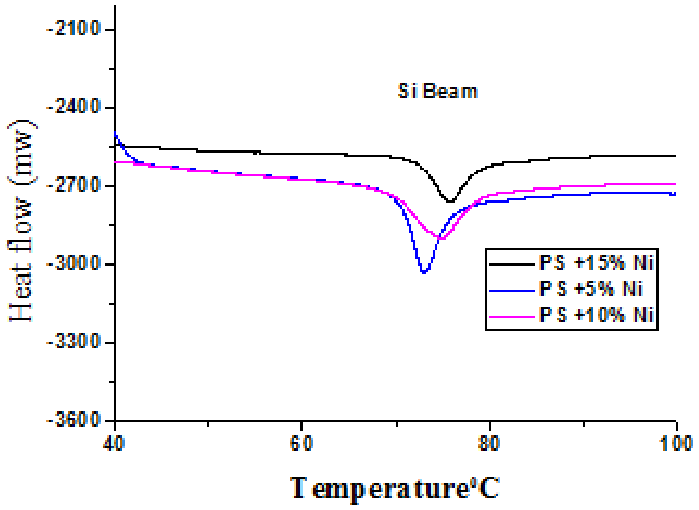

(c)

Fig. 5.11 DSC spectra for (a) Pristine (b) C beam (c) Si beam composites

effect) when islands of nanoparticles are bonded with polymeric chains. This lowers the mobility of the chains, and as a result the glass transition temperature increases in the nanocomposites [27]. So after irradiation, glass transition temperature was shifted further towards higher temperature, this further reveals cross linking between nanoparticles and polymer matrix which is also corroborated with XRD analysis.

5.2.3 Optical response:

The absorption of light energy by polymeric materials in the UV and visible region involves promotion of electrons in the orbital from ground state to the higher energy states. UV–Vis spectroscopy provides valuable information on optical band gap energy (Eg). The electronic transitions (→) that are involved in the ultraviolet and visible regions are of the following type σ → σ *, n → π*, and π → π* [27]. The absorbance edge of the UV-Vis spectra of pristine nanocomposites and irradiated by

C and Si ions is shown in Fig 5.12 (a-e). The absorbance in aromatic compounds is due to the π to π^* transition. This is very sensitive to the change in the environment around the phenyl ring [28]. Ion beam interaction with polymers generates damage which leads to the formation of new defects and new charge states. It is observed that optical absorption increases with increasing energy loss and this absorption shifts from UV–Vis to the visible region for all irradiated nanocomposite samples. With increase of electronic energy loss the nanocomposites become gradually opaque to the visible light and the absorption edge shifted from UV to the visible region. The increase in absorption with irradiation may be attributed to the formation of a conjugated system of bonds due to bond cleavage and reconstruction [29]. The shifting of absorption edge towards visible is generally considered to result from carbonization of the material under irradiation [30] which is also corroborated to the dielectric results.

Determination of optical band gap:

Optical feature of the pristine and irradiated samples have been studied by Perkin-Elmer 25 Lambda UV-Visible spectroscope in the frequency range 200-600 cm^{-1} as illustrated in Fig. 5.12 (a-e). The optical band gap E_g is obtained by tauc's equation [17] as described in chapter 2 in section 2.3.3 by relation 2.2.4.

i. e. $\omega\varepsilon(\lambda) = (\hbar\omega - E_g)^2$

Where $\varepsilon(\lambda)$ is the optical absorbance and λ is the wavelength. The intersection of the extrapolated spectrum with the abscissa of the plot $\varepsilon^{1/2}/\lambda$ versus $1/\lambda$ yields the gap wavelength λ_g from which the energy gap is derived as $E_g = hc/\lambda_g$. It is noticed that the band gap (energy gap) value shifted to lower energy from 4.35 eV upto 3.43 eV due to doping of nickel nanoparticles and also upon irradiation with both the ions.

This behavior of the optical gap of ion-irradiated samples can be explained following the model of Robertson and O Reilly [32, 33].

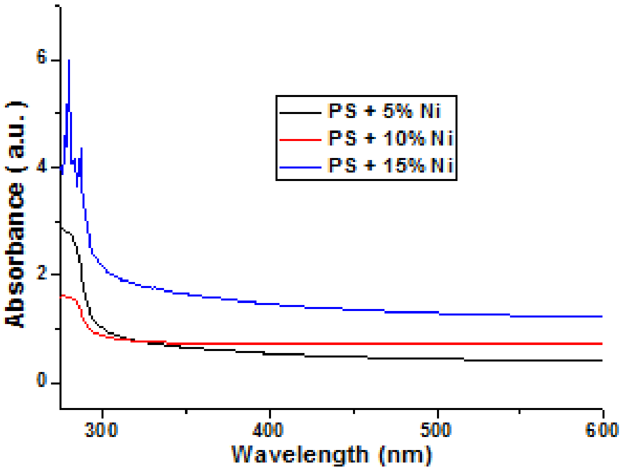

(a)

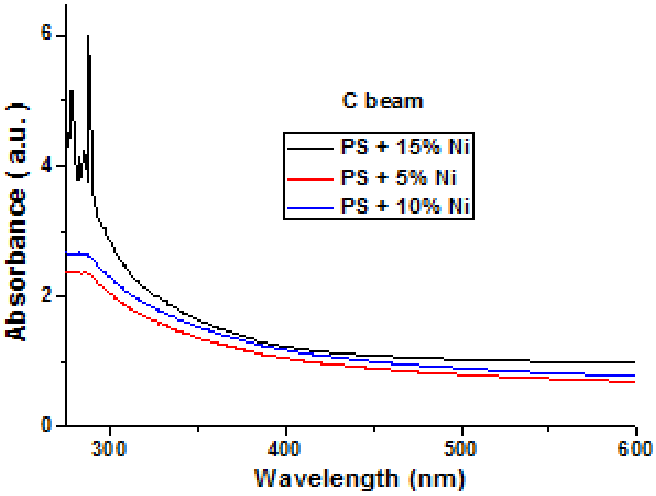

(b)

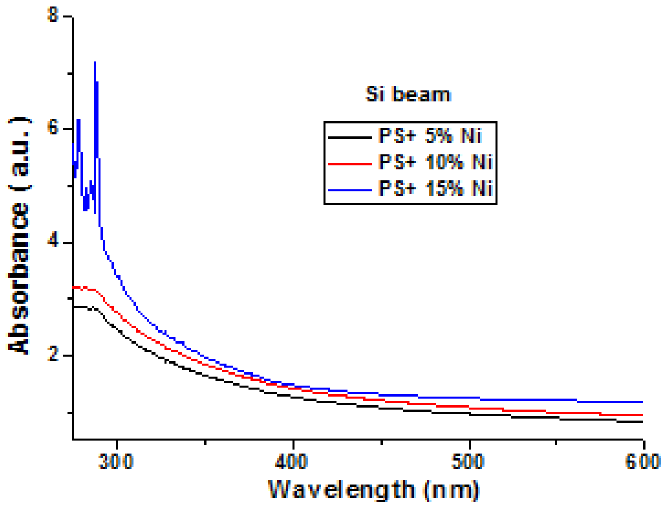

(c)

Fig. 5.12 Absorbance spectra of (a) Pristine (b) C beam (c) Si beam composites

The number of carbon hexagon rings in the cluster (M) is then found from the relation 2.2.6 [32] as discussed in chapter 2 in section 2.3.3.

$E_g \approx 2\,|\beta|\,\sqrt{M}$

Where, |β| is a bond integral that represents the interaction energy of two π atomic orbitals. A theoretical value for |β| proposed by Robertson and O Reilly is 2.9 eV, which according to Compagnini et al. [34] is an overestimation of the true value. So, the best-fit value of |β| given by them is 2.2 eV. In the present study on the aromatic polymer, given equation has been used to calculate the value of M and its behaviour with different ions is summarized in Table 5.6. The number of rings (M) reveals constant with the filler and upon irradiation except for Si-ions at a fluence of 1x 10^{12} ions/cm^2.

Table 5.6 Band gap by direct allowed transitions, number of carbon atoms in pristine and irradiated composites.

Sample	Pristine		C Beam		Si Beam	
	Band gap in eV	No. of carbon hexagon rings	Band gap in eV	No. of carbon hexagon rings	Band gap in eV	No. of carbon hexagon rings
PS + 5%Ni (1 x 10^{11} ions/cm^2)	4.35	~1	4.30	~1	4.08	~1
PS + 5%Ni (1 x 10^{12} ions/cm^2)	4.32	~1	4.04	~1	3.98	~1
PS + 10%Ni (1 x 10^{11} ions/cm^2)	4.20	~1	3.95	~1	3.88	~1
PS + 10%Ni(1 x 10^{12} ions/cm^2)	4.14	~1	3.88	~1	3.75	~1
PS + 15%Ni (1 x 10^{11} ions/cm^2)	4.12	~1	3.81	~1	3.60	~1
PS + 15%Ni(1 x 10^{12} ions/cm^2)	4.02	~1	3.75	~1	3.43	~2

5.2.4 Surface morphology:

Fig. 5.13(a–c) shows the SEM images of pristine, composites and irradiated composite films with magnification of X250. The analysis shows that the filled partilces are distributed randomly in the matrix which display continuous contact between themselves and formed conducting paths. The surface becomes smoothen upon irradiation.The decrease in roughness with Ni-nanoparticles may be attributed to the decrease in density of metal particles on the surfaces of the films, which is also responsible for increase in crystallinity of the material on irradiations revealed by XRD analysis.

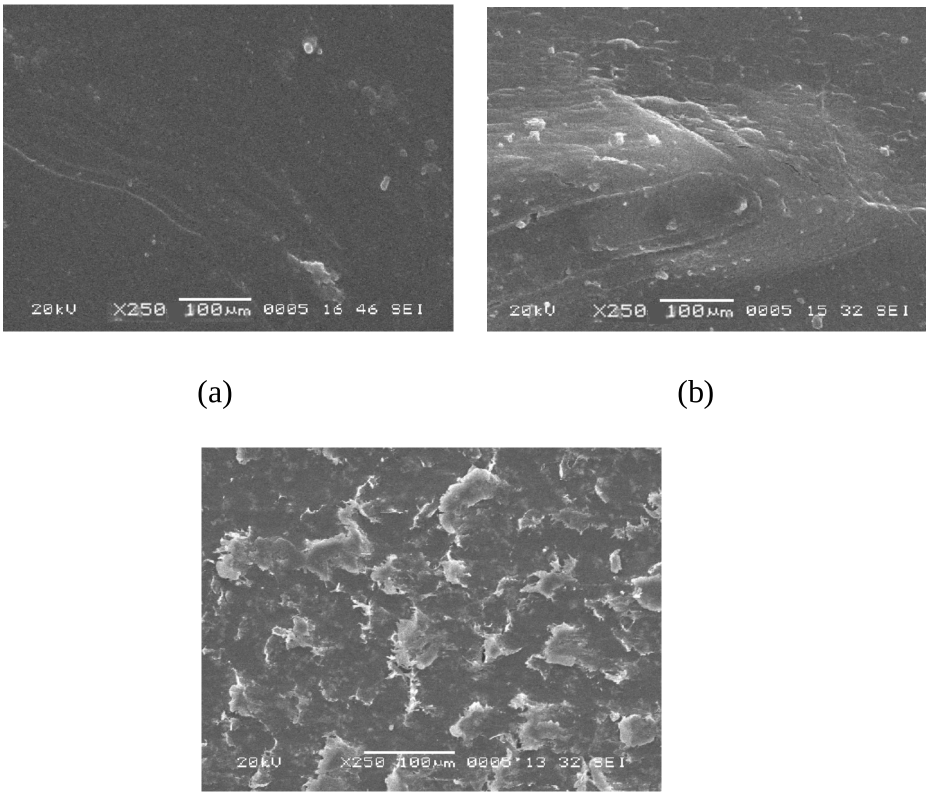

(a) (b)

(c)

Fig. 5.13 SEM images of (a) PS+ 15 % Ni (pristine) (b) PS + 15 % Ni (C beam) (c) PS + 15 % Ni (Si beam)

5.2.5 Magnetic properties:

The static and dynamic magnetic properties were measured by using Quantum Design, over a broad range of magnetic fields. The dc magnetic characteristic was done by using field-cooled-zero-field cooled (FC-ZFC) and M-H hysteresis loop measurements. The FC-ZFC measurements were carried out from 5-300 K at applied field of 500 Oe. Hysteresis measurements were carried out at 300 K with magnetic field swept from 50 kOe to -50 kOe.

The magnetic measurement of Ni/PS nano composites having Ni concentration of 15% by weight is discussed here. The Fig. 5.14 (a, b, c) shows the M-H curves for the pristine and irradiated samples. The magnetic parameters extracted from the measurements are listed here, saturation magnetization (M_S) ~0.070 emu/gm, coercive field (H_C) ~136 Oe, remnant magnetization (M_R) ~0.014 emu/gm for pristine and M_S ~ 0.097 emu/gm, H_C ~145 Oe, $M_{R\sim}$ 0.019 emu/gm and M_S ~ 0.109 emu/gm, H_C ~155 Oe, $M_{R\sim}$ 0.022 emu/gm for irradiated by 85 MeV C ions and 120 MeV Si ions respectively. The saturation magnetization in nanoparticle system is generally lower than that of the bulk materials and is strongly influenced by the supporting matrix. M_S increases after irradiation may be attributed to the change in exchange and dipolar interactions mediated by the matrix. However unlike the saturation magnetization, the remnant magnetization is also strongly dependent on the inter particles interaction which is governed by the particles inside the polymer matrix [35]. The enhancement in coercive field upon irradiation is also due to the inter particles interaction.

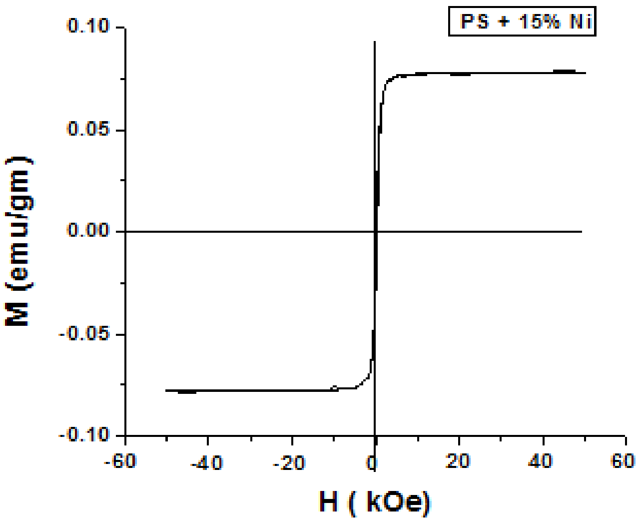

(a)

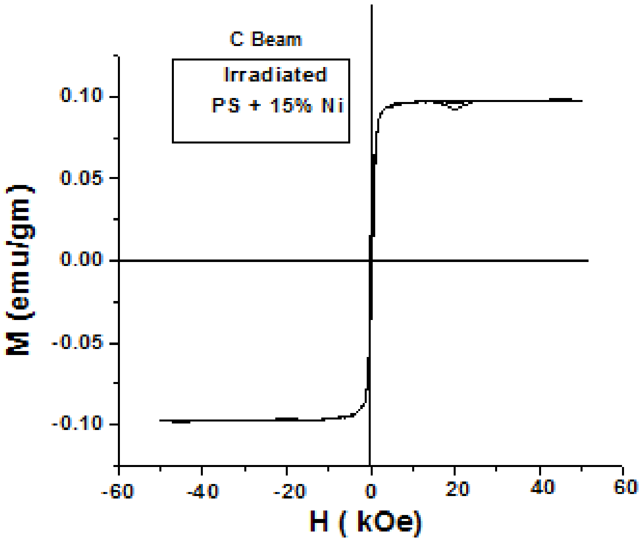

(b)

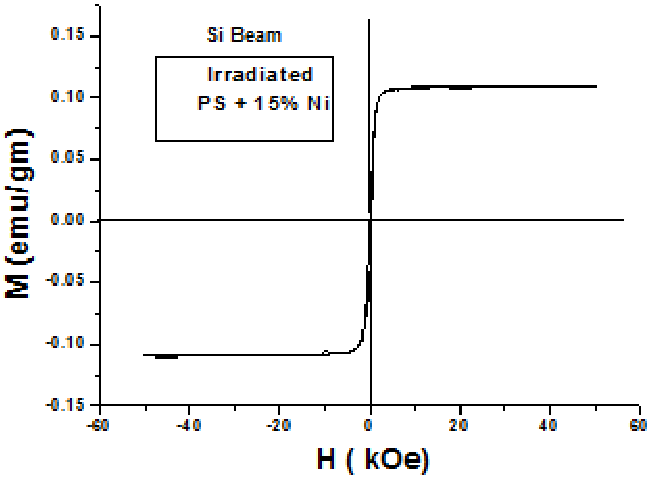

(c)

Fig. 5.14 M-H curves for pristine and irradiated samples

Fig 5.15 shows the comparison of FC-ZFC curves for nanocomposites. For the zero-field-cooled (ZFC) measurements, the sample was cooled down from room temperature to 5 K in the absence of an external magnetic field and the magnetic data were acquired during the warming run in a constant external field. In the field-cooled

(FC) measurements, the samples were initially cooled down to 5 K in the presence of a magnetic field and the FC data were recorded during the warm up cycle in the same magnetic field. The FC–ZFC measurements were carried out in the temperature range 5–300 K at applied field of 500 Oe as shown in Fig. 5.15 for pristine and irradiated samples, respectively. None of these curves show any characteristic sharp change in magnetization associated with the well established ferromagnetic to super paramagnetic transition in single domain nanoparticles. This indicates that the particles (mostly in clusters) in the polymer matrix are predominantly ferromagnetic [22]. Magnetization was increased upon irradiation which may be attributed to the creation of free radicals and interaction of particles mediated by the matrix which is also corroborated with the M-H measurements.

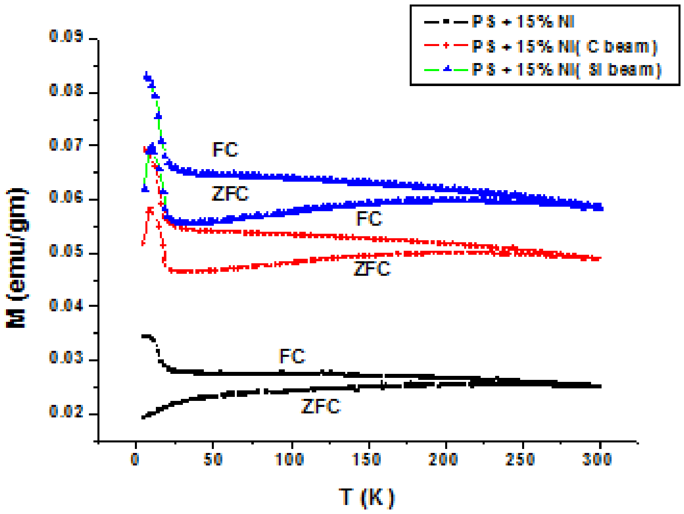

Fig. 5.15 ZFC-FC curves for pristine and irradiated samples

5.2.6 AC electrical frequency response:

Conductivity: The conductivity behavior of the PS/Ni nanocomposite films depends on the concentration of the nickel nano particles under an ac field as shown in Fig. 5.16 (a-e). The conductivity of nanocomposite films increases with increasing nanoparticles loading, while the influence of frequency on the conductivity is stronger than the influence of the concentration of nano-Ni particles, which shows a strong dependence of the conductivity at higher frequency range. Charge carriers are transported mainly through the amorphous phase. The impurity content in the amorphous region is hop to increase with the increasing concentration of nano-Ni particles. The electronic charge carriers transport will be simpler due to the function of impurity and resulting in an increase in the sample conductivity. The conductivity is influenced by the hopping processes of charge carriers in a material and barrier height. The disordered morphology causes the ac mobility to increase with the frequency of the applied electric field and was found to be strongly frequency dependent. Therefore hopping carriers transport became easier, resulting in an increase in conductivity of the films [36]. It is also examined that the conductivity increases upon irradiation. Irradiation is supposed to endorse the metal-polymer bonding and convert it into the hydrogen depleted carbon network due to the emission of hydrogen and/or other volatile gases. It is this carbon network that is believed to make the polymers more conductive [37].

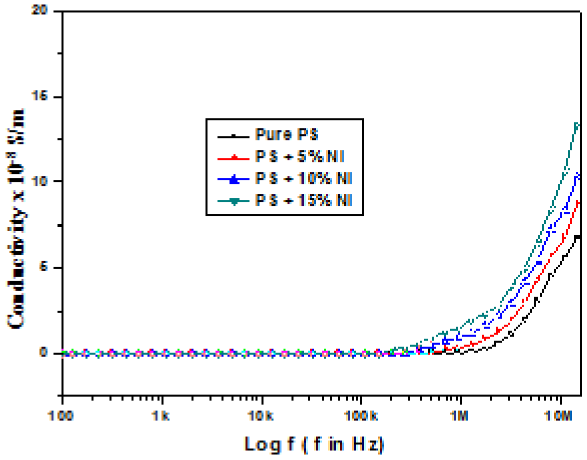

(a)

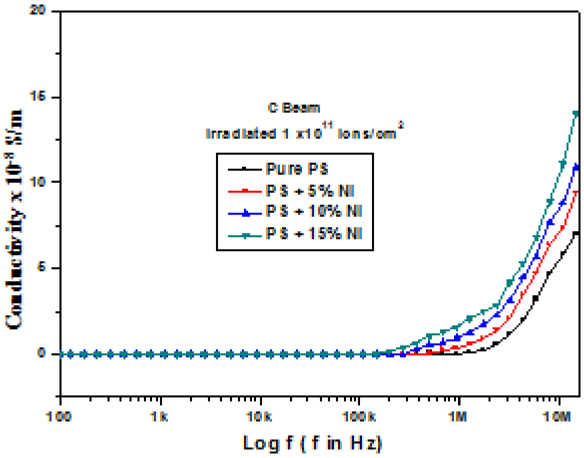
20
15
10
5
0
Conductivity x 10^{-8} S/m
C Beam
Irradiated 1 x10^{11} Ions/cm^2
Pure PS
PS + 5% NI
PS + 10% NI
PS + 15% NI
100
1k
10k
100k
1M
10M
Log f (f in Hz)

(b)

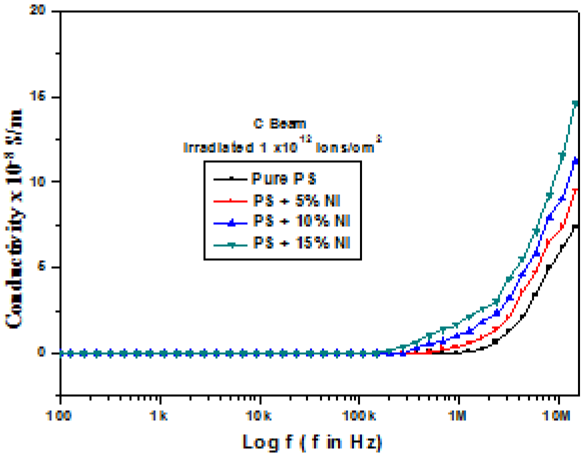
20
15
10
5
0
Conductivity x 10^{-8} S/m
C Beam
Irradiated 1 x10^{12} Ions/cm^2
Pure PS
PS + 5% NI
PS + 10% NI
PS + 15% NI
100
1k
10k
100k
1M
10M
Log f (f in Hz)

(c)

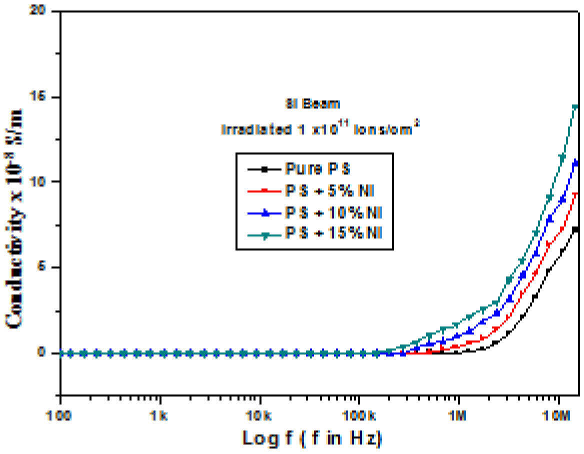
20
15
10
5
0
Conductivity x 10^{-8} S/m
SI Beam
Irradiated 1 x10^{11} Ions/cm^2
Pure PS
PS + 5% NI
PS + 10% NI
PS + 15% NI
100
1k
10k
100k
1M
10M
Log f (f in Hz)

(d)

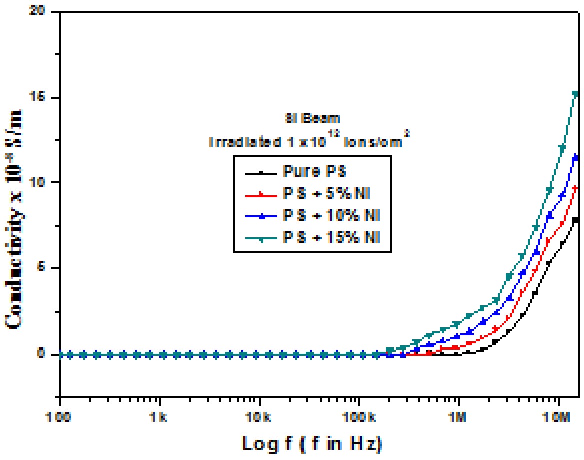

(e)

Fig. 5.16 Conductivity Vs Log f for (a) pristine (b) C beam (1 x 10^{11} ions/cm^2) (c) C beam (1 x 10^{12} ions/cm^2) (d) Si beam (1 x 10^{11} ions/cm^2) (e) Si beam (1 x 10^{12} ions/cm^2)

Dielectric properties of composites:

As can be seen in Fig 5.17(a-e), the value of the dielectric permittivity for PS/Ni nanocomposites depends both on the measuring frequency and the nanofiller concentration. Especially, the dielectric behaviors of PS/Ni nanocomposites with different nickel nanoparticles concentrations in the low frequency range are found to be increased which is due to the interfacial space charge polarization. The higher the nanofiller loading level, the larger the total effective area of the interfaces between the polymer matrix and the filler, and the thinner the insulating spacers separating nickel nanoparticles, resulting in the considerable increment of the interfacial space-charge

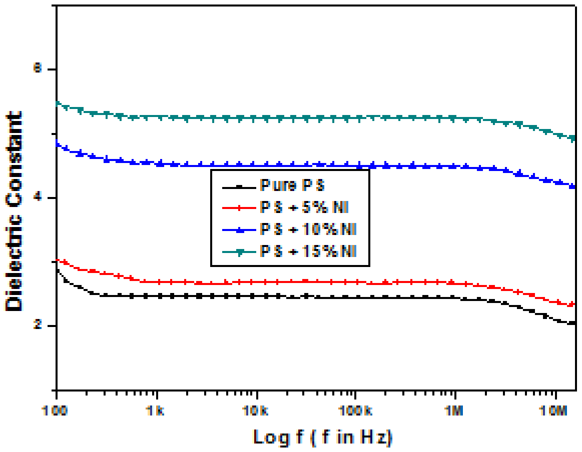
Dielectric Constant
2
4
6
100
1k
10k
100k
1M
10M
Log f (f in Hz)
Pure PS
PS + 5% NI
PS + 10% NI
PS + 15% NI

(a)

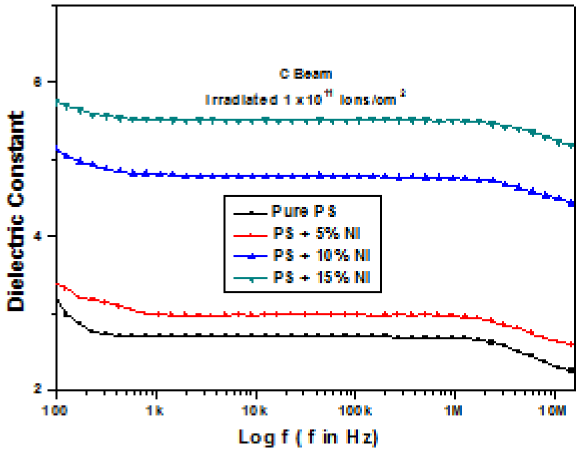
C Beam
Irradiated 1 x10^11 Ions/cm^2
Dielectric Constant
2
4
6
100
1k
10k
100k
1M
10M
Log f (f in Hz)
Pure PS
PS + 5% NI
PS + 10% NI
PS + 15% NI

(b)

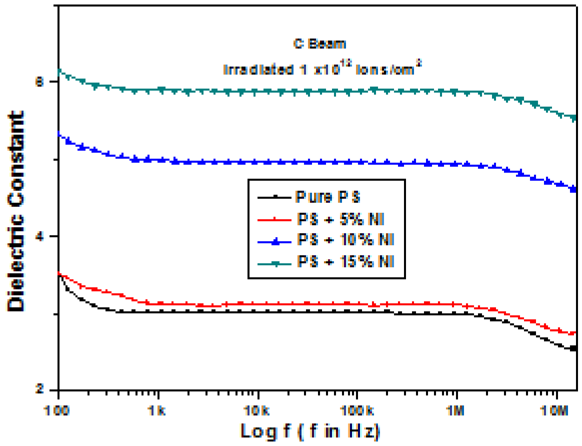
C Beam
Irradiated 1 x10^12 Ions/cm^2
Dielectric Constant
2
4
6
100
1k
10k
100k
1M
10M
Log f (f in Hz)
Pure PS
PS + 5% NI
PS + 10% NI
PS + 15% NI

(c)

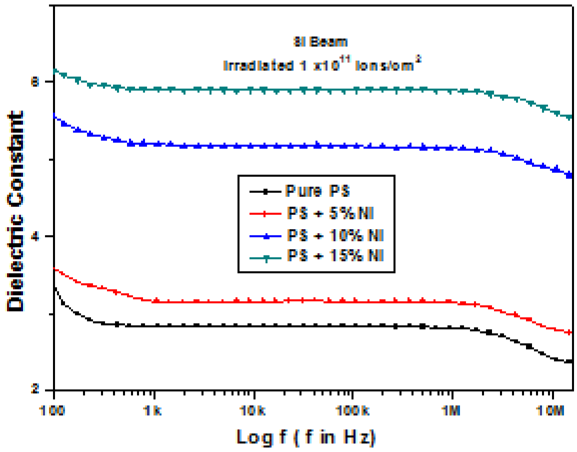

(d)

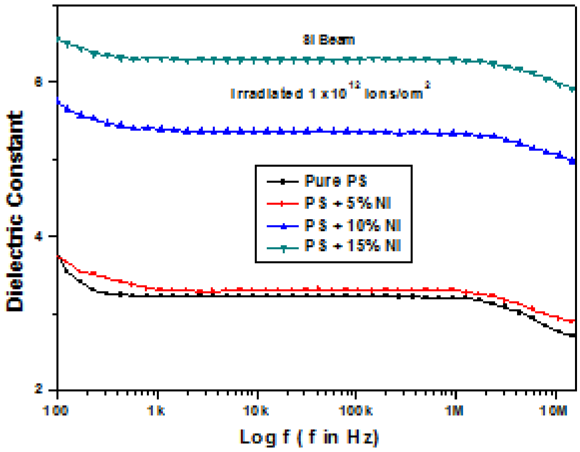

(e)

Fig. 5.17 Dielectric Constant Vs Log f for (a) pristine (b) C beam (1 x 10^{11} ions/cm^2) (c) C beam (1 x 10^{12} ions/cm^2) (d) Si beam (1 x 10^{11} ions/cm^2) (e) Si beam (1 x 10^{12} ions/cm^2)

polarization at these frequency range [36]. As observed from figure, the dielectric constant remains almost constant up to 100 kHz. At these frequencies, the motion of free charge carriers assumed to be constant through the polymer. It is also observed that dielectric constant increases upon irradiation. The increase in dielectric constant may be attributed to the chain scission, cross linking and as a result the increase in the number of free radicals, unsaturation etc. At higher frequency regions, (i.e., beyond 100 kHz), the charge carriers migrate through the dielectric and get trapped against a defect sites and induced an opposite charge in its vicinity. So, the polarization of trapped and bound charges cannot take place and that reduced the dielectric constant [38].

Fig. 5.18(a-e) shows the variation of dielectric loss with log frequency for pristine and irradiated samples of pure PS and nickel nanoparticles dispersed PS films at different concentrations. In general, the dielectric loss of the dielectric material causes

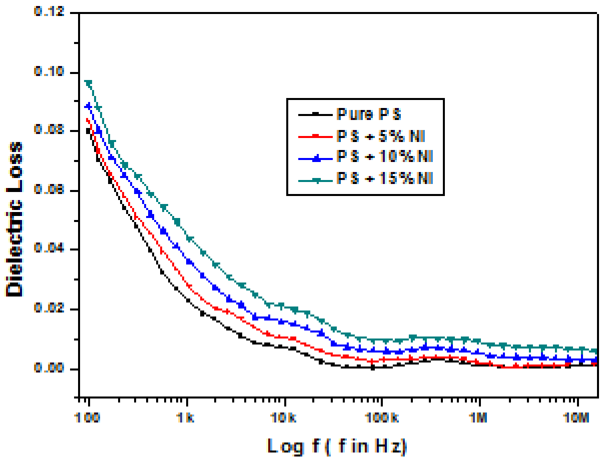

(a)

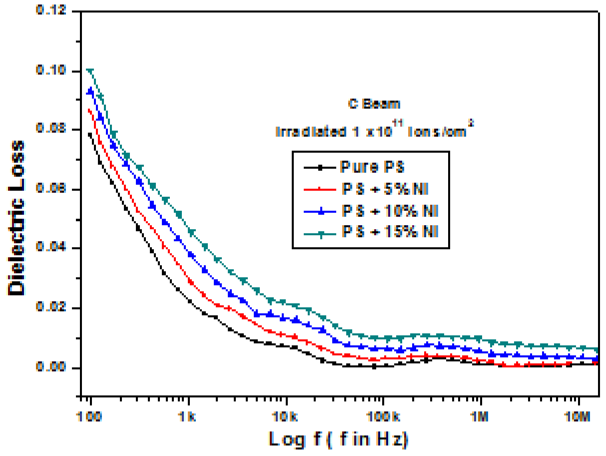
0.12
0.10
0.08
0.06
0.04
0.02
0.00
Dielectric Loss
100
1k
10k
100k
1M
10M
Log f (f in Hz)
C Beam
Irradiated 1 x10^{11} Ions/cm^{2}
Pure PS
PS + 5% NI
PS + 10% NI
PS + 15% NI

(b)

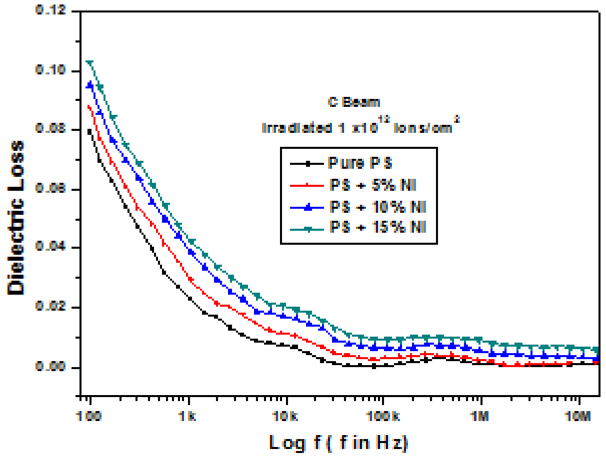
0.12
0.10
0.08
0.06
0.04
0.02
0.00
Dielectric Loss
100
1k
10k
100k
1M
10M
Log f (f in Hz)
C Beam
Irradiated 1 x10^{12} Ions/cm^{2}
Pure PS
PS + 5% NI
PS + 10% NI
PS + 15% NI

(c)

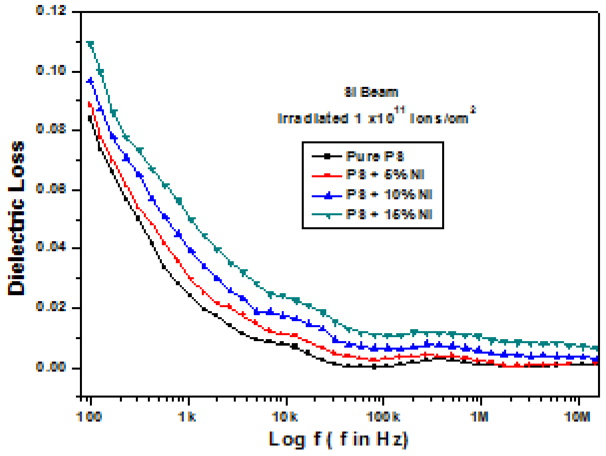
0.12
0.10
0.08
0.06
0.04
0.02
0.00
Dielectric Loss
100
1k
10k
100k
1M
10M
Log f (f in Hz)
Si Beam
Irradiated 1 x10^{11} Ions/cm^{2}
Pure PS
PS + 5% NI
PS + 10% NI
PS + 15% NI

(d)

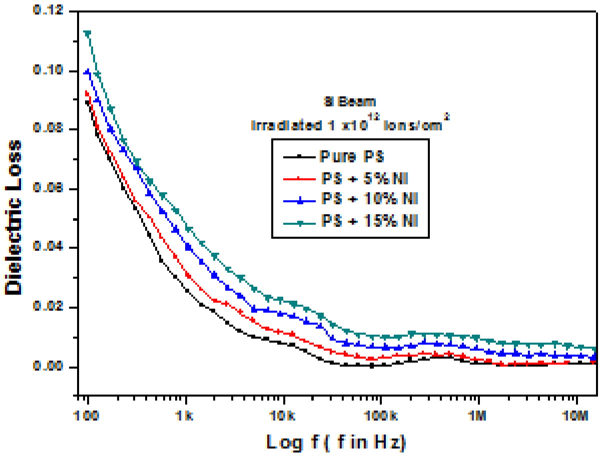

(e)

Fig. 5.18 Dielectric loss Vs Log f for (a) pristine (b) C beam (1 x 10^{11} ions/cm^2) (c) C beam (1 x 10^{12} ions/cm^2) (d) Si beam (1 x 10^{11} ions/cm^2) (e) Si beam (1 x 10^{12} ions/cm^2)

from distortional, dipolar, interfacial, and conduction loss. The dielectric loss decreases moderately with the increase of log frequency as shown in figure. It is observed that dielectric loss increases moderately with the concentration of filler and also with the fluence which may be featured by the interfacial polarization mechanism of the heterogeneous system [39].

Conclusion:

The ion beam irradiation of polymer nanocomposites leads to chain scission and cross linking. As a result of that there are changes in physical properties of composites. It is observed that the crystalline size increased upon irradiation as revealed from XRD analysis. This might be featured to rupture of some polymeric bonds, which is also confirmed by DSC analysis. The magnetic properties enhanced after irradiation which may be attributed to the exchange dipolar interaction of particles in the matrix and generation of free radicals. The AC electrical studies signify that the conductivity increases on increasing the frequency and also upon irradiation. Dielectric constant is observed to change upon irradiation. This might be attributed to breakage of chemical bonds and resulting in the increase of free radicals, unsaturation, etc.

5.3 Summary:

Two different composites have been studied using two different ion beam (C and Si - ions) irradiation. Structural, optical, thermal, magnetic properties, electrical properties and surface morphology have been examined by different characterization techniques.

In XRD, the results show that the crystallite size of fillers decreases slightly upon both ion beams irradiations in PMMA nanocomposites. It is also observed that the intensity of the peak decreases and to some extent broadening of the peak after irradiation offers confirmation of decrease in crystallinity. Since no significant change in the peak position is observed, this reveals that lattice parameters do not change significantly in both ion beams irradiations. Rather in the case of PS nanocomposites, crystallite size of fillers increases upon both ion beams irradiations which may be attributed to cross linking effect.

In DSC thermograms, the Tg value decreases upon irradiations in PMMA nanocomposites and increases upon irradiations in PS composites. This behavior probably arises due to branching (cross-linking effect) when islands of nanoparticles are bonded with polymeric chains. This lowers the mobility of the chains, and as a result, the glass transition temperature increases in the nanocomposites. Decrease in Tg was explained by thin film model. When the inter-particles distance is small enough, then the polymer between two particles can be considered as a thin film. Assuming that there is small or no interfacial interaction between the filler and matrix exists and then Tg decreases.

The band gap values for both composites were increased upon concentration of fillers and both ions irradiations. It was observed from the UV- visible spectroscopy analysis that the band gap value moved to the lower energy.

SEM images showed that increase in density in PMMA nanocomposites and decrease in density in PS nanocomposites upon irradiations.

Ac electrical conductivity of all pristine and irradiated samples at different filler concentrations is shown in Fig.5.19. The conductivity of nanocomposite films increases with increasing nanoparticles loading, while the influence of frequency on the conductivity is stronger than the influence of the concentration of nano-Ni particles, which shows a strong dependence of the conductivity at higher frequency range. Charge carriers are transported mainly through the amorphous phase. The impurity content in the amorphous region is hop to increase with the increasing concentration of nano-Ni particles. The electronic charge carriers transport will be simpler due to the function of impurity and resulting in an increase in the sample conductivity. The conductivity is influenced by the hopping processes of charge carriers in a material and barrier height. The disordered morphology causes the ac mobility to increase with the frequency of the applied electric field and was found to be strongly frequency dependent. Therefore hopping carriers transport became easier, resulting in an increase in conductivity of the films. Conductivity is further observed to increase upon irradiation. Irradiation is expected to promote the metal to polymer bonding and convert polymeric structure into hydrogen depleted carbon network. It is this carbon network that is believed to make the polymer more conductive. Fig. 5.20 shows comparison of conductivity of all composites before and after irradiation. For the sake of comparison filler concentration (5, 10, 15 wt%) at a fluence of 1 x 10^{12} ions/cm^2 for C and Si ions beam at a frequency 10 MHz have considered. Similar study for dielectric constant of all composites has been done and shown in Fig 5.20 at a frequency of 10 MHz.

Dielectric loss was studied for all pristine and irradiated samples and result shows frequency and fluence dependent behaviour for all cases. In general, the natures of the curves of electrical response for all samples are same but the magnitude varies with filler material.

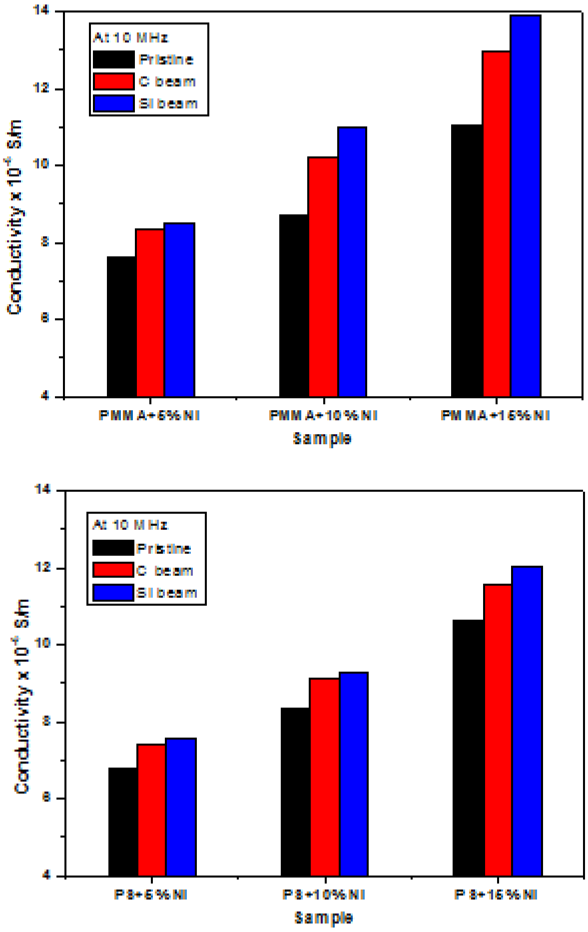

Fig. 5.19 Comparison of conductivity of pristine and irradiated samples at 10 MHz

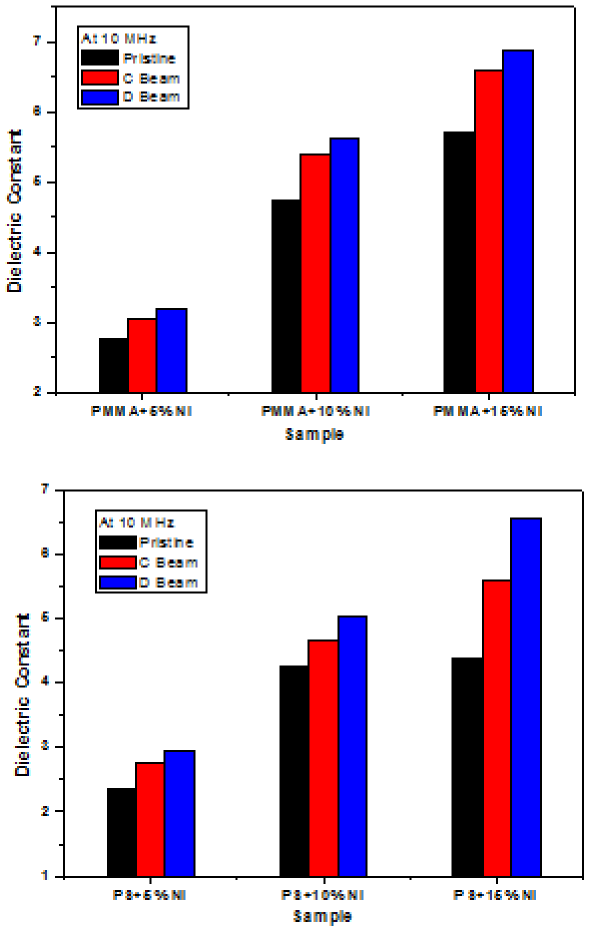

Fig. 5.20 Comparison of dielectric constant of pristine and irradiated samples at 10 MHz

References

[1] D. R. Sharma , Rashi Mathur , S.R. Vadera , N. Kumar , T.R.N. Kutty, Journal of Alloys and Compounds 358 (2003) 193-204.

[2] Xingyi Huang, Chonung Kim, Pingkai Jiang, Yi Yin, Zhe Li, Journal of Applied Physics 105 (2009) 014105 (10 pages).

[3] F. C. Fonseca, G. F. Goya, R. F. Jardim, R. Muccillo, N. L. V. Carren˜o, E. Longo, E. R. Leite, Physical Review B 66 (2002) 104406-104410.

[4] K. Akamatsu, K. Nakahashi, S. Ikeda, H. Nawafune, Eur. Phys. J. D 24 (2003) 377–380.

[5] N L Singh, Anjum Qureshi, A K Rakshit And D K Avasthi, Bull. Mater. Sci. 29(6) (2006) 605-609.

[6] C.J. Bedell, C.J. Solfield, L.B. Bridwell, I.M. Brown, J. Appl. Phys. 67 (1990) 1736-1740.

[7] V. Hnatowicz, J. Kvitek, V. Svorcik, V. Rybka, Appl. Phys. A 58 (1994) 349-352.

[8] N. L. Singh, Chaitali Gavade, P. K. Khanna, Defect and Diffusion Forum,341 (2013) 51-68.

[9] Chaitali Gavade, N. L. Singh, P. K. Khanna, Sunil Shah, Sanjeev Kumar, Advance materials letters (communicated).

[10] R. Kumar, U. De, R. Prasad, Nucl. Instrum. Methods B 248 (2006) 279-283.

[11] P. Scherrer, Gott Nachar, 2 (1918) 98–100.

[12] N. L. Singh, D. Singh, A. Qureshi, Radiation Effects & Defects in Solids 66(8-9) (2011) 640–647.

[13] A. Semwal, A. Negi, R. G. Sonkawade, J. M. S. Rana, R. C. Ramola, Indian J of pure and App Phy 48 (2010) 496-499.

[14] H S Virk , P S Chandi And A K Srivastava, Bull. Mater. Sci. 24(5), 529 (2001)

[15] L. Singh, K. Singh Samra, Radiation Physics and Chemistry 77 (2008) 252–258.

[16] A. Das, S. Dhara and A. Patnaik Physical Rev B 59 (1999) 11069.

[17] Anjum Qureshi , Dolly Singh , N.L. Singh, S. Ataoglu , Arif N. Gulluoglu , Ambuj Tripathi ,D.K. Avasthi, Nuclear Instruments and Methods in Physics Research B 267 (2009) 3456.

[18] A. K. Srivastava, H. S. Virk, J. Polym. Mater., 17 (2000) 325.

[19] S. Shah, N.L. Singh, A. Qureshi, D. Singh, K.P. Singh, V. Shrinet, A. Tripathi, Nucl. Instrum. Methods B 226 (2008) 1768.

[20] R. Vijaya Kumar, Yu. Koltypin, O. Palchik, A. Gedanken, Journal of Applied Polymer Science 86 (2002) 160–165.

[21] S. Manna, A. K. Deb, J. Jagannath, and S. K. De, J. Phys. Chem. C 112 (29) (2008) 10659-10662.

[22] Chaitali Gavade, N. L. Singh, D. K. Avasthi, Alok Banerjee, Nuclear Instruments and Methods in Physics Research B, 268 (2010) 3127–3131.

[23] P. Balaji Bhargav, B. A. Sarada, A. K. Sharma And V.V. R. N. Rao, Journal of Macromolecular Science, Part A: Pure and Applied Chemistry 47 (2010) 131–137.

[24] N. L. Singh, S. Shah, A. Qureshi, A Tripathi, F Singh, D. K. Avasthi, P. M. Raole, Bull. Mater. Sci.34(1) (2011) 81–88.

[25] T. Phukan, D. Kanjilal, T. D. Goswami, Nucl. Instr. And Meth. B, 234 (2005) 520.

[26] D. Singh, N.L. Singh, A. Qureshi, P. Kulriya, A. Tripathi, D.K. Avasthi, A.N. Gulluoglu, J. Non-Cryst. Solids, 356 (2010) 856–863.

[27] X. Yan, T. Xu, S. Xu, S. Wang, Nanotechnology, 15 (2004) 1759–1762.

[28] Rajesh Kumar, S. Asad Ali, A.K. Mahur, H.S. Virk, F. Singh, S.A. Khan, D.K. Avasthi, Rajendra Prasad, Nuclear Instruments and Methods in Physics Research B 266 (2008) 1788–1792.

[29] S. Saravanana, M.R. Anantharaman, S. Venkatachalam, D.K. Avasthi, Vacuum 82 (2008) 56–60.

[30] L.S. Farenza, R.M. Papaleo, A. Hallen, M.A. Araujo, R.P. Livi, B.U.R. Sundqvist, Nucl. Instr. and Meth. B 105 (1995) 134.

[31] Zhiyong Zhu, Yunfan Jin, Changlong Liu, Youmei Sun, Mingdong Hou, Chonghong Zhang, Zhiguang Wang, Jie Liu, Xiaoxi Chen, Baoquan Li, Yanbin Wang, Nuclear Instruments and Methods in Physics Research B 169 (2000) 83-88.

[32] J. Robertson, E.P. O Reilly, Phys. Rev. B 35 (1987) 2946.

[33] Lakhwant Singh, Kawaljeet Singh Samra, Ravinder Singh, Nuclear Instruments and Methods in Physics Research B 255 (2007) 350–356.

[34] G. Sui, S. Jana, W. H. Zhong, M. A. Fuqua, C. A. Ulven, Acta Mater., 56 (2008) 2381–2388.

[35] J. L. Wilson, P. Poddar, N.A. Frey, H. K. Srikanth, J. P. Mohomed, H. Kotha, S. J. Wachsmuth, J. Appl. Phys., 95 (2004) 1439-1443.

[36] Huang XY, Jiang PK, Kim CU, Journal of Applied Physics, 102 (2007) 124103-8.

[37] Qureshi A, Singh NL, Shah S, Singh F, Avasthi DK, Journal of Macromolecular Science, Part A: Pure and Applied Chemistry, 45 (2008) 265-270.

[38] A. K. Jonscher, Dielectric Relaxation in Solids; Chesla Dielectric Press: London, 1983.

[39] N. L. Singh, S.Shah, A. Qureshi, K. P. Singh, V. Shrinet, A. Tripathi, Radiat. Eff. Def. Solids, 163 (2) (2008) 169–177.

Chapter - VI

Summary and conclusion

Abstract

This chapter summarizes the results derived from the present investigations. The comparative study of various properties of the composites with respect to filler concentration, different ions and ion fluence is presented. It also derives the conclusions of the present study and future perspectives.

Summary and conclusions

This thesis is concerned the high energy ion beam irradiation effects in polymer composites which fascinated considerable attention for purposes of polymers in radiation environment and also in the improvement of new electronic devices. To achieve this goal, polymers have traditionally been considered as an excellent host matrix for composite materials and mixing with metal nanoparticles. SHI irradiation of polymers/polymer composites alters the chemico-physical properties considerably. The nature of changes depends upon properties of polymer composites, such as the composition and molecular weight, and on the mass and energy of the incident ions and other conditions also.

The composite films of different concentrations of metal nanoparticles silver (Ag), copper (Cu), and Nickel (Ni) powder in PMMA and PS were prepared by casting method in which THF and toluene was used as a solvent respectively. The films prepared at Department of Physics, The M. S. University of Baroda, Vadodara. These films were irradiated with 85 MeV C- ions and 120 MeV Si-ions at fluences of 1 x 10^{11}, 1 x10^{12} ions/cm^2 using high energy ion beam facility of Inter University Accelerator Centre (IUAC), New Delhi, India. Energetic ion beams play a vital role in the field of research and it has been exploited by researchers in different ways in materials science. Due to the interaction of radiation/energetic particle with polymer composite material absorbs its energy and active species such as radicals are produced initiating various chemical reactions. The different responses to radiation for different polymers are intrinsically related to the chemical structures of the polymer /polymer composite materials. The synthesized polymer nanocomposites were subjected to different characterizations, mainly structural, thermal, optical, magnetic and electrical properties and surface morphology before and after irradiation. The comparative results are summarized as follow;

(I) Structural modification:

The crystallite size of pristine and irradiated composites was studied by means of X-ray diffraction. The crystallite size was calculated using Scherrer’s formula as discussed in chapter 2. It is appearant that crystallite size increases with filler concentartions which is responsible to the crytalline nature of filler in both composites. In the case of PMMA/Ag(/Cu/Ni) nanocomposites, crystallite size of fillers decreases slightly upon irradiation with both the ions. It is also observed that the intensity of the peak decreases and to some extent broadening of the peak after irradiation offers confirmation of decrease in crystallinity. Since no significant change in the peak position is observed, this reveals that lattice parameters do not change significantly with both ion beams irradiations. Results show that the ion beam irradiation causes large amount of energy deposition in the material which leads to decrease in crystallite size. It may be attributed to splitting of crystalline grains due to absorption of large amount of energy and it also reflects the formation of disorder system. The irradiation may induce chain scissioning, which is also corroborated by DSC analysis, assumed to be responsible for the reduction in crystallinity of the composite. Rather in the case of PS/Ag(/Cu/Ni) nanocomposites, the diffraction patterns of the irradiated samples by 85 MeV C-ions and 120 MeV Si ions exhibited an increase in the peak intensity and a decrease in the full width at half maximum (FWHM) corresponding to all observed peaks of Ag/Cu/Ni nano particles. This behaviour may be attributed to cross-linking effect and resulted in the alignment of the polymeric chains, which is also corroborated by the results of DSC analysis. The results for highest concentration and fluence are summarized in Table 6.1.

Table 6.1(a): Crystallite size of composites for PMMA+ Ag/Cu/Ni systems

Sample	Pristine		C Beam	Si Beam
	2θ	Crystallite size (nm)	Crystallite size (nm) (1x10^{12}) ions/cm^2	Crystallite size (nm) (1x10^{12}) ions/cm^2
PMMA+ 15%Ag	38.07	32.64	30.14	29.98
	44.24	33.17	30.67	29.34
	Average	32.91	30.41	29.66
PMMA + 15%Cu	46.39	12.36	11.68	10.54
	58.01	12.24	11.22	10.39
	Average	12.30	11.45	10.47
PMMA + 15%Ni	44.60	10.40	11.05	10.67
	51.27	11.10	10.21	9.58
	Average	11.52	10.63	10.13

Table 6.1(b): Crystallite size of composites for PS+ Ag/Cu/Ni systems

Sample	Pristine		C Beam	Si Beam
	2θ	Crystallite size (nm)	Crystallite size (nm) (1x10^{12}) ions/cm^2	Crystallite size (nm) (1x10^{12}) ions/cm^2
PS+ 15%Ag	37.87	37.98	38.51	38.88
	44.11	37.87	38.19	38.90
	Average	37.93	38.35	38.89
PS + 15%Cu	46.18	11.89	12.98	13.52
	57.23	12.06	13.11	13.78
	Average	11.97	13.05	13.65
PS + 15%Ni	44.60	10.40	11.50	11.88
	51.27	11.10	11.75	12.24
	Average	10.75	11.62	12.06

(II) Thermal response:

The glass transition temperature (Tg) of pristine and irradiated samples was studied by DSC thermograms. At the glass transition temperature, the weak secondary bonds that stick the polymer chains together are broken, and the macromolecule starts to move. The influence of metal nanoparticles and irradiation on the glass transition behaviour of polymer matrix (PMMA/PS) was investigated with dynamic DSC technique. When the inter-particles distance is small enough, then the polymer between two particles can be considered as a thin film. Assuming that there is small or no interfacial interaction between the filler and matrix exists and then Tg decreases as explained by Ash et al according to thin film model. It reveals that the ion irradiation leads to polymer chain scissioning and a subsequent reduction in the molecular weight. As a result, the system moved toward the more disordered state in the case of PMMA+Ag (/Cu/Ni) nanocomposites. The Tg of pristine composites increases with filler concentration and also further increases upon irradiation in PS/Ag(/Cu/Ni) nanocomposites. This behaviour probably arises due to branching (cross-linking effect) when islands of nanoparticles are bonded with polymeric chains. This lowers the mobility of the chains, and as a result, the glass transition temperature increases in the nanocomposites. These results are also corroborated with XRD results. The results for highest concentration and fluence are summarized in Table 6.2.

Table 6.2(a): Glass transition temperature of composites for PMMA+ Ag/Cu/Ni systems

Sample name	Tg (Pristine)	Tg (C beam)	Tg (Si beam)
PMMA + 15 %Ag	71.4	65.8	64.2
PMMA + 15 %Cu	71.9	61.8	61.5
PMMA + 15 %Ni	77.8	76.8	72.8

Table 6.2(b): Glass transition temperature of composites for PS+ Ag/Cu/Ni systems

Sample name	Tg (Pristine)	Tg (C beam)	Tg (Si beam)
PS + 15 %Ag	71.9	72.7	73.2
PS + 15 %Cu	72.9	73.3	74.8
PS + 15 %Ni	71.5	73.7	75.7

(III) Optical response:

UV–vis spectroscopy is an important tool to investigate the value of optical band gap energy (Eg). It is observed that optical absorption increases with increasing energy loss and this absorption shifts from UV–vis to visible region for all irradiated nanocomposite samples. With increase of electronic energy loss the nanocomposites become gradually opaque to the visible light and the absorption edge shifted from UV towards the visible. This is consistent with the observation that the material changes from transparent to opaque with increase of energy deposition. The increase in absorption with irradiation may be attributed to the formation of a conjugated system of bonds due to bond cleavage and reconstruction. The shifting of absorption edge towards visible is generally considered to result from carbonization of the material under irradiation which is also corroborated to the dielectric results. It is noticed that band gap values shifted to lower energy in composites for irradiated samples. The obtained results for highest concentration and fluence are summarized in Table 6.3.

Table 6.3(a): Band gap energy of composites for PMMA+ Ag/Cu/Ni systems

Sample	Pristine		C Beam		Si Beam	
	Band gap in eV	No. of carbon atoms(N)	Band gap in eV	No. of carbon atoms(N)	Band gap in eV	No. of carbon atoms(N)
Pure PMMA	4.58	56	4.38	61	4.26	65
PMMA + 15%Ag	3.82	80	3.65	88	3.21	114
PMMA + 15%Cu	3.78	82	3.55	90	3.22	113
PMMA + 15%Ni	3.84	80	3.55	90	3.43	100

Table 6.3(b): Band gap energy of composites for PS+ Ag/Cu/Ni systems

Sample	Pristine		C Beam		Si Beam	
	Band gap in eV	No. of carbon hexagon rings	Band gap in eV	No. of carbon hexagon rings	Band gap in eV	No. of carbon hexagon rings
Pure PS	4.38	~1	4.21	~1	3.89	~1
PS + 15%Ag	3.90	~1	3.60	~1	3.30	~2
PS + 15%Cu	3.98	~1	3.65	~1	3.40	~2
PS + 15%Ni	4.02	~1	3.75	~1	3.43	~2

(IV) Surface morphology:

Surface morphology was studied by means of scanning electron microscope (SEM) which gives 2-D surface topography of sample surface. The analysis shows that the filled partilces are distributed randomly in the matrix which display continuous contact between themselves and formed conducting paths. After irradiation, significant changes in surface morphology were observed. Considerable damage in the polymeric structure was observed after irradiation, which is also responsible for decrease in crystallinity of the material as indicated by XRD analysis in PMMA nanocomposites. This may be attributed to large sputtering effect due to irradiation in PMMA nano composites. Wherea in PS nanocomposites, the surface becomes smoothen upon irradiation.The decrease in roughness may be attributed to the decrease in density of metal particles on the surfaces of the films, which is also responsible for increase in crystallinity of the material as indicated by XRD analysis. This is attributed to the defect enhanced surface diffusion in the case of PS nano composites.

(V) Magnetic properties:

The temperature (T) and magnetic field (H) variations of the magnetization (M) were measured with a SQUID (superconducting quantum interference device) magnetometer. The temperature variations of M for the zero field- cooled (ZFC) and the field-cooled (FC) cases were measured from 5-300 K at applied field ,H = 500 Oe. Hysteresis measurements were carried out at 300 K with magnetic field swept from 50 kOe to -50 kOe. The magnetic parameters extracted from the measurements are listed in Table 6.4.

The increase in the values of M_S and H_C after irradiation may be attributed to the change in exchange and dipolar interactions mediated by the matrix.

FC magnetization decreases continuously with the increase of temperature. Such characteristic behavior of FC magnetization data is attributed to ferromagnetism in material in both nanocomposites.

Table 6.4: Magnetic properties of composites for PMMA+Ni and PS+Ni systems.

Sample		Pristine	C Beam	Si Beam
PMMA+15%Ni	Saturation Magnetization (M_S) (emu/gm)	0.085	0.107	0.120
	Coercive Field (H_C) (Oe)	138	147	150
	Remnant Magnetization (M_R) (emu/gm)	0.015	0.020	0.022
PS + 15%Ni	Saturation Magnetization (M_S) (emu/gm)	0.077	0.097	0.109
	Coercive Field (H_C) (Oe)	136	145	155
	Remnant Magnetization (M_R)(emu/gm)	0.014	0.019	0.022

(VI) AC electrical properties:

Conductivity: The AC electrical properties of all composites were studied in the frequency range of 100 Hz to 10 MHz at an ambient temperature.

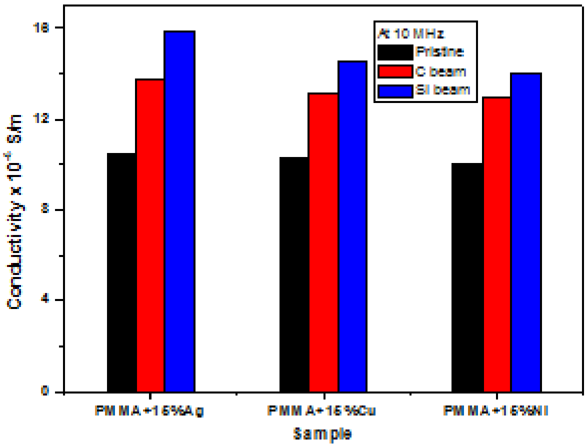

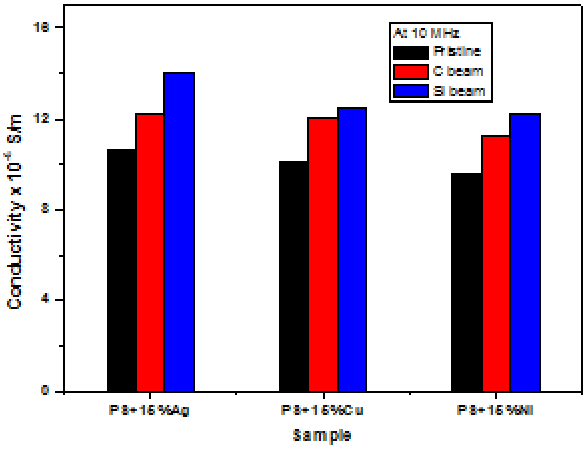

Fig.6.1 Comparison of conductivity of pristine and irradiated samples at 10 MHz

Ac electrical conductivity of all pristine and irradiated samples at different ion species and at a constant concentration (15%) and constant frequency (10MHz) is shown in Fig.6.1. The increase in conductivity with metal nanoparticles concentration for pristine samples may be attributed to the conductive phase formed by dispersed metal nanoparticles in polymer matrix. The increase in conductivity is related to a possible increase in the number of conduction paths created between the filler particles aggregates in the composite and as a consequence electrical path in the polymer matrix in addition to a decrease in the width of the potential barriers within the bulk region of high conductivity. Therefore more charge carriers may be able to 'hop' by tunnelling; resulting in the increase in the bulk conductivity and it also increases with increasing filler concentration. Conductivity is further observed to increase upon irradiation. Irradiation is expected to promote the metal to polymer bonding and convert polymeric structure into hydrogen depleted carbon network. It is this carbon network that is believed to make the polymer more conductive.

Dielectric constant: The dielectric constant of all composites was calculated in the frequency range of 100 Hz to 10 MHz.

The values of the dielectric permittivity for nanocomposites depend both on the measuring frequency and also nano filler concentration. Especially, the dielectric behaviors of nanocomposites with different metal nanoparticles concentrations in the low frequency range (< 1kHz) are found to be increased which is due to the interfacial space charge polarization. The higher the nanofiller loading level, the larger the total effective area of the interfaces between the polymer matrix and the filler, and the thinner the insulating spacers separating nanoparticles, resulting in the considerable increment of the interfacial space-charge polarization at these frequency range. As observed from figure, the dielectric constant remains almost constant up to 100 kHz. At these frequencies, the motion of free charge carriers assumed to be constant through the polymer. It is also observed that dielectric constant increases upon irradiation. The increase in dielectric constant may be attributed to the chain scission, cross linking and as a result the increase in the number of free radicals, unsaturation etc. At higher frequency regions, (i.e., beyond 100 kHz), the charge carriers migrate through the dielectric and get trapped against a defect sites and induced an opposite charge in its vicinity. So, the polarization of trapped and bound charges cannot take place and that reduced the dielectric constant. According to the Dissado and Hill theory, in intra-cluster motions, the relaxation of a dipole will produce a ‘chain’ response in its neighbouring dipoles and the reaction of the neighbouring dipoles will, in turn, affect the first dipole, so the overall effect will be seen as a single-cluster dipole moment relaxation. This reduces the dielectric constant at these frequencies. For the sake of comparison, the dielectric constant of all pristine and irradiated samples at different ion species and at a constant concentration (i.e. 15%) and constant frequency (10MHz) is shown in Fig.6.2.

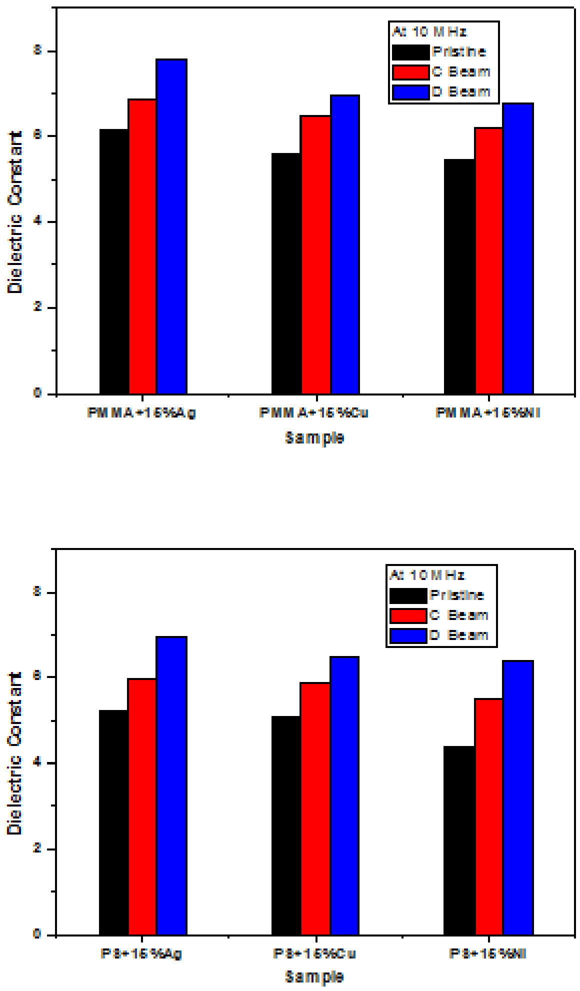

Fig. 6.2 Comparison of dielectric constant of pristine and irradiated samples at 10 MHz

Dielectric loss: The dielectric loss of all composites was studied in the frequency range of 100 Hz to 10 MHz. In general, the dielectric loss of the dielectric material causes from distortional, dipolar, interfacial, and conduction loss. The dielectric loss decreases exponentially with the increase of log frequency. It is observed that dielectric loss increases moderately with the concentration of filler and also with the ion fluence which may be featured by the interfacial polarization mechanism of the heterogeneous system. Positive value of dielectric loss in all the cases represents the inductive behavior of the material.

Conclusion:

Present work deals with the synthesis of polymer nanocomposites and effect of ion beam irradiation on these nanocomposites. Based on this study, we have concluded that ion beam irradiations alter all the properties of polymer nanocomposites. An XRD analysis reveals that the crystallite size of the composites decreased after ion beam irradiation which is also corroborated by the DSC analysis due to the chain scissioning upon irradiation in PMMA nanocomposites. In PS nano composites, we observed cross linking effect upon irradiation. It was observed from the UV- visible spectroscopy analysis that the band gap value moved to the lower energy on doping with metal nanoparticles, as well as upon irradiation. SEM images showed damages upon ion beam irradiation. The magnetic properties enhanced after ion beam irradiation which may be attributed to the exchange dipolar interaction of particles in the matrix and generation of free radicals. The dielectric properties of the composites increased with the increase of metal content. These phenomena could be interpreted from interfacial polarization of heterogeneous systems. It is evsigaed taht the new composite materials synthesized in the present work have potential applications such as microelectronics, satellite, telecommunication, packaging, biomaterials etc where material with low dielectric constant is required. Rather material with high dielectric constant can be used for EMI shielding application.

Future Plan

Physical properties of bimetallic nanoparticles embedded polymer matrix by ion beam irradiation

During the past decade, the design and synthesis of bimetallic nanomaterials have attracted considerable attention, because they show multiple functionalities and prominent catalytic activity, electrical, chemical and optical properties over monometallic nanomaterials. Polymer nanocomposites have received significant attention because of the new and superior properties (*e.g.* electrical, thermal and mechanical) to conventional composites of these materials and may be synthesized using surprisingly simple and inexpensive techniques. Synthesis of nanocomposite polymers is easy due to their ease of processing, solubility and less toxicity. The modification of polymeric material by irradiation with swift heavy ions has gained considerable interest in the last two decades because of significant change in the chemico-physical properties of the materials. The nature of changes depends upon properties of polymers, such as the composition and molecular weight, and on the mass and energy of the incident ions and other conditions also. The samples will be prepared by chemical route method in which different bimetallic nanoparticles dispersed in polymer matrix and will be irradiated by different ion beams. These samples will be characterized by X-ray diffraction, TEM/SEM, DSC, UV-Visible spectroscopy, SQUID measurements and dielectric spectroscopy.